Technical Report

TR-13-12

Investigation of sulphide production in core-drilled boreholes in Äspö Hard Rock Laboratory

Boreholes KA3110A, KA3385A and KA3105A

Henrik Drake, Isochron Geoconsulting

Lotta Hallbeck, Karsten Pedersen
Microbial Analytics Sweden AB

Anette Rosdahl, Sweco Environment AB

Eva-Lena Tullborg, Terralogica AB

Bill Wallin, Geokema AB

Bertil Sandberg, Thomas Blomfeldt
Swerea KIMAB

July 2014

Svensk Kärnbränslehantering AB
Swedish Nuclear Fuel
and Waste Management Co

Box 250, SE-101 24 Stockholm
Phone +46 8 459 84 00

ISSN 1404-0344
SKB TR-13-12
ID 1403211

Investigation of sulphide production in core-drilled boreholes in Äspö Hard Rock Laboratory

Boreholes KA3110A, KA3385A and KA3105A

Henrik Drake, Isochron Geoconsulting

Lotta Hallbeck, Karsten Pedersen
Microbial Analytics Sweden AB

Anette Rosdahl, Sweco Environment AB

Eva-Lena Tullborg, Terralogica AB

Bill Wallin, Geokema AB

Bertil Sandberg, Thomas Blomfeldt
Swerea KIMAB

July 2014

Keywords: Instrumentation, Equipment, Microbiological analyses, Sulphate reducing bacteria, Dissolved gases, Stable isotopes, Isotopes in gases, Corrosion.

Abstract

The purpose of the activities described in this report was to investigate the conditions and the main energy sources for microbial sulphide production in groundwater in isolated sections of core drilled boreholes. The idea was to study and compare the microbiological and chemical characteristics of boreholes with different sulphide concentrations and water chemistry.

The study consists of two parts;

1. Analyses of time-series of sulphide and sulphide related parameters in delimited borehole sections during stagnant conditions (boreholes KA3110A and KA3385A).
2. Investigations of borehole sections and fracture waters in KA3105A and KA3385A, before retrieval of borehole instrumentation and investigation of the equipment after retrieval, studying corrosion, microorganisms and secondary precipitates.

The study has showed the importance of performing a thorough investigation of the hydraulic performance of the borehole instrumentation before sampling from a borehole section. Due to problems with the instrumentation and accidental addition of ethanol during sampling, some of the activities were not fully performed in accordance to the activity plans. The results from the sampling campaigns and analyses were to some extent affected by these deviations.

The similarity in ongoing processes between the different boreholes has been evidenced by results from different methods, representing different disciplines. Overall, the results from the boreholes studied showed relatively similar features regarding secondary mineralogy, groundwater chemistry evolution between fracture and section water as well as the stable isotope ratios in water and minerals. Also, with one exception, there was no significant difference between the numbers of sulphate reducing bacteria on the surface of the different materials of the instrumentation. The exception was the stainless steel surfaces, where the number of sulphate reducing bacteria was lower; however, the pattern was the same disregarding borehole and sulphide concentration. Remaining parameters that were not considered or thoroughly investigated in this study are the hydrogeological conditions of the boreholes and the species of sulphate reducing bacteria and other bacteria. These features are likely to affect the sulphide that may be produced and observed when analysing sulphide in groundwater.

Contents

1 Introduction

1.1 Background

In the safety assessment of spent nuclear fuel disposal according to the KBS-3 design, sulphide concentrations in groundwater play a key role in the long-term stability of the copper canisters (Tullborg et al. 2010a, b). In an anaerobic environment, sulphide will cause corrosion of the copper canisters and it is of importance to understand how concentrations of sulphide vary in granitic groundwater.

During the site investigation and the subsequent monitoring of groundwater chemistry it has been found that there was a large variation, between 0.001–0.1 mM, in the measured sulphide concentration both between groundwater from different boreholes and sections but also over time in one borehole section. Pronounced differences were found between the sulphide contents measured during the complete chemical characterisation (CCC) and the later groundwater monitoring. The latter were performed after the permanent installations were put in place in the boreholes (Tullborg et al. 2010a, b). Data from the site investigation (CCC sampling) showed no correlation between the numbers of sulphate-reducing bacteria (SRB) and the sulphide concentrations either in Laxemar groundwater or in the groundwater in Forsmark. There was on the other hand a significant correlation between the number of SRB and the measured Eh at sites (Hallbeck and Pedersen 2008a), suggesting that there is an ongoing sulphate-reduction to sulphide in the groundwater. At some point it was found that high sulphide concentrations were developed in the water within the borehole section after a period during which the section had not been flushed and sampled (Nilsson et al. 2010).

The following questions were raised within the SR-Site project (Tullborg et al. 2010a, b):

- What are the representative sulphide concentrations in the fracture groundwater?
- Why does the number of SRB not relate with the measured sulphide concentrations?
- What may trigger an increased sulphide production in the borehole sections?
  - Does the equipment in the boreholes support the sulphide production by SRB?
  - Is there a difference between the equipment materials in different boreholes?
  - Or, does the difference in sulphide production depend on the groundwater characteristics and thereby different microbial fauna?

Other studies of microbial sulphide production have been performed at the Äspö HRL. Determination of the number of SRB has been done in three boreholes at the Microbe site in the Äspö tunnel (Hallbeck and Pedersen 2008a). In those studies, there was a clear difference in the number of SRB (MPN-most probable number) and sulphide concentrations between the different boreholes. The borehole instrumentation in the Microbe site was made of PEEK (polyetheretherketone) and no metal was used. The results in Hallbeck and Pedersen (2008a) indicated that the concentration of sulphide increased during periods of slow water flow. In the MiniCan (miniature canister) experiment (Smart et al. 2012), the MPN of SRB had increased in the water enclosed in the void volume close to the miniature capsules that were installed at Äspö HRL in 2007 and investigated in 2011 (Lydmark and Hallbeck 2011). Small holes were deliberately made at the top and/or bottom of the miniature copper canisters, so that water could enter and start the corrosion of the cast iron insert. In 2009 surface boreholes were investigated at Laxemar and Äspö (Rosdahl et al. 2011). In this study, elevated concentrations of sulphide and SRB were found in standpipes and section water that had not been subjected to previous pumping. The sulphide concentration in the sections decreased during continuous pumping.

1.2 Aim and scope

The aim of the investigations described in this report was to study the processes behind microbial sulphide production in delimited sections of core drilled boreholes to be able to explain;

- why the concentration of sulphide differs between boreholes both in the borehole section and in the fractures intersecting the sampled section,
- why the concentration of sulphide increases in borehole sections during periods of more stagnant conditions and decrease when discharging water.

1.3 Conceptual idea and method

The idea was to look for differences between borehole sections with observed different sulphide concentrations in order to be able to include or exclude components involved in microbial sulphide production. Such components may be of chemical, geological, biological and hydrological character or a combination of these. Also, a part of the investigation focused on determining any influence on the sulphide production from the materials included in the instrumentation in core-drilled boreholes. The investigation strategy was to sample section water (stagnant water in the packed off borehole section) and compare it with fracture water (water flowing into the borehole section from the surrounding rock, in general sampled after 10 section volumes have been discharged).

The investigations were performed in three boreholes in the Äspö HRL and included analyses of groundwater in delimited sections and analyses of solid samples from borehole equipment (precipitates and biofilm). The analysis programme included chemical components, microbiology, dissolved gases and stable isotopes in water (C (Carbon), O (Oxygen), H (Hydrogen) and S (Sulphur)) and in gases (C, O, H). The investigations in this report were a continuation of a previous study performed in core drilled boreholes at Äspö and Laxemar (Rosdahl et al. 2011).

1.4 Quality assurance

The work presented in this report was carried out in accordance with activity plans and other documents listed in Table 1-1. Both activity plan and measurement system descriptions are SKB's internal controlling documents. This report presents hydrogeochemical and microbiological data from field work carried out during the period of March 2010 to February 2011. The obtained data from the listed activity plans are stored in the Sicada database and are traceable by the activity plan number.

Table 1-1. Controlling documents for the performance of the activity.

Project plan	**Number**	**Version**
Investigation of sulphide production processes in groundwaters at Äspö and Laxemar.	SKBdoc 1233091	1.3
Activity plan		
Cirkulation och provtagning av grundvatten i KA3385A och KA3110A – undersökning av sulfidproduktion.	APTDKBP4001-10-019	1.0
Cirkulation och provtagning av grundvatten I KA3385A och KA3110A etapp 2 – undersökning av gassammansättning och isotoper i gaser.	AP TD KBP4001-10-041	1.0
Utspädningsmätning och kapacitetstest I KA3110A och KA3385A inom Sulfidprojektet KBP4001.	AP TDKBP4001-11-019	1.0
Uttag och provtagning av borrhålsutrustning I KA3110A och KA3385A I Äspö HRL.	AP TDKBP4001-11-098	1.0
Measurement system descriptions	**Number**	**Version**
Metodbeskrivning för sprickmineralanalys.	SKB MD 144.001	1.0
Metodbeskrivning för hydrogeologisk monitering i Äspötunneln.	SKB MD 368.004 (applicable parts)	1.0
Metodbeskrivning för grundvattenmonitering vid SKB:s platsundersökningar.	SKB MD 360.002 (applicable parts)	2.0
Instructions		
Provtagning och analys-kemilaboratorium – enligt kemilaboratoriets ledningssystem.	SKB MD 452.001-019	

1.5 Report Structure

This study consists of two parts; 1) *in situ* investigation of sulphide production in groundwater between packed-off boreholes sections, 2) investigation of borehole instrumentation (packers, etc).

The introduction of the report includes a general description of the site location and the groundwater chemistry sampled from the investigated borehole sections. A background to microbial sulphide production processes, gases dissolved in groundwater and stable isotopes are given in Chapters 1, 2 and 3. A description of the boreholes and instrumentation is given in Chapter 4. Chapter 5 includes the circulation experiment and Chapter 6 the investigation of borehole instrumentation. Chapter 7 discusses the results from Chapters 5 and 6 and Chapter 8 gives the project conclusions.

Key to abbreviations used throughout the report:

AA: Autotrophic acetogens

ANME: Anaerobic methanotroph

CCC: Complete chemical characterisation

CDT: Canyon diablo troilite

DOC: Dissolved organic carbon

EPDM: Ethylene-polypropylene rubber

IAP: Ionic activity product

IRB: Iron-reducing bacteria

HRL: Hard Rock Laboratory (Äspö)

MPN: Most probable number

PDB: Pee dee belemnite

pmC: Percent modern carbon

PUR: Poly urethane rubber

PVC Polyvinylchloride

SI: Saturation index

SIMS: Secondary ion mass spectrometer

SMOW: Standard mean oceanic water

SRB: Sulphate-reducing bacteria

TNC: Total number of cells

TOC: Total organic carbon

2 Microbial sulphide producing processes

2.1 Sulphate reducing bacteria

Sulphate reduction at temperatures and pressures prevailing in deep groundwater environment is a microbiological process. The chemical reduction to hydrogen sulphide at these conditions is extremely slow as revealed by the calculated half-life for thermo-chemical sulphate reduction in the presence of acetate and elemental sulphur at 100°C that is 372,000 years (Cross et al. 2004).

The sulphate-reducing bacteria (SRB) use the S atom in the sulphate molecule as an electron-acceptor and the reduced product is hydrogen sulphide. The energy and electron donor for SRB can be either organic compounds or hydrogen. With a general organic compound, written as CH_2O, the reaction with sulphate can be written (Equation 2−1):

$$2(CH_2O) + SO_4^{2-} + 2H^+ \rightarrow 2HCO_3^- + HS^- + 3H^+ \qquad \text{Equation 2−1}$$

Organic compounds that can be used by different types of SRB are fermentation products like short chain organic acids, fatty acids and higher molecular weight hydrocarbons. Many SRB, especially of the genus *Desulfovibrio,* can grow on lactate. The lactate molecule is incompletely oxidized to acetate and carbon dioxide and the electrons are transported to electron transport enzymes in the cell membrane and then further to the sulphate reduction enzymes in the cytoplasm. The overall reaction is written (Equation 2−2):

$$2 \text{ lactate} + SO_4^{2-} + 2H^+ \rightarrow 2 \text{ acetate} + 2CO_2 + HS^- + H^+ + 2H_2O \qquad \text{Equation 2−2}$$

In this metabolism lactate is used as an energy and electron source as well as a carbon source for biomass production.

There are also SRB that utilize hydrogen as electron donor and energy source. The reaction for the reduction of SO_4^{2-} with H_2 is written (Equation 2−3):

$$4H_2 + SO_4^{2-} + 2H^+ \rightarrow H_2S + 4H_2O \qquad \text{Equation 2−3}$$

Note that there is no carbon involved in this energy transforming reaction (Equation 2−3). The carbon sources for H_2 oxidising SRB are either short chain organic compounds like acetate or carbon dioxide. The carbon is used for biomass production and the biosynthesis is energy consuming. Acetate and carbon dioxide are incorporated into the cell metabolism via the molecule acetyl coenzyme A (acetyl-CoA) to produce pyruvate in the following way (Equation 2−4):

$$CH_3COO^- – CoA + CO_2 + H_2 \rightarrow CH_3COCOO^- + CoA + H_2O \qquad \text{Equation 2−4}$$

The pyruvate then enters the cell metabolism and will be incorporated into new bio molecules.

Recently, SRB strains isolated from marine sediments have been shown to directly extract the electrons from iron metal into their energy metabolism (Dihn et al. 2004, Enning et al. 2012). It was demonstrated that this type of SRB corroded iron metal faster than chemotrophic SRB using organic energy sources and/or the hydrogen produced in the anaerobic corrosion process. One of the two strains isolated was heterotrophic SRB using acetate as carbon source and the second one was lithotrophic using CO_2 as carbon source (Enning et al. 2012).

Finally, some microbial consortia can use methane as a source of energy and produce hydrogen sulphide.

$$CH_4 + SO_4^{2-} \text{g } HCO_3^- + HS^- + H_2O \qquad \text{Equation 2−5}$$

For methane to act as an energy source requires the SRB to have a symbiotic relationship with anaerobic methane oxidation *Archaea* methanogens (ANME); a situation which until now has been demonstrated only in sea bed sediments (Lösekann et al. 2007). Similar hydrogeochemical, isotopic and microbiological signatures have been observed under deep bedrock conditions in Olkiluoto (Pedersen et al. 2008) and from calcite studies at Laxemar (Drake et al. 2012). The calcites are of unknown age, but presumably within 10 Ma.

2.2 Energy and carbon sources

In shallow groundwater the energy and carbon originate from photosynthesis. In groundwater at several hundreds of metres depth the energy sources may also originate from the inner of the Earth. The actual depth for the shift from carbon and energy coming from the phototrophic surface processes is not established for Fennoscandian groundwater and is probably also varying depending on soil layer depth, groundwater flows etc. It has been observed in Laxemar, Äspö and in Forsmark that in some zones there is a transport of Baltic Seawater, and thus photosynthesised carbon, from the surface to depths of 500 m below sea level (Tullborg et al. 2010a, b). Hydrogen gas is used by several physiological groups of microorganisms, among them SRB, methanogens and acetogens. There are several origins of hydrogen in deepground water and they are discussed in Section 2.4 Dissolved gases. Hydrogen is also produced in metal corrosion as discussed in Section 2.3 below. Methane is another energy rich gas that can be used by microorganisms. Anaerobic oxidation of methane has not yet been conclusively demonstrated in the laboratory but there are environmental indications that this microbial processes occurs in natural systems. The origin of methane is discussed in Section 2.4 below.

Metals in borehole installations can act as energy source by anaerobic corrosion with H_2 formation. The formed H_2 can then act as energy source for many species of SRB. The SRB process using electrons directly from metallic iron is also a possible energy source without H_2 see Section 2.3 below.

SRB most often use short organic acids and other partially oxidised organic compounds. There are reports claiming that SRB can grow on plasticisers from different plastic materials (Tsuchida et al. 2011). This is still to be elucidated regarding tubing and tape used in the borehole installations. The investigation of microbial presence on the different materials used in the installations was an initial approach to this question.

2.3 Anaerobic bio-corrosion of metals

Hydrogen sulphide is a compound that can mediate anaerobic corrosion of metals. There are steel materials in the investigated monitoring boreholes that may corrode and generate hydrogen sulphide by means of SRB. The oxidation of metallic iron with sulphate is regarded as the principal reaction in anaerobic corrosion of iron. The suggested reaction mechanism for the corrosion, see scheme in Figure 2-1, is that the negative redox potential (Fe^{2+}/Fe, $E_0^{'}$[1] = −0.44 V) of iron can liberate hydrogen ($2H^+/H_2$, $E_0^{'}$ = −0.41 V) and may in this way indirectly act as an electron donor for SRB (Cord-Ruwisch 2000).

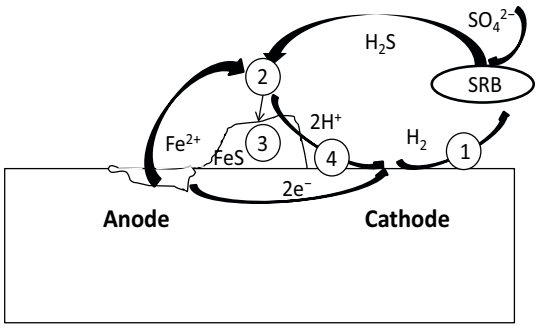

Figure 2-1. *The principle of anaerobic corrosion of metallic iron mediated by SRB. 1. The hydrogen produced by the reduction of protons by electrons from the oxidation of iron is consumed by SRB. 2. The H_2S produced precipitates with the Fe^{2+} and is deposited as 3. FeS on the iron surface. 4. During the precipitation protons are liberated.*

[1] E_0 means the standard redox potential of a redox reaction (for example the redox couple Fe^{2+}/Fe) when all substances are in their standards states of unit activity. $E_0^{'}$ denote the E_0 for the half-reaction at pH 7.

Another possible mechanism in anaerobic corrosion has been proposed: a direct utilization of the electrons liberated during the oxidation of metallic iron ($Fe^0 \rightarrow Fe^{2+} + 2e^-$) $E_0 = -0.469$ V. This mechanism is kinetically more favourable than consumption of the electrochemically formed H_2. A recent study showed that two isolated strains of SRB grew in culture media with coupons of iron as energy and electron source (Enning et al. 2012). One strain was autotrophic and used CO_2 as carbon source. The other strain needed acetate as carbon source but did not oxidise this with sulphate as electron acceptor but grew only when metallic iron was present. The corrosion rate of iron was 0.7 mm $year^{-1}$. The study also showed that the precipitated FeS functioned as a semi-conductor transporting electrons from the metal surface via the FeS to the SRB cells that grew on the surface of the precipitates.

In the anaerobic copper corrosion in the presence of sulphide produced by SRB, electrons from the metal reduce protons to hydrogen, see Equation 2-6.

$$2Cu + HS^- + H^+ \rightarrow Cu_2S + H_2 \qquad \text{Equation 2-6}$$

The produced hydrogen can be used by SRB that produce more hydrogen sulphide, and the overall reaction then becomes:

$$2Cu + 0.75\ HS^- + 0.25\ SO_4^{2-} + 1.25\ H^+ \rightarrow Cu_2S + H_2O$$

It is therefore of great importance to characterize the potential for hydrogen sulphide production in groundwater in a repository for spent nuclear fuel. One set of the parameters that are of consequence is that governing the growth kinetics of SRB when grown on different energy sources.

2.4 Dissolved gases

Gaseous species are taken to be substances that exist as gases under the range of temperatures and pressures that include those of the sampled drill holes. In this investigation, 9 different gaseous compounds were found at various concentrations above trace amounts in the investigated groundwater. The process of formation and the place of origin differ for different geosphere gas species. It can be biological processes in the atmosphere, radioactive decay at different places or thermogenic, chemical processes in deep crustal and mantle layers of Earth. Several gases have a primordial origin, meaning that they were formed before the Earth was formed; they were aggregated during the condensation of the Earth, and have been degassing to the atmosphere, through the geosphere since then. To fully understand the differences in groundwater chemistry that affect sulphide production, dissolved gases have to be included.

Hydrogen

Hydrogen is the most abundant element in the universe and consists of three isotopes with mass number 1, 2 and 3. Hydrogen gas (H_2) is explosive in oxygenic environments and it can act as a strong reducing agent as is revealed by the negative redox potential of proton/hydrogen ($2H^+/H_2$, $E_0' = -0.41$ V). H_2 can be formed in microbiological biological fermentation processes and by a range of different processes not involving life. Fermentation occurs in anaerobic systems such as water logged soils and anoxic groundwater, i.e. in the geosphere. Fermentative processes cannot produce high concentrations of hydrogen (Madigan and Martinenko 2006); hydrogen produced during fermentation is commonly combined with carbon dioxide to methane by methanogens. The radiolysis of water has been proposed by Lin et al. (2005) as a possible H_2 generation process occurring in the Precambrian granitic system including the Fennoscandian Shield (yield rate calculated to 9.4×10^{-9}nM s^{-1}). Radiolysis of water to oxygen and H_2 can consequently produce small amounts of H_2 in the geosphere, but the main natural source of hydrogen to the geosphere is likely transport from deep layers by diffusion and advection. Anaerobic corrosion of metals, mainly iron and steel, in engineered borehole installations will also produce H_2.

There are at least six possible processes by which crustal H_2 is generated: (1) reaction between dissolved gases in the C-H-O-S system in magmas, especially in those with basaltic affinities; (2) decomposition of methane to carbon (graphite) and hydrogen at temperatures above 600°C; (3) reaction between CO_2, H_2O, and CH_4 at elevated temperatures in vapours; (4) radiolysis of water

by radioactive isotopes of uranium and thorium and their decay daughters and by radioactive isotopes of potassium; (5) cataclasis of silicates under stress in the presence of water; and (6) hydrolysis by ferrous minerals in mafic and ultramafic rocks (Apps and van de Kamp 1993).

H_2 is not expected to react chemically at significant rates under the conditions found in KLX06 and the KAS drill holes. However, H_2 is an important compound in several anaerobic microbial metabolisms in deep groundwater, such as methanogenesis by autotrophic methanogens and acetate production by acetogens (Kotelnikova and Pedersen 1997). There are also autotrophic iron- and sulphate-reducing bacteria that can use H_2 as an energy and electron source, concomitant with iron or sulphate reduction (Badziong and Thauer 1978). The main products from biological anaerobic reactions are methane and acetate. H_2 can be used by SRB with sulphide as the final reaction product and by bacteria that reduce ferric iron to ferrous iron. If oxygen is available, H_2 is oxidised by some bacteria to water. H_2 can thereby contribute to the reduction of oxygen via microbial processes. Biological reactions consequently remove H_2 from groundwater.

Carbon dioxide

Most of the world's carbon is contained in the geosphere, primarily in the form of carbonate rocks. Carbon dioxide is mainly contained in the oceans and to some extent in the atmosphere. The processes of formation of carbon dioxide and places of origin are a complex system, as it includes gas-water-mineral reactions, combustion of fossil and modern fuels, biological respiration of organic material and processes in the mantle. Inherent in this is that the places of origin are diverse as well.

Dissolved carbon dioxide, is important to natural mineralogical processes that occur in the geosphere. It dissolves readily to form carbonate and bicarbonate, which can take part in a large number of chemical processes, for example the well-known dissolution-precipitation reaction of fracture filling carbonates (calcite),

$$CO_2 + H_2O + CaCO_3\,(s) \leftrightarrow Ca^{2+} + 2HCO_3^-\,(aq) \qquad \text{Equation 2-7}$$

and the weathering of minerals in the rock matrix (here exemplified by the weathering reaction of Ca-feldspar, anorthite, into kaolinite):

$$CaAl_2Si_2O_8(s) + 2H_2CO_3(aq) + H_2O \rightarrow Al_2Si_2O_5(OH)_4(s) + 2HCO_3^- + Ca^{2+} \qquad \text{Equation 2-8}$$

Carbon dioxide is reduced to organic carbon by photosynthetic organisms and by chemolithotrophic bacteria. Photosynthesis is not a possible process in the geosphere. Chemolithotrophy includes methanogenesis and acetogenesis reducing carbon dioxide to methane and acetate, respectively.

Methane

Methane forming processes comprise thermogenic, hydrolysis and biogenic reaction routes. Thermogenic generation occurs in deep crustal layers, while hydrolysis processes such as serpentinisation of ferrous materials can occur in both the geosphere in shallow layers and in deep layers. The oxidation of ferrous material is coupled to the reduction of water to hydrogen, carbon dioxide to carbon or carbon to methane. Biological methane production takes place in anaerobic systems with hydrogen and carbon dioxide, within the temperature limits of life, i.e. < 113°C. Methane can also form by biological degradation of C-1 compounds such as methanol and formic acid and by degradation of acetate. Biological methane formation then is restricted to the geosphere and the shallow part of deep layers.

There are no chemical reactions that involve CH_4 in groundwater under the conditions in this investigation. However, microorganisms can readily oxidise CH_4 with O_2. Intruding O_2 to the geosphere will be reduced with CH_4 if present (Chi Fru 2008). Anaerobic CH_4 oxidation with sulphate can occur (Boetius et al. 2000, Lösekann et al. 2007).

3 Isotope fractionation processes

3.1 General

The various isotopes of an element have slightly different chemical and physical properties because of their mass differences. Under the proper circumstances, such differences can manifest themselves as a mass-dependent isotope fractionation effect. As a result of fractionation processes, unique isotopic compositions develop (ratios of heavy to light isotopes) that may be indicative of their source or the processes that formed them.

Two main types of phenomena produce isotopic fractionations: isotope exchange reactions and kinetic processes. Isotope exchange reactions can be viewed as a subset of kinetic isotope reactions where the reactants and products remain in contact in a closed, well-mixed system such that back reactions can occur and chemical equilibrium can be established. Under such circumstances, isotopic equilibrium can be also established. By measurement of stable isotopes $\delta^{2}H$, $\delta^{13}C$, $\delta^{34}S$ in organic and inorganic compounds, reactions such as those involved in the sulphate reduction processes can be determined.

3.2 Biological (microbial) fractionations

Biological processes are generally unidirectional and are excellent examples of kinetic isotope reactions. Microorganisms preferentially use the lighter isotopic species because of the lower energy "costs" associated with breaking the chemical bonds in these molecules, resulting in significant fractionations between the substrate (heavier) and the biologically mediated product (lighter). Kinetic isotopic fractionations of biologically-mediated processes vary in magnitude, depending on reaction rates, concentrations of products and reactants, environmental conditions, and – in the case of metabolic transformations – species of the organism.

The variability of the fractionations makes interpretation of isotopic data difficult, particularly for nitrogen and sulphur. The fractionations due to microbial activity are typically larger than the equivalent inorganic equilibrium reaction. The magnitude of the fractionation depends on the reaction pathway utilized (i.e. which is the rate-limiting step) and the relative energies of the chemical bonds severed and formed by the reaction. In general, slower reaction steps show greater isotopic fractionation than faster steps because the organism has time to be more selective (i.e. the organism saves internal energy by preferentially breaking light-isotope bonds).

If the substrate concentration is large enough and the isotopic composition of the reservoir undergoes small changes by the reaction it will represent an "open system model" (O'Leary 1981). In contrast, if there is a considerable change in isotopic composition of the residual reservoir substrate relative to the product then it can be defined by the so called Rayleigh equation as described in the section below (Mariotti et al. 1981).

3.3 The Rayleigh distillation equations

The Rayleigh distillation equation describes the isotope fractionation system very well in a closed system (the equations are so-named because the original equation was derived by Lord Rayleigh for the case of fractional distillation of mixed liquids). The principle relates to an exponential relation that describes the partitioning of isotopes between two reservoirs as one reservoir decreases in size. The equation is commonly referred to;

$$R = R_o\, f^{(a-1)}$$

Where R = ratio of the isotopes (e.g. $^{34}S/^{32}S$) in the reactant, R_o = initial ratio, f = fraction of initial substrate remaining, α = fractionation factor.

The equation can be used to describe an isotope fractionation process for sulphate reduction processes if, a) material is continuously removed from a mixed system containing molecules of two or more isotopic species (e.g. $^{34}S/^{32}S$), b) the fractionation accompanying the removal process is described by the fractionation factor α, and c) α does not change during the process. The enrichment factor of $\delta^{34}S$ relative to $\delta^{32}S$ for sulphate when it is progressively reduced to sulphide can be calculated using the method as described by Strebel et al. (1990).

3.4 Stable isotopes in the present project

Stable isotope signatures in groundwater and minerals were analysed in the present study and can be used to indicate conditions and processes in the groundwater or during mineral formation, such as organic influence (proportion of organic carbon), bacterial activity, salinity, groundwater origin, "closed or open systems" with regards to sulphate, mixing of different groundwater and temperature fluctuations (Laaksoharju et al. 2008, 2009, Tullborg et al. 2008, Wallin 2011).

3.4.1 Oxygen isotopes in groundwater and fracture minerals

Oxygen isotopes ($\delta^{18}O$) are considered to be a relatively conservative (non-reactive) in the deep groundwater as they do not change composition (interact) readily with the wall rock during low temperatures and can thus be used to trace the source and mixing proportion of different groundwater, as oppose to hydrothermal water-rock interaction which can result in significant "oxygen shift" between water and rock (Truesdell and Hulston 1980). Fractionation of $\delta^{18}O$ is temperature dependent, and cold water, such as glacial water commonly has low $\delta^{18}O$ signatures (c. –21‰ SMOW), which distinguishes it from modern meteoric water with higher $\delta^{18}O$ (~ –10‰) (Laaksoharju et al. 2009). Marine or brackish water; Baltic Seawater and ancient Littorina Sea water, has on the other hand relatively high $\delta^{18}O$, which makes components of these waters traceable in the deep groundwater (along with other marine tracers (Laaksoharju et al. 2009).

Oxygen isotopes in fracture-coating calcite has been analysed, both at Äspö and at Laxemar-Simpevarp (Drake and Tullborg 2009, Drake et al. 2009a, b, 2012, Tullborg et al. 1999, Wallin and Peterman 1999). Hydrothermal precipitates with very low $\delta^{18}O$ values dominates, but low temperature calcite of possible recent age (possibly Quaternary) have also been identified, by their $\delta^{18}O$ and $^{87}Sr/^{86}Sr$ signature being in the range expected from precipitates from the present groundwater (except in waters with a substantial glacial component (Drake et al. 2012). Although several groundwater types may have left precipitates in single fractures, reflecting fluctuation of the fresh/saline water interface (Tullborg et al. 1999), oxygen isotopes in calcite have been shown to match the general variation in groundwater $\delta^{18}O$ with depth, with meteoric precipitates near the surface and more saline-brackish precipitates at greater depth (Drake and Tullborg 2009, Drake et al. 2012). Near the surface, above the redox front, calcite is dissolved (Drake et al. 2009a). Regarding influence from microbial activity, depletions in $\delta^{18}O$ values of a few per mil in calcite as a consequence (bi-product) of SRB activity have been indicated from field observations elsewhere (Machel 1987) and in theoretical considerations (Sass et al. 1991). However, such depletions are only significant if the system is limited with respect to sulphate supply (i.e. closed system) (Machel et al. 1995).

In the current study, oxygen isotopes can give input about salinity and perhaps also temperature fluctuations and pH fluctuation. However, of main interest is to explore whether SRB activity has affected the $\delta^{18}O$ composition in the groundwater (i.e. whether there is systematic difference between section water and fracture water) and if calcite has $\delta^{18}O$ values in line with what is expected from the groundwater composition at the current borehole temperature (using literature fractionation data), or if the calcite shows anomalous $\delta^{18}O$ composition due to local SRB-related $\delta^{18}O$-modification.

3.4.2 Carbon isotopes in groundwater and fracture minerals

The carbon isotope values in the groundwater have been shown to vary with depth. At Laxemar for instance, the groundwater showed $\delta^{13}C$ values of –13 to –27‰ PDB (mainly –15 to –20‰ PDB; Pee Dee Belemnite (Laaksoharju et al. 2009)). The near surface waters showed $\delta^{13}C$ (–6 to –22‰ PDB).

The proposed simplified evolution of the $\delta^{13}C$ values in descending waters is as follows (modified after Laaksoharju et al. 2009); the near surface recharge waters with atmospheric $\delta^{13}C$ (> –8‰ PDB), increase their HCO_3^- concentration when entering the bedrock due to microbial degradation of organic material which decrease the $\delta^{13}C$ value of the water, as organic matter is depleted in $\delta^{13}C$ to different degree depending on origin (e.g. the most common plants; those utilizing the C_3 and C_4 methabolic pathways during carbon fixation have –34 to –23‰ and –23 to –6‰, respectively (Faure and Mensing 2005).

Fracture minerals analysed for $\delta^{13}C$ have been restricted to calcite at Äspö and Laxemar (see references above). The $\delta^{13}C$ in calcite can reveal organic or inorganic influence on the fluid during formation of the calcite, and measurements of an extensive data set of calcites have shown how this influence has varied with depth. Low organic influence is generally seen in the deepest waters, where the hydraulic conductivity is low and to which depth only small amounts of organic material (e.g. from soil) has descended (< 800 m) (Drake and Tullborg 2009, Drake et al. 2012). Above this depth, organic influence is common in the calcites, i.e. they have low $\delta^{13}C$, in many cases probably due to microbial oxidation of organic matter during SRB activity (or other microbial activity; Fe-reduction, Mn-reduction etc), as oppose to older inorganic hydrothermal precipitates which has higher $\delta^{13}C$ values. In some cases, both at Äspö and at Laxemar, the $\delta^{13}C$ values are so low (down to –70 to –100‰ in rare cases), that anaerobic oxidation of methane (i.e. biogenic based on the low $\delta^{13}C$) is the only possible explanation (cf. Drake et al. 2012). At Äspö, these observed extreme values of $\delta^{13}C$ are found closer to the ground surface than at Laxemar, where they cluster around –300 to –700 m (Drake and Tullborg 2009, Drake et al. 2012, Tullborg 2003). However, neither analyses for methane oxidisers (e.g. archaea) (Hallbeck and Pedersen 2008b), nor stable isotope composition of methane has been included in the investigations. Noteworthy is that extremely low $\delta^{13}C$ values have been observed in fracture calcites from Forsmark (Sandström and Tullborg 2009), whereas at Olikluoto, Finland, methanogenesis is more commonly traced (high $\delta^{13}C$ in calcite (Sahlstedt et al. 2010), but both of these sites show dominance of moderately depleted $\delta^{13}C$ values in calcite, indicative of degradation of organic matter during microbial activity in the fractures, in line with the common observation at Laxemar and Äspö for low-temperature calcite.

In the present study, $\delta^{13}C$, in similarity with the $\delta^{18}O$ aids to explore whether the "primary" composition of the water (the fracture water) has changed over time in the stagnant section (the section water). Large deviations between $\delta^{13}C$ in calcite and in the section water can indicate local microbial activity and related $\delta^{13}C$-modification in parts of the section. In order to investigate any influence from organic carbon from the instrumentation, $\delta^{13}C$ in calcite and dissolved carbonate was compared with a $\delta^{13}C$ measurement of the tape.

3.4.3 Sulphur isotopes in groundwater and fracture minerals

As stated in Wallin (2011), $\delta^{34}S$ isotopes can be used as a tool for monitoring groundwater changes, biological cycling and specifically sulphate reduction. On the other hand, in some systems $\delta^{34}S$ isotopes can contribute to the understanding of groundwater mixing, when used together with conservative parameters such as $\delta^{18}O$ and dissolved Cl^-, as shown at Äspö (Wallin 2011). $\delta^{34}S$ isotopes can be used to trace microbial activity because SRB fractionate the $\delta^{34}S$ composition during their metabolism in which ^{32}S is favoured, leaving a ^{34}S-enriched fluid behind (Kaplan and Rittenberg 1964). Fractionation during bacterial sulphate reduction can vary considerably depending on the species involved (Detmers et al. 2001) but also be due to other factors such as sulphate supply, reduction rate and temperature (Canfield 2001b, Faure and Mensing 2005, Hoefs 2004).

Sulphur isotope analysis in the groundwater has mainly been carried out on SO_4^{2-}, both during the site investigations at Laxemar-Simpevarp (Kalinowski 2009, Laakosharju et al. 2009) and at Äspö, summarized in Wallin (2011). Groundwater in the Laxemar-Simpevarp area has elevated $\delta^{34}S$ values in the upper hundreds of meters and lower values at greater depth. At Laxemar the values overall was +9 to +37‰ (Gimeno et al. 2009). Values higher than marine signature (~ 21‰) were found in groundwater with chloride contents < 6,500 mg/L and at depths down to about –400 m. The highest $\delta^{34}S$ values correspond to samples of low dissolved sulphate concentrations, and can thereby be interpreted as being produced *in situ* by SRB (Laakosharju et al. 2009), dominantly in closed conditions. Below about 350 m a switch towards lower $\delta^{34}S$ values, generally with decreasing $\delta^{34}S$ with increasing sulphate content. A lower SRB activity (if any) and gypsum dissolution may collectively

be responsible for the lower $\delta^{34}S$ values in the deeper groundwaters. At Äspö, the $\delta^{34}S$ isotope signatures of the dissolved sulphate suggest multiple sources for the sulphur, although two sulphur sources are dominant, namely, Baltic Sea water ($\delta^{34}S$: ~ +19‰ to +20‰) and Deep Saline groundwater ($\delta^{34}S$: ~ +10‰) (Wallin 2011). Early sampling from Äspö before tunnel construction revealed $\delta^{34}S$ signatures that decreased gradually with depth, in similarity with observations at Laxemar. In contrast to these two sulphur sources and $\delta^{34}S$ values discussed above, values of +19 to +28‰ found at depths of approximately 100–400 m are significantly higher and indicative of bacterial sulphate reduction.

During fracture mineral investigations, pyrite has been analysed for its $\delta^{34}S$ composition using conventional technique (~ 5 mg bulk samples), and has shown values indicative of bacterial sulphate reduction, in open (low $\delta^{34}S$) and sulphate-limited systems (strong enrichment of ^{34}S), (Drake and Tullborg 2009, Pedersen et al. 1997). However, no detailed expensive comparison between co-precipitated calcite and groundwater were carried out from these pyrites and it therefore remains unresolved whether they are potential recent precipitates or represent Paleozoic or older precipitation. In a recent study on Laxemar, a detailed approach involving multiple *in situ* SIMS analyses (Secondary Ion Mass Spectrometer) of $\delta^{34}S$ within individual pyrite crystals from fractures where calcite with stable isotope composition similar to that of the present groundwater existed were performed (Drake et al. 2013). In this study, the evolution of $\delta^{34}S$ in each analysed crystal, and consequently each fracture, could be explored and compared with the groundwater composition. It was shown in the Laxemar study that *in situ* $\delta^{34}S$ analyses of fracture pyrite, co-precipitated with calcite, give detailed information on the sulphur system and on the activity of SRB during natural conditions in the bedrock. The main findings were:

- $\delta^{34}S_{pyr}$ showed huge variations across individual crystals (up to –32 to +73‰) and extreme minimum (–50‰) and maximum (+91‰) values indicative of SRB activity.
- Increase in $\delta^{34}S_{pyr}$ values across individual crystals was a common feature for pyrite residing in low-flow fractures, revealing that sulphate has been limited (up to > 90% consumed) and SRB have caused isotopic fractionation in a closed system that has undergone Rayleigh distillation.
- Current-day groundwater with $\delta^{34}S_{SO4}$ values up to +37‰ cannot explain the highest $\delta^{34}S_{pyr}$ values of +40‰ to +91‰. These pyrites probably reflect conditions developed in delimited near stagnant parts of the fracture system, whereas the groundwater data are dominantly represented by more sulphate-rich waters from highly flowing parts of the structures, in which open system often prevails as indicated by constant $\delta^{34}S_{pyr}$ during crystal growth.
- Mineral-groundwater comparisons ($\delta^{34}S_{pyr}$–$\delta^{34}S_{SO4}$ and $\delta^{18}O_{calcite}$–$\delta^{18}O_{groundwater}$) indicate that precipitation has occurred during conditions similar to the present and that precipitation from the current groundwater cannot be ruled out.

In the current study, the same *in situ* SIMS technique as in the study mentioned above (Drake et al. 2013) is used. This means that the $\delta^{34}S$ evolution within single crystals can be explored (and thus the evolution of the local groundwater composition at the site of pyrite precipitation). Furthermore, the SIMS technique utilizes a very small spot size and thus very small samples can be used, which is crucial because the pyrite precipitates in the current study are generally very fine-grained, and bulk samples were very much too small to allow conventional analysis. This detailed knowledge of the pyrite $\delta^{34}S$ composition provides valuable input to the understanding of the SRB activity and S^{2-} production in the borehole sections, and completes the groundwater data. The groundwater data can in itself give valuable information about SRB activity in the fracture water and in the section water, as well as about variation in fractionation of sulphur isotopes because both $\delta^{34}S_{sulphate}$ and $\delta^{34}S_{sulphide}$ was measured for the fracture water and for the section water. However, the groundwater data give a bulk value for the whole water volume sampled and do not provide any time constraints. Therefore, the detailed pyrite analysis provides valuable input regarding the evolution of the sulphur isotopes with time at very local spots ("micro environments") in the borehole sections.

4 Investigated boreholes

4.1 Site locations in Äspö HRL

The investigated boreholes are located in the Äspö HRL at –410 m (KA3110A and K3105A) and –425 m (KA3385A). The depths are all meters below sea level (m.b.s.l).The locations are shown in Figure 4-1.

The two boreholes that were initially chosen for the study; KA3110A and KA3385A, were selected due to their different sulphide concentrations (12 mg L^{-1} and 0.1 mg L^{-1}) and diverging chemical water composition (see Section 4.2). These values were retrieved from sampling of section water 2009-09-21 (data stored in Sicada) and sampled after discharge of only 1 L of water in each borehole section (KA3110A:1, KA3385A:1).

In addition the water volumes of the sections were of a suitable size (about 14.5 and 4.5 L respectively for KA3110A and KA3385A). Larger volumes would make it more difficult to get an effective mixing of the water before sampling. In the activity involving investigation of the borehole instrumentation, boreholes KA3105A and KA3385A were investigated. Borehole KA3110A was excluded from the investigation since the instrumentation had been accidentally cemented during previous injection activities in Äspö HRL. Pressure responses indicate that at least section 1 of this borehole was affected by the grouting (see Section 4.3).

4.2 Hydrogeochemistry of investigated fractures

The evolution of the groundwater chemistry in the boreholes KA3110A and KA3385A has been obtained from the groundwater samples taken in connection with the groundwater monitoring at Äspö, which were analysed for major chemistry and environmental isotopes. For these two boreholes the time span covered reaches from 1995 to 2009 with almost annual sampling. Close to KA3110A, a borehole named KA3105A is situated; from it only a few analyses are available but a similar evolution to KA3110A is indicated and therefore they probably are connected to the same fracture system. The elevation is –415 to –420 m whereas borehole KA3385A represents greater depth (elevation about –450 m).

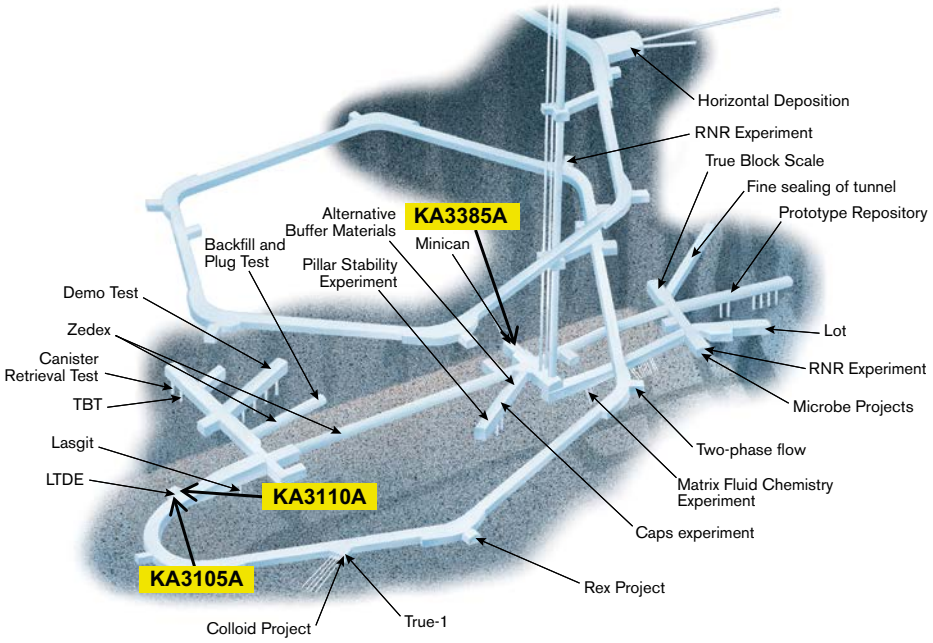

Figure 4-1. *Äspö HRL, locations of experimental sites and investigated boreholes in the present investigation*

Groundwater samples from KA3385A represent a relatively stable composition of major ions during the entire sampling period. The groundwater can be described as Na-Ca (Mg) Cl-SO_4 in type with a Cl content around 7,000 mg L^{-1} and a generally very low HCO_3 content (≤ 20 mg L^{-1}), cf. Table 4-1. Using the classification by Mathurin et al. (2012) this is a water of mixed origin with a portion of marine (probably Littorina water) mixed with deep saline and glacial melt water.

The water in KA3110A (and KA3105A) in contrast has changed composition significantly during the operational phase of the Äspö tunnel. The evolution can be generally described as an exchange of Littorina type groundwater (mixture of Littorina Sea water and glacial melt water) which with time has largely been replaced by present day Baltic Sea water. The measured tritium values around 10 TU indicate that the portion of modern water during the recent years is large. This indicates that the borehole is connected to one of the vertical to sub-vertical fracture zones which introduces Baltic Sea water to great depth in the South East part of the tunnel system at Äspö (a result of draw down). This phenomenon can also be seen in other boreholes, cf. Figure 4-2.

Table 4-1. Water composition in fractures of boreholes KA3110A (section 1) and KA3385A (section 1), after discharge of at least 10 section volumes.

Parameter	KA3110A	KA3385A
Section no/ secup–seclow (m)	Section 1/ 20.05–26.83	Section 1/ 32.05–34.18
pH	7.4	7.6
Conductivity (mS m^{-1})	1,000	2,100
Cl^- (mg L^{-1})	3,100	7,600
HCO_3^- (mg L^{-1})	190	20
SO_4^{2-} (mg L^{-1})	330	420
HS^- (mg L^{-1})	0.2	0.02
Fe^{2+} (mg L^{-1})	1.3	0.2
TOC (mg L^{-1})	6.4	4.3
SRB* (cells mL^{-1})	800	13

* Sulphate reducing bacteria.

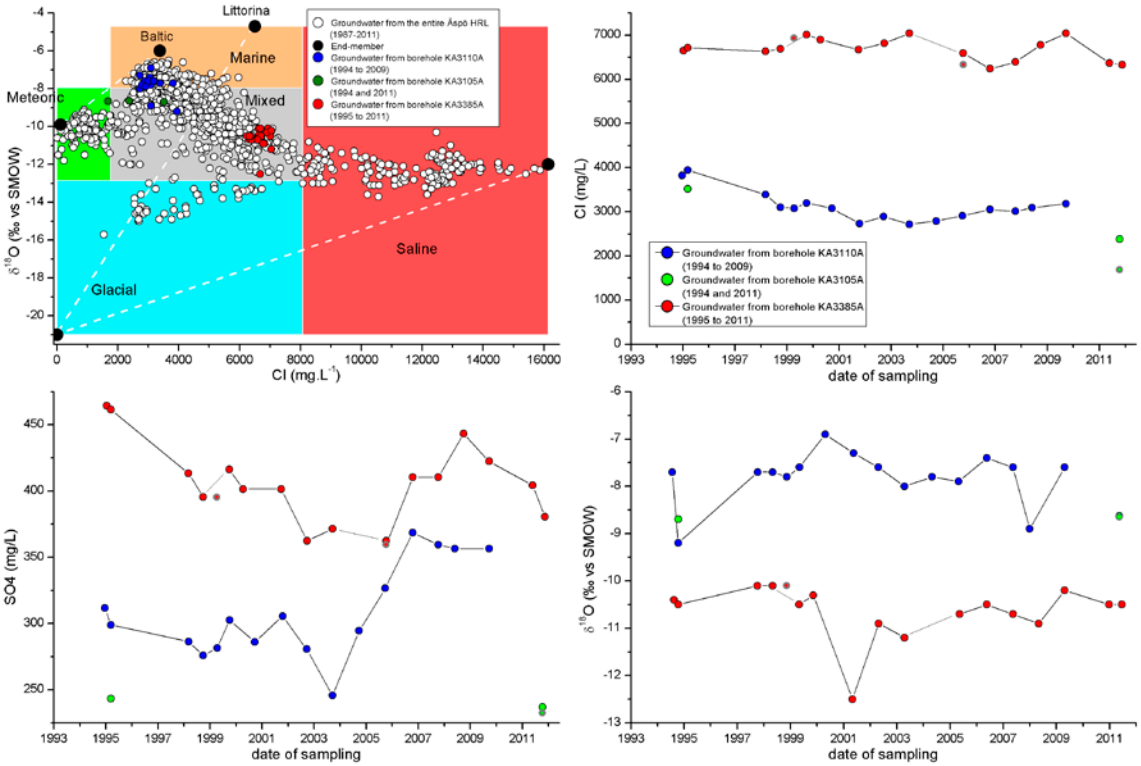

Figure 4-2. *Evolution of Cl, SO_4, and $\delta^{18}O$ with time for boreholes KA3110A, KA3105A and KA3385A. Figure from Mathurin et al. (2012).*

Boreholes KA3110A and KA3385A each holds two isolated sections. The samples sections correspond to the inner sections (section 1) in both boreholes. A complete set of analytical data is given in Appendix F.

4.3 Hydrogeology of investigated borehole sections

To determine the natural groundwater flow in the fractures intersecting the investigated sections in KA3110A and KA3385A, groundwater flow measurements using the dilution technique was performed. The principle of a dilution test is to inject a tracer solution into a borehole section and then monitor the decrease in tracer concentration over time. The water was circulated and during the time it takes to exchange one section volume the tracer was injected with a flow rate corresponding to 1/100 of the circulation flow rate. Continuous sampling was carried out during circulation by extracting a constant small flow (constant leak) which was collected by a fractional sampler and analysed. Flow rates were calculated from the decrease in tracer concentration versus time through dilution with natural unlabelled groundwater, c.f. Gustafsson (2002). A more detailed description of the performance and results is given in Appendix G. The assessment of the natural groundwater flow through a section is important for understanding the transport of solutes and the turnover time for water in the section. For KA3105A there are no available data for the groundwater flow through the sections.

It has been suggested in previous investigations (Rosdahl et al. 2011, Tullborg et al. 2010a, b) that the location and hydraulic conductivities of water-bearing fractures may influence the observed sulphide concentration in water samples. Depending on the array in the boreholes section, very large volumes could be needed to be discharged in order to obtain a representative fracture water sample. Information about number and locations of flow anomalies is scarce, because flow logging and investigation using borehole image processing system (BIPS) was not carried out (only for KA3385A in 1995, see below). Flow measurements were however carried out in KA3385A (section 1), which showed 2×10^{-8} m^2/s (unknown number of anomalies) and in KA3110A (section 1), in which it was estimated to 5×10^{-7} m^2/s. Due to this lack of detailed information about flow anomalies in the section, the volume needed to be discharged before sampling of a representative fracture water was not possible to calculate. Therefore, there is a possibility that the samples regarded as pure fracture water may include a small portion of section water, similarly to what has been observed in monitoring sections in surface drilled boreholes from the site investigations (Nilsson et al. 2010, Tullborg et al. 2010a). However, it should be noted that the tunnel drilled boreholes have a favourable pressure gradient, which is towards the tunnel, and therefore discharge of the entire section volume is more likely.

The dilution test performed in KA3385A indicated a groundwater flow of 40 mL L^{-1} and a transmissivity of 2×10^{-8} m^2 s^{-1}. A previous flow logging investigation in KA3385A was performed in 1995. The logging showed an area with higher groundwater flow into the borehole at about 32,5–33,3 meters borehole length, which is in the middle of section 1 (32.05–34.18 m).

During circulation of KA3110A:1, unexpected pressure responses were found. The results from groundwater flow measurement in KA3110A:1, capacity test as well as earlier sampling, are probably significantly affected by some unfavourable condition in the borehole section and should not be regarded as representative for undisturbed conditions. A likely explanation is that grouting has penetrated the section in between the outlets of the inner and outer circulation tubes. The explanation is strengthened by that the instrumentation was not possible to dismantle (for details see Chapter 3 in Appendix G), the results of the hydraulic tests in KA3110A are therefore questionable.

4.4 Activities in borehole sections

Boreholes KA3110A, KA3105A and KA3385A are all core-drilled boreholes with diameter 56 mm, drilled in 1994–1995. An overview of the investigated sections in this study, lengths and the performed field activities are given in Table 4-2 and sampling occasions are shown in a timeline in Figure 4-3. Schematic drawings of the boreholes, sections and instrumentation features are compiled in Appendices A–C.

Table 4-2. Investigated borehole sections, section lengths and performed activities.

		Performed activity			
Borehole: Section no	**Secup–Seclow (m)/ Elevation (m.b.s.l.)**	**Circulation experiment**	**Dilution test**	**Sampling of borehole instrumentation**	**Water sampling**
KA3110A:1	20.05–26.83 415.58–416.24	X	X		X
KA3110A:2	6.55–19.05 414.29–415.48				X
KA3385A:1	32.05–34.18 448.27–448.42	X	X	X	X
KA3385A:2	6.05–31.05 446.46–448.20			X	X
KA3105A:1	53.01–68.95 418.06–419.50			X	X
KA3105A:2	25.51–52.01 415.75–417.97			X	X
KA3105A:3	22.51–24.51 415.51–415.67			X	X
KA3105A:4	17.01–19.51 415.26–415.06			X	X
KA3105A:5	6.51–16.01 414.98–414.18			X	X

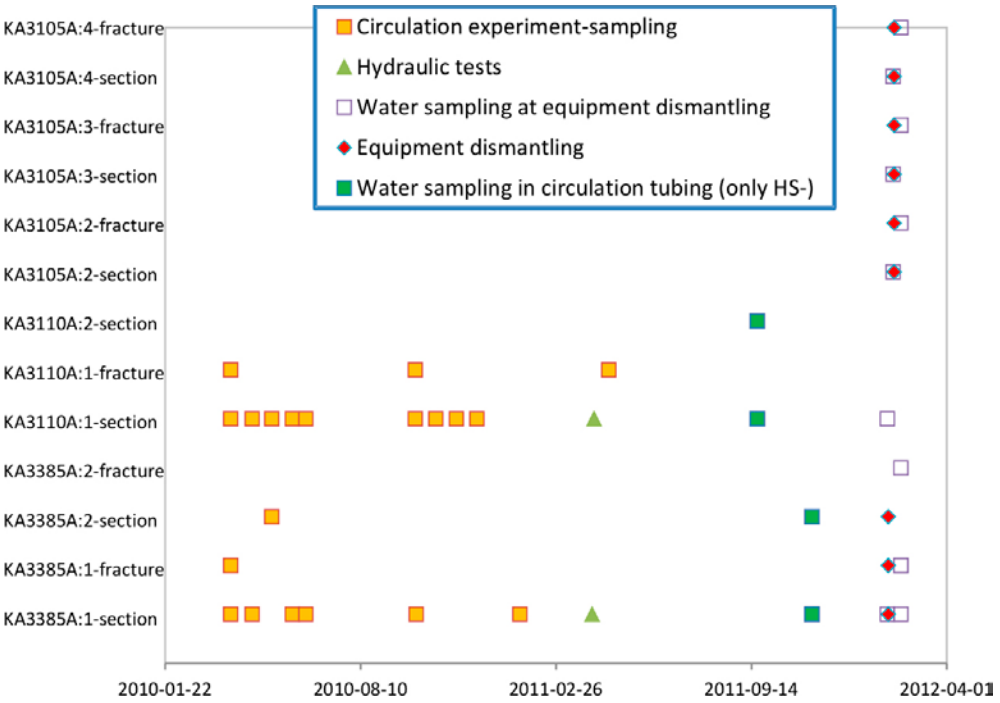

Figure 4-3. *Timeline for the borehole investigations.*

5 Circulation system for *in situ* investigation

5.1 Experimental setup and analyses

Observations from a previous investigation of sulphide concentration in a core-drilled borehole at Laxemar and results from hydrochemical monitoring in several boreholes in Forsmark suggest that the sulphide concentration decreases as water is discharged from a section (Hallbeck and Pedersen 2008a, Rosdahl et al. 2011). In periods with stagnant water, between discharging of water, the sulphide builds up in concentration. The decrease in sulphide concentration with discharged water volume is reproducible when conducting the pumping under similar conditions (pumping rate, time etc) (Tullborg et al. 2010a, b, Rosdahl et al. 2011). The experiments have shown that sulphide build up in concentration in a matter of days or a couple of weeks.

The conceptual idea of the circulation experiment was to follow the build-up of sulphide in a borehole section while analysing time-series of components that are related to sulphide production. An important aspect was to compare two boreholes in which the sulphide concentration in stagnant borehole sections had different concentrations; one in which the sulphide concentration (sampled after 1L of discharge) had increased to 12 mg/L since last sampling (1 year earlier), and one with 0.1 mg/L. Äspö HRL was a suitable place for conducting the experiment, since the location underground facilitates sampling of dissolved gas and in addition the installed equipment does not include water standpipes. When water is discharged from a section an equal amount of water is added from the fractures, as a consequence water in a sample consist of a mixture of section and fracture water in which the proportion of fracture water increase as more water is discharged. Water was sampled and analysed from the fractures of each section in order to be able to compare with the analyses from the time-series of section water.

A circulation system for the study of sulphide production processes in a packed-off borehole section (circulation section) was assembled (Figure 5-1). The section water is circulated under maintained pressure (about 30 bars in KA3110A and 25 bars in KA3385A) using a circulation pump located outside the borehole. The difference in pressure between the in- and outlet of the circulation pump was about 8 bars in order to be able to circulate the water, however, the pressure difference in the borehole section itself was only about 1 or 2 bars as compared to the absolute pressure of the section of 25 or 30 bars. Tubing at the two ends of the section enables circulation/mixing of water in the section before small volumes of water samples are collected and analysed as time-series. The direction of the groundwater circulation was by drawing water from the outbound tubing at the top of the section and returning it at the bottom at the section through the inbound tubing.

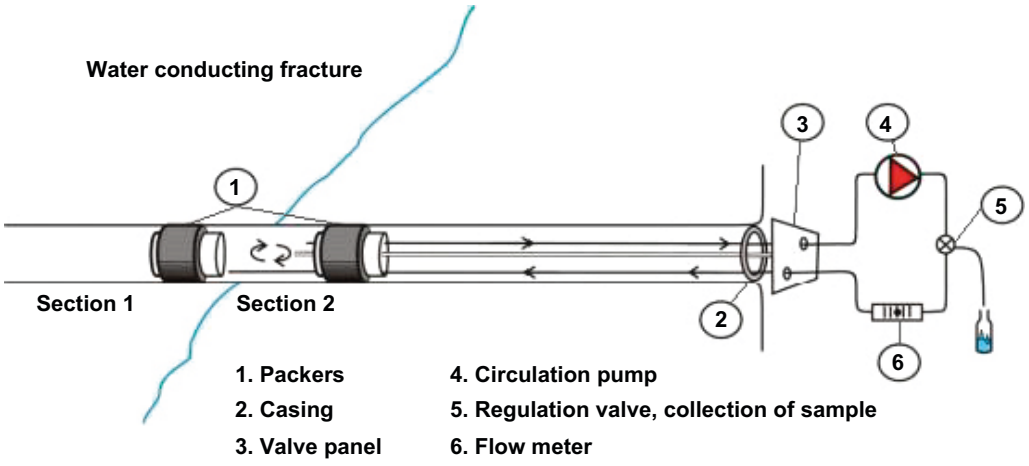

Figure 5-1. *Schematic experimental setup of circulation system for in situ investigations in borehole sections. The pumping equipment is located outside the borehole. In the present study section 1 (the inner section) was investigated for boreholes KA3110A and KA3385A.*

The experiment was divided into two parts with partly different analytical programmes since the volume of water between the packers is limited. The analytical programmes are given in Appendices D, E. The first part focused on sulphide and related components and included sulphide, sulphate and other dissolved chemical compounds, microorganisms (sulphate reducing bacteria, iron reducing bacteria, acetogenic bacteria) and dissolved gases. The second part focused on analyses of stable isotopes to determine reaction pathways and origin of reactants and products; $\delta^{34}S$ in dissolved sulphide and sulphate dissolved inorganic carbon (hydro carbonate) and dissolved organic carbon and stable isotopes in gases ($\delta^{13}C$ in CH_4 and CO_2 and $\delta^{2}H$ in CH_4 and H_2).

5.2 Sampling procedure

The sampling procedures in boreholes KA3110A and KA3385A are described in Appendices D, E.

One sampling occasion corresponds to several analyses having one and the same SKB number. A sampling occasion consisted of several steps as described below;

1. The tubing to the sections contains groundwater (inbound and outbound tubing). Before sampling, the volume of water in the tubing was discharged so that the sample corresponded to section water (and a minor proportion of fracture water). This sample is denoted “Section water”.
2. Sampling and analysis of HS^- and Fe (II) for every Litre of circulated water.
3. A complete set of components were analysed after circulation of one section volume. The sample is denoted “Section water, mixed” and represents more or less the groundwater in the borehole section. Each sampling campaign was made up of successive discharge with increasing water volumes. With each sampling, the proportion of fracture water in the sample will be increased by the volume discharged/section volume.
4. After discharge of 10 section volumes, it was assumed (could not be calculated due to lack of knowledge about position and number of flow anomalies) that when collecting a sample, the water would represent the fracture water. This sample is denoted “Fracture water”.

Step 1 to 3 was performed at every sampling occasion, while step 4 was only performed after collecting an initial sample of section water. Sampling occasions and discharged volumes are listed in Appendix F.

5.3 Deviations from the activity plans

The circulation experiments in boreholes KA3110A and KA3385A were associated with several unexpected incidents and consequently deviations from the activity plan;

1. Mix-up of tubing in KA3385A

The tubing for borehole KA3385A had been rearranged before the beginning of this activity; it was discovered from pressure measurements (HMS system) during circulation and sampling. Unfortunately, during the first three sampling occasions (2010-03-30, 2010-04-21 and 2010-05-11), water was drawn from section 1 and returned to section 2, resulting in discharging of water from section 1 instead of circulating the water in section 1 as planned. The following sampling sessions were performed by circulation the water with the correct inner and outer circulation tubing to section 1.

2. Grouting of tubing in KA3110A

The dilution tests revealed that previous injection tests performed in the Äspö HRL had an effect on the circulation tubing in KA3110A. The registered pressures in the section and a nearby section suggest that the connection between the inner and outer circulation tubing has been cut off due to previous grouting injection in section 1. During circulation water was flowing from the outer tubing and returned to the inner tubing. However, due to the grouting, water was not circulated as planned

but discharged from the section. The water that was sampled from the inner tubing was a mixture of section water and fracture water and the proportion of fracture water increased as water was sampled. This situation persisted during the entire experiment.

3. Contamination with ethanol in KA3110A and KA3385A

Analysed samples from KA3110A and KA3385A for DOC and TOC showed high and varying concentrations (up to several hundreds of mg L^{-1} DOC). In addition the concentrations of acetate were elevated (up to 115 mg L^{-1}). Normally in deep groundwater the DOC concentrations is a few mg L^{-1} as well as the acetate. In order to find the source distilled water was filtrated through the filters used and analysed. Any leakage of organic carbon from the sample container itself was also investigated. The results showed no elevated concentrations of organic carbon from the sample preparation and storage of samples. Finally, the pumping system (pump, tubing and pressure gauge) was investigated and it was concluded that he contamination of organic carbon in the samples was a result of traces of ethanol from the inside of the pumping system. Ethanol and distilled water was used during the cleaning procedure of the inside of the pumping system prior to connecting it to the tubing of the borehole section. Ethanol was excluded from the cleaning procedure in October 2010 (from the sampling campaign 2010-10-26 and forward). However, the effect of ethanol persisted for a longer time as can be seen from the elevated numbers of SRB, sulphide and DOC (Section 5.4 and Appendix F).

5.4 Results from *in situ* circulation experiments

The data obtained from the circulation experiments must be interpreted with caution due to several unexpected incidents during the performance of the activity as described in Section 5.3. The incidents have affected both the analyses and the concept of the experiment, which was to achieve as small discharge of fracture water as possible during sampling and analysis of chemical and biological components during the production of sulphide in a section.

5.4.1 Microbiological analyses

Results from samples collected for microbiological analyses, organic carbon (dissolved (DOC) and total (TOC)), acetate and sulphide are shown in Table 5-1 and Table 5-2. All samples, except number S1:3 were taken after the volume of the tubing from the section was discharged and one section volume circulated. Circulation was performed twice before sampling for sample S1:2 and once for all other samples. Sample S1:3 was collected after discharging a volume corresponding to 10 times the section volume, which was about 145 L for borehole KA3110A and about 45 L for borehole KA3385A. Samples for microbiological analyses were taken with sterile and anoxic syringes and needles and transferred to anaerobic and sterile flasks sealed with rubber stoppers and aluminium crimps. Growth media and analyses were described in Hallbeck and Pedersen (2008a) and in Rosdahl et al. (2011).

Total number of cells (TNC) in water from borehole KA3110A was determined at eight occasions in the first sampling session (series 1) and at two occasions in sampling series 2. The TNC ranged from 1.7×10^4 mL^{-1} in fracture water in sample S1:3 at start of Sulphide 1, to 2.7×10^5 mL^{-1} in samples corresponding to mixed section water, collected in May 2010 (S1:7). TNC in groundwater from borehole KA3385A was determined eight times in Sulphide 1 and once in Sulphide 2. The TNC in samples from the borehole KA3385A, varied with the lowest number in the sample from April 2010 (S1:5) with 5.2×10^3 mL^{-1} and the highest in the sample from January 2011 (S2:2), with 1.5×10^6 mL^{-1}. The variation in TNC for the two boreholes, KA3110A and KA3385A are shown in Table 5-1, where all data from the microbial analyses are compiled. The TNC in KA3110A varied 15 times between the highest and the lowest value. In KA3110A, each sampling corresponded to a discharge of water and hence diluting section water with fracture water each time a sample was collected. The variation in KA3385A was 290 times, which is a significant difference. It has to be remembered that the tubing in KA3385A was erroneously labelled and that the wrong tubes were used until the sampling in 2010-06-01, when the correct circulation path was used. The mix up of tubing meant that water was discharged from section 1 and returned to section 2 instead of circulating the water in section 1, cf. Figure 5-1.

Table 5-1. Series 1 and 2. Borehole KA3110A, TNC, SRB, acetate, TOC and DOC.

Sample/ SKB no	Date	TNC (mL^{-1})	MPN SRB (l and u)* (mL^{-1})	%SRB of TNC	TOC ($mg\ L^{-1}$)	DOC ($mg\ L^{-1}$)	Acetate ($mg\ L^{-1}$)	Sample description
Sampling series 1								
S1:2/20136	2010-03-30	64,000 ± SD 11,000	11,000 (4,000–30,000)	17	29	20	5	Section water, mixture
S1:3/20137	2010-03-30	17,000 ± SD 2,100	800 (300–2,500)	0.05	6	8	3	Fracture water
S1:5/20154	2010-04-21	160,000 ± SD 8,300	8,000 (3,000–25,000)	0.05	78	148	5	Section water mixed
S1:7/20180	2010-05-11	270,000 ± SD 72,000	30,000 (10,000–120,000)	11	38	58	39	Section water mixed
S1:9/20248	2010-06-01	260,000 ± SD 24,000	14,000 (6,000–36,000)	0.05	13	8	17	Section water mixed
S1:10/20216	2010-06-15	1100,000 ± SD 260,000	110,000 (40,000 –300,000)	10	–	–	–	After tube
S1:11/20262	2010-06-15	150,000 ± SD 54,000	35,000 (16,000–82,000)	23	84	16	7	Section water mixed
Sampling series 2								
S1:20/20357	2010-10-05	200,000 ± SD 15,000	3,000 (1,000–12,000)	0.02	112	112	3	Section water, mixture
S2:2/20359	2010-10-05	110,000 ± SD 23,000	3,000 (1,000–12,000)	0.03	15	15	3	Fracture
S2:15/20372	2010-12-07	130,000 ± SD 1,400	2,300 (900–8,600)	0.02	5	6	2	Section water mixed

* Lower and upper limits of 95% confidence interval.

Table 5-2. Series 1 and 2. Borehole KA3385A, TNC, SRB, acetate, TOC and DOC.

Sample/ SKB nr	Date	TNC (mL^{-1})	MPN SRB (lower and upper limit)* (mL^{-1})	%SRB of TNC	TOC ($mg\ L^{-1}$)	DOC ($mg\ L^{-1}$)	Acetate ($mg\ L^{-1}$)	Sample description
S1:2/20134	2010-03-30	23,000 ± SD 5,000	50 (20–150)	0.2	23	38	2	Section water mixed
S1:3/20135	2010-03-30	47,000 ± SD 2,100	13 (5–39)	0.3	4	5	1	Fracture water
S1:5/20153	2010-04-21	5,200 ± SD 2,000	110 (40–300)	2	–	–	4	Section water mixed, (ethanol)
S1:7/20179	2010-05-11	6,100 ± SD 2,200	1,300 (500–3,900)	21	9	6	6	Section water mixed (ethanol)
S1:9/20247	2010-06-01	710,000 ± SD 64,000	160,000 (60,000–130,000)	22	127	28	10	Section water mixed, correct flow from here (ethanol)
S1:10/20383	2010-06-15	350,000 ± SD 59,000	7,000 (3,000–21,000)	2	127	28	–	After tube (ethanol)
S1:11/20263	2010-06-15	330,000 ± SD 20,000	1,700 (700–4,800)	0.5	415	222	25	Section water mixed (ethanol)
S1:15/20346	2010-10-05	330,000 ± SD 54,000	300,000 (100,000–1200,000)	91	562	564	74	Section water mixed (ethanol)
S2:2/20573	2011-01-20	1500,000 ± SD 840,000	>160,000	_	14.1	14.5	27	Section water mixed

* Lower and upper limits of 95% confidence interval.

5.4.2 Sulphate reducing bacteria

The number of sulphate-reducing bacteria (SRB) determined with the MPN method in samples from the borehole KA3110A, varied from 800 mL^{-1} in the fracture water sample S1:3 to 3.5×10^4 mL^{-1} in sample S1:11. In samples from borehole KA3385A the MPN of SRB varied from 13 mL^{-1} in the fracture water S1:3 sampled in March 2010 and up to 3.0×10^5 mL^{-1} in the S2:4 sampled in

January 2011. In Table 5-1, the results from MPN of SRB from the sampling occasions are compiled. The number of SRB, in fracture water, sample S1:3, was 800 SRB mL^{-1}, with lower limit 300 mL^{-1} and upper limit 2,500 mL^{-1}, in KA3110A and 13 mL^{-1} in KA3385A. This sample was taken after 10 section volumes of 14.5 L, 145 L in KA3110A and 10 section volumes of 5 L, 50 L, in KA3385A, were discharged and the water in the section was then circulated once before sampling. A second sample of fracture water was sampled from borehole KA3110A in October 2010 and the number of SRB was then 3,000 mL^{-1} with lower limit of 1,000 mL^{-1} and upper limit of 12,000 mL^{-1}. These numbers represent the number of SRB in the fracture water supplying the sampled section in borehole KA3110A.

In borehole KA3110A, SRB in the section water was one to 1.5 times higher than in fracture water both with high and low concentration of organic material in the water, see Figure 5-2. Figure 5-2 also shows a shift to higher numbers of SRB and TNC in samples from borehole KA3385A when the water was circulated in the intended manner (and not discharged), from sample S1:9 (2010-06-01) and forward.

After discharging water from the section at the end of the experiment, the number of SRB in groundwater from KA3110A went back to the original number after that the incidental addition of ethanol had increased the number of SRB in the section. The number of SRB in section water from KA3385A increased to around 10^5 cells mL^{-1} during the experiment and since water was not discharged from the section after the circulation experiment in 2010-10-06, it had not decreased at the last sampling occasion in January 2011. The number of SRB in fracture water in KA3385A at that time (January 2011) is unknown since no such sample was taken.

5.4.3 Acetogenic bacteria (AA)

The number of acetogenic bacteria (AA) in water from KA3110A varied from below 10 mL^{-1} up to 280 mL^{-1} during the time of the project. The highest number was determined in June 2010 and the lowest number was obtained in the samples from October 2010. In the fracture water sampled in March there was 9 mL^{-1}. The number of AA in KA3385A was below 10 $mL^{-1}$with an increase in the sample from 15th of June in 2010, to 130 mL^{-1}. The number of AA in fracture water of KA3385A was 2.3 mL^{-1}.

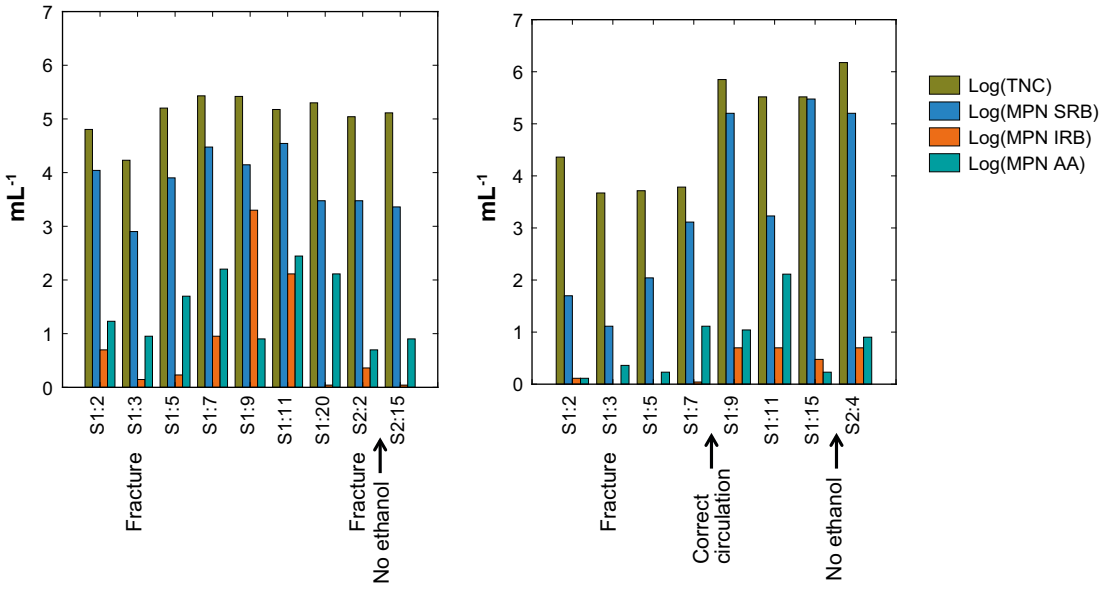

Figure 5-2. *Total numbers of cells (TNC), the most probable number of sulphate-reducing bacteria, iron-reducing bacteria and autotrophic acetogens, MPN SRB, MPN IRB, MPN AA, respectively, in the water from boreholes KA3110A (left) and KA3385A (right) during Sulphide 1 and Sulphide 2.*

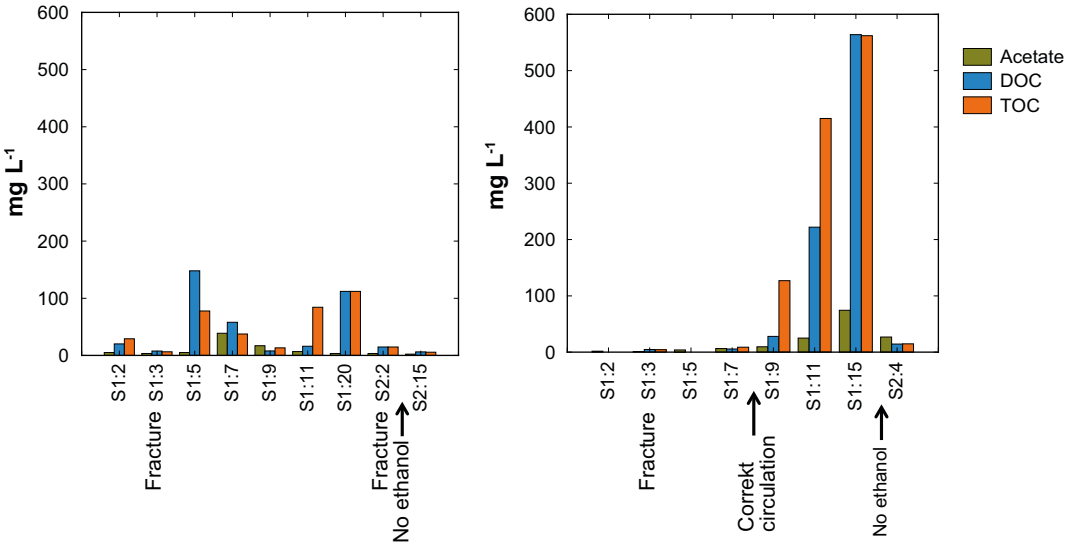

Figure 5-3. *The concentrations of acetate, DOC and TOC in the water from boreholes KA3110A (left) and KA3385A (right) during Sulphide 1 and Sulphide 2.*

5.4.4 Iron reducing bacteria (IRB)

In water from borehole KA3110A the number of IRB were below 10 mL^{-1}, except in samples from 1st and 15th of June 2010 when the IRB increased to 2,000 mL^{-1} and 130 mL^{-1}, respectively. The number of IRB in water from borehole KA3385A was below10 mL^{-1}, except in samples from 1st and 15th of June 2010 when the IRB increased to 130 mL^{-1} and 11 mL^{-1}, respectively.

5.4.5 Sulphide and sulphate

The concentration of sulphate in groundwater from the sampled boreholes KA3110A and KA3385 differ but the difference is minor. The concentration in KA3110A varied during Sulphide 1 and Sulphide 2 from 285 mg L^{-1} in sample S1:9 to 358 mg L^{-1} in sample S1:20. The sulphate concentration in groundwater from borehole KA3385A varied between 357 mg L^{-1} to 417 mg L^{-1}. A comparison between the sulphate concentration data from KA3110A and KA3385A is found in Figure 5-5.

The sulphide concentrations in groundwater samples from KA3110A and KA3385A collected during Sulphide 1 and Sulphide 2 are shown in Figure 5-4 and in Figures 5-7 and 5-8. The sulphide concentration in groundwater from KA3385A did not increase until sample S1:9 (2010-06-01), which was when circulation of water during sampling was made, instead of discharge of water. In Figure 5-4, the sulphide corresponds to concentrations obtained after circulating (or discharging) one section volume (14.5 L in KA3110A and 4.5 L in KA3385A). Figures 5-7 and 5-8 correspond to analyses of sulphide during circulation of the section volumes. Samples were collected and analysed for sulphide and iron (II) after discharge of water in tubing and after every circulated Litre of water. For KA3110A and KA3385A (up until 2010-06-01), the circulation corresponded to a discharge of water from the sections. The sulphide concentration in water from KA3110A varied from below detection limit in fracture water from March 2010 and up to 26 mg L^{-1}in sample S1:9 (section water) from June 2010. After discharge of water from the tubing 2010-05-11, the sulphide concentration was 106 mg L^{-1}. The highest sulphide concentration measured in water from KA3385A was 3.6 mg L^{-1} after circulation of a section volume, while after only discharging water from the tubing the concentration was 27 mg L^{-1} (2010-05-11).

Sampling and analysis of sulphide in KA3110A and KA3385A (both sections 1 and 2) was performed after completion of the circulation experiments in September and November 2011. Samples were collected on section water from the inner and outer circulation tubing and pressure tubing (cf. Figure 5-1 and Appendix G). In KA3385A, the sulphide concentration differed by a factor of 300 between inner tubing at the bottom of the section and the outer tubing at the top of the section. In KA3110A, there was no significant difference between the tubing. The analyses also show that the sulphide concentrations are at the same level as before the addition of ethanol.

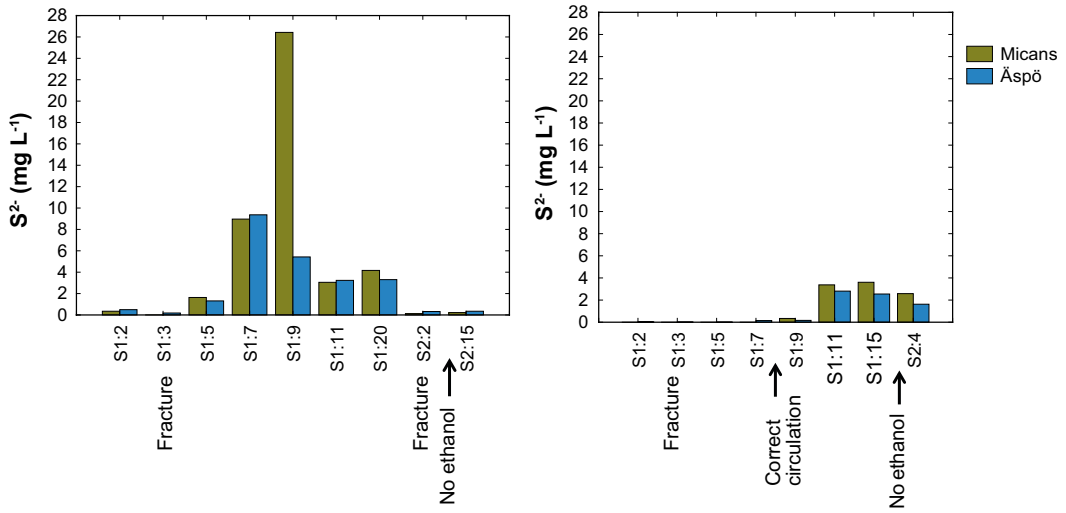

Figure 5-4. *The concentrations of sulphide in the water from boreholes KA3110A (left) and KA3385A (right) during Sulphide 1 and Sulphide 2. The figure shows data from analyses made by Microbial Analytics (Micans) and the Äspö laboratory. See text for details.*

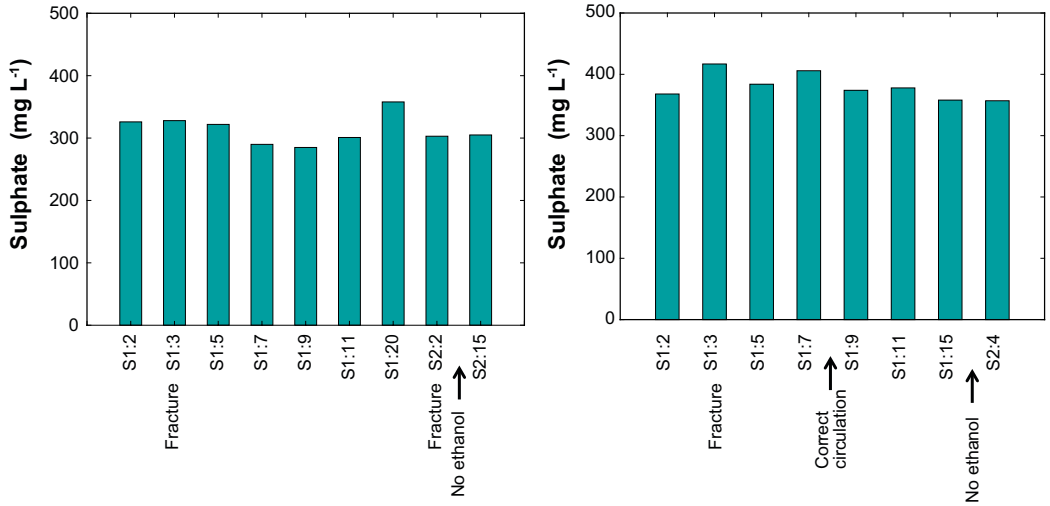

Figure 5-5. *The concentrations of sulphate in the water from boreholes KA3110A (left) and KA3385A (right) during Sulphide 1 and Sulphide 2.*

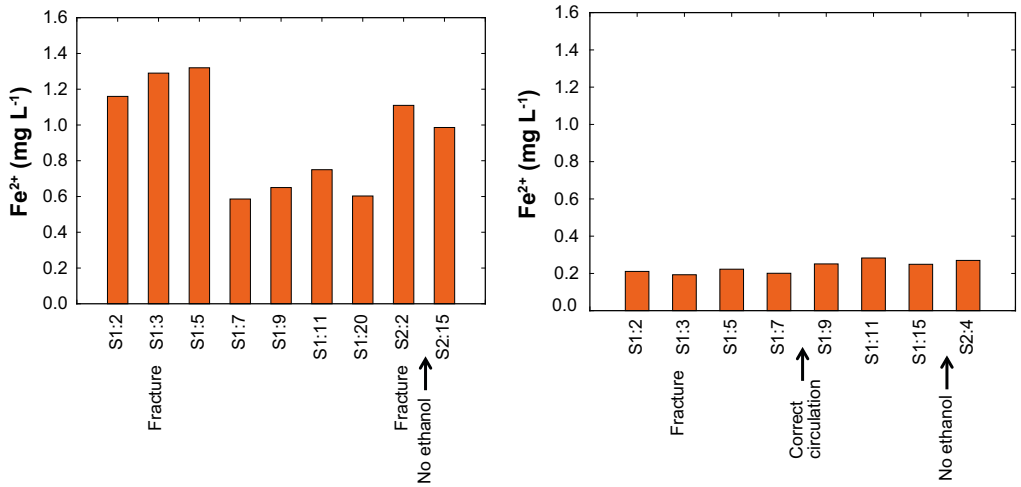

Figure 5-6. *The concentrations of ferrous iron in the water from boreholes KA3110A (left) and KA3385A (right) during Sulphide 1 and Sulphide 2. The figure shows data from analyses made by Äspö water chemistry laboratory.*

Table 5-3. Analyses of sulphide from different tubing in KA3110A and KA3385A (after circulation experiment).

Date	Borehole:section	Tubing	SKB number	HS^- (mg L^{-1})
2011-09-20	KA3110A:1	Pressure	20950	11 ± 4
	KA3110A:1	Inner circulation	20951	15 ± 5
	KA3110A:2	Pressure	20952	0.3 ± 0,1
2011-11-15	KA3385A:1	Inner circulation	22012	0.11 ± 0,04
	KA3385A:1	Outer circulation	22013	3 ± 1
	KA3385A:2	Pressure	22014	3 ± 1

5.4.6 Sulphide and ferrous iron during circulation

It was discovered that the sulphide concentration decreased dramatically after circulation and discharge of water for sampling. This occurred both in KA3110A and KA3385A, but more pronounced in KA3110A. In order to understand the reason behind the decrease in concentration sulphide and ferrous iron was analysed in the field for every litre of water that was circulated (Figures 5-7 and 5-8). The analysis data is compiled in Appendix F. The reason for this could be the blocking of the tubing by grout and consequently discharge of water from section 1 in KA3110A (instead of circulation). In KA3385A, section 1, until 2010-05-11 water was discharged instead of circulated due to a mistake in the labelling of tubing. From 2010-06-01 and forward, the water is circulated as intended. Ethanol was added to the borehole sections during the period 2010-04-21 to 2010-10-05.

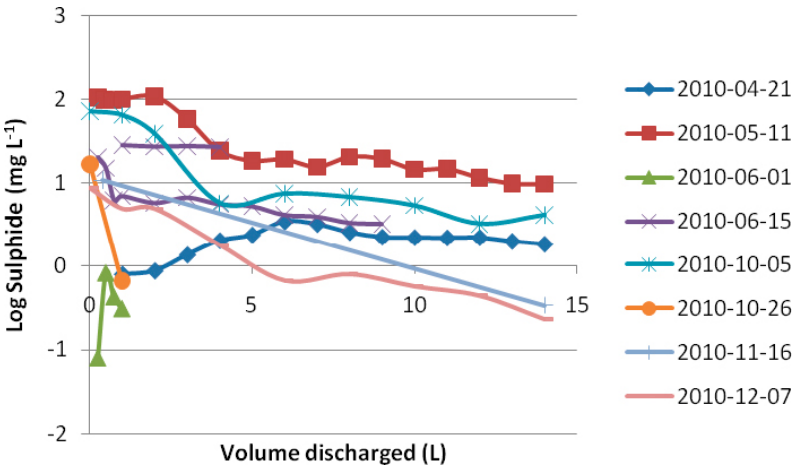

Figure 5-7. Borehole KA3110A, sulphide during discharge of water in section 1.

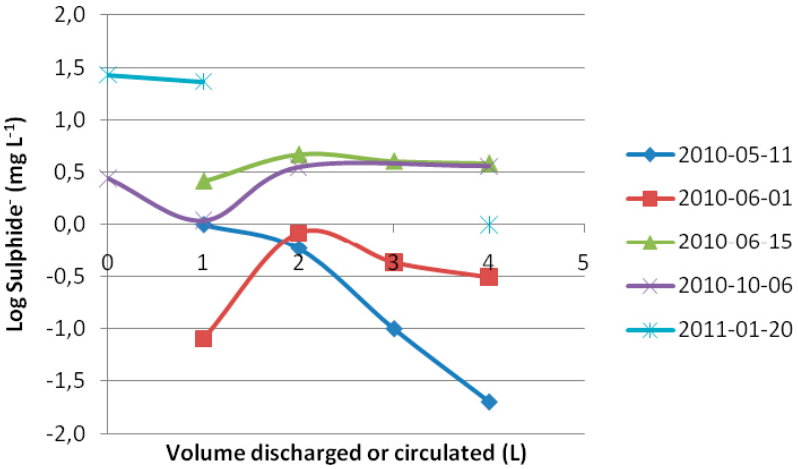

Figure 5-8. Borehole KA3385A, sulphide during discharge (2010-05-11) and circulation (2010-06-01 and forward) of water in section 1.

5.4.7 Analysis of sulphide and solubility product of monosulphide

The pH-dependent equilibrium between the different sulphide species in natural water is described by the following equations and equilibrium constants:

$H_2S(aq) \rightarrow H^+ + HS^-$ $\quad K_1(H_2S) = 10^{-7.01}$

$H_2S(aq) \rightarrow 2H^+ + S^{2-}$ $\quad K_2(H_2S) = 10^{-14.9}$

The value of the equilibrium constant K_1 implies that at pH around 7, the concentrations of dissolved H_2S and HS^- are roughly the same. At pH values above 7, the concentration of HS^- will dominate over H_2S.

The Swedish standard method for determination of sulphide in groundwater (SIS 2004) is a colorimetric method. The method is based on the complexation of sulphide and paraaminodimethylaniline (N, N-dimethyl-p-phenylenediamine), which form methyleneblue in an excess solution of iron (II). Ammoniumphosphate is used for complex formation with the excess iron (III) ions. The methyleneblue-method for sulphide measurements includes a preservation step where the sulphide (H_2S, HS^- and S^{2-}) is precipitated as ZnS(s). In this step the pH is raised to a high pH and all sulphide will be captured in the precipitate. All metal sulphides that are soluble in acid including sulphide in possible FeS will be analysed (Greenberg et al. 1985).

Ionic products (log IAP) were calculated for FeS (s) for samples collected and analysed for Fe (II) and HS^- in KA3110A and KA3385A, cf. Figures 5-9 and 5-10. Each collected sample is a mixture of section and fracture water or consists of more or less entirely fracture water (it should be noted that very minor parts of the section water may still be present even though discharge representing many sections volumes have been flushed out, depending on the distribution of flow anomalies along the section and the layout of the equipment). In an equilibrium or steady state situation with corresponding physical and chemical conditions, the ionic product should be approximately the same in all samples. As can be seen in the figures this is not the situation in any of the boreholes. The ionic product in the fracture water is slightly lower than in the corresponding sample consisting of a mixture of section and fracture water. The reason for the higher ionic product in the latter is the higher sulphide content in the section water, for various reasons (e.g. ethanol injection [if used at the time], SRB activity, corrosion etc). For the following samples of section/fracture water mixture, the ionic product increase drastically. This coincides with the contamination of ethanol and increase in sulphide concentration. The solubility product for monosulphide or pyrite has not been determined previously for the groundwater in Äspö, since all components in the water samples were not analysed in the earlier studies.

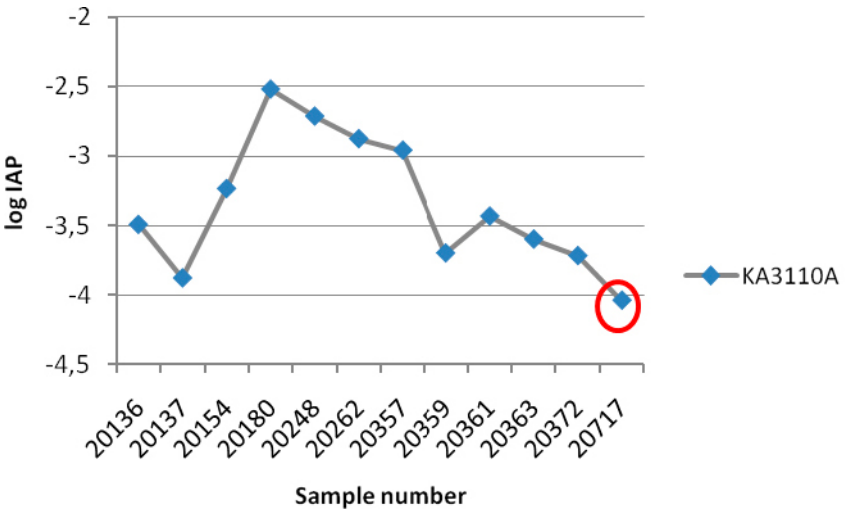

Figure 5-9. *Ionic products for FeS (s) in samples from KA3110A. The red ring represents fracture water, others are section water or mixtures of section and minor fracture water.*

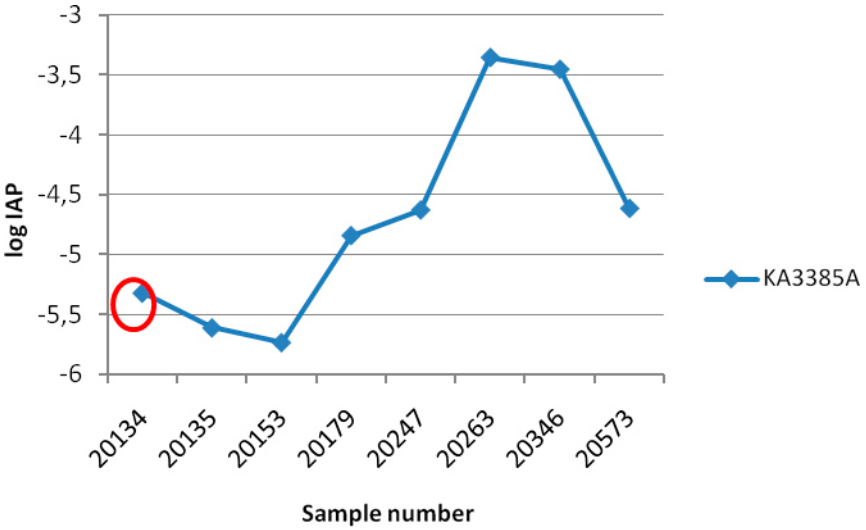

Figure 5-10. *Ionic products for FeS (s) in samples from KA3385A. The red ring represents fracture water, others are section water or mixtures of section and minor fracture water.*

However, the solubility product for amorphous monosulphide was determined for sulphidic groundwater in the Laxemar area to log K = –2.908 by Gimeno et al. (2006) using PHREEQC and WATEQ4F database. The solubility product for pyrite was not determined. The monosulphide is the first sulphide-phase to crystallise and will relatively rapidly re-crystallise to pyrite, which is the stable form in this environment. Mineralogical analyses, shown later in this report (Chapter 6.3.3–6.3.6), confirm the presence of both of these phases on the equipment in borehole KA3105A and KA3385A.

5.4.8 Acetate and dissolved organic carbon

Figure 5-2 shows the concentrations of acetate, dissolved organic carbon (DOC) and Total organic carbon (TOC) in groundwater samples from the boreholes in KA3110A and KA3385A. The high values of TOC and DOC originated most certainly from remaining ethanol in the circulation pump. The concentrations in samples from KA3385A were higher than in samples KA3110A because of the smaller volume in the sampled section in KA3385A (a similar amount of ethanol mixed in a smaller volume gave a higher concentration). The concentrations of acetate, DOC and TOC increased in the water of KA3385A from sample S1:9, when water was circulated in the section (section 1) instead of discharged to section 2. Overall the concentration of acetate was rather low in comparison with DOC and TOC, although higher than usually found in deep groundwater (Hallbeck and Pedersen 2008a).

5.4.9 Isotopes in groundwater

Data for stable isotopes and pmC (Percent modern Carbon) are compiled in Appendix F. Measurements of $\delta^{34}S$ in dissolved sulphate and sulphide are compiled in Tables 5-4 and 5-5. Stable isotopes of C (inorganic and organic carbon), O, H and pmC in groundwater are given in Tables 5-6 and 5-7. The fractionation of $\delta^{34}S$ between dissolved sulphide and sulphate in section water of KA3110A varies between 13.4 and 32.6‰ CDT (Canyon Diablo Troilite) ($\delta^{34}S_{sulphate}$–$\delta^{34}S_{sulphide}$). Samples with high sulphide concentration have, as expected, a large fractionation. In KA3385A, there are two samples from the circulation experiment; 2010-10-06 and 2011-01-20. The fractionation in $\delta^{34}S$ ($\delta^{34}S_{sulphate}$–$\delta^{34}S_{sulphide}$) is less pronounced in these two samples (–0.4 and 3.4‰ CDT) compared to KA3110A and does not seem to relate to the sulphide concentration (2.6 and 0.2 mg L^{-1}). After the circulation experiment was completed in KA3385A, samples were collected from the section water and fracture water (samples 22088 and 22153 with $\delta^{34}S_{sulphide}$ –0.5 and –10.7‰ CDT, respectively). The dissolved sulphate showed similar $\delta^{34}S$ values (18.6 and 20.2‰ CDT, respectively) as measured during the circulation experiment (samples 20346 and 20573). This indicates that the smaller $\delta^{34}S_{sulphate}$–$\delta^{34}S_{sulphide}$ in the section water may be due to the higher sulphide values (maybe higher sulphide production) in the section compared with the fracture water.

Table 5-4. $\delta^{34}S$ in dissolved sulphate and sulphide, borehole KA3110A.

Date	Sample/SKB no	Water type	$\delta^{34}S_{sulphate}$ (dev CDT)	$\delta^{34}S_{sulphide}$ (dev CDT)	$\delta^{34}S_{sulphate}$–$\delta^{34}S_{sulphide}$
2010-10-05	20357	Section	27.0	13.6	13.4
2010-10-05	20359*	Fracture	26.8	*	–
2010-10-26	20361	Section	27.1	4.1	23
2010-11-16	20363	Section	27.7	–4.9	32.6
2010-12-07	20372	Section	26.7	*	–

* Not possible to measure due to low sulphide concentration in sample.

Table 5-5. $\delta^{34}S$ in dissolved sulphate and sulphide, borehole KA3385A.

Date	Sample/SKB no	Water type	$\delta^{34}S_{sulphate}$ (dev CDT)	$\delta^{34}S_{sulphide}$ (dev CDT)	$\delta^{34}S_{sulphate}$–$\delta^{34}S_{sulphide}$
2010-10-06	20346	Section	18.9	19.3	–0.4
2011-01-20	20573	Section	20.8	17.4	3.4
2012-01-31	22088	Section	18.6	–0.5	19.1
2012-02-14	22153	Fracture	20.2	–10.7	30.9

The $\delta^{13}C$ signature in HCO_3^- for KA3110A varies between –13.7 and –6.3‰. The $\delta^{13}C$ values in organic carbon are lower; between –34.9 and –26.5‰. The values in KA3385A vary between –22.5 and –11.9‰ in HCO_3^- and –28.0 and –23.1 in organic carbon. This indicates generally lower values for $\delta^{13}C$ in HCO_3^- for KA3385A than for KA3110A. The values for $\delta^{13}C$ in the fracture water in both borehole sections are similar; –9.9 and –11.9 respectively in KA3110A and KA3385A. This implies a generally higher degree of fractionation of carbon isotopes in KA3385A than in KA3110A. This could be due to the presence of ethanol and a smaller section volume (less dilution and higher concentration of ethanol) in KA3385A. It is especially distinct that $\delta^{13}C$ is low after several months without discharging water from the section (2011-01-20), while in KA3110A the $\delta^{13}C$ signature is more similar in the section and fracture water. The $\delta^{13}C$ signature in organic carbon (DOC) is in the same order of magnitude as the carbon from oil produced plastics e.g. the tape (about –29‰) in section KA3385A:1 (see Section 7.2.2). The preparation of the sample for analysis of $\delta^{13}C$ in DOC involves evaporation of the water phase; it is therefore unlikely that ethanol has affected the analysis. The $\delta^{13}C$ signature of ethanol was not analysed, but if the ethanol was produced from fossil oil it should be devoid of ^{14}C. As can be seen in Figure 6-10b, in KA3385A, section 1 some calcite crystals have significantly lower $\delta^{13}C$ values compared to section 2 and to the calcites in borehole KA3105A. Since ethanol was added to section 1, but not to any of the other sections, this may indicate that the analysed calcite was produced recently, after the addition of ethanol. A formation of HCO_3^- from ethanol with low or absent ^{14}C is supported by pmC_{HCO3} in samples 20346 and 20573, which is significantly lower than pmC_{HCO3} in samples collected in KA3385A section 1 sometime after the addition of ethanol (see Table 5-7). Typically, the pmC_{HCO3} in borehole KA3110A is higher than in KA3385A. A similar effect of ethanol in KA3110A as in KA3385A is indicated in sample 20357 with lower pmC_{HCO3} than in the samples collected at later occasions. Since there are no measurements of pmC in calcite it cannot be concluded whether the calcite is produced from ethanol or if calcite is more ancient.

Table 5-6. Stable isotopes in C, O and H and pmC in borehole KA3110A.

Date	Sample/ SKB no	Water type	$\delta^{13}C$ in HCO_3^-	pmC	$\delta^{13}C$ in organic carbon/DOC	pmC organic carbon	$\delta^{18}O$	$\delta^{3}H$	$\delta^{2}H$
2010-10-05	20357	Section	–13.70	70.50	–34.90	74.20	–8.30	n.a.	–64.3
2010-10-05	20359*	Fracture	n.a.	n.a.	–34.70	88.70	–8.20	n.a.	–61.2
2010-10-26	20361	Section	–10.00	81.00	–33.60	89.80	–7.80	n.a.	–58.3
2010-11-16	20363	Section	–6.30	82.40	–30.00	88.20	–7.80	n.a.	–59.1
2010-12-07	20372	Section	–9.10	82.80	–26.50	90.09	–7.90	n.a.	–75.4
2011-04-21	20717	Fracture	–9.90	80.90	n.a.	n.a.	n.a.	n.a.	n.a.

* Due to an accident at the analysing laboratory, $\delta^{13}C$ in $HCO_3^-$was not analysed in fracture water 2010-10-05. The corresponding analysis was performed in 2011-04-21 (sample 20717). n.a. = not analysed.

Table 5-7. Stable isotopes in C, O and H and pmC in borehole KA3385A.

Date	Sample/ SKB no	Water type	$\delta^{13}C$ in HCO_3^-	pmC	$\delta^{13}C$ in organic carbon/D^{OC}	pmC organic carbon	$\delta^{18}O$	$\delta^{3}H$	$\delta^{2}H$
2010-10-06	20346	Section	–18.90	34.30	–28.00	54.80	–11.00	n.a.	n.a.
2011-01-20	20573	Section	–22.50	32.80	–23.10	62.40	–10.80	n.a.	–84.2
2012-01-31	22088	Section	–13.00	42.80	n.a.	n.a.	–11.10	2.10	–77.4
2012-02-14	22153	Fracture	–11.90	47.80	n.a.	n.a.	–10.70	2.40	–77.1
2012-11-14	22433	Section	–12.60	39.46	n.a.	n.a.	n.a.	n.a.	n.a.
2012-11-14	22435	Fracture	–10.90	46.18	n.a.	n.a.	n.a.	n.a.	n.a.

n.a. = not analysed.

5.4.10 Dissolved gases

The data from gas analyses in groundwater from the boreholes KA3110A and KA3385A during sampling session 1 are compiled in Table 5-8, Table 5-9 and Appendix F. Gas analyses from sampling session 2 are compiled in Appendix F. The gas samples in Sulphide 2 were primarily collected for analysis of stable isotopes. Accidently, the gas cylinders in Sulphide 2 were not filled with neon gas used for counter pressure during sampling. This may have affected the total gas volume and the volumes of the respective gases, but not the analyses of stable isotopes. For this reason, the stable isotopes and not the composition of dissolved gases in Sulphide 2 is discussed in the report. The total gas volume in KA3110A (Sulphide 1) varied between 43.3 mL L^{-1} in sample S1:2 and 52.9 mL L^{-1} in sample S1:11. The gas volume in groundwater from borehole KA3385A varied between 60.4 mL L^{-1} in sample S1:5 and 79.9 mL L^{-1} in sample S1:7. The groundwater from KA3385A has larger content of dissolved gases than KA3110A. The major differences in gas composition between the boreholes are a significant larger volume of helium in the water from KA3385A than in water from KA3110A (about 25 times) and larger volume of CO_2 in water from KA3110A than in water from KA3385A (about 10 times). These results are in agreement with the interpretations of the groundwater chemistry (Section 4.2) showing that the water in KA3385 represent longer residence times in the bedrock, which results in larger volume of He (to the largest extent produced by alpha decay of Uranium and Thorium in the bedrock). The lower CO_2 volume measured in the water from KA3385 is in accordance with the lower HCO_3^- in this borehole.

The gas that varies the most is hydrogen gas. It is most abundant in fracture water in KA3385A (sample S1:3/20135) and in section water from KA3110A (samples S1:2/20136 and S1:5/20154). Hydrogen gas is difficult to measure; it is a mobile light gas, the concentrations normally found in deep groundwater are low and the sampling and analysis is associated with uncertainties. Furthermore, it is an energy source for several microbial species and in this perspective it is interesting to mention that hydrogen is higher in the fracture than in the section water for KA3385 whereas KA3110A show the opposite trend although less significant.

Table 5-8. Gas concentrations in groundwater samples from borehole KA3110A at 1 atm and 22°C. Sample S1:3/20137 corresponds to fracture water, others to section water.

Sample/ SKB no.	H_2 (µL L^{-1})	H_2 (µmol L^{-1})	He (mL L^{-1})	He (µmol L^{-1})	N_2 (mL L^{-1})	N_2 (µmol L^{-1})	CO (µL L^{-1})	CO (µmol L^{-1})	CO_2 (mL L^{-1})	CO_2 (µmol L^{-1})	CH_4 (mL L^{-1})	CH_4 (µmol L^{-1})	Total gas (mL L^{-1})	Total gas (mmol L^{-1})
S1:2/20136	135.00	6.01	0.32	14.50	42.3	1,890	0.44	0.02	2.7	122	0.2	9	43.3	1.93
S1:3/20137	32.80	1.46	0.38	17.10	41.3	1,840	0.38	0.02	2.2	100	0.2	9	44.4	1.98
S1:5/20154	180.70	8.06	0.41	18.13	42.9	1,912	1	0.05	2.2	96	0.2	10	46.3	2.07
S1:7/20180	95.80	4.27	0.41	18.20	45.8	2,040	0.8	0.04	1.7	75	0.3	13	48.9	2.18
S1:9/20248	94.50	4.21	0.41	18.10	47.0	2,100	0.58	0.03	2.6	116	0.3	11	50.8	2.27
S1:11/20262	0.47	0.02	0.36	15.90	49.6	2,210	1.3	0.06	2.0	89	0.3	12	52.9	2.36

Table 5-9. Gas concentrations in groundwater samples from borehole KA3385A at 1 atm and 22°C. Sample S1:3/20135 corresponds to fracture water, others to section water.

Sample/ SKB no.	H_2 (µL L^{-1})	H_2 (µmol L^{-1})	He (mL L^{-1})	He (µmol L^{-1})	N_2 (mL L^{-1})	N_2 (µmol L^{-1})	CO (µL L^{-1})	CO (µmol L^{-1})	CO_2 (mL L^{-1})	CO_2 (µmol L^{-1})	CH_4 (mL L^{-1})	CH_4 (µmol L^{-1})	Total gas (mL L^{-1})	Total gas (mmol L^{-1})
S1:2/20134	14	0.60	6.2	278.00	62.5	2,790	1.4	0.06	0.14	6	0.1	7	69.34	3.10
S1:3/20135	156	6.97	7.9	351.00	65.8	2,930	0.56	0.02	0.07	3	0.1	5	74.56	3.33
S1:5/20153	11.3	0.51	5.8	260.00	53.8	2,400	2.06	0.09	0.14	6	0.1	6	60.35	2.69
S1:7/20179	2.6	0.11	9.5	424.00	57.1	2,550	1.94	0.09	0.11	5	0.1	6	79.92	3.57
S1:9/20247	36	1.58	6.5	284.00	55.1	2,460	2.09	0.09	0.16	7	0.1	6	61.06	2.72
S1:11/20263	12	0.52	6.2	277.00	64.6	2,880	1.93	0.9	0.29	13	0.1	6	71.26	3.18

5.4.11 Stable isotopes in gases

Stable isotopes C, H and O were analysed in dissolved gases H_2, CH_4 and CO_2 (Table 5-10). Samples 20347 and 20358 correspond to measurements in samples of released gases collected from fracture water with a gas trap, in order to collect enough gas to for measurement of δ^2H in H_2. However, the concentration of H_2 was too low for a successful measurement. The measurements succeeded in 3 out of 10 analysed samples.

The data for stable isotopes in gases are compiled in Appendix F and stable isotopes in groundwater in Appendix F. The $\delta^{13}C$ stable isotopes in the methane show relative uniform patterns, with average $\delta^{13}C$ values around –46‰ PDB and δ^2H values between –97.7 and –160‰ PDB, with an average of –124‰. The values are within the same interval irrespective of which boreholes is sampled and also if fracture water or water from the section itself is sampled. The $\delta^{13}C$ values are relatively high but a biogenic origin is nevertheless probable.

The fractionation of both $\delta^{13}C$ and δ^2H in the methane could be interpreted as the result of several processes. One possibility is that the methane is derived from acetate fermentation. A gas generated during such a process may attain such values as those measured here. The equilibrium exchange between CH_4 and water in the low temperature systems at Äspö is certainly minimal. Hence the δ^2H isotope signatures we observe in the methane are due to a fractionation during the consumption of the organic matter. One possibility for the origin of the CO_2, other than oxidation of organic matter, is a microbial oxidation of methane. If so, it would have taken place to a larger extent in borehole KA3110A than in KA3385A due to the relative higher measured concentrations of CO_2. The higher $\delta^{13}C$ values of the CO_2 gas (around –25‰ PDB) could be a product of anaerobic methane oxidation. As mentioned above, the ^{13}C isotopes of CO_2 during the acetate fermentation, may give ^{13}C values which coincide with the observed numbers. It is also possible that the isotopic values of the methane may have been influenced by microbial oxidation of methane.

Table 5-10. Stable isotopes in gases, boreholes KA3110A and KA3385A.

Date	Sample/SKB no	Water type	δ^2H in H_2	δ^2H in CH_4	$\delta^{13}C$ in CH_4	$\delta^{13}C$ in CO_2	$\delta^{18}O$ in CO_2
KA3110A							
2010-10-05	20357	Section	–830	–117	–41.3	–19.5	35.7
2010-10-05	20358	Fracture	n.a.	*	n.a.	n.a.	n.a.
2010-10-05	20359	Fracture	–837	–97.7	–46.1	–19.5	34.3
2010-10-26	20461	Section	–817	–142.7	–49.1	–23.7	28.2
2010-11-16	20363	Section	*	–131.3	–49.3	–23.9	29.6
2010-12-07	20372	Section	*	–160	–46.9	–19.3	35.8
KA3385A							
2010-10-06	20346	Section	*	–120.2	–47.5	–22.7	28.5
2010-10-06	20347	Fracture	*	n.a.	n.a.	n.a.	n.a.
2010-10-06	20348	Fracture	*	–113.9	–46.4	–23.3	27.1
2011-01-20	20573	Section	*	–111.1	–46.3	–24.2	31.6

* Not possible to analyse due to low concentration of dissolved hydrogen gas.

5.4.12 Stable isotopes

The values are within the same interval irrespective of which boreholes is sampled and also if fracture water or water from the section itself is sampled. The $\delta^{13}C$ values of methane are relatively high but a biogenic origin is still probable. The fractionation of $\delta^{2}H$ is here the strongest indicator of the source for the methane. Accordingly, the $\delta^{2}H$ values of the methane are fingerprinted from the isotope content of the organic matter and of course the water which is participating in the reaction. The biogenic origin of the methane is also supported by the isotope signatures revealed from the CO_2. The $\delta^{13}C$ values of the CO_2 gas reflect typical numbers expected from a degradation of organic matter.

The fractionation of both $\delta^{13}C$ and $\delta^{2}H$ in the methane could be due to several possible reactions of methanogenesis. In the borehole KA3110A, the methane concentration is about twice as high as the measured values in KA3385A. However, the processes according to the isotope results and observations made from the microbial studies seem to be the same in both boreholes. The methane content as well as the isotopic composition is also similar in the fracture and section water from each section, which indicates that methane is not involved in any section specific microbial activities. Furthermore, fractionation of $\delta^{34}S$ between dissolved sulphide and sulphate in section water of KA3110A was much higher (13.4 and 32.6‰ CDT) than in KA3385A (–0.4 and 3.4‰ CDT). Samples with high sulphide concentration have, as expected, a large fractionation, thus showing a clear difference between these boreholes.

6 Investigation of borehole instrumentation

This chapter describes the dismantling of borehole instrumentation from boreholes KA3105A and KA3385A and related investigations of precipitates, corrosion and microbiology. Hydrochemical data from the borehole section and fracture water are included as well.

6.1 Borehole instrumentation and materials

The instrumentation in core-drilled boreholes in Äspö HRL consists of different parts. A list of the instrumentation details and materials is given in Table 6-1 (see also Appendices A–C). A connection pipe of Aluminium runs through the whole length of the borehole. Inflatable packers of rubber on a stainless steel supporting frame are connected to the pipe in order to create delimited sections. Each section is connected by tubing of Polyamide to valves at a panel located outside the borehole in tunnel atmosphere. The tubing is fastened to the connection pipe by black tape about every 30 cm. Some sections are so called pressure sections where it is possible to measure the groundwater pressure, other sections (normally 1 or 2 sections in each borehole) are in addition prepared for water sampling and performance of dilution tests (so called circulation sections).

The construction of instrumentation in surface boreholes differs in several aspects from boreholes in the Äspö HRL. In surface boreholes, each borehole section is connected by tubing to a standpipe in the wider upper part of the borehole. This standpipe is supplied with a pressure transducer for groundwater level monitoring and in the case of circulation sections an additional stand pipe allows lowering of a pump for water sampling. More detailed information on the instrumentation in surface boreholes is given in Rosdahl et al. (2011).

The rods used in the tunnel boreholes in the Äspö HRL are generally made of aluminium.

Later installations in surface boreholes drilled during the site investigations in Forsmark and Oskarshamn, used stainless steel due to the better resistance to corrosion in chemically demanding environment. The tubing has always been made of polyamide but different brands and physical properties have been used. The packers were initially of EPDM rubber, but were exchanged for PUR (Poly Urethane Rubber) during the site investigations. Only a very small part of the packers (about 5 cm^2) is in contact with the groundwater when inflated.

Most plastics contain some plasticizers. PVC may contain up to about 65% plasticisers. Polyamide plastics may also contain plasticisers and also surfactants (Page 2000). The plasticisers have a number of improving properties on the plastics such as; easier machining and more regular pore-size distribution during fabrication, a better shape stability and in particular a barrier to the absorption of water. There are references from the literature that show that SRB can use plasticisers as a source of electrons while oxidising sulphide to sulphate (Tsuchida et al. 2011).

Acid-proof steel is more suitable than stainless steel for chemically demanding environments such as groundwater with high concentrations of chloride. Acid-proof steel contains besides iron and Chromium also Nickel and Manganese and smaller amounts of Molybdenum, Niobium and Titanium.

Table 6-1.Instrumentation details and materials.

Instrumentation part	Material
Rod	Aluminium
Tubing	Polyamide (Tecalan)
Packers (rubber)	EPDM[1]-rubber
Connection pipes and supporting frame	Stainless steel
Black tape	PVC[2] (Brand: Nitto)

[1] Ethylene-Polypropylene Rubber.
[2] Polyvinylchloride.

6.2 Methodology of the investigations

6.2.1 Performance

The activity focused on whether microbial sulphate reducing processes were related to the instrumentation in the borehole and to a certain material or process, such as for instance metal corrosion or plasticisers in plastics. An important aspect in the investigation was to compare instrumentation from boreholes with high and low sulphide concentrations. The investigation included visual observations as well as a number of analyses. The section water and fracture water was sampled 1–2 days before dismantling of the instrumentation and analysed for a number of chemical components including sulphate and sulphide as well as for stable isotopes in carbon, sulphide and oxygen. The surfaces of the instrumentation was sampled and analysed for microbiological parameters, secondary minerals and stable isotopes of secondary minerals. In KA3385A, which was part of the circulation experiment, the section water had not been extracted since November 2011 (in October 2011 for KA3105A). The instrumentation was dismantled more than a year after the circulation experiment was finished. Analyses performed on water samples and minerals are listed in Table 6-2.

6.2.2 Microbiological analyses

The microbial analyses chosen for the investigation of the borehole installations were TNC, MPN of SRB and DNA sequencing. The DNA, if enough material could be sampled, would be used for cloning and sequencing of the 16S rRNA gene for identification of microorganism present on the equipment. TNC gives the total amount of cells in a sample and are used together with the MPN of SRB which then show how large proportion of the population that is sulphate reducing microorganisms. DNA identification tells what types of microorganisms there are in a sample and in this case, especially which SRB species.

Samples were collected from the surfaces of five different materials of which the installation was composed, aluminium, rubber, stainless steel, plastic tubing and the precipitate that were in connection with the tape. This approach was used to elucidate if some material was preferred by SRB.

The samples collected from equipment surfaces were prepared for analyses of TNC, MPN of SRB and for DNA extraction from microorganisms present on the surfaces. The sampling was made with sterile cotton swabs that were placed in anaerobic tubes with growth medium for the MPN determination of SRB and in a formaldehyde solution for the TNC samples. Sampling for DNA extraction was done with sterile DNA swabs prepared for the extraction and frozen within 2 hours. The inoculations for the MPN of SRB were done directly after sampling. Counting of TNC samples were done in the laboratory less than three day after sampling. DNA extraction samples were transported frozen and extracted in two day from sampling. Sampling and analyses followed protocols described in Hallbeck and Pedersen (2008a) and Hallbeck et al. (2011).

Table 6-2. Water and mineral analyses from sections where the borehole instrumentation was dismantled (sampling just after the dismantling [minerals], just before dismantling [section water], just after sampling for section water, or after instrumentation was re-installed [fracture water].

Borehole	Type	Section	Metals	Anions	DOC	REE**	δ^2H	$\delta^{18}O$	^{14}C	$\delta^{13}C$	$\delta^{34}S_{SO4}$	$\delta^{34}S_{HS}$	HS^-	$\delta^{34}S_{py}$	$\delta^{13}C_{cal}$	$\delta^{18}O_{cal}$
KA3385A	Fracture	1	x	x	x		x	x	x	x	x	x	x			
KA3385A	Section	1	x	x*			x	x	x	x	x	x	x	x	x	x
KA3385A	Fracture	2											x			
KA3385A	Section	2												x	x	x
KA3105A	Fracture	2	x	x	x		x	x	x	x	x	x	x			
KA3105A	Section	2	x	x*	x		x	x	x	x	x	x	x	x	x	x
KA3105A	Fracture	3	x	x	x		x	x	x	x	x	x	x			
KA3105A	Section	3	x	x*	x		x	x	x	x	x	x	x	x	x	x
KA3105A	Fracture	4	x	x	x	x	x	x	x	x	x	x	x			
KA3105A	Section	4	x	x*	x		x	x	x	x	x	x	x	x	x	x

* = not HCO_3, F. **Rare earth elements. py = pyrite. cal = calcite.

6.2.3 Secondary minerals and stable isotopes

Samples of precipitates were scraped off from the permanent borehole equipment using a chisel and tweezers, shortly after extraction from the borehole in the tunnel. Each sample bag was flushed with nitrogen gas, vacuum-pumped and sealed using a heating device directly after sampling, in order to keep the sample in an oxygen-free environment until analysis. Each sample bag was then transferred to a second, Al-coated, sample bag, which was vacuum-pumped and sealed.

Scanning electron microscopy and microanalysis

In the laboratory, the sample bags were opened and the samples were quickly examined under the stereomicroscope, and a representative portion (based on microscopical observation) of each sample was then placed on a copper tape on a glass slide and investigated with a scanning electron microscope (SEM) equipped with an EDS detector (energy dispersive spectrometer).

Crystals of calcite and pyrite were then hand-picked with tweezers under the stereomicroscope, for both conventional analysis (bulk samples of several calcite crystals each) and *in situ* analysis (pyrite) using SIMS (secondary ion mass spectrometer). Crystals for SIMS analysis were mounted in epoxy, polished until the crystal interiors were exposed, gold-coated (30 nm) and before the analysis investigated with SEM (back-scatter) in order to identify any zonation or overgrowth and any cracks or impurities.

6.2.4 Corrosion

Investigation of corrosion was only performed by visual inspection. Interesting observations were documented by photo. Together with analyses of precipitations and microbiological analyses the type of corrosion as well as cause of attack was evaluated.

6.3 Results from investigation of borehole instrumentation

6.3.1 General observations

From visual observations, the appearance of the dismantled instrumentations from the two boreholes was similar. Some common features were:

- Corrosion of Aluminium where plastic tape or tubing were in contact with the metal rod.
- White precipitation in connection to the tape when it was in contact with the Aluminium rod.
- There was no white precipitation where the tape was in contact with stainless steel parts.
- Grey precipitation on Aluminium rods and stainless steel part of the packers.
- Black precipitation on parts of the Aluminium rod (no obvious pattern).

However, there was more black precipitation on the aluminium rods from borehole KA3105A than on the ones from KA3385A (possibly due to less frequent discharge of water from KA3105A).

Figure 6-1. *Photograph of rod, tubing, tape and stainless steel part of a packer in borehole KA3385A.*

6.3.2 Microbiological analyses in KA3385A and KA3105A

The results from the microbiological analyses of samples taken from different materials in the borehole installations in borehole KA3105A and KA3385A are compiled in Table 6-3 and presented in Figure 6-2. There was no difference in TNC on the different materials or between the boreholes when the standard deviation was taken into account. The only significant difference in the number of SRB on the equipment was a ten times less abundance on the stainless steel compared to the other materials sampled.

Table 6-3. Microbiology results from sampling of borehole installations in KA3385A and KA3105A.

Sample name	Material	Micans-number	SKB number	TNC (± SD) (cm^{-2})	SRB MPN (lower and upper 95% confidence interval) (cells cm^{-2})	SRB MPN (lower and upper 95% confidence interval) (cells cm^{-3})
KA3105A Sample 1	Aluminium	120001	22096	4.4×10^5 ($\pm 2.7\times10^5$)	2,400 (1,100–6,400)	
KA3385A Sample 2	Aluminium	120007	22092	1.5×10^5 ($\pm 8.3\times 10^4$)	1,200 (444–3,300)	
KA3105A Sample 3	Tecalan tube	120003	22098	2.2×10^5 ($\pm 1.7\times10^4$)	890 (333–2,780)	
KA3385A Sample 3	Tecalan tube	120008	22093	5.7×10^4 ($\pm 2.9E\times10^4$)	89 (33.3–278)	
KA3105A Sample 4	Rubber	120004	22099	6.4×10^4 ($\pm 4.6\times10^4$)	56 (22–189)	
KA3385A Sample 1	Rubber	120006	22091	3.5×10^5 ($\pm 1.8\times10^5$)	780 (333–2,330)	
KA3105A Sample 5	Stainless steel	120005	22100	5.9×10^4 ($\pm 3.1\times10^4$)	0.26 (0.1–0.9)	
KA3385A Sample 5	Stainless steel	120010	22095	6.1×10^4 ($\pm 4.4\times10^4$)	0.26 (0.1–0.9)	
KA3105A Sample 2	Precipitation	120002	22097	*n.d.		560 (222–1,890)
KA3385A Sample 4	Precipitation	120009	22094	*n.d.		56 (22–189)

* n.d. = not detected.

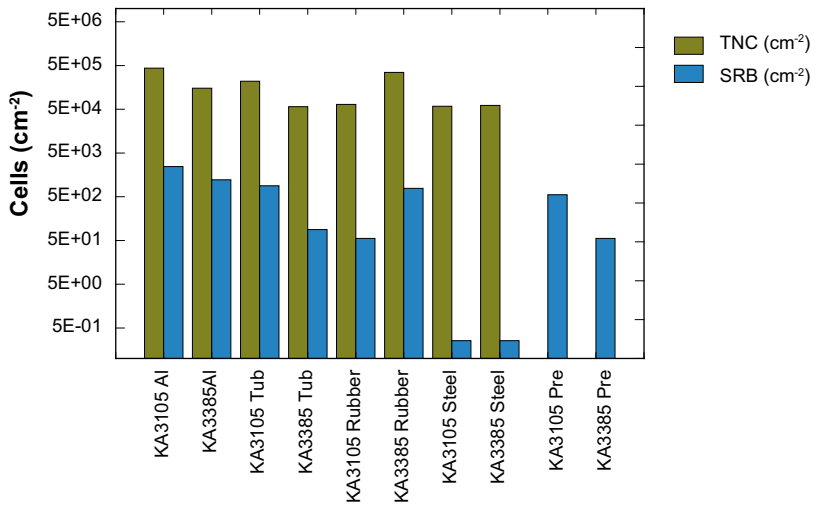

Figure 6-2. The number of cells and the most probable number of cells in samples taken from different materials in the borehole installations in the boreholes KA3385A and KA3105A. Note the logarithmic scale. The MPN of SRB in the precipitate is given in cm^{-3} and that TNC could not be determined in the precipitate. Al = rod in aluminium, Tub = tubing in Tecalane, Rubber = Packers, Steel = Connection pipes and supporting frame, Prec = precipitate close to the tape.

6.3.3 Secondary minerals in borehole KA3385A

The precipitates retrieved from the borehole equipment showed variation in mineralogical composition depending on what type of equipment they were sampled from. White precipitates in a soft substance around the tape on the Aluminium-rods (Figure 6-3), were dominated by Al-rich amorphous substances, with varying amounts of S and Si (with or without Cl, Ca, Na, Fe; chemical analyses are presented in Appendix J). Organic-rich material and salts ($NaCl/CaCl_2$) were also present in various amounts. Very small amounts of pyrite and barite were detected underneath the tape.

Precipitates at the stainless steel parts of the packer connections were totally dominated by calcite (Figure 6-4). The crystals had large c-axis/a-axes ratio (scalenohedral habit, Figure 6-5) and were generally around 100–300 µm, but larger crystals (> 500 µm) were observed as well. Pyrite and barite ($BaSO_4$) were found in various but overall small amounts together with calcite (Figure 6-6). Pyrite was commonly euhedral and showed cubic habit but anhedral/subhedral crystals were also observed. Maximum grain size of pyrite was 100 µm but most crystals were much smaller (10–50 µm). Amorphous monosulphide (FeS) was present on many calcite crystals, as tiny grains (< 25 µm, Figure 6-7), often in fine-grained aggregates, but were too small (especially too thin) for stable isotope analysis. Barite crystals were generally smaller than 50 µm.

The Tecalan (polyamide) tubing close to the packer connections and the Aluminium-rods featured the same minerals as observed on the steel packer connections, but the minerals proportions differed slightly. The precipitates on the Tecalan tubing were mainly calcite in similarity with those on the packer connections, but on the Aluminium-rods the precipitates generally contained a higher sulphide/calcite-ratio (mainly due to lower amounts of calcite) than at the steel parts of the packer connections (Figure 6-4). More extensive sample descriptions and SEM-images of precipitates are given in Appendix H.

At the start of borehole KA3385A, just at tunnel-borehole interface, gypsum had precipitated together with salts (e.g. NaCl – cubic halite crystals) on the Al-rod.

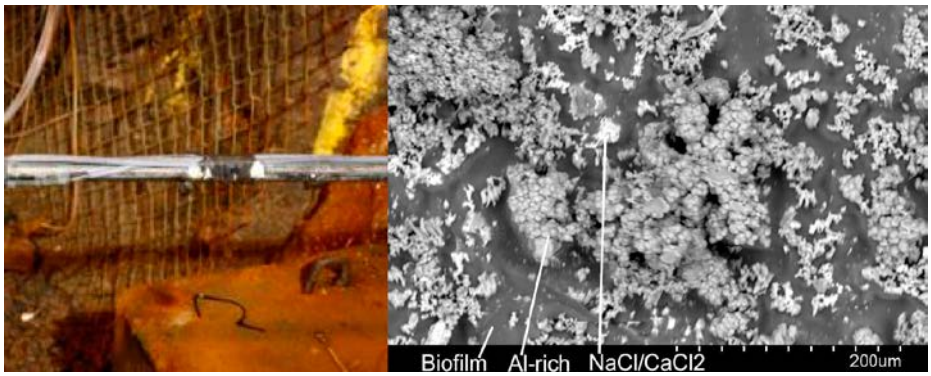

Figure 6-3. *(Left) Photograph of sample 22104 (borehole KA3385A) (the white substance adjacent to the black tape). (Right) Back-scattered SEM image of the white substance showing black organic-rich material), Al-rich substance and $NaCl/CaCl_2$.*

Figure 6-4. *(Left) Photograph of grey precipitates (calcite-dominated) on packer steel connections. Sample 22111 (KA3385A). (Right) Photograph of grey precipitates (calcite-dominated) and black precipitates (sulphide-rich) on the Al-rod. Sample 22131 (KA3105A).*

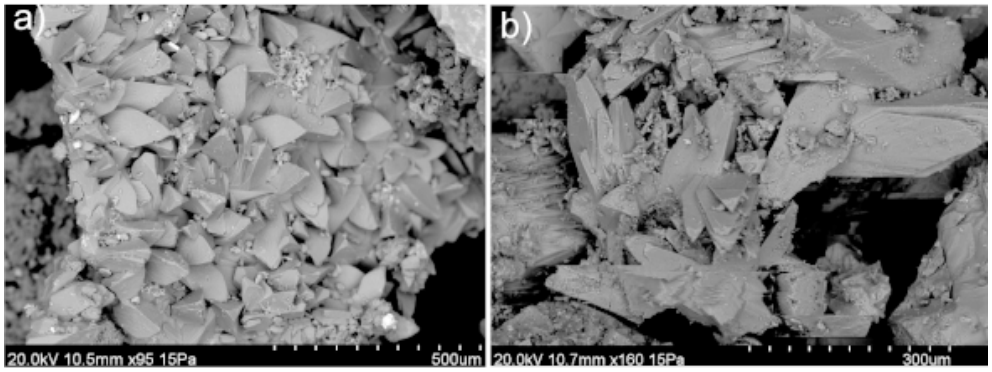

Figure 6-5. *Back-scattered SEM-images of calcite of scalenohedral habit (high c-axis/a-axes ratio), scraped off from the equipment in KA3385 section 1 (a, sample 22113) and KA3105A section 4 (b).*

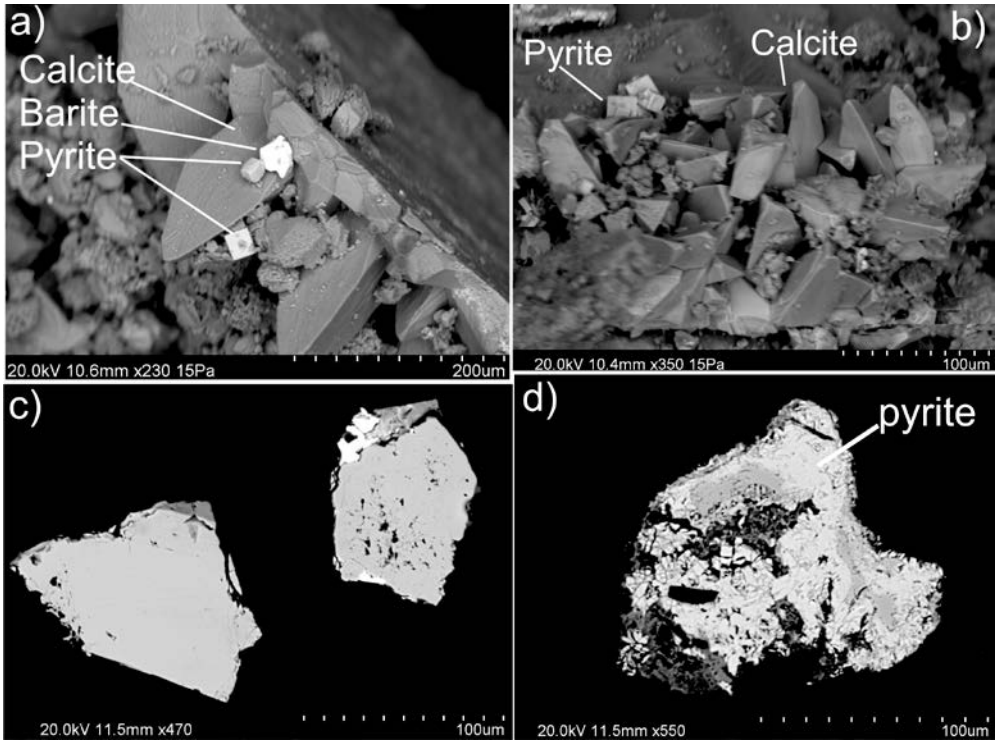

Figure 6-6. *Back-scattered SEM images of pyrite. (a and b, from sample 22113, KA3385A and sample 22128, KA3105A) Cubic pyrite crystals together with calcite and barite (only in a). (c and d) Polished pyrite crystals mounted in epoxy. Crystals were euhedral and homogenous (c, sample 22010, KA3385A), or, in a minor number of samples, very-fine-grained and intergrown with other phases (d, 22131, KA3105A).*

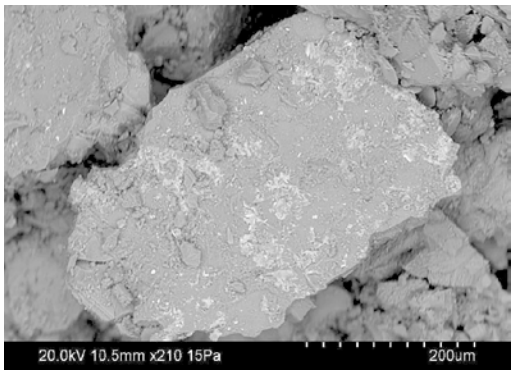

Figure 6-7. *Back-scattered SEM image showing fine-grained FeS (light grey) on calcite from the steel connections of the packer. Sample 22132, KA3105A.*

6.3.4 Secondary minerals in borehole KA3105A

In similarity with borehole KA3385A, the precipitates retrieved from the borehole equipment in KA3105A showed variation in mineralogical composition depending on what type of equipment material they were sampled from. White precipitates around the tape on the Al-rods were found here as well, dominated by Al-rich amorphous substances, with varying amounts of S and Si (with or without Cl, Ca, Na, Fe; chemical analyses are presented in Appendix J). Organic-rich material and salts ($NaCl/CaCl_2$) were also present in various amounts. Very small amounts of pyrite and barite were also present underneath the tape.

Precipitates at the steel parts of the packer connections were totally dominated by calcite (Figure 6-4). The crystals had large c-axis/a-axes ratio (scalenohedral habit) and were generally around 100–300 µm, but the ratio was generally slightly smaller than in KA3385A calcites. Pyrite and barite ($BaSO_4$) were found in various but overall small amounts together with calcite. Pyrite was commonly euhedral and showed cubic habit but anhedral/subhedral crystals were also observed. Maximum grain size of pyrite was 100 µm but most crystals were much smaller (10–50 µm). Amorphous monosulphide (FeS) was present on many calcite crystals, as tiny grains (< 25 µm), often in fine-grained aggregates, but were too small (especially too thin) for stable isotope analysis. Barite crystals were generally smaller than 50 µm.

The Tecalan (polyamide) tubing close to the packer connections and the Al-rods featured the same minerals as observed on the steel packer connections, but the minerals proportions differed slightly. The Tecalan hose was dominated by calcite in similarity with the packer connections, but the Al-rods generally contained a higher sulphide/calcite-ratio (mainly due to lower amounts of calcite) than at the steel parts of the packer connections (Figure 6-4).

Fluorite (packer connection), magnetite (Al-rod) and quartz (Al-rod) were observed in single samples. The amount of pyrite in each sample was very small and a maximum of five pyrite crystals from each sample suitable for analysis were retrieved.

6.3.5 Stable isotopes in borehole KA3385A

Pyrite showed an overall large range in $\delta^{34}S$ values (–35.7 to +33.8‰ in section 2 and –17.6 to +33.1‰ in section 1 (Figure 6-8). The range within individual crystals was generally quite small (< 10‰, in all but one crystal) compared to the overall range in the samples and in the whole sections. The $\delta^{34}S$ values commonly increased with growth and in a few cases, SEM investigations revealed clear morphological sub-generations (overgrowths) within the crystals (Figure 6-9). The range in $\delta^{34}S$ values was large for pyrite sampled from both kinds of equipment (Tecalan tubing and steel connections at the packers).

The waters showed differing $\delta^{34}S$ values between the fracture water and the section water (only measured in section 1), see Section 5.4.9. The section water was lower in $\delta^{34}S_{sulphate}$ (by 1.7‰) and higher in $\delta^{34}S_{sulphide}$ than the fracture water (by 10.2‰). The difference between sulphate and sulphide ($\Delta\delta^{34}S_{sulphate–sulphide}$) was larger (range: 30.9‰) for the fracture water than for the corresponding section water (19.0‰). The maximum range in $\delta^{34}S$ values in the waters was thus smaller than in the pyrite.

Calcite showed $\delta^{18}O$ values between –11.2 and –8.9‰ and $\delta^{13}C$ values between –22.9 and –12.3‰, although the –22.9‰ is somewhat of an outlier when compared also with samples from KA3105A. All calcite samples from section 1 (water from section 2 was not analysed for stable isotopes) was within the range expected from precipitates from the current groundwater (Section 5.4.9), using the equation $1{,}000\ \ln\alpha = 2.78(10^6T^{-2})–2.89$ (O'Neil et al. 1969) to calculate the fractionation factor (α) between oxygen in water and in calcite and taking into account the variation in temperature during this sampling and variation in $\delta^{18}O$ in these sections during previous samplings (Figure 6-10a). In the section where both fracture water and section water were analysed, the section water showed lower $\delta^{18}O$ values, although only by 0.4‰. For $\delta^{13}C$, all calcites were lower than in hypothetical calcite precipitated from the current groundwater, using $\delta^{13}C$ values together with fractionation factor ($\alpha = 1.00185 \pm 0.00023$ at 20°C, with temperature dependence of 0.000035 ± 0.000013/°C) from Emrich et al. (1970) to calculate the fractionation factor (α) between carbon in HCO_3^-(aq) and calcite. Tape from the Al-rods showed $\delta^{13}C$ values of –29.1 to –28.9‰. The section water showed lower $\delta^{13}C$ values than the fracture water, by 1.1‰, but earlier measurements of $\delta^{13}C_{HCO3^-}$ representing the circulation experiment when ethanol was added show lower values (–18.9 and –22.5‰) in the section. One possibility is therefore that the low and variable $\delta^{13}C$ values in the calcites relate to the condition in the section during this part of the experiment.

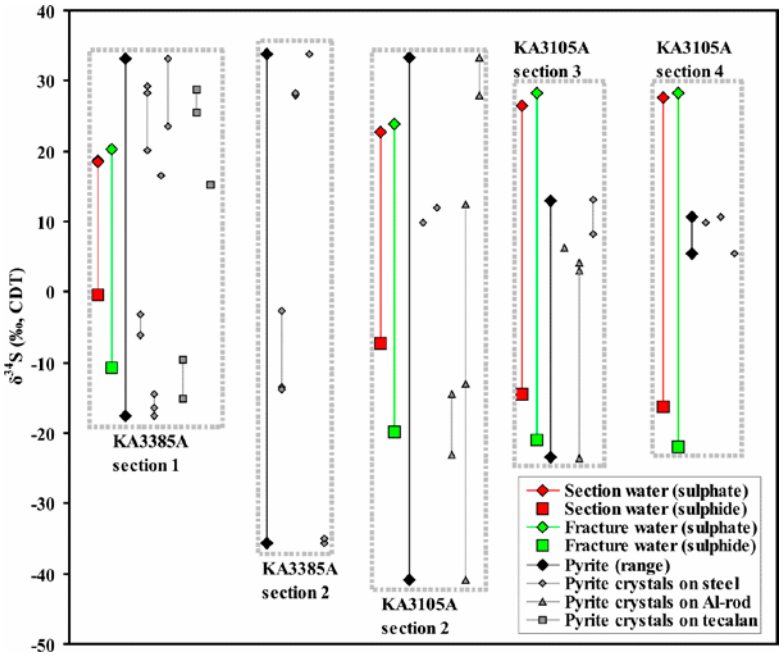

Figure 6-8. *$\delta^{34}S$ composition of water (fracture and section; values from sulphate and sulphide connected by a line) and pyrite (both range: black; and individual analyses in different crystals: grey, with different symbols depending on which type of equipment it was precipitated on).*

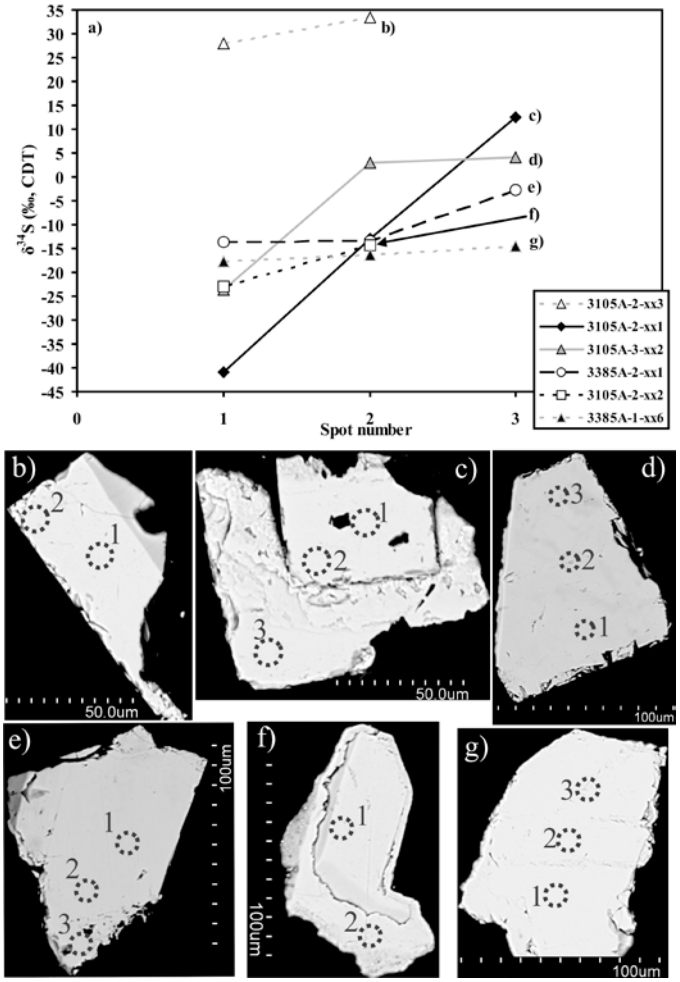

Figure 6-9. *(a) Evolution of $\delta^{34}S$ composition during growth of pyrite crystals, (b–g) showing spot location in back-scattered SEM images.*

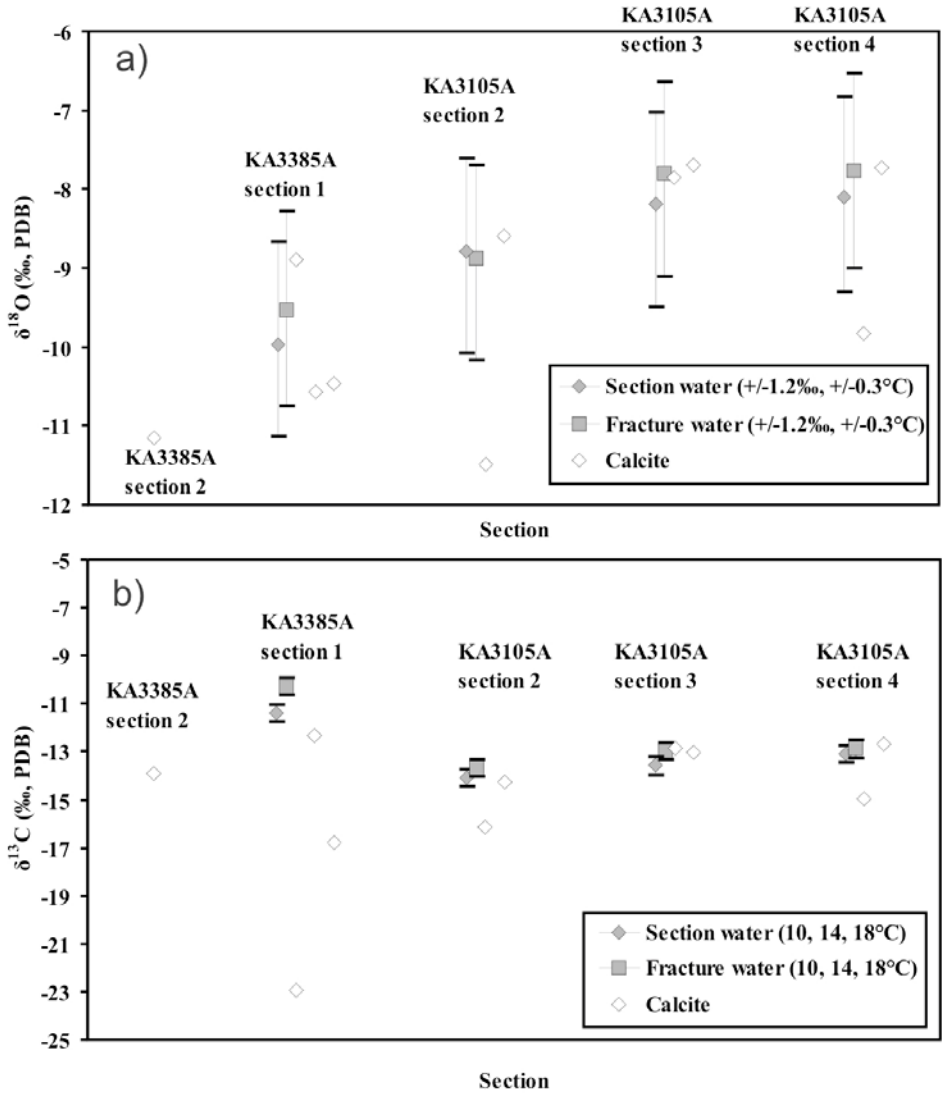

Figure 6-10. *Stable isotopes in calcite and associated section water and fracture water. (a) $\delta^{18}O$ in calcite and the range for hypothetical calcite precipitated from the current fracture or section water at present borehole temperatures (~ 14°C), using the equation 1,000 lnα = 2.78(10^6T^{-2})–2.89 (O'Neil et al. 1969) to calculate the fractionation factor (α) between oxygen in water and calcite. The range bar is based on a measured variation of ~ 1.2‰ (variation during previous sampling) and 0.3°C (variation during the current sampling. (b) $\delta^{13}O$ in calcite and the range for hypothetical calcite precipitated from the current fracture or section water at present borehole temperatures (~ 14°C), using fractionation factors (α = 1.00185 ± 0.00023 at 20°C, with temperature dependence of 0.000035 ± 0.000013/°C) from Emrich et al. (1970) to calculate the fractionation factor (α) between carbon in HCO_3^-(aq) and calcite. Because previous measurements of $\delta^{13}C$ and temperature are lacking, a temperature range of 10–18°C was used.*

6.3.6 Stable isotopes in borehole KA3105A

Pyrite showed an overall large range in $\delta^{34}S$ values (–40.8 to +33.3‰), largest in section 2, Figure 6-8. The sample with the smallest range is probably not representative because only three analyses could be carried out from very fine-grained pyrite intergrown with other phases. The range within individual crystals was generally quite small (< 10‰ in all but two crystals) compared to the overall range in the samples and in the whole sections. The $\delta^{34}S$ values commonly increased with growth and in a few cases, SEM investigations revealed clear morphological sub-generations (over-growths) within the crystals. The range in $\delta^{34}S$ values was large for pyrite sampled from all kinds of equipment (Al-rods, Tecalan tubing and steel connections at the packers).

The waters showed differing $\delta^{34}S$ values between the fracture water and the section water. The section water was in all cases lower in $\delta^{34}S_{sulphate}$ (by 0.7–1.8‰) and higher in $\delta^{34}S_{sulphide}$ than the fracture water (by 5.7–12.6‰). The difference between sulphate and sulphide ($\Delta\delta^{34}S_{sulphate-sulphide}$) was therefore always larger (range: 43.8–50.2‰) for the fracture water than for the corresponding section water (30.0–44.2‰). The maximum range in $\delta^{34}S$ values in the waters was thus smaller than in the pyrite.

Calcite showed $\delta^{18}O$ values between –11.5 and –7.7‰ and $\delta^{13}C$ values between –16.2 and –12.7‰. Calcite from KA3105A generally showed higher $\delta^{18}O$ values than in KA3385A, which is also reflected in the waters, which had higher $\delta^{18}O$ values in KA3105A. In four samples out of six the calcite was within the range expected from precipitates from the current groundwater, using the equation $1000\ \ln\alpha = 2.78(10^6T^{-2})-2.89$ (O'Neil et al. 1969) to calculate the fractionation factor (α) between oxygen in water and calcite and taking into account the variation in temperature during this sampling and variation in $\delta^{18}O$ in these sections during previous samplings (). In two out of three sections, the section water showed lower $\delta^{18}O$ and $\delta^{13}C$ values than in the fracture water, although only by 0.3–0.4‰ and 0.2–0.6‰, respectively. For $\delta^{13}C$, calcites where in four out of six cases lower than in hypothetical calcite precipitated from the current groundwater, using $\delta^{13}C$ values together with fractionation factor ($\alpha = 1.00185 \pm 0.00023$ at 20°C, with temperature dependence of 0.000035 ± 0.000013/°C) from Emrich et al. (1970) to calculate the fractionation factor (α) between carbon in HCO_3^-(aq) and calcite.

6.3.7 Material balance calculation in borehole KA3385A

The material balance calculations reported below show that the amount of dissolved organic carbon (DOC) in fracture groundwater is enough for producing the observed sulphide in the borehole section. It is not clear however, why the DOC would not have been consumed already in the fractures. Plasticizers from the adhesive tape are, alone, not likely to be responsible for the production of the observed sulphide. In addition, the amount of formed hydrogen gas calculated from corrosion and the amount of dissolved hydrogen gas in the groundwater (fracture water) are not alone large enough to explain the observed sulphide production.

Plasticizers

One of the most common plasticizers in polyvinylchloride (the base material for the adhesive electric tape) is bis(2-ethylhexyl) phthalate. Other names are di(2-ethylhexyl)phthalate and DEHP. It is added to make the plastics flexible. The molecular weight is 390.56 g $mole^{-1}$ and the chemical formula $C_{24}H_{38}O_4$. Suppose DEHP was used by SRB to produce sulphide, then the stoichiometric reaction would look like this;

$$4\ C_{24}H_{38}O_4 + 20\ H_2O + 63\ SO_4^{2-} \rightarrow 63\ HS^- + 96\ HCO_3^- + 33\ H^+$$

The reaction give a molar relationship between DEHP and HS^- of 4:63, i e 63 moles of sulphide can be produced from 4 moles of DEHP (ratio about 1:16), assuming that bacteria can use the whole molecule as substrate for production of sulphide.

The results from the hydrotests in borehole KA3385A, section 1 implied that the groundwater flow through the fractures in the section is 40 mL hr^{-1} (corresponds to the turnover rate). The equipment was installed 17 years ago, in 1995. Assuming that the sulphide concentration in the borehole section is 1 mg L^{-1} and has been constant since the installation of equipment (in accordance with the results obtained in this investigation), then the total amount of sulphide that has been produced and removed from the borehole section by the flowing groundwater during the last 17 years will be:

Sulphide = 40 mL hr^{-1} (borehole turnover rate)×17 year×1 mg L^{-1}
(concentration in borehole section) = 5.96 g or 0.18 moles

The sulphide produced may be a larger amount than observed, since there may be sulphide that has been continuously precipitated on the walls of the borehole or the instrumentation and that will not be accounted for in this analysis. Assuming that DEHP is the only substrate for production of sulphide it is possible to calculate the amount of DEHP that is needed to produce 0.18 moles of sulphide:

Phthalate (mole) = sulphide (moles)×4/63 (see stoichiometric reaction above) = 0.011 moles
Phthalate (g) = 0.011 moles× 390.56 g $moles^{-1}$ = 4.47 g

This implies that the amount of phthalate needed to keep the sulphide concentration in the borehole section to 1 mg L^{-1} during 17 years is 4.47 g.

The amount of DEHP to produce the observed amount of sulphide in the section is 0.011 mole or almost 5 g of DEHP. The amount of tape with plasticizers that is required in an isolated section can be estimated;

The tape is 0.2 mm thick and 19 mm wide and has a density of 1.4 g/cm^3. From that follows that 1 cm of the tape has a weight of 0.05 g. PVC (Poly vinyl chloride) plastics may consist of as much as 50% plasticizers. Assuming 50-weight% DEHP, 5 g of DEHP would correspond to 10 g of tape, which is about 200 cm of tape.

In the sections, the rod and the tubing were tightened together using tape. The distance between these tightenings differed slightly between sections. The amount of tape in section 1 in KA3385A was estimated to be at most about 100 cm. The estimation was made by the following assumptions; the diameter of the rod is 2 cm (perimeter 6 cm), the tape was winded around the rod at about 10 cm in length in double layers. This gives a total length of tape of about 60 cm. The result implies that plasticizers alone may not be responsible for microbial sulphide production.

Dissolved organic carbon

The results for DEHP can be compared to the other available source of organic carbon, DOC (atomic mass of ~ 12 g $mole^{-1}$). The concentration of DOC in the borehole section and in the fracture water flowing into KA3385A is about 1 mg L^{-1} (sampled section and fracture water in November 2012, SKB numbers 22433 and 22435 in Appendix F, Table A6-1) The amount of DOC in the incoming fracture water during these 17 years (at a rate of 40 mL hr^{-1}) corresponds to;

DOC = 40 mL hr^{-1} (borehole turnover rate)×17 year×1 mg L^{-1}
(concentration in borehole section) = 6 g C or 0.5 moles

Assuming the following reaction to produce sulphide from DOC, two carbon atoms are needed to produce one sulphide molecule:

$2(CH_2O) + SO_4^{2-} + 2H^+ \rightarrow 2HCO_3^- + HS^- + 3H^+$

The DOC transported with fracture water to the section is in total 0.5 moles, and to produce 0.18 moles sulphide we need only 0.36 moles DOC, so the amount of DOC in the incoming groundwater is theoretically enough to produce the observed sulphide concentration in the borehole section. A question to be asked is why the DOC in the groundwater has not been already used by microbes while the groundwater has slowly been transported to the borehole section. This suggests that the natural DOC is of a nature that is not suitable for sulphate reduction or that the rate of DOC degradations is very slow. Alternative explanations might be that the environment in the fractures is not as favourable for SRB, or that some nutrients in the plastics, tape and metals of the borehole section are needed for SRB.

Hydrogen gas

Hydrogen gas (H_2) is available naturally in deep groundwater, but is also produced in corrosion reactions. Assume the following reactions for the corrosion of Aluminium;

$2Al + 4H_2O \rightarrow 2Al(OH)_3 + H_2$

The rod in section 1, KA3385A, was subjected to corrosion under the tape. The depth of the corrosion was about 1µm on a surface of 10 cm with the perimeter of 6 cm, in total 60 cm^2. This means that 0.006 cm^3 of Aluminium had been depleted from the rod. This corresponds to 0.0162 g of Aluminium (density 2.7 g cm^{-3}) or 0.4 moles (molecular weight 27 g $mole^{-1}$). The production of H_2 from corrosion corresponds to 0.2 moles. The amount can be compared to the natural content of H_2 dissolved in groundwater which is 0.2 µmoles L^{-1} or 0.012 moles (0.024 g) during 17 years.

The stoichiometric reaction for production of sulphide from H_2 can be written as;

$4H_2 + SO_4^{2-} + 2H^+ \rightarrow H_2S + 4H_2O$

1 mole sulphide is produced from 4 moles of H_2, which means that 0.72 mole of H_2 is required to produce 0.18 mole sulphide. The produced amount of H_2 from corrosion under the tape is less and estimated to about ¼ of the required amount and so is the amount of H_2 transported through the section dissolved in the groundwater.

In conclusion: the amount of dissolved organic carbon from fracture groundwater is enough for producing the observed sulphide in the section. Plasticizers alone are likely not responsible for the production of the observed sulphide. Calculated hydrogen gas from corrosion or measured dissolved hydrogen gas from fractures is not enough for production of the observed sulphide.

6.3.8 Corrosion

The general corrosion observations are summarized in Appendix I. At the anode electrons are released and at the same time an oxidation of the metal takes place. At the cathode, the electrons are taken up and a substance in the water is reduced. Figure 6-11 illustrates the electrochemical corrosion process for steel in an aerobic environment.

The electrons are relocated in the metal from the anode to the cathode, resulting in a current going in the opposite direction. A circuit must be closed in a continuous flow in order for the so-called corrosion cell to work (Figure 6-12). In an aquatic environment the current is transported by ions that are dissolved in the water.

The attack in the joint between the two Aluminium rods situated about 1 cm outside of the rock wall (borehole KA3385A) shown in Figure 6-13, was probably caused by the chloride-rich rock water. The attack starts as crevice corrosion, probably accelerated by chloride enrichment due to evaporation. As the corrosion attack proceeds deeper, the water will come in contact with the stainless steel junction and the corrosion process is accelerated by galvanic corrosion where the Aluminium sacrifices itself for the stainless steel, see Figure 6-14.

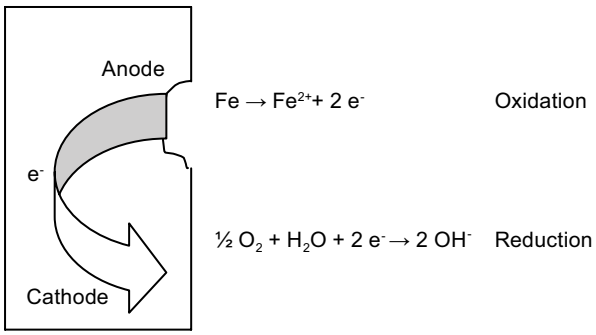

Figure 6-11. *Corrosion reactions in aerobic environment.*

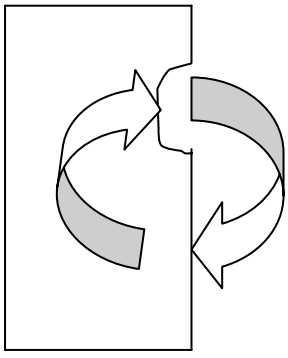

Figure 6-12. *Current flow in a corrosion cell.*

Figure 6-13. *Attack in the joint between two rods, 1 cm outside the tunnel wall (KA3385A).*

Figure 6-14. *Galvanic corrosion between Aluminium (rod) and stainless steel (junction).*

The area from the rock wall and a distance into the borehole, KA3105A is well aerated (no sealing of the casing). The rod has been in direct contact with the casing and has been subjected to severe galvanic corrosion, where oxygen has acted as the oxidizing agent (see Appendix I for overview of aerobic and anaerobic areas in the boreholes and Figures 6-15 to Figure 6-19 for photographs).

If we assume that the borehole was filled with water, an estimation of the magnitude of galvanic corrosion can be performed:

The resistance of the corrosion cell is dominated by the transition resistance between the metal surfaces and the surrounding water, which can be calculated with the following equation:

$$R = 0.315 \cdot \frac{\rho}{\sqrt{A}}$$

Where ρ is the water resistivity, 0.315 is a constant and A the metal surface exposed to water. The water has equivalent salinity as the Baltic Sea why the resistivity is approximately 1 Ωm. The stainless steel inner surface of the casing is about 4,000 cm^2 and the surface of 2 m rod is roughly 1,250 cm^2. This gives $R_{stainless}$ = 0.5 Ω and $R_{aluminum}$ = 0, 89 Ω. The potential difference between stainless steel and aluminium is about 0.7 V. When coupled to each other, a galvanic current starts to flow and the driving voltage decreases as the surfaces polarize. At steady state a potential difference of about 0.2 V is normally measured. This gives a current of:

$$I = \frac{\Delta U}{R} = \frac{0.2}{0.89 + 0.5} = 0.144 A$$

Aluminium corrodes with a rate of about 3 kg per year at a leakage current of 1 A. This means that with the leakage current of 0.144 A the theoretical amount of dissolved Aluminium should be approximately 6.48 kg after 15 years. However, the 2 m Aluminium rod weighs only 1.7 kg and should have been corroded away after only 4 years. This can be explained by that either the borehole has not been completely filled with water or the amount of oxidizing agent; oxygen has been limited by diffusion. Another explanation is that a protective passive oxide coating on the surface was formed.

Figure 6-15. *Severe corrosion on the whole surface of the first 2 m of rod (KA3105A) outside the borehole wall.*

Figure 6-16. *Local pitting in the outer aerobic part (KA3385A, area 3, outside section 2).*

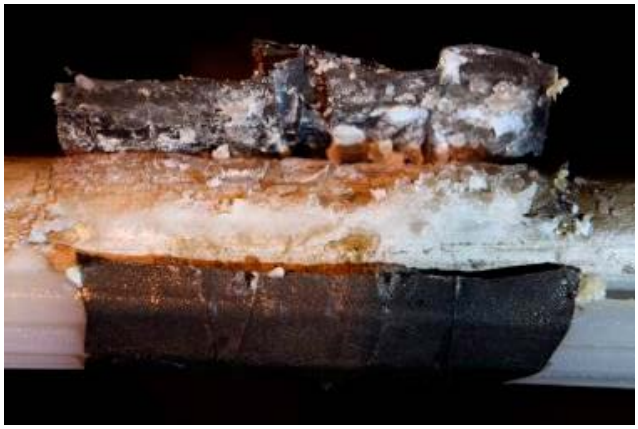

Figure 6-17. *Severe corrosion under PVC-tape in the outer aerobic section (KA3385A, area 3, outside section 2).*

Figure 6-18. *Local pitting in the inner anaerobic zones (KA3385A, area 2, section 2).*

Figure 6-19. *Severe corrosion under the PVC-tape in the inner anaerobic zones (KA3385A and KA3105A).* This photo is from KA3385A, area 1, section 1.

At the end of the casing (Appendix I) large amounts of sulphide precipitation was observed, which indicates that the environment has been anaerobic in this part of the casing. Precipitations of sulphide to the same extent were not observed on adjacent parts of the Aluminium rod. In this more anaerobic part of the casing, H^+ has been the oxidizing agent instead of O_2 in the galvanic corrosion process. This is a clear indication that the corrosion process has also contributed to increased precipitation of sulphide in the borehole. The amount of precipitations is related to heavy galvanic corrosion on Aluminium in an anaerobic environment. Nothing indicates participation of SRB in this corrosion process.

Severe corrosion was found on the rods basically wherever electrical tape had been wrapped around the rods (Figures 6-17 and 6-19). Voluminous corrosion products pushed out around the tape. To explain the mechanism that caused these attacks under the tape, we have taken note of the following observations:

- Precipitation of calcite on stainless steel surfaces in metallic contact with the rods.
- No or marginal precipitation of calcite on stainless steel surfaces isolated from the rods.
- No or negligible galvanic corrosion on freely exposed aluminium surfaces in direct connection to the stainless steel surfaces.

The precipitates of calcite on the stainless steel tubes of the packers show that the water in the vicinity to the steel surface has had an elevated pH. An excess alkalinity always occurs at the cathode surface in a corrosion cell independent of the reduction that takes place (oxygen consumption, hydrogen evolution, etc.). The calcite precipitation therefore indicates that the steel surface acted as cathode. In an anaerobic environment the cathode reaction is the reduction of H_2O or H^+.

No anodic reaction (metal dissolution) corresponding to the cathode reactions had occurred on the surface of the stainless steel. This shows that we have a macro-cell, with separate anode and cathode surfaces. The anodic surfaces of the corrosion cell must therefore be on the aluminium surfaces of the rods. Apart from a few local attacks of pitting on the free aluminium surfaces, all the corrosion was observed under the PVC-tape. If corrosion is to be classified as a pure galvanic corrosion attack it should primarily be generated on the parts of the rods adjacent to the stainless steel tubes, as in the case of galvanic corrosion in the stainless steel casing in bore hole KA3105A. It can therefore be concluded that we observe a different corrosion process than a pure galvanic corrosion.

We believe that the following corrosion process has occurred. The Aluminium rod has initially functioned as anode surface in a galvanic corrosion cell with the stainless steel tubes of the packer as the cathode. Relatively soon, however, the environment under the tape will be unfavourable for the cathode reaction as the oxidizing agents will be depleted (see below). The attack under the PVC-tape can be characterized as deposit corrosion. When the corrosion starts, the anode and cathode surfaces are small and evenly distributed over the Aluminium surface under the tape, see Figure 6-20. The reduction taking place at the cathode surfaces causes a depletion of oxidizing agents under the tape. Nature, however, is inventive and strives to break down metals. Outside the deposit the environment is not depleted of oxidizing agents and new agents is more easily supplied by diffusion. By moving the cathode reaction to the area outside the tape, the corrosion process can proceed despite the absence of oxidizing agents under the PVC-tape (Figure 6-20). If SRB were present and active under the PVC-tape, the oxidizing agent could be sulphide; however in the present study there are no data to support or deny such theory.

The Aluminium surfaces outside of the deposit (tape) are, however, in turn anodic to the stainless steel tubes why the cathode reaction will be moved to these surfaces. Corrosion attack i.e. the anodic reaction, which requires no oxidizing agent will proceed under the PVC-tape. This is why we refer to the corrosion process to be a mixture of deposit corrosion and galvanic corrosion, see Figure 6-21.

Precipitation of calcite has not occurred on the stainless steel clamping rings packer connection, see Figure 6-22. These rings are not in contact with the aluminium rods and are therefore not taking part in the above described corrosion cell. The fact that the rings are isolated prohibits cathode reactions to take place on the metal surface and therefore there is no increase in pH and precipitation of calcite, which is a support for the above suggested theory.

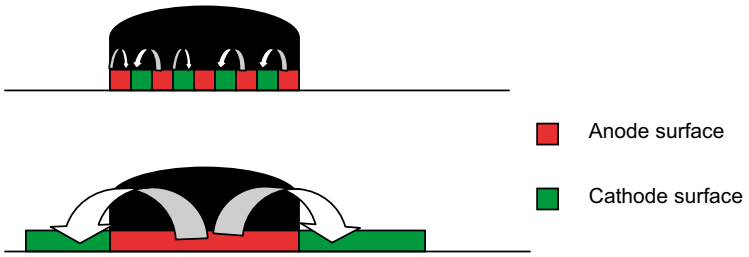

Figure 6-20. *Principle mechanism for deposit corrosion. After an initial uniform attack the corrosion is transformed into a local attack under the deposit.*

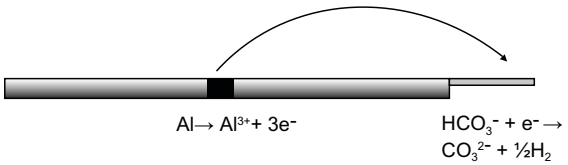

Figure 6-21. *Combined deposit and galvanic corrosion with the anode on Aluminium under the PVC tape and the cathode on stainless steel tubes.*

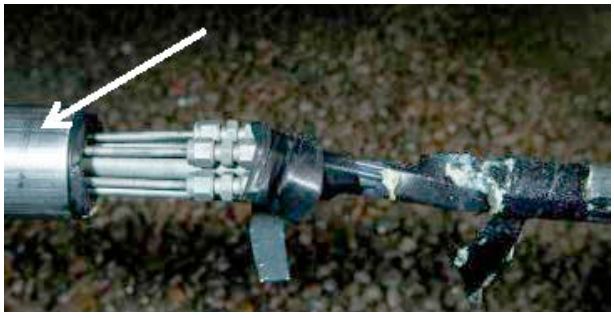

Figure 6-22. *Lack of calcite precipitation on stainless steel clamping ring.*

The oxidizing agent (H^+) originally existing under the tape can have been produced by SRB. The environment under the tape should namely be good prospects for high SRB activity, referring to its stagnant conditions and nutrition, in the form of the plasticizer in PVC. That SRB can use the plasticizer as nutrition has been reported in the literature (Tsuchida et al. 2011). The PVC-tape should even be considered as a huge source of nutrition for the SRB, since the material consists of 50% plasticizers (or more). Furthermore, the PVC tape extracted from the bore holes was very stiff and has significant loss of plasticizer. The polyamide tubes do also contain plasticizers, however not in the same contents as the PVC-tape, however it is important to not neglect that the plasticizer in the polyamide tubes might contribute as an additional source over a longer time period. H_2S is known to cause breakdown of passivity. If SRB activity caused increased sulphide concentration under the PVC-tape then this would have contributed to the initiation. After this initial stage, however, the cathode reaction shifted to the stainless steel surfaces of the tubes connected to the packer connection. If bacterial activity is as high on these freely exposed surfaces, SRB may have contributed significantly to corrosion, in the steady state. Otherwise, naturally occurring hydrogen sulphide may be the main fuel in the corrosion process.

The fact that corrosion also was observed under tubes indicates that a possible increased SRB activity under the PVC-tape did not have a significant impact on the corrosion process. In Figure 6-23, we can see that the attacks occurred in the gap between tube and rod but not under the tape In this case the tube was firmly attached to the Aluminium surface, while the tape was not. This indicates that a close gap between the polymer and the Aluminium surface, creating an anode surface in a macro cell, might be more important than that the additives in the polymer (plasticizer) acting as a nutrition.

Regardless of if the observed corrosion attacks have been accelerated by supply of oxidizing agent produced by SRB or not, it is very likely that corrosion has contributed to an increase in precipitation of sulphide in the water (decrease of sulphide in the water). In area 1, section 1, in the borehole KA3385A one of the heaviest attacks under tape was observed. As an average the rod diameter had decreased from 20 to 18.7 mm. The tape wrapped on a length of 50 mm. The volume lost due to corrosion has been estimated to be 2 cm^3, which corresponds to about 5.5 g of Aluminium. Let us assume that the following reactions are included in the corrosion process:

$$Al \rightarrow Al^{3+} + 3e^-$$

$$H_2S + Fe^{2+} + 2\,e^- \rightarrow FeS + H_2$$

2 moles of Aluminium, corresponds to 3 moles of sulphide. 5.5 g of Aluminium is 0.2 moles. These 0.2 moles generates 0.3 moles or 9.6 g sulphide or 26.4 g FeS. This is quite a lot of sulphide. Probably the other proposed cathode reaction dominates, namely:

$$HCO_3^- + e^- \rightarrow CO_3^{2-} + \tfrac{1}{2}\,H_2$$

Produced CO_3^{2-} reacts with Ca^{2+} to form precipitation of calcite $CaCO_3$ on the stainless steel surfaces.

The corrosion has therefore contributed to the precipitation of both FeS and $CaCO_3$. To get an estimation of the magnitude of this contribution it would be interesting to inspect a borehole where all equipment is made of stainless steel and where corrosion do not contribute to the quantity of precipitation.

Figure 6-23. *Corrosion under tubing.*

7 Discussion

This chapter summarizes and discusses the observations of microbiology, hydrochemistry, mineralogy (including stable isotopes) and corrosion from both the circulation experiments and the investigation of borehole equipment. The latter two are restricted to the investigation of borehole equipment. Hydrochemistry and mineralogy are discussed jointly.

7.1 Microbiology

7.1.1 Microbiology in circulation experiment

Three deviations occurred; 1) blocking of the circulation tubing in borehole section KA3110A:1 due to grouting, 2) erroneous labelling of the tubing in borehole KA3385A (which was discovered after some time and corrected) and 3) unintended introduction of small amounts of ethanol into the experiment sections of the two boreholes (regards experiments performed before 2010-10-26). To get the most out of the experiments the data obtained will be considered together with the circumstances that prevailed.

For the data from KA3110A it has to be remembered that all samples taken as section water were in fact a mixture of fracture water and section water except for the samples S1:3 and S2:2 which were fracture water Samples S1:2 and S1:20 were collected from the section water of section 1. Thereafter, 10 section volumes (145 L), was discharged. Sampling of S1:3 and S2:2 followed directly after this discharge. The data for TNC and SRB for fracture water (S1:3 and S2:2), give the same numbers within the standard deviation of the methods. The amount of SRB in fracture water of KA3110A was around 1,000 mL^{-1} both at start and at the end of the *in situ* circulation experiments. The data on acetate and organic carbon together with sulphide show that the ethanol gave an increase in sulphide concentration from April to June 2010. The increase in number of SRB was around 10 times the number in fracture water. After the ethanol was removed, the values went back to the start values. During April and June 2010, the iron concentration decreased from 1.2 mg L^{-1} to between 0.6 and 0.8 mg L^{-1}, possibly due to precipitation with sulphide. Interestingly, the number of IRB increased in section water when ethanol was added, the highest value detected was 2×10^3 mL^{-1}, in sample S1:9. Also the number of AA increased during this period. The conclusion from evaluating the data from KA3110A is that there is a population of SRB in the fracture water of around 1,000 SRB mL^{-1}.This is supported by the results from a MPN of SRB made in 2007, which gave 2,200 SRB mL^{-1} (lower limit 1,000 and upper limit 5,800) (Eydal et al. 2009).

There was only one sample of fracture water collected from borehole KA3385A, S1:3, and in that sample the number of SRB was 13 mL^{-1}. The samples taken in March, April and May 2010 showed no or very small increase in acetate and organic carbon even though ethanol probably was introduced in the borehole like in KA3110A, presumably because the water in section 1 was supplied with fracture water, since water was discharged from the section instead of circulated. When the water was circulated and less diluted by fracture water, resulted in high concentrations of organic carbon and increased numbers of TNC and SRB (samples S1:9, S1:11 and S1:15). In January 2011, sample S2:4, the numbers of TNC and SRB were still high but the organic carbon had decreased almost back to start values. The strong change in concentrations of organic compounds and numbers of microorganisms in KA3385A was likely due to the small volume of section 1, 4.5 L compared to 14.5L in section 1 of KA3110A. Unfortunately there was no sample of fracture water collected at the last sampling occasion. It is therefore unknown if the number of TNC and SRB still were the same as at start in fracture water in KA3385A.

The addition of ethanol to the sections in KA3110A and KA3385A showed that the microbial populations in the two boreholes responded differently to the introduced organic compound. The amount of sulphide that can be produced by oxidation of ethanol to inorganic carbon is given by the following overall reaction,

$$CH_3CH_2OH + 1.5\ SO_4^{2-} \rightarrow 2HCO_3^- + 1.5\ HS^- + 0.5\ H^+ + H_2O$$

In KA3110A, the highest measured concentration of DOC, 148 mg L^{-1}, which equals 6.15 mM of ethanol, would give a maximum sulphide concentration of 9.2 mM or 305 mg L^{-1}. The highest measured sulphide concentration (after discharging the 0.3 L tubing volume) was 106 mg L^{-1}, which is in the range of the calculated sulphide concentrations. In KA3385A, on the other hand, the highest measured DOC concentration was 564 mg L^{-1}, which equals 23 mM of ethanol. If complete oxidation by SRB is presumed, this concentration would theoretically give a sulphide concentration of 35 mM or 1,165 mg L^{-1}. However, in this case, the highest measured sulphide concentration was 26 mg L^{-1} (sample 20576, collected after circulation of 1 L of water). The two examples show that the presence of organic carbon is not the only parameter that determines active sulphate reduction in these borehole sections. A review article (Plugge et al. 2011), presented findings indicating that SRB can have different metabolisms, sulphate-reducing or fermenting. The fermenting metabolism was induced when the amount of organic carbon is high. This is a possible explanation to the observed different conditions in the two borehole sections.

7.1.2 Microbiology in investigation of borehole equipment

The results from microbiological analyses of the different material surfaces showed that there was no significant difference in TNC or SRB numbers between the two installations in the boreholes KA3385A and KA3105A. The only significant difference found in the investigation was that the TNC and numbers of SRB were lower on stainless steel than on the other materials; rubber, aluminium, plastic tubing and the precipitate in connection to tape. Since there were too small amounts of DNA in the samples, it was not possible to identify the species of microorganisms on the equipment. The number of SRB at the corroded aluminium surface beneath the tape is unknown, since no samples were collected from this site.

In the miniature canister experiment (MiniCan), which is a corrosion experiment performed at Äspö HRL, TNC on the copper surface of the canister was about 10 times lower and SRB 10 times higher in comparison with the instrumentation in this study. In the Minican experiment almost the total microbial population on the canister surface was SRB (Hallbeck et al. 2011). The DNA sequencing data from the MiniCan canister gave indications that a part of the microorganisms were SRB species that can use the electrons directly from metal surfaces. The aim of the MiniCan experiment was to study corrosion of the cast iron insert when a hole was introduced in the outer copper canister. The corrosion process resulted in formation of hydrogen gas available for sulphide production.

Previous investigations of the microbial populations, presence of SRB and sulphide production in boreholes were performed both at Laxemar and Äspö surface boreholes (Rosdahl et al. 2011) and at the so called Microbe site in Äspö HRL (Hallbeck and Pedersen 2008a), where groundwater samples and circulation experiments from three different fractures in three boreholes, KJ0052F01, KJ0052F03 and KJ0050F01 showed that there were different numbers of SRB and concentrations of sulphide in the water. In KJ0052F01, the number of SRB was 3.0×10^4 cells mL^{-1} compared to 280 and 30 cells mL^{-1} in KJ0052F03 and KJ0050F01, respectively. The sulphide concentration was at one sampling occasion 0.250 mg L^{-1} in KJ0052F01, 0.006 mg L^{-1} in KJ0052F03 and 0.010 in KJ0050F01. In these systems the volume of the section was kept to a minimum (about 0.3 L) and there were only PEEK material in the instrumentation. These results show that differences in the number of SRB and sulphide concentrations were not coupled to the materials in the borehole. It is still unknown what the key parameters are, but presumably it is the energy sources and substrates for sulphate-reduction that are most important. H_2 is a strong energy source candidate. The measured hydrogen concentration in groundwater from the three microbe boreholes were 40.6 µL L^{-1} in KJ0052F01 but 7.5 and 1.4 µL L^{-1}, respectively, in the boreholes KJ0050F01 and KJ0052F03 However, the sampling and analysis of hydrogen gas is in general coupled to uncertainties.

7.2 Stable isotopes in waters and minerals

7.2.1 Stable isotopes in waters in circulation experiment

The fractionation of $\delta^{34}S$ between dissolved sulphide and sulphate in section water of KA3110A varied between 13.4 and 32.6‰ CDT ($\delta^{34}S_{sulphate}$–$\delta^{34}S_{sulphide}$) and samples with high sulphide

concentration had, as expected, a large fractionation. The fractionation in $\delta^{34}S$ ($\delta^{34}S_{sulphate}$–$\delta^{34}S_{sulphide}$) is less pronounced in two samples from KA3385A (–0.4 and 3.4‰ CDT) compared to KA3110A. After the circulation experiment was completed in KA3385A, samples were collected from the section water and fracture water ($\delta^{34}S_{sulphide}$ –0.5 and –10.7‰ CDT, respectively and 18.6 and 20.2‰ CDT, respectively). This indicates that the smaller $\delta^{34}S_{sulphate}$–$\delta^{34}S_{sulphide}$ in the section water may be due to the higher sulphide values (maybe higher sulphide production) in the section compared with the fracture water.

There was an indicated higher degree of fractionation of carbon isotopes in KA3385A than in KA3110A. This could be due to the presence of ethanol and a smaller section volume (less dilution and higher concentration of ethanol) in KA3385A. It is especially distinct that $\delta^{13}C$ is low after several months without discharging water from the section (2011-01-20), while in KA3110A the $\delta^{13}C$ signature is more similar in the section and fracture water. The $\delta^{13}C$ signature in organic carbon (DOC) is in the same order of magnitude as the carbon from oil produced plastics e.g. the tape (about –29‰).

7.2.2 Stable isotopes in waters and minerals in the investigation of borehole equipment

Presence of pyrite (FeS_2) and iron monosulphide (FeS) on all types of material investigated (stainless steel packer connections, Aluminium-rods, Tecalan tube and even beneath the tape) is a strong indication of prevailing reducing conditions and bacterial sulphate reduction in all of the packed off sections ever since the equipment was installed in 1995, shortly after drilling of the boreholes. The amounts of crystals suitable for analysis were however small. Although no FeS could be analysed, the $\delta^{34}S$ values of pyrite are also representative for FeS, because fractionation of sulphur isotopes is small or insignificant during both precipitation of FeS from H_2S or HS^- (Böttcher et al. 1998) and transformation of FeS to FeS_2 (Wilkin and Barnes 1996). In contrast, during microbial reduction of sulphate by SRB fractionation is commonly large (Goldhaber and Kaplan 1975, Canfield 2001a, Wortmann et al. 2001, Sim et al. 2011) because SRB favour ^{32}S over ^{34}S (Canfield 2001a, Seal 2006), although occasionally fractionation can be as low as 2‰ (Berner et al. 1985, Brüchert et al. 2001, Canfield 2001b, Detmers et al. 2001)).

The overall markedly higher $\delta^{34}S_{sulphate}$ than $\delta^{34}S_{sulphide}$ in the section water and in the fracture water is a clear indication of influence of SRB. The elevated $\delta^{34}S_{sulphate}$ values (up to 28.3‰, compared to deep saline groundwater ~ +10‰, and Baltic Sea water 19–20‰) are in line with earlier measurements of indicatively SRB-influenced groundwaters in the upper 100–400 m at Äspö (Wallin 2011). The systematic difference in $\Delta\delta^{34}S_{sulphate-sulphide}$ between the fracture water and the section water is enigmatic but may be due to activity of different microbial species in the fractures and in the section, as fractionation during bacterial sulphate reduction can vary considerably depending on the species involved (Detmers et al. 2001) but may also be due to other factors such as sulphate supply and reduction rate which also influence the fractionation (Canfield 2001b). It is for instance reasonable to believe that the section water was exchanged to a larger extent during sampling than the fracture water, which may have affected the fractionation and resulted in a lower level of fractionation in sulphide. Another possible explanation is that the sulphate reduction activity is higher in the fracture than in the section. However, since the sulphide concentration is apparently lower in the fracture, this would imply that sulphide is removed from the water before or during sampling.

Pyrite samples from both of the boreholes showed similar maximum range in $\delta^{34}S$, although the range varied between different packed off sections in the boreholes (> 50‰ in three sections, 27‰ in one section and 5.2‰ in one – not thought to be representative (Figure 6-8). The increase in $\delta^{34}S$ values during crystal growth in many crystals shows that the bacterial sulphate reduction has proceeded in a (semi-closed) system where the rate of sulphate consumption by SRB exceeded the rate of sulphate supplied by advection plus diffusion, which lead to progressively heavier $\delta^{34}S$ in pyrite and residual sulphate as precipitation proceeded (i.e. Rayleigh distillation, (Ohmoto and Rye 1979, McKibben and Eldridge 1989, 1994). The generally small range in $\delta^{34}S$ values within some single pyrite crystals indicates that they reflect precipitation at different phases of the Rayleigh distillation process. Alternatively, the pyrite crystals may have precipitated at different events, reflecting

changes in conditions in the borehole sections due to previous sampling occasions (and perhaps during ethanol injection, which however is only a limited time period in the history of the borehole), which may have resulted in the replacement of the stagnant, sulphate-depleted water with high $\delta^{34}S_{sulphate}$ by inflowing of sulphate-rich water (low $\delta^{34}S_{sulphate}$) from nearby fractures. In addition, this may partly be a polishing effect; crystals are of different size and some fractions may thus not have been polished to the centre of the crystal. Consequently, for these crystals, transect analyses will represent the same growth layer in the cubic pyrite, resulting in measurement of relatively uniform $\delta^{34}S$ values.

The higher $\delta^{34}S$ values in the pyrite than in the groundwater are unexpected because pyrite produced as a result of SRB activity will always have lower $\delta^{34}S$ values than the corresponding groundwater. In order to precipitate this pyrite, the $\delta^{34}S_{sulphate}$ values must have been well above 35‰. These very high pyrite $\delta^{34}S$ values may represent precipitation in local micro-environments in the borehole sections where the waters have been stagnant and where Rayleigh distillation during SRB-induced pyrite precipitation has led to a local progressive increase in $\delta^{34}S_{sulphate}$ values, compared to the mean (and measured) value of the water in the whole section. The very light pyrite $\delta^{34}S$ values (down to –40.8‰) show that the fractionation during bacterial sulphate reduction has been large. The lightest $\delta^{34}S$ values would require larger fractionation (~ 62‰) than commonly identified for SRB (~ 46‰) (Kaplan and Rittenberg 1964, Canfield 2001a) in order to be accomplished from an initial $\delta^{34}S_{SO4}$ pool of +22.7‰ (the current $\delta^{34}S_{sulphate}$ in the section water), but is still within the range of fractionations in natural settings and laboratory (Wortmann et al. 2001, Sim et al. 2011).

The preferential location of calcite precipitates to the steel bars at the packer connections can be due to corrosion-induced increase of the pH, which has led to local supersaturation with respect to calcite and consequently precipitation. Calcite precipitation may also be an effect of SRB activity, because SRB may oxidize organic matter to hydrogen sulphide and CO_2,which ultimately leads to an increase in the amount of carbonate ions in solution and consequently an increase in the calcite saturation index (SI) (Visscher et al. 2000, Baumgartner et al. 2006). Limited positive influence on the SI may also be due to differences in pCO_2 between fractures in the rock volume and the borehole. But none of the latter explanations, as oppose to corrosion-induced precipitation, can explain why calcite is most common on the stainless steel, which hosted lower number of SRB cells than other types of equipment (see microbiology Section 7.1.2).

The generally lower $\delta^{13}C$ values in calcite compared to the waters may reflect influence of microbial activity, because microorganisms can oxidize carbon (cf. Hoefs 2004), and during this step, fractionation of the carbon isotopes can occur, as a rule leading to precipitation of $\delta^{13}C$-depleted calcite, as shown in studies elsewhere (Andres et al. 2006, Breitbart et al. 2009, Brady et al. 2010). For instance, carbon isotope fractionation during metabolism of lactate by *Desulfovibrio desulfuricans* have been shown to result in a depletion of $\delta^{13}C$ by 5.5 to 12.8‰ in the released CO_2 (Kaplan and Rittenberg 1964). Alternatively carbon from the tape ($\delta^{13}C$: –29.2 to –28.8‰) or possibly carbon from other plastic materials (tubing, rubber) may also have influenced the low $\delta^{13}C$ in the calcite and the generally lower $\delta^{13}C$ in the section water compared to the fracture water. The influence of ethanol in KA3385A is another possible explanation (Section 5.3) as well as oxidation of carbon produced from autotrophic, phototrophic or lithotrophic metabolism. As shown in Chapter 6.3.7, SRB-related sulphate reduction can theoretically take place by consuming natural DOC only. The PVC can provide some organic carbon as well. Up to 50% of the sulphide production can have taken place using plasticizer. DOC is constantly consumed, but also produced (PVC is stiff due to loss of plasticizers which indicates addition of DOC), so the fact that there is still significant amounts DOC in the section water do not tell whether DOC has been suitable as nutrients for SRB or not. Hydrogen from corrosion can alone explain only 25% of the corrosion. Therefore it is likely that naturally occurring DOC, DOC from plasticizer material and hydrogen from corrosion and natural sources all can have been important nutrients for SRB, thus contributing to sulphide production in stagnant borehole water.

The different groundwater $\delta^{18}O$ values between the two boreholes partly reflect the different water types. Water with a deep saline component (such as in KA3385A: 6,800 ± 300 mg L^{-1} Cl) commonly has lower $\delta^{18}O$ values (–11 to –10‰ V-PDB) than the less saline water type in KA3105A

($\delta^{18}O$: –10 to –9‰ V-PDB, ~ 3,000 ± 300 mg L^{-1} Cl, based on data from adjacent KA3110A) (data extracted from SKB database Sicada), and this small borehole-related difference is also reflected in the $\delta^{18}O$ values of most calcites. Regarding the salinity, the dominantly scalenohedral crystal habit has in earlier studies (e.g. at Laxemar closeby) been proposed to indicate precipitation from saline or brackish water (Milodowski et al. 1997, 2005), and similar relation is seen in these fairly saline borehole sections; the more saline water in KA3385A, correlates with calcites with generally more elongated crystals compared to in KA3105A (although there is slight variation in crystal habit in the latter borehole). The slightly lower groundwater $\delta^{18}O$ in section 2 (–10.1 to –10.0‰) of KA3105A compared to sections 3 and 4 (–9.4 to –8.9‰) also correlates with a higher salinity in section 2 (2,800 mg L^{-1} Cl) compared to 3 and 4 (~ 2,300 mg L^{-1} Cl).

Some calcites show lower $\delta^{18}O$ than expected for precipitates from the sampled water. Lower $\delta^{18}O$ in calcite than expected could also be due to high precipitation rates (Dietzel et al. 2009), which has certainly prevailed due to the local increase in pH at the stainless steel. Most of the calcite samples did however show predicted $\delta^{18}O$ values, which indicates that SRB activity has not significantly influenced the $\delta^{18}O$ signature in most of these local systems.

Mineralogical and isotopic observations can be summarised as:

- Overall, the results from the two boreholes studied showed relatively similar features regarding secondary mineralogy, groundwater chemistry evolution between fracture and section water as well as the stable isotope ratios in water and minerals.
- Precipitates of calcite, amorphous FeS, pyrite, Al-oxyhydroxides (close to tape), biofilm (close to tape), Si-rich precipitates (close to tape), salts (Na/Ca-Cl) and small amounts of barite have been identified on the equipment.
- The amounts of calcite were higher on the stainless steel parts indicating an association between calcite precipitation and the cathode reactions at these surfaces, i.e. an increase in pH leading to saturation of calcite.
- The $\delta^{34}S$ in the dissolved sulphide and sulphate showed SRB-activity in both section water and fracture water, although there was a slight, but significant difference between the $\delta^{34}S$ signatures, which is still unexplained. These features were similar in both of the boreholes and points towards a higher fractionation in the fracture water, although frequent discharge of water in the section (during the sampling process) may have resulted in a lower fractionation in the section water due to mixing with incoming fracture water.
- The stable isotope analyses of the pyrite show large variations in $\delta^{34}S$ between grains but also within single grains; with progressively higher $\delta^{34}S$ with growth: $\delta^{34}S_{rim} > \delta^{34}S_{centre}$. Some of the pyrite grains showed very high $\delta^{34}S$ values which suggest precipitation in local micro-environments in the borehole sections where the waters have been close to stagnant and the sulphide production have been faster than the supply of sulphate causing progressive increase in $\delta^{34}S_{sulphide}$ values in the produced sulphide.
- Calcite showed $\delta^{18}O$ values within the range expected for precipitates from the current section and fracture water at the current water temperatures. However, in a few cases, the $\delta^{18}O$ values in calcite were lower than expected, probably due to very fast precipitation.
- $\delta^{13}C$ values in calcite were either within or lower than the range expected for precipitates from the groundwater $\delta^{13}C$ composition. The lower values may be due to local fractionation of carbon during oxidation of organic matter to HCO_3^- which is eventually incorporated into calcite. There may be several, more or less likely explanations for this; 1) $\delta^{13}C$-depleted organic C from the decomposed tape and related plasticizers may also explain the depleted $\delta^{13}C$ signal in HCO_3^- and calcite (locally to lower values in calcite than in the water in the whole section), 2) $\delta^{13}C$-depleted carbon originates from oxidation of organic material that was produced from autotrophic, phototrophic or lithotrophic metabolism. 3) Oxidation of ethanol. It cannot be concluded from this study which explanation/s is most likely to apply in this case.

7.3 Corrosion

Corrosion observations can be summarised as:

- The corrosion of Aluminium under the PVC-tape is considered to be caused by a combination of galvanic corrosion and deposit corrosion.
- The corrosion of Aluminium has probably led to increased precipitation of sulphide as a consequence of the alkalization due to the cathode reaction on the stainless steel surfaces.
- Corrosion may have been stimulated by the SRB, but the required oxidizing agent (H^+ in H_2S/HS^-) may also have existed naturally in the rock water, in the form of H_2CO_3.
- Increased SRB activity under the tape is possible but this may only have had a marginal effect on the corrosion and only during an initial stage of the corrosion process.
- SRB activity and/or dissolved sulphide may have been influenced in three ways by the presence of the corrosion or any degradation of plastics in the equipment:
  - H_2 produced at the cathode act as nutrient for SRB.
  - PVC plasticizers supply organic carbon for SRB metabolism.
  - Precipitation of sulphide as FeS at cathode sites.

8 Project conclusions

The circulation experiment suffered from unexpected problems and uncertainties concerning the borehole installations including the tubing and also some unconformities during sampling, therefore it is not possible to make a thorough comparison and evaluation of what happened in the different borehole sections. In addition, it was not possible to compare the equipment in KA3385A and KA3110A due to grouting in KA3110A. From the experiences gained in this study some conclusions may be drawn regarding both the results and the methods:

- Before performing any kind of sampling activity from a borehole section it is important to find out if the instrumentation is functioning properly. A simple way to check for defects is to study pressures measurements while opening the valves of the section to be sampled as well as the adjacent sections. However, in some cases (such as this), it is justified to perform a more advanced functionality test; a so called dilution test to determine the functionality of the instrumentation.
- An adequate comparison of two borehole sections requires also estimations of the groundwater flow in transecting fractures. Performance of a dilution test gives this information on hydrogeological properties.
- It is clear from this investigation that ethanol may be used as an energy source for SRB. Therefore ethanol should not be used for sterilizing purposes in studies involving microbiological analyses and sulphide, unless under intended and controlled conditions.
- The results presented in this report are valid for core drilled boreholes in a tunnel and may not necessarily fully apply for boreholes drilled from the surface. These boreholes have a different kind of instrumentation (described in detail in Rosdahl et al. 2011) and other conditions concerning supply of nutrients occur.
- Groundwater from transecting fractures must be compared, and in these, different compositions for KA3110A and KA3385A were observed (i.e. higher number of SRB and higher concentrations of DOC and Fe^{2+}, but also higher H_2 in fracture water from KA3110A). Some of these differences may explain the higher sulphide concentrations in fracture water from KA3110A, although the processes are not made clear from this investigation.

It was in most cases impossible to determine δ^2H in Hydrogen gas due to low concentrations of dissolved hydrogen gas in the groundwater. It may require an improved sampling technique as well as a development of more advanced analysis techniques to succeed.

- The results from the two boreholes studied showed relatively similar features regarding secondary mineralogy, corrosion characteristics, and microbes on the installation surfaces and groundwater chemistry evolution between fracture and section water. Also the stable isotope ratios in water and minerals showed the same evolution.
- Scoping calculations show that neither the plasticizers in the PVC tape nor the H_2 gas produced by corrosion can, alone, account for the sulphide produced in the section water. Although it is possible that both have acted as energy sources for SRB it is not likely that the instrumentation alone is responsible for elevated sulphide concentrations in core drilled boreholes. It may be the case that the DOC in the groundwater is high enough to account for the sulphide production in the section, but obviously the DOC that originally was introduced into the rock with recharging fresh waters at least partly has not been attractive as an energy source for microbial processes. It could not be concluded from the analyses of $\delta^{13}C$ in water, precipitated calcite and dissolved gases (methane and carbon dioxide) what processes were involved in the production of carbon dioxide and dissolved carbonate. The fractionation of both $\delta^{13}C$ and δ^2H in the methane could be interpreted as the result of several processes. One possibility is that the methane is derived from acetate fermentation. One possibility for the origin of the CO_2, other than oxidation of organic matter, is microbial oxidation of methane. Addition of ethanol in KA3385A and lack of isotope data for precipitated calcite and gases in KA3110A and KA3105A make the interpretation and formulation of a theory impossible.

- The interaction between the groundwater and the material of the instrumentation has modified the chemical environment in the borehole sections, however, if and in what way SRB is involved or affected has not been clarified by the present study.
- The analyses of stable isotope $\delta^{34}S$ in dissolved sulphide and sulphate show that sulphide production is on-going in the section as well as in the fracture. It cannot be concluded from this study whether the rate of production is higher or lower in the fractures than in the sections.
- The composition of microbes in a borehole/fracture may tell us the potential for sulphide production and what energy source may be used to produce sulphide. If the potential is there and the right substrate is present or added it may give rise to sulphide production. However, it remains to be established if and why the sulphide concentration reaches a higher level in a borehole section than in the corresponding fracture.
- At the site investigations no correlation between number of SRB and sulphide concentrations was detected, and sulphate reduction was confirmed. The present investigations show that instrumentation and sampling affect the sulphide concentrations and similar processes took place in each borehole independent of water composition of these specific boreholes. The process indicated in the section water reflects ongoing processes mainly, because the sulphide content in the fracture water is significantly lower than in the borehole section water. Sulphide production may occur in the fracture water as well, because there is dissolved sulphide in this water, which also has a difference between sulphate and sulphide in terms of $\delta^{34}S$ that can only be produced by SRB. Implications for site investigations include that several different analytical methods, like in this study, apart from hydrochemical data only, adds to the understanding of ongoing processes. However, the water sampling methods used influence the sulphide concentration measured.

References

SKB's (Svensk Kärnbränslehantering AB) publications can be found at www.skb.se/publications.

Andres M S, Sumner D Y, Reid R P, Swart P K, 2006. Isotopic fingerprints of microbial respiration in aragonite from Bahamian stromatolites. Geology 34, 973–976.

Apps J A, van der Kamp P C, 1993. Energy gases of abiogenic origin in the Earth's crust. In Howell D G (ed). The future of energy gases. Washington, DC: United States Government Printing Office. (U.S. Geological Survey Professional Paper 1570), 81–132.

Badziong W, Thauer R K, 1978. Growth yields and growth rates of *Desulfovibrio vulgaris* (Marburg) growing on hydrogen plus sulphate and hydrogen plus thiosulphate as the sole energy sources. Archives of Microbiology 117, 209–214.

Baumgartner L K, Reid R P, Dupraz C, Decho A W, Buckley D H, Spear J R, Przekop K M, Visscher P T, 2006. Sulfate reducing bacteria in microbial mats: changing paradigms, new discoveries. Sedimentary Geology 185, 131–145.

Berner R A, De Leeuw J W, Spiro B, Murchison D G, Eglinton G, 1985. Sulphate reduction, organic matter decomposition and pyrite formation [and discussion]. Philosophical Transactions of the Royal Society of London 315, 25–38.

Boetius A, Ravenschlag K, Schubert C J, Rickert D, Widdel F, Gieseke A, Amann R, Jørgensen B B, Witte U, Pfannkuche O, 2000. A marine microbial consortium appparently mediating anaerobic oxidation of methane. Nature 407, 623–626.

Brady A, Slater G F, Omelon C R, Southam G, Druschel G, Andersen A, Hawes I, Laval B, Lim D S S, 2010. Photosynthetic isotope biosignatures in laminated micro-stromatolitic and non-laminated nodules associated with modern, freshwater microbialites in Pavilion Lake, B.C. Chemical Geology 274, 56–67.

Breitbart M, Hoare A, Nitti A, Siefert J, Haynes M, Dinsdale E, Edwards R, Souza V, Rohwer F, Hollander D, 2009. Metagenomic and stable isotopic analysis of modern freshwater microbialites in Cuatro Ciénegas, Mexico. Environmental Microbiology 11, 16–34.

Controls on stable sulfur isotope fractionation during bacterial sulfate reduction in Arctic sediments. Geochimica et Cosmochimica Acta 65, 763–776.

Böttcher M E, Smock A M, Cypionka H, 1998. Sulfur isotope fractionation during experimental precipitation of iron(II) and manganese(II) sulfide at room temperature. Chemical Geology 146, 127–134.

Canfield D E, 2001a. Biogeochemistry of sulphur isotopes. Reviews in Mineralogy 43, 607–636.

Canfield D E, 2001b. Isotope fractionation by natural populations of sulfate-reducing bacteria. Geochimica et Cosmochimica Acta 65, 1117–1124.

Chi Fru E, 2008. Constraints in the colonization of natural and engineered subterranean igneous rock aquifers by aerobic methane-oxidizing bacteria inferred by culture analysis. Geobiology 6, 365–375.

Cord-Ruwisch R, 2000. Microbially influenced corrosion of steel. In Lovley D E (ed). Environmental microbe–metal interactions. Washington, DC: ASM Press, 159–173.

Cross M M, Manning D A C, Bottrell S H, Worden R H, 2004. Thermochemical sulphate reduction (TSR): experimental determination of reaction kinetics and implications of the observed reaction rates for petroleum reservoirs. Organic Geochemistry 35, 393–404.

Crowe D E, Vaughan R G, 1996. Characterization and use of isotopically homogenous standards for in situ laser microprobe analysis of $^{34}S/^{32}S$ ratios. American Mineralogist 81, 187–193.

Detmers J, Brüchert V, Habicht K S, Kuever J, 2001. Diversity of sulfur isotope fractionations by sulfate-reducing procaryotes. Applied and Environmental Microbiology 67, 888–894.

Dietzel M, Tang J, Leis A, Köhler S, 2009. Stable isotopic fractionation during inorganic calcite precipitation – Effects of temperature, precipitation rate and pH. Chemical Geology 268, 107–115.

Dihn H T, Kuever J, Mußmann M, Hassel A W, Startmann M, Widdel F, 2004. Iron corrosion by novel anaerobic microorganisms. Nature 427, 829–832.

Drake H, Tullborg E-L, 2009. Paleohydrogeological events recorded by stable isotopes, fluid inclusions and trace elements in fracture minerals in crystalline rock, Simpevarp area, SE Sweden. Applied Geochemistry 24, 715–732.

Drake H, Tullborg E-L, Mackenzie A B, 2009a. Detecting the near-surface redox front in crystalline bedrock using fracture mineral distribution, geochemistry and U-series disequilibrium. Applied Geochemistry 24, 1023–1039.

Drake H, Tullborg E-L, Page L, 2009b. Distinguished multiple events of fracture mineralisation related to far-field orogenic effects in Paleoproterozoic crystalline rocks, Simpevarp area, SE Sweden. Lithos 110, 37–49.

Drake H, Tullborg E-L, Hogmalm K J, Åström M E, 2012. Trace metal distribution and isotope variations in low-temperature calcite and groundwater in granitoid fractures down to 1 km depth. Geochimica et Cosmochimica Acta 84, 217–238.

Drake H, Åström M E, Tullborg E-L, Whitehouse M, Fallick A E, 2013. Variability of sulphur isotope ratios in pyrite and dissolved sulphate in granitoid fractures down to 1 km depth – evidence for widespread activity of sulphur reducing bacteria. Geochimica et Cosmochimica Acta 102, 143–161.

Emrich K, Ehhalt D H, Vogel J C, 1970. Carbon isotope fractionation during the precipitation of calcium carbonate. Earth and Planetary Science Letters 8, 363–371.

Enning D, Venzlaff H, Garrelfs J, Dinh H T, Meyer V, Mayrhofer K, Hassel A W, Stratmann M, Widdel F, 2012. Marine sulfate-reducing bacteria cause serious corrosion of iron under electroconductive biogenic mineral crust. Environmental Microbiology 14, 1597–1803.

Eydal H S C, Jägevall S, Hermansson M, Pedersen K, 2009. Bacteriophage lytic to *Desulfovibrio aespoeensis* isolated from deep groundwater. The ISME Journal 3, 1139–1147.

Faure G, Mensing T M, 2005. Isotopes: principles and applications. 3rd ed. Hoboken, NJ: John Wiley & Sons.

Gimeno M J, Auqué L F, Gómez J B, 2006. PHREEQC modeling. In Hydrochemical evaluation. Preliminary site description. Laxemar subarea – version 2.1. SKB R-06-70, Appendix 3, 175–210.

Gimeno M J, Auqué L F, Gómez J B, Acero P, 2009. Water–rock interaction modelling and uncertainties of mixing modelling. Site descriptive modeling, SDM-Site Laxemar. SKB R-08-110, Svensk Kärnbränsehantering AB.

Goldhaber M B, Kaplan I R, 1975. Controls and consequences of sulphate reduction rates in recent marine sediments. Soil Science 119, 42–55.

Greenberg A E, Trussell R R, Clesceri L S, 1985. Standard methods for the examination of water and wastewater. American Public Health Ass. American Water Works Ass. Water Polution Control Fed. American Public Healh Association, Washington DC.

Gustafsson E, 2002. Bestämning av grundvattenflödet med utspädningsteknik. Modifiering av utrustning och kompletterande mätningar. SKB R-02-31, Svensk Kärnbränslehantering AB. (In Swedish.)

Hallbeck L, Pedersen K, 2008a. Characterization of microbial processes in deep aquifers of the Fennoscandian shield. Applied Geochemistry 23, 1796–1819.

Hallbeck L, Pedersen K, 2008b. Explorative analyses of microbes, colloids, and gases together with microbial modelling. Site description model. SDM-Site Laxemar. SKB R-08-109, Svensk Kärnbränslehantering AB.

Hallbeck L, Edlund J, Eriksson L, 2011. Microbial analyses of groundwater and surfaces during the retrieval of experiment 3, A04, in MINICAN. SKB P-12-01, Svensk Kärnbränslehantering AB.

Hoefs J, 2004. Stable isotope geochemistry. 5th ed. Berlin: Springer-Verlag.

Kalinowski B E (ed), 2009. Background complementary hydrogeochemical studies. Site descriptive modelling, SDM-Site Laxemar. SKB R-08-111, Svensk Kärnbränslehantering AB.

Kaplan I R, Rittenberg S C, 1964. Carbon isotope fractionation during metabolism of lactate by *Desulfovibrio desulfuricans*. Journal of General Microbiology 34, 213–217.

Kotelnikova S, Pedersen K, 1997. Evidence for methanogenic *Archaea* and homoacetogenic *Bacteria* in deep granitic rock aquifers. FEMS Microbiology Reviews 20, 339–349.

Laaksoharju M, Smellie J, Tullborg E-L, Gimeno M, Hallbeck L, Molinero J, Waber N, 2008. Bedrock hydrogeochemistry Forsmark. Site descriptive modelling, SDM-Site Forsmark. SKB R-08-47, Svensk Kärnbränslehantering AB.

Laaksoharju M, Smellie J, Tullborg E-L, Wallin B, Drake H, Gascoyne M, Gimeno M, Gurban I, Hallbeck L, Molinero J, Nilsson A-C, Waber N, 2009. Bedrock hydrogeochemistry Laxemar. Site descriptive modelling, SDM-Site Laxemar. SKB R-08-93, Svensk Kärnbränslehantering AB.

Lin L-H, Slater G F, Sherwood Lollar B, Lacrampe-Couloumbe G, Onstott T C, 2005. The yield and isotopic composition of radiolytic H_2, a potential energy source for the deep subsurface biosphere. Geochimica et Cosmochimica Acta 69, 893–903.

Lydmark S, Hallbeck L, 2011. Results report. Sampling and analyses of gases andmicroorganisms in the water from MINICAN in 2007, 2008 and 2010. SKB P-11-32, Svensk Kärnbränslehantering AB.

Lösekann T, Knittel K, Nadalig T, Fuchs B, Niemann H, Boetius A, Amann R, 2007. Diversity and abundance of aerobic and anaerobic methane oxidisers at the Haakon Mosby mud volcano, Barents Sea. Applied and Environmental Microbiology, 73, 3348–3362.

Machel H G, 1987. Saddle dolomite as a by-product of chemical compaction and thermochemical sulfate reduction. Geology 15, 936–940.

Machel H G, Krouse H R, Sassen R, 1995. Products and distinguishing criteria of bacterial and thermochemical sulfate reduction. Applied Geochemistry 10, 373–389.

Madigan M T, Martinenko J M, 2006. Brock biology of microorganisms. 11th ed. Upper Saddle River, NJ: Pearson Prentice Hall.

Mariotti A, Germon J C, Hubert P, Kaiser P, Letolle E, Tardieux A, Tardieux P, 1981. Experimental determination of nitrogen kinetic isotope fractionation some principles; illustration for the denitrification and nitrification process. Plant and Soil 62, 413–430.

Mathurin F A, Åström M E, Laaksoharju M, Kalinowski B E, Tullborg E-L, 2012. Effect of tunnel excavation on source and mixing of groundwater in a coastal granitoidic fracture network. Environmental Science & Technology 46, 12779−12786.

McKibben M A, Eldridge C S, 1989. Sulfur isotopic variations among minerals and aqueous species in the Salton Sea geothermal system; a SHRIMP ion microprobe and conventional study of active ore genesis in a sediment-hosted environment. American Journal of Science 289, 661–707.

McKibben M A, 1994. Micron-scale isotopic zoning in minerals: a record of large-scale geologic processes. Mineralogical Magazine 58A, 587–588.

Milodowski A E, Gillespie M R, Metcalfe R, 1997. Relationship between mineralogical transformations and groundwater chemistry at Sellafield, N.W. England: a tool for studying Quaternary palaeohydrogeology. In Hendry J P, Carey P F, Parnell J, Ruffell A H, Worden R H E (eds). Geofluids II ’97: Contributions to the second international conference on fluid evolution, migration and interaction in sedimentary basins and orogenic belts, Belfast, 10–14 March 1997. Belfast: The Queens University.

Milodowski A E, Tullborg E-L, Buil B, Gómez P, Turrero M-J, Haszeldine S, England G, Gillespie M R, Torres T, Ortiz J E, Zachariáš J, Silar J, Chvátal M, Strnad L, Šebek O, Bouch J E, Chenery S R, Chenery C, Shepherd T J, McKervey J A, 2005. Application of mineralogical, petrological and geochemical tools for evaluating the palaeohydrogeological evolution of the PADAMOT study sites. Padamot Project, Technical Report WP2, UK Nirex Ltd.

Moench A F, 1985. Transient flow to a large-diameter well in an aquifer with storative semiconfining layers. Water Resources Research 21, 1121–1131.

Nilsson A-C (ed), Berg C, Harrström J, Jönsson S, Thur P, Borgiel M, Qvarfordt S, 2010. Forsmark site investigation. Hydrochemical monitoring of groundwaters and surface waters. Results from water sampling in the Forsmark area, January–December 2009. SKB P-10-40, Svensk Kärnbränslehantering AB.

Ohmoto H, Rye R O, 1979. Isotopes of sulfur and carbon. In Barnes H L (ed). Geochemistry of hydrothermal ore deposits. 2nd ed. New York: John Wiley & Sons, 517–612.

O'Leary M H, 1981. Carbon isotope fractionation in plants. Phytochemistry 20, 553–567.

O'Neil J R, Clayton R N, Mayeda T K, 1969. Oxygen isotope fractionation in divalent metal carbonates. Journal of Chemical Physics 51, 5547–5558.

Page I B, 2000. Polyamides as engineering thermoplastic materials. Rapra Review Reports: expert overviews covering the science and technology of rubber and plastics 11, number 1, Rapra Technology Ltd.

Pedersen K, Ekendahl S, Tullborg E-L, Furnes H, Thorseth I, Tumyr O, 1997. Evidence of ancient life at 207 m depth in a granitic aquifer. Geology 25, 827–830.

Pedersen K, Arlinger J, Hallbeck A, Hallbeck L, Johansson J, 2008. Numbers, biomass and cultivable diversity of microbial populations related to depth and borehole-specific conditions in groundwater from depths of 4– 450 m in Olkiluoto, Finland. The ISME Journal 2, 760–775.

Plugge C M, Zhang W, Scholten J C M, Stams A J M, 2011. Metabolic flexibility of sulphate-reducing bacteria. Frontiers in Microbiology 2, 1–8.

Rosdahl A, Pedersen K, Hallbeck L, Wallin B, 2011. Investigation of sulphide in core drilled boreholes KLX06, KAS03 and KAS09 at Laxemar and Äspö. Chemical-, microbiological- and dissolved gas data from groundwater in four borehole sections SKB P-10-18, Svensk Kärnbränslehantering AB.

Sahlstedt E, Karhu J A, Pitkänen P, 2010. Indications for the past redox environments in deep groundwaters from the isotopic composition of carbon and oxygen in fracture calcite, Olkiluoto, SW Finland. Isotopes in Environmental and Health Studies 46, 370–391.

Sandström B, Tullborg E-L, 2009. Episodic fluid migration in the Fennoscandian Shield recorded by stable isotopes, rare earth elements and fluid inclusions in fracture minerals at Forsmark, Sweden. Chemical Geology 266, 126–142.

Sass E, Bein A, Algomi-Labin A, 1991. Oxygen-isotope composition of diagenetic calcite in organic-rich rocks: evidence for ^{18}O depletion in marine anaerobic pore water. Geology 19, 839–842.

Seal R R, 2006. Sulfur isotope geochemistry of sulfide minerals. Reviews in Mineralogy & Geochemistry 61, 633–677.

Sim M S, Bosak T, Ono S, 2011. Large sulfur isotope fractionation does not require disproportionation. Science 333, 74–77.

SIS, 2004. SS 02 81 15: Vattenundersökningar – Bestämning av sulfidkoncentrationen hos renvatten och icke förorenat naturvatten – Kolorimetrisk metod (Determination of sulphide content of pure water and non-polluted natural water – Colorimetric method). Stockholm: Swedish Standards Institute. (In Swedish.)

Smart N R, Rance A P, Reddy B, Fennell P, Winsley R J, 2012. Analysis of SKB MiniCan. Experiment 3. SKB TR-12-09, Svensk Kärnbränslehantering AB.

Strebel O, Böttcher J, Fritz P, 1990. Use of isotope fractionation of sulfate-sulfur and sulfate-oxygen to assess bacterial desulfurication in a sandy aquifer. Journal of Hydrology 121, 155–172.

Truesdell A H, Hulston J R, 1980. Isotopic evidence on environments of geothermal systems. In Fritz P, Fontes J C (eds). Handbook of environmental isotope geochemistry. Vol 1, The terrestrial environment, A. Amsterdam: Elsevier, 179–226.

Tsuchida D, Kajihara Y, Shimidzu N, Hamamura K, Nagese M, 2011. Hydrogen sulphide production by sulphate-reducing bacteria utlilizing additives eluted from plastic resins. Waste Management & Research 29, 594–601.

Tullborg E-L, 2003. Palaeohydrogeological evidences from fracture filling minerals – Results from the Äspö/Laxemar area. In Oversby V M, Werme L O (eds). Scientific basis for nuclear waste management XXVII: symposium held in Kalmar, Sweden, 15–19 June 2003. Warrendale, PA: Materials Research Society. (Materials Research Society Symposium Proceedings 807), 873–878.

Tullborg E-L, Landström O, Wallin B, 1999. Low-temperature trace element mobility influenced by microbial activity – indications from fracture calcite and pyrite in crystalline basement. Chemical Geology157, 199–218.

Tullborg E-L, Drake H, Sandström B, 2008. Palaeohydrogeology: a methodology based on fracture mineral studies. Applied Geochemistry 23, 1881–1897.

Tullborg E-L, Smellie J, Nilsson A-C, Gimeno M J, Auqué L F, Brüchert V, Molinero J, 2010a. SR-Site – Sulphide content in the groundwater at Forsmark. SKB TR-10-39, Svensk Kärnbränslehantering AB.

Tullborg E-L, Smellie J, Nilsson A-C, Gimeno M J, Auqué L F, Wallin B, Blüchert V, Molinero J, 2010b. SR-Site – sulphide content in the groundwater at Laxemar. SKB R-10-62, Svensk Kärnbränslehantering AB.

Visscher P T, Reid R P, Bebout B M, 2000. Microscale observations of sulfate reduction: correlation of microbial activity with lithified micritic laminae in modern marine stromatolites. Geology 28, 919–922.

Wallin B, 2011. Bacterial sulphate reduction and mixing processes at the Äspö Hard Rock Laboratory indicated by groundwater $\delta^{34}S$ isotope signatures. SKB R-11-13, Svensk Kärnbränslehantering AB.

Wallin B, Peterman Z, 1999. Calcite fracture fillings as indicators of paleohydrology at Laxemar at the Äspö Hard Rock Laboratory, southern Sweden. Applied Geochemistry 14, 953–962.

Whitehouse M J, Kamber B S, Fedo C M, Lepland A, 2005. Integrated Pb- and S-isotope investigation of sulphide minerals from the early Archaean of southwest Greenland. Chemical Geology 222, 112–131.

Wilkin R T, Barnes H L, 1996. Pyrite formation by reactions of iron monosulfides with dissolved inorganic and organic sulfur species. Geochimica et Cosmochimica Acta 60, 4167–4179.

Wortmann U G, Bernasconi S M, Böttcher M E, 2001. Hypersulfidic deep biosphere indicates extreme sulfur isotope fractionation during single-step microbial sulfate reduction. Geology 29, 647–650.

Appendix A

Layout of borehole KA3110A

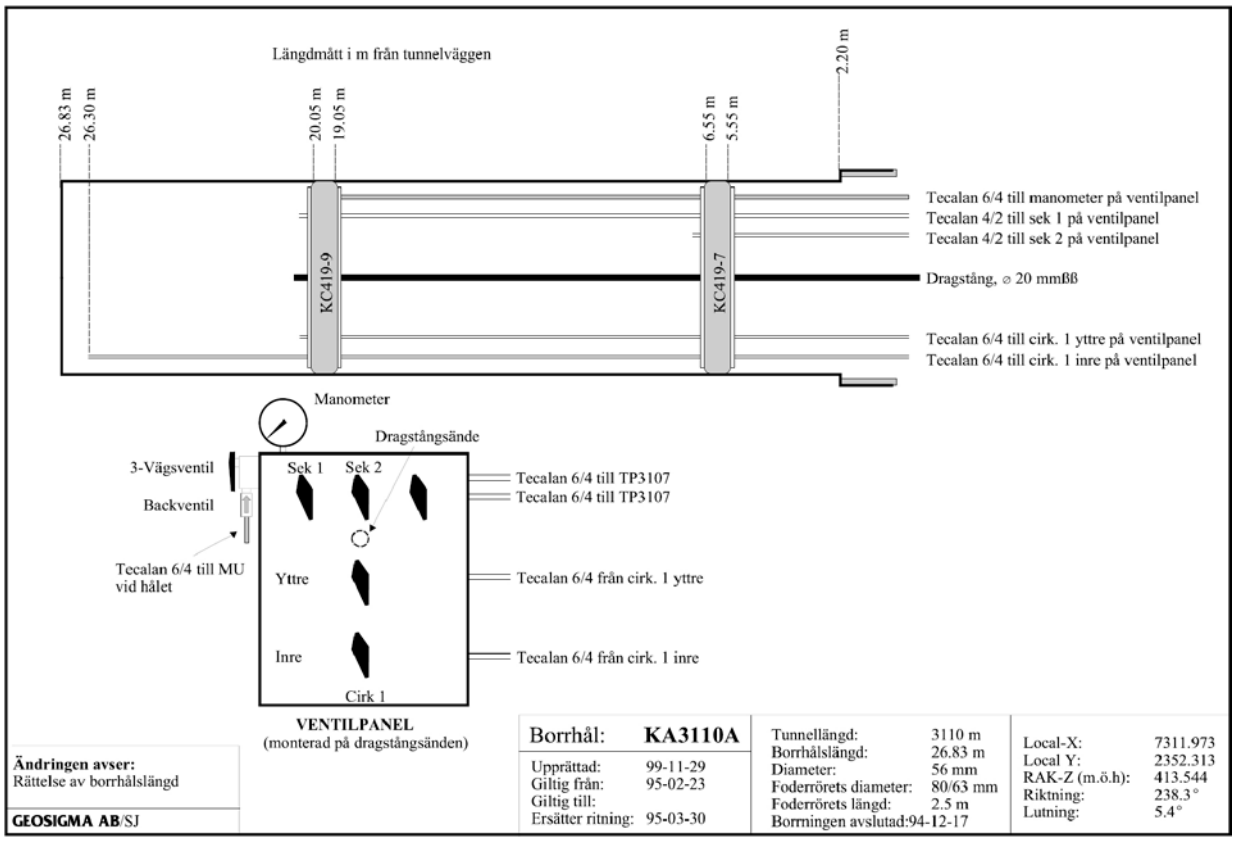

Layout of borehole KA3385A

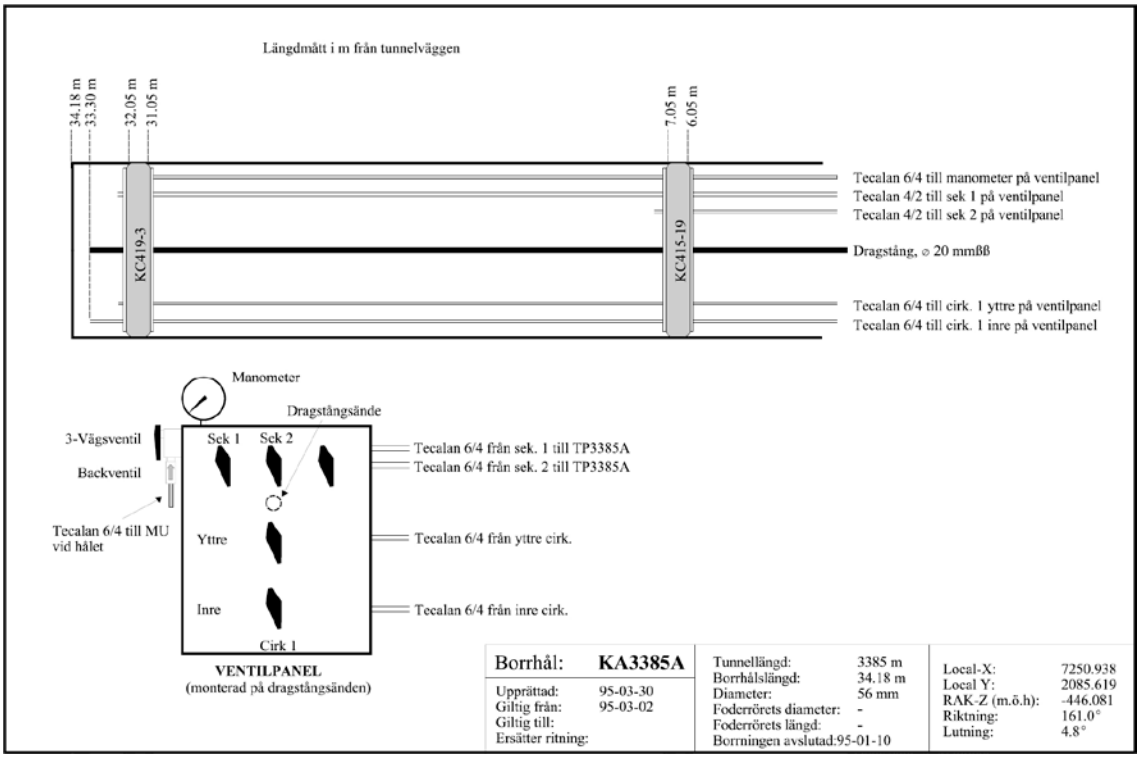

Layout of borehole KA3105A

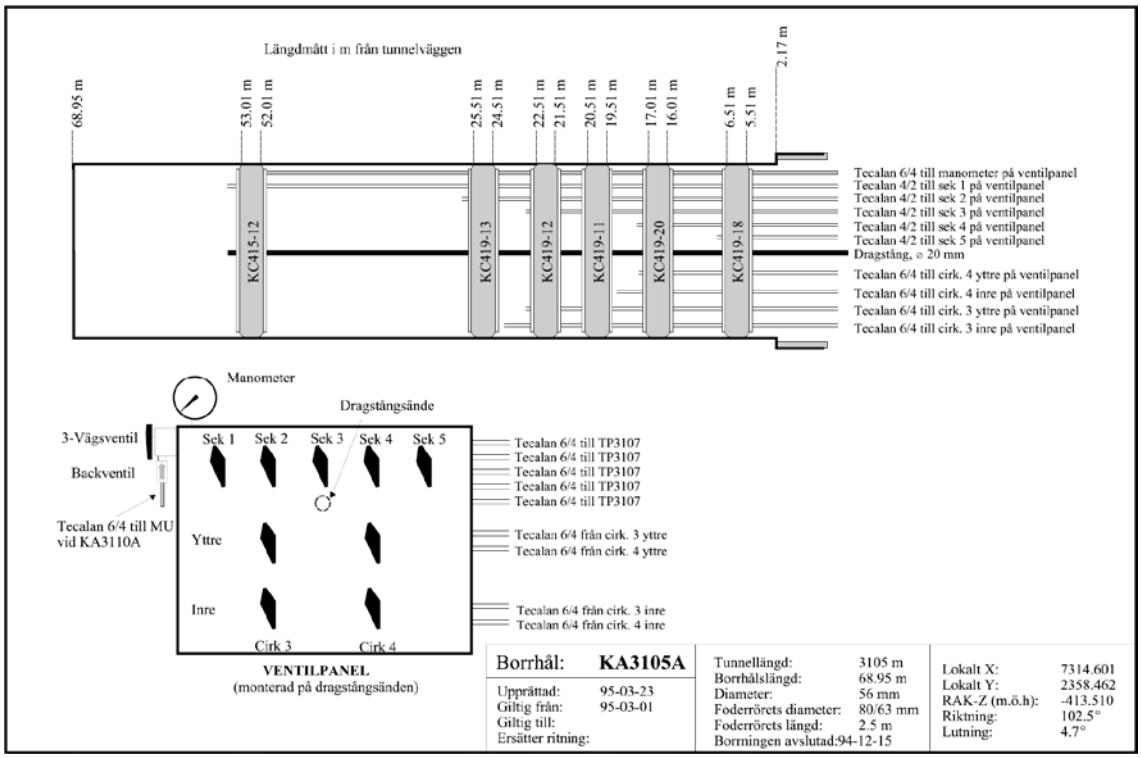

Appendix D

Sampling procedure during circulation experiments

Sampling in borehole KA3110A

The intergroup order of the samples during sampling corresponds to the lists given in Table D-1 and Table D-2.

Table D-1. Circulation and sampling of section water and fracture water in KA3110A, section 1.

Date	Performance before collected sample	SKB number	Analytical programme	Water type/ sample volume
Sampling session 1				
2010-03-30	Discharge of water in outer tubing (volume 0,3 L)	20156	HS–, Fe(II)	Section water, Sampling volume 0,05 L
2010-03-30	Circulation of 2 section volumes	20136	Gases (composition), HS^- and Fe(II) (field), Microbiology 1, Acetate, pH and redox (field), HS^-(Äspö), pH, conductivity, Anions, Fe(II)+Fe(total), major cations, environmental cations, lantanoids, DOC and TOC	Section water, mixed
2010-03-30	Discharge of 10 section volumes, circulation of 1 section volume	20137	Gases (composition), HS^- and Fe(II) (field), Microbiology 1, Acetate, pH and redox (field), HS^-(Äspö), pH, conductivity, Anions, Fe(II)+Fe(total), major cations, environmental cations, lantanoids, DOC and TOC	Fracture water
2010-04-20	Discharge of water in outer tubing (volume 0,3 L)	20157	HS^-, Fe(II) – field	Section water
2010-04-20	Sampling after circulation of 1, 2…14 L	20158–20172	HS^-, Fe(II) – field	Section water
2010-04-20	Circulation of 1 section volume (14,5 L)	20154	Gases (composition), HS^- and Fe(II) (field), Microbiology 1, Acetate, pH and redox (field), HS^-(Äspö), pH, conductivity, Anions, Fe(II)+Fe(total), major cations, environmental cations, lantanoids, DOC and TOC	Section water, mixed
2010-05-11	Discharge of water in outer tubing (volume 0,3 L)	20181	HS^-, Fe(II) – field	Section water
2010-05-11	Sampling after circulation of 1, 2…14 L	20182–20198	HS^-, Fe(II) – field	Section water
2010-05-11	Circulation of 1 section volume (14,5 L)	20180	Gases (composition), HS^- and Fe(II) (field), Microbiology 1, Acetate, pH and redox (field), HS^-(Äspö), pH, conductivity, Anions, Fe(II)+Fe(total), major cations, environmental cations, lantanoids, DOC and TOC	Section water, mixed
2010-06-01	Sampling from outer tubing	20216	HS^-, Fe(II) – field, acetate, pH, SRB	Water in tubing/section
2010-06-01	Discharge of water in outer tubing (volume 0,3 L)	20217	HS^-, Fe(II) – field	Section water
2010-06-01	Sampling after circulation of 0,250 L, 0,500 L, 0,750 L and 1, 2…14 L	20218–20234	HS^-, Fe(II) – field	Section water
2010-06-01	Circulation of 1 section volume (14,5 L)	20248	Gases (composition), HS^- and Fe(II) (field), Microbiology 1, Acetate, pH and redox (field), HS^-(Äspö), pH, conductivity, Anions, Fe(II)+Fe(total), major cations, environmental cations, lantanoids, DOC and TOC	Section water, mixed
2010-06-15	Discharge of water in outer tubing (volume 0,3 L)	20264	HS^-, Fe(II) – field	Section water
2010-06-15	Sampling after circulation of 0,250 L, 0,500 L, 0,750 L and 1, 2…14 L	20265–20282	HS^-, Fe(II) – field	Section water
2010-06-15	Circulation of 1 section volume (14,5 L)	20262	Gases (composition), HS^- and Fe(II) (field), Microbiology 1, Acetate, pH and redox (field), HS^-(Äspö), pH, conductivity, Anions, Fe(II)+Fe(total), major cations, environmental cations, lantanoids, DOC and TOC	Section water, mixed

Date	Performance before collected sample	SKB number	Analytical programme	Water type/ sample volume
Sampling session 2				
2010-10-05	Discharge of water in outer tubing (volume 0,3 L)	20349	HS^-, Fe(II) – field	Section water
2010-10-05	Sampling after circulation of 1, 2…12 L	20350–20356	HS^-, Fe(II) – field	Section water
2010-10-05	Circulation of 1 section volume (mixing)	20357	Gases (composition and stable isotopes), HS^- and Fe(II) (field), Microbiology 2, Acetate, $\delta^{13}C$ in Acetate, pH and redox (field), TOC and DOC, $\delta^{13}C$ and pmC in HCO_3^-, $\delta^{13}C$ and pmC in DOC, pH, anions, HS^-, Fe(II)+Fe(total), major cations, $\delta^{34}S$ in HS^- and SO_4^{2-}, $\delta^{18}O$	Section water, mixed
2010-10-05	Discharge of 10 section volumes (>145 L)	20358	Gas trap for sampling of released gas and analysis of δ^2H in Hydrogen gas	Fracture water
2010-10-05	Discharge of 10 section volumes (>145 L)	20359[1]	Gases (composition and stable isotopes), HS^- and Fe(II) (field), Microbiology 2, Acetate, $\delta^{13}C$ in Acetate, pH and redox (field), TOC and DOC, $\delta^{13}C$ and pmC in HCO_3^-, $\delta^{13}C$ and pmC in DOC, pH, anions, HS^-, Fe(II)+Fe(total), major cations, $\delta^{34}S$ in HS^- and SO_4^{2-}, $\delta^{18}O$	Fracture water
2010-10-26	Discharge of water in outer tubing (volume 0,3 L)	20360	HS^-, Fe(II) – field	Section water
2010-10-26	Circulation of 1 section volume (14,5 L)	20361	Gases (composition and stable isotopes), HS^- and Fe(II) (field), Acetate, $\delta^{13}C$ in Acetate, pH and redox (field), TOC and DOC, $\delta^{13}C$ and pmC in HCO_3^-, $\delta^{13}C$ and pmC in DOC, pH, anions, HS^-, Fe(II)+Fe(total), major cations, $\delta^{34}S$ in HS^- and SO_4^{2-}, $\delta^{18}O$	Section water, mixed
2010-11-16	Discharge of water in outer tubing (volume 0,3 L)	20362	HS^-, Fe(II) – field	Section water
2010-11-16	Circulation of 1 section volume (14,5 L)	20363	Gases (composition and stable isotopes), HS^- and Fe(II) (field), Acetate, $\delta^{13}C$ in Acetate, pH and redox (field), TOC and DOC, $\delta^{13}C$ and pmC in HCO_3^-, $\delta^{13}C$ and pmC in DOC, pH, anions, HS^-, Fe(II)+Fe(total), major cations, $\delta^{34}S$ in HS^- and SO_4^{2-}, $\delta^{18}O$	Section water, mixed
2010-12-07	Discharge of water in outer tubing (volume 0,3 L)	20364	HS^-, Fe(II) – field	Section water
2010-12-07	Sampling after circulation of 1, 2…12 L	20365–20371	HS^-, Fe(II) – field	Section water
2010-12-07	Circulation of 1 section volume	20372	Gases (composition and stable isotopes), HS^- and Fe(II) (field), Microbiology 2, Acetate, $\delta^{13}C$ in Acetate, pH and redox (field), TOC and DOC, $\delta^{13}C$ and pmC in HCO_3^-, $\delta^{13}C$ and pmC in DOC, pH, anions, HS^-, Fe(II)+Fe(total), major cations, $\delta^{34}S$ in HS^- and SO_4^{2-}, $\delta^{18}O$	Section water, mixed
Sampling in connection to hydrotests				
2011-04-21	Discharge of 2 section volumes (>30 L)	20717	pH, anions, Fe(II)+Fe(total), HS^-, major cations. TOC, DOC, $\delta^{13}C$ and pmC in HCO_3^-	Fracture water
Additional sampling after completion of circulation experiment				
2011-09-20	Section 1, pressure tubing	20950	HS^-	Section water
2011-09-20	Section 2, pressure tubing	20951	HS^-	Section water
2011-09-20	Section 1, inner circulation tubing	20952	HS^-	Section water

[1] Sample 20359 was accidently acidified at Ångström Laboratory. The sample and analysis of pmC and ^{13}C in hydrocarbonate was replaced on 21st of April by SKB number 20717.

The first sampling session was completed in 2010-06-15 and the second sampling session began 2010-10-05. There was no discharge of water from the borehole section in between two sampling sessions. After completion of the circulation experiment in December 2010, additional samples were collected for analysis of sulphide in September 2011. Samples were collected from inner circulation and pressure tubing in section 1 and from the pressure tubing in section 2. The inlet of the pressure tubing is at the top of the section, while the inner circulation tubing is at the bottom of the section.

Sampling in borehole KA3385A

The intergroup order of the samples during sampling corresponds to the list given in Table D-2.

Table D-2. Circulation and sampling of section water and fracture water in KA3385A, section 1.

Date	Performance before collected sample	SKB number	Analytical programme	Note
Sampling session 1				
2010-03-30	Circulation of 2 section volumes (9,0 L)	20134	Gases (composition), HS^- and Fe(II) (field), Microbiology 1, Acetate, pH and redox (field), HS^-(Äspö), pH, conductivity, Anions, Fe(II)+Fe(total), major cations, environmental cations, lantanoids, DOC and TOC	Section water, mixed
2010-03-30	Discharge of 10 section volumes (>45 L), circulation of 1 section volume	20135	Gases (composition), HS^- and Fe(II) (field), Microbiology 1, Acetate, pH and redox (field), HS^-(Äspö), pH, conductivity, Anions, Fe(II)+Fe(total), major cations, environmental cations, lantanoids, DOC and TOC	Fracture water
2010-04-20	Discharge of water in outer tubing (volume 0,4 L)	20173	HS^-, Fe(II) – field	Section water
2010-04-20	Circulation of 1 section volume (4,5 L)	20153	Gases (composition), HS^- and Fe(II) (field), Microbiology 1, Acetate, pH and redox (field), HS^-(Äspö), pH, conductivity, Anions, Fe(II)+Fe(total), major cations, environmental cations, lantanoids, DOC and TOC	Section water, mixed
2010-05-11	Discharge of water in outer tubing (volume 0,4 L)	20199	HS^-, Fe(II) – field	Section water
2010-05-11	Sampling after circulation of 1, 2…4 L	20200–20203	HS^-, Fe(II) – field	Section water
2010-05-11	Circulation of 1 section volume (4,5 L)	20179	Gases (composition), HS^- and Fe(II) (field), Microbiology 1, Acetate, pH and redox (field), HS^-(Äspö), pH, conductivity, Anions, Fe(II)+Fe(total), major cations, environmental cations, lantanoids, DOC and TOC	Section water, mixed
2010-06-01	Discharge of water in outer tubing (volume 0,4 L)	20235	HS^-, Fe(II) – field	Section water
2010-06-01	Sampling after circulation of 1, 2…4 L	20236–20239	HS^-, Fe(II) – field	Section water
2010-06-01	Circulation of 1 section volume (4,5 L)	20247	Gases (composition), HS^- and Fe(II) (field), Microbiology 1, Acetate, pH and redox (field), HS^-(Äspö), pH, conductivity, Anions, Fe(II)+Fe(total), major cations, environmental cations, lantanoids, DOC and TOC	Section water, mixed
2010-06-15	Discharge of water in outer tubing (volume 0,4 L)	20283	HS^-, Fe(II) – field, Microbiology (TNC, SRB)	Section water
2010-06-15	Sampling after circulation of 1, 2…4 L	20284–20287	HS^-, Fe(II) – field	Section water
2010-06-15	Discharge of water in outer tubing (volume 0,4 L)	20264	HS^-, Fe(II) – field	Section water
2010-06-15	Circulation of 1 section volume (4,5 L)	20263	Gases (composition), HS^- and Fe(II) (field), Microbiology 1, Acetate, pH and redox (field), HS^-(Äspö), pH, conductivity, Anions, Fe(II)+Fe(total), major cations, environmental cations, lantanoids, DOC and TOC	Section water, mixed
Sampling session 2				
2010-10-06	Discharge of water in outer tubing (volume 0,4 L)	20349	HS^-, Fe(II) – field	Section water
2010-10-06	Circulation of 1 section volume (4,5 L)	20346	TOC and DOC, $\delta^{13}C$ and pmC, pH, anions, HS^-, Fe(II)+Fe(total), major cations, $\delta^{34}S$ in HS^- and SO_4^{2-}, $\delta^{18}O$	Section water, mixed

Date	Performance before collected sample	SKB number	Analytical programme	Note
2010-10-06	Discharge of 10 section volumes (>45 L)	20347	Gas trap for sampling of released gas and analysis of δ^2H in Hydrogen gas	Fracture water
2010-10-06	Discharge of 10 section volumes (>45 L)	20359	Gases (composition), HS^- and Fe(II) (field), Microbiology 1, Acetate, pH and redox (field), HS^-(Äspö), pH, conductivity, Anions, Fe(II)+Fe(total), major cations, environmental cations, lantanoids, DOC and TOC	Fracture water
2011-01-20	Discharge of water in outer tubing (volume 0,4 L)	20576	HS^-, Fe(II) – field	Section water
2011-01-20	Sampling after circulation of 1 and 2 L	20577, 20578	HS^-, Fe(II) – field	Section water
2011-01-20	Circulation of 1 section volume (4,5 L)	20573	Dissolved gas, microbiology TOC and DOC, $\delta^{13}C$ and pmC, pH, anions, HS^-, Fe(II)+Fe(total), major cations, $\delta^{34}S$ in HS^- and SO_4^{2-}, $\delta^{18}O$	Section water, mixed
Additional sampling after completion of circulation experiment				
2011-11-15	Section 1: discharge of water in inner tubing (volume 0,4 L)	22012	HS^-	Section water
2011-11-15	Section 1: discharge of water in outer tubing (volume 0,4 L)	22013	HS^-	Section water
2011-11-15	Section 2: discharge of water in pressure tubing (volume 0,4 L)	22014	HS^-	Section water

The first sampling session was completed in 2010-06-15 and the second sampling session began 2010-10-06. There was no discharge of water from the borehole section in between two sampling sessions. In January 2011, a complementary sample was collected and analysed, in order to compensate for the samples collected during discharge of water.

After completion of the circulation experiment in December 2010, additional samples were collected for analysis of sulphide in November 2011. Samples were collected from inner circulation and pressure tubing in section 1 and from the pressure tubing in section 2. The inlet of the pressure tubing is at the top of the section, while the inner circulation tubing is at the bottom of the section.

Appendix E

Performed analyses during circulation experiment

Table E-1. Performed analyses in sampling series 1 and 2.

		Sampling series 1	Sampling series 2
Component/group	**Component/element**	**2010-03-30–2010-06-15**	**2010-10-05-2011-01-20**
pH		X	X
Conductivity		X	X
HS^-		X	X
Fe(II)[2] and Fe(tot)[3]		X	X
Major cations	Na, K, Ca, Mg, S(tot), Si(tot), Fe, Mn, Li, Sr	X	X
Environmental cations	Al, As, Ba, B, Cd, Co, Cr, Cu, Hg, Mo, Ni, P, Pb, V, Zn		X
Lantanoids	Sc, Rb, Y, Zr, I, Sb, Cs, La, Hf, Tl, Ce, Pr, Nd, Sm, Eu, Gd, Tb, Dy, Ho, Er, Tm, Yb, Lu, U, Th		
Anions	HCO_3^-, Cl^-, SO_4^{2-}, Br^-,	X	X
DOC (dissolved organic carbon)		X	X
TOC (total organic carbon)		X	X
Acetate		X	X
$\delta^{18}O$			X
$\delta^{34}S$ in dissolved HS^-, SO_4^{2-}		X	X
$\delta^{13}C$, pmC in HCO_3^-			X
$\delta^{13}C$ and pmC in DOC			X
Dissolved gases, composition	He, Ar, N_2, CH_4, CO_2, Ne, O_2, CO, H_2, C_2H_6, C_2H_4, C_2H_2, C_3H_6, C_3H_8	X	X
Dissolved gases, stable isotopes	$\delta^{13}C$ in CH_4 and CO_2, δ^2H in CH_4 and H_2		X
Released gas	δ^2H in H_2		X
Microbiology 1	TNC, CHAB, MPN IRB, MPN SRB, MPN AA, Q-PCR RNA 16S all bacteria, Q-PCR RNA 16S methanogens, Q-PCR RNA 16S all fungi, Q-PCR apsA DNA SRB, Q-PCR apsA SRB activity, Q-PCR fthfs DNA acetogens, Q-PCR fthfs RNA acetogens activity	X	
Microbiology 2	TNC, CHAB, MPN IRB, MPN SRB, MPN AA, Q-PCR DNA 16S all bacteria, Q-PCR DNA 16S all fungi, Q-PCR apsA DNA SRB, Q-PCR fthfs DNA acetogens		X

[1] Sulphide was analysed by two different laboratories; Microbial Analytics Sweden AB and Äspö Water Chemistry Laboratory.

[2] Fe (II) was analysed in field by the HACH method and at Äspö Water Chemistry Laboratory /, Fe (tot)[3] was analysed at Äspö Water Chemistry Laboratory.

Sulphide (HS^-) and Fe (II) was analysed with two different laboratories; Microbial Analytics Sweden AB and Äspö water chemistry Laboratory. The methods for sulphide are similar and based on that sulphide and N, N-dimetyl-p-fenylendiamin reacts to form methyleneblue in a Fe^{3+} rich solution (Svensk Standard SIS 028115). The HACH method is described in Hach DR/2500 Laboratory Spectrophotometer Handbook, method 8146, Ferrous iron Phenanthroline Method. Hach Company, USA, 2003.

More detailed information on analyses, methods and consulted laboratories used in the circulation experiments are given in Rosdahl et al. (2011).

Appendix F

Analysis results circulation experiments

Circulation experiments – Water composition (in all tables: n.a. = not analysed, b.d. = below detection limit, – = lower than).

Idcode	Sampling date	Secup m	Seclow m	SKB no.	Water type	Na^+ mg L^{-1}	K^+ mg L^{-1}	Ca^{2+} mg L^{-1}	Mg^{2+} mg L^{-1}	HCO_3^- mg L^{-1}	Cl^- mg L^{-1}	SO_4^{2-} mg L^{-1}	SO_4_S mg L^{-1}	Br^- mg L^{-1}	F^- mg L^{-1}	Si^{2+} mg L^{-1}	Fe–tot mg L^{-1}
KA3105A	2010-03-30 15:15	53.01	68.95	20138	Section	n.a.	n.a.	n.a.	n.a.	n.a.	n.a.	n.a.	n.a.	n.a.	n.a.	n.a.	n.a.
KA3385A	2010-03-30 09:40	32.05	34.18	20134	Section	2,230	10.4	1,890	65.1	25.7	6,490	368	140	39.4	1.42	6.6	0.22
KA3385A	2010-03-30 14:20	32.05	34.18	20135	Fracture	2,410	11	2,270	61.6	19.6	7,560	417	157	49.3	1.43	6.25	0.207
KA3385A	2010-04-21 11:26	32.05	34.18	20153	Section	2,090	9.57	1,850	65.2	26.4	6,770	384	134	44.1	1.26	6.66	0.249
KA3385A	2010-05-11 13:41	7.05	31.05	20179	Section	2,300	10.5	2,230	65.3	20.9	7,500	406	154	47.3	1.48	6.4	0.179
KA3385A	2010-06-01 10:21	32.05	34.18	20247	Section	2,010	9.5	2,030	63.6	21.7	7,100	374	140	43.8	1.58	6.3	0.368
KA3385A	2010-06-15 13:09	32.05	34.18	20263	Section	2,080	10.1	2,110	66.9	25	6,990	378	144	42.6	1.5	6.31	0.289
KA3385A	2010-10-06 08:50	32.05	34.18	20346	Section	2,200	10	1,900	63	30.7	6,819	358	138	41.5	1.46	6.33	0.299
KA3385A	2011-01-20 09:30	32.05	34.18	20573	Section	2,260	10.3	2,010	69.6	28.6	6,759	357.5	137	41.4	1.45	6.39	0.314
KA3385A	2011-11-15 09:21	32.05	34.18	22012	Section	n.a.	n.a.	n.a.	n.a.	n.a.	n.a.	n.a.	n.a.	n.a.	n.a.	n.a.	n.a.
KA3385A	2011-11-15 09:30	32.05	34.18	22013	Section	n.a.	n.a.	n.a.	n.a.	n.a.	n.a.	n.a.	n.a.	n.a.	n.a.	n.a.	n.a.
KA3385A	2011-11-15 09:39	7.05	31.05	22014	Section	n.a.	n.a.	n.a.	n.a.	n.a.	n.a.	n.a.	n.a.	n.a.	n.a.	n.a.	n.a.
KA3110A	2010-03-30 11:15	20.05	26.83	20136	Section	1,580	39	334	133	185	3,110	326	120	12.3	1.39	6.56	1.17
KA3110A	2010-03-30 15:30	20.05	26.83	20137	Fracture	1,540	39.1	338	134	185	3,120	328	123	12.2	2.09	6.74	1.32
KA3110A	2010-04-21 10:25	20.05	26.83	20154	Section	1,470	35.1	332	132	187	3,130	322	116	13.5	1.38	6.3	0.895
KA3110A	2010-05-11 10:42	20.05	26.83	20180	Section	1,450	34	335	130	193	3,120	290	135	11.6	1.32	6.62	0.557
KA3110A	2010-06-01 10:31	20.05	26.83	20248	Section	1,360	34.3	344	130	190	3,080	285	123	12	1.47	6.3	0.641
KA3110A	2010-06-15 10:12	20.05	26.83	20262	Section	1,300	32.1	329	123	188	3,070	301	105	12.1	1.48	6.09	0.691
KA3110A	2010-10-05 10:07	20.05	26.83	20357	Section	1,480	35.8	328	124	189.4	3,018	303	118	11.5	1.5	6.29	0.653
KA3110A	2010-10-05 14:42	20.05	26.83	20359	Fracture	1,490	36.3	328	124	185.5	3,006	313.9	111	11.5	1.47	6.45	1.1
KA3110A	2010-10-26 10:08	20.05	26.83	20361	Section	1,440	35.2	341	126	187.2	3,005	293	114	11.6	1.35	6.36	0.891
KA3110A	2010-11-16 09:55	20.05	26.83	20363	Section	1,500	35.2	319	121	185.8	3,015	301	104	11.9	1.41	6.41	0.875
KA3110A	2010-12-07 16:48	20.05	26.83	20372	Section	1,420	32.9	347	135	187.8	3,057	305.2	114	11.8	1.59	6.31	1.08
KA3110A	2011-04-21 08:45	20.05	26.83	20717	Fracture	1,470	36.1	348	127	183.7	3,037	294.1	104	11.9	1.55	6.58	1.32
KA3110A	2011-09-20 09:03	20.05	26.83	20952	Section	n.a.	n.a.	n.a.	n.a.	n.a.	n.a.	n.a.	n.a.	n.a.	n.a.	n.a.	n.a.
KA3110A	2011-09-20 09:17	20.05	26.83	20950	Section	n.a.	n.a.	n.a.	n.a.	n.a.	n.a.	n.a.	n.a.	n.a.	n.a.	n.a.	n.a.
KA3110A	2011-09-20 09:23	6.55	19.05	20951	Section	n.a.	n.a.	n.a.	n.a.	n.a.	n.a.	n.a.	n.a.	n.a.	n.a.	n.a.	n.a.

Idcode	Sampling date	Secup m	Seclow m	SKB no.	Water type	Fe-tot mg L^{-1}	Fe^{2+} mg L^{-1}	Mn^{2+} mg L^{-1}	Li^{+} mg L^{-1}	Sr^{2+} mg L^{-1}	pH	Cond. mS m^{-1}	TOC mg L^{-1}	DOC mg L^{-1}	HS^{-*} mg L^{-1}	HS^{-**} mg L^{-1}	P–tot mg L^{-1}
KA3105A	2010-03-30 15:15	53.01	68.95	20138	Section	n.a.	n.a.	n.a.	n.a.	n.a.	n.a.	n.a.	n.a.	n.a.	0.248	n.a.	n.a.
KA3385A	2010-03-30 09:40	32.05	34.18	20134	Section	0.221	0.211	0.473	1.41	35.9	7.58	1,890	22.7	37.8	0.041	n.a.	–0.04
KA3385A	2010-03-30 14:20	32.05	34.18	20135	Fracture	0.207	0.193	0.477	1.83	43.3	7.55	2,140	4.3	4.7	0.023	< 0,01	–0.04
KA3385A	2010-04-21 11:26	32.05	34.18	20,153	Section	0.233	0.223	0.497	1.21	33.6	7.52	1,860	27.8	15.6	0.015	n.a.	–0.04
KA3385A	2010-05-11 13:41	7.05	31.05	20179	Section	0.232	0.201	0.445	1.56	40.8	7.63	2,080	8.8	5.7	0.13	n.a.	–0.04
KA3385A	2010-06-01 10:21	32.05	34.18	20247	Section	0.261	0.251	0.446	1.26	34.6	7.49	1,970	127	28.1	0.17	0.35	–0.04
KA3385A	2010-06-15 13:09	32.05	34.18	20263	Section	0.291	0.283	0.468	1.32	36	7.46	1,960	415	222	2.81	3.38	–0.04
KA3385A	2010-10-06 08:50	32.05	34.18	20346	Section	0.253	0.249	0.448	1.55	36.9	7.56	1,915	562	564	2.551	3.61	n.a.
KA3385A	2011-01-20 09:30	32.05	34.18	20573	Section	0.29	0.27	0.5	1.34	36	7.54	1,878	14.8	14.5	0.163	2.6	n.a.
KA3385A	2011-11-15 09:21	32.05	34.18	22012	Section	n.a.	n.a.	n.a.	n.a.	n.a.	n.a.	n.a.	n.a.	n.a.	0.111	n.a.	n.a.
KA3385A	2011-11-15 09:30	32.05	34.18	22013	Section	n.a.	n.a.	n.a.	n.a.	n.a.	n.a.	n.a.	n.a.	n.a.	3.26	n.a.	n.a.
KA3385A	2011-11-15 09:39	7.05	31.05	22014	Section	n.a.	n.a.	n.a.	n.a.	n.a.	n.a.	n.a.	n.a.	n.a.	2.92	n.a.	n.a.
KA3110A	2010-03-30 11:15	20.05	26.83	20136	Section	1.16	1.16	0.777	0.184	5.77	7.5	1,000	29.2	20.2	0.502	0.355	0.0199
KA3110A	2010-03-30 15:30	20.05	26.83	20137	Fracture	1.29	1.29	0.804	0.186	5.79	7.44	999	6.4	7.7	0.186	< 0,01	0.0212
KA3110A	2010-04-21 10:25	20.05	26.83	20154	Section	0.804	0.8	0.891	0.158	5.52	7.57	988	77.8	148	1.32	1.64	0.024
KA3110A	2010-05-11 10:42	20.05	26.83	20180	Section	0.594	0.586	0.758	0.159	5.15	7.51	1,020	37.6	58	9.37	8.97	0.0187
KA3110A	2010-06-01 10:31	20.05	26.83	20248	Section	0.659	0.646	0.744	0.196	4.94	7.5	972	13.4	7.9	5.43	26.43	0.0192
KA3110A	2010-06-15 10:12	20.05	26.83	20262	Section	0.749	0.745	0.712	0.193	4.74	7.48	965	84.3	16.1	3.24	3.06	0.0201
KA3110A	2010-10-05 10:07	20.05	26.83	20357	Section	0.617	0.603	0.712	0.173	5.47	7.56	957	112	112	3.309	4.17	n.a.
KA3110A	2010-10-05 14:42	20.05	26.83	20359	Fracture	1.118	1.11	0.742	0.169	5.47	7.5	956	14.8	14.9	0.327	0.122	n.a.
KA3110A	2010-10-26 10:08	20.05	26.83	20361	Section	0.847	0.84	0.738	0.164	5.52	7.54	955	6.4	6.3	0.796	0.67	n.a.
KA3110A	2010-11-16 09:55	20.05	26.83	20363	Section	0.91	0.91	0.715	0.158	5.48	7.5	953	6.1	19.8	0.502	0.34	n.a.
KA3110A	2010-12-07 16:48	20.05	26.83	20372	Section	1.01	0.99	0.784	1.63	5.12	7.71	954	5.6	6.2	0.351	0.23	n.a.
KA3110A	2011-04-21 08:45	20.05	26.83	20717	Fracture	1.22	1.21	0.747	0.195	6.58	7.52	945	5.8	5.8	0.137	n.a.	n.a.
KA3110A	2011-09-20 09:03	20.05	26.83	20952	Section	n.a.	n.a.	n.a.	n.a.	n.a.	n.a.	n.a.	n.a.	n.a.	15.072	n.a.	n.a.
KA3110A	2011-09-20 09:17	20.05	26.83	20950	Section	n.a.	n.a.	n.a.	n.a.	n.a.	n.a.	n.a.	n.a.	n.a.	11.034	n.a.	n.a.
KA3110A	2011-09-20 09:23	6.55	19.05	20951	Section	n.a.	n.a.	n.a.	n.a.	n.a.	n.a.	n.a.	n.a.	n.a.	0.303	n.a.	n.a.

Circulation experiments – Environmental metals.

Idcode	Sampling date	Secup m	Seclow m	SKB no.	Water type	Al µg L^{-1}	Ba µg L^{-1}	Cd µg L^{-1}	Cr µg L^{-1}	Cu µg L^{-1}	Co µg L^{-1}	Hg µg L^{-1}	Ni µg L^{-1}	Mo µg L^{-1}	Pb µg L^{-1}	V µg L^{-1}	Zn µg L^{-1}
KA3385A	2010-03-30 09:40	32.05	34.18	20134	Section		76.2	–0.05				–0.002				0.0738	
KA3385A	2010-03-30 14:20	32.05	34.18	20135	Section		85.6	–0.05				–0.002				0.0672	
KA3385A	2010-04-21 11:26	32.05	34.18	20153	Section		75.6	–0.05				–0.002				–0.05	
KA3385A	2010-05-11 13:41	7.05	31.05	20179	Section	4.56	80.2	–0.05	0.674	–0.5	–0.05	–0.002	4.64	41.7	–0.3	0.167	–2
KA3385A	2010-06-01 10:21	32.05	34.18	20247	Section	678	79.6	0.106	6.15	0.572	0.265	–0.002	33.9	47.1	–0.3	0.388	123
KA3385A	2010-06-15 13:09	32.05	34.18	20263	Section	145	72.6	–0.05	11.3	–0.5	0.213	–0.002	33.7	39.3	–0.3	0.353	4.84
KA3110A	2010-03-30 11:15	20.05	26.83	20136	Section		114	–0.02				–0.002				0.595	
KA3110A	2010-03-30 15:30	20.05	26.83	20137	Section		113	–0.02				–0.002				0.565	
KA3110A	2010-04-21 10:25	20.05	26.83	20154	Section		118	–0.02				–0.002				0.615	
KA3110A	2010-05-11 10:42	20.05	26.83	20180	Section	6.63	111	–0.02	1.02	–0.2	0.0595	–0.002	1.38	3.41	–0.1	0.571	12
KA3110A	2010-06-01 10:31	20.05	26.83	20248	Section	7.5	98.6	–0.02	0.612	–0.2	–0.02	–0.002	0.521	4.63	–0.1	0.53	–0.8
KA3110A	2010-06-15 10:12	20.05	26.83	20262	Section	13.2000	93.8000	–0.0200	–0.0200	–0.2000	0.0405	–0.0020	2.8000	5.5300	–0.1000	0.7030	1.5400

Circulation experiments – Trace elements.

Idcode	Sampling date	Secup m	Seclow m	SKB no.	Water type	U µg L^{-1}	Th µg L^{-1}	Sc µg L^{-1}	Rb µg L^{-1}	Y µg L^{-1}	Zr µg L^{-1}	Sb µg L^{-1}	Cs µg L^{-1}	Hf µg L^{-1}	Tl µg L^{-1}
KA3385A	2010-03-30 09:40	32.05	34.18	20134	Section	0.0682	–0.2000	–0.5000	31.8000	0.2050	–0.3000		2.9500	–0.0500	–0.1000
KA3385A	2010-03-30 14:20	32.05	34.18	20135	Section	0.0554	–0.2000	–0.5000	33.5000	0.2280	–0.3000		3.1500	–0.0500	–0.1000
KA3385A	2010-04-21 11:26	32.05	34.18	20153	Section	0.0474	–0.2000	–0.5000	32.3000	0.1940	–0.3000		2.9600	–0.0500	–0.1000
KA3385A	2010-05-11 13:41	7.05	31.05	20179	Section	0.0767	–0.2000	–0.5000	35.0000	0.5180	0.5640	0.1340	2.7100	–0.0500	–0.1000
KA3385A	2010-06-01 10:21	32.05	34.18	20247	Section	0.1030	–0.2000	–0.5000	30.8000	0.4960	–0.3000	0.1410	2.5900	–0.0500	–0.1000
KA3385A	2010-06-15 13:09	32.05	34.18	20263	Section	0.0604	–0.2000	–0.5000	31.7000	0.3380	–0.3000	0.1310	2.5600	–0.0500	–0.1000
KA3110A	2010-03-30 11:15	20.05	26.83	20136	Section	0.6230	–0.2000	–0.4000	51.6000	0.2970	0.2280		5.0200	–0.0200	–0.0500
KA3110A	2010-03-30 15:30	20.05	26.83	20137	Section	0.6450	–0.2000	–0.4000	53.2000	0.2940	0.2500		5.1000	–0.0200	–0.0500
KA3110A	2010-04-21 10:25	20.05	26.83	20154	Section	0.6050	–0.2000	–0.4000	53.2000	0.2420	0.2200		5.5900	–0.0200	–0.0500
KA3110A	2010-05-11 10:42	20.05	26.83	20180	Section	0.4270	–0.2000	–0.4000	50.4000	0.3660	0.4140	–0.1000	4.6900	–0.0200	–0.0500
KA3110A	2010-06-01 10:31	20.05	26.83	20248	Section	0.5300	–0.2000	–0.4000	54.0000	0.3020	0.1830	–0.1000	5.4700	–0.0200	–0.0500
KA3110A	2010-06-15 10:12	20.05	26.83	20262	Section	0.5690	–0.2000	–0.4000	56.3000	0.2990	0.1700	–0.1000	5.9000	–0.0200	–0.0500

Circulation experiments – Trace elements (rare earth elements).

Idcode	Sampling date	Secup m	Seclow m	SKB no.	Water type	La µg L^{-1}	Ce µg L^{-1}	Pr µg L^{-1}	Nd µg L^{-1}	Sm µg L^{-1}	Eu µg L^{-1}	Gd µg L^{-1}	Tb µg L^{-1}	Dy µg L^{-1}	Ho µg L^{-1}	Er µg L^{-1}	Tm µg L^{-1}	Yb µg L^{-1}	Lu µg L^{-1}
KA3385A	2010-03-30 09:40	32.05	34.18	20134	Section	0.0956	–0.0500	–0.0500	–0.0500	–0.0500	–0.0500	–0.0500	–0.0500	–0.0500	–0.0500	–0.0500	–0.0500	–0.0500	–0.0500
KA3385A	2010-03-30 14:20	32.05	34.18	20135	Section	0.1320	0.0802	–0.0500	–0.0500	–0.0500	–0.0500	–0.0500	–0.0500	–0.0500	–0.0500	–0.0500	–0.0500	–0.0500	–0.0500
KA3385A	2010-04-21 11:26	32.05	34.18	20153	Section	0.0577	–0.0500	–0.0500	–0.0500	–0.0500	–0.0500	–0.0500	–0.0500	–0.0500	–0.0500	–0.0500	–0.0500	–0.0500	–0.0500
KA3385A	2010-05-11 13:41	7.05	31.05	20179	Section	0.1200	0.0600	–0.0500	–0.0500	–0.0500	–0.0500	–0.0500	–0.0500	–0.0500	–0.0500	–0.0500	–0.0500	–0.0500	–0.0500
KA3385A	2010-06-01 10:21	32.05	34.18	20247	Section	3.2400	3.3700	0.2840	1.0400	0.0778	–0.0500	0.0585	–0.0500	–0.0500	–0.0500	–0.0500	–0.0500	–0.0500	–0.0500
KA3385A	2010-06-15 13:09	32.05	34.18	20263	Section	1.0400	0.9970	0.0857	0.2660	–0.0500	–0.0500	–0.0500	–0.0500	–0.0500	–0.0500	–0.0500	–0.0500	–0.0500	–0.0500
KA3110A	2010-03-30 11:15	20.05	26.83	20136	Section	0.2100	0.2490	0.0258	0.1120	0.0217	–0.0200	–0.0200	–0.0200	0.0225	–0.0200	–0.0200	–0.0200	0.0224	–0.0200
KA3110A	2010-03-30 15:30	20.05	26.83	20137	Section	0.1450	0.1980	0.0232	0.0969	–0.0200	–0.0200	0.0243	–0.0200	0.0214	–0.0200	0.0214	–0.0200	0.0209	–0.0200
KA3110A	2010-04-21 10:25	20.05	26.83	20154	Section	0.3260	0.2800	0.0271	0.1190	–0.0200	–0.0200	–0.0200	–0.0200	–0.0200	–0.0200	–0.0200	–0.0200	–0.0200	–0.0200
KA3110A	2010-05-11 10:42	20.05	26.83	20180	Section	0.1580	0.1980	0.0243	0.1350	0.0214	–0.0200	0.0259	–0.0200	–0.0200	–0.0200	–0.0200	–0.0200	–0.0200	–0.0200
KA3110A	2010-06-01 10:31	20.05	26.83	20248	Section	0.1280	0.1750	0.0222	0.0947	–0.0200	–0.0200	0.0216	–0.0200	–0.0200	–0.0200	–0.0200	–0.0200	–0.0200	–0.0200
KA3110A	2010-06-15 10:12	20.05	26.83	20262	Section	0.1420	0.1760	–0.0200	0.0933	–0.0200	–0.0200	–0.0200	–0.0200	–0.0200	–0.0200	–0.0200	–0.0200	–0.0200	–0.0200

Circulation experiments – Isotopes.

Idcode	Sampling date	Secup m	Seclow m	SKB no.	Water type	pmC	C13 dev PDB	AGe_BP year	AGE_BP _CORR year	PMC_ORG	C13_ORG dev PDB	AGE_BP _ORG year	AGE_BP _CORR year	S34_SO4 dev CDT	S34_HS dev CDT	D dev SMOW	TR TU	O18 dev SMOW
KA3385A	2010-10-06 08:50	32.05	34.18	20346	Section	34.30	–18.90	8,536	593	54.80	–28.00	4,778	241	18.9	19.3	n.a.	n.a.	–11.00
KA3385A	2011-01-20 09:30	32.05	34.18	20573	Section	32.80	–22.50	8,892	632	62.40	–23.10	3,734	170	20.8	17.4	–84.2	n.a.	–10.80
KA3385A	2011-11-15 09:21	32.05	34.18	22012	Section	n.a.	n.a.	n.a.	n.a.	n.a.	n.a.	n.a.	n.a.	n.a.	n.a.	n.a.	n.a.	n.a.
KA3385A	2011-11-15 09:30	32.05	34.18	22013	Section	n.a.	n.a.	n.a.	n.a.	n.a.	n.a.	n.a.	n.a.	n.a.	n.a.	n.a.	n.a.	n.a.
KA3385A	2011-11-15 09:39	7.05	31.05	22014	Section	n.a.	n.a.	n.a.	n.a.	n.a.	n.a.	n.a.	n.a.	n.a.	n.a.	n.a.	n.a.	n.a.
KA3110A	2010-10-05 10:07	20.05	26.83	20357	Section	70.50	–13.70	2,754	44	74.20	–34.90	2,341	52	27.0	13.6	–64.3	n.a.	–8.30
KA3110A	2010-10-05 14:42	20.05	26.83	20359	Fracture	n.a.	n.a.	n.a.	n.a.	88.70	–34.70	2,754	44	26.8	b.d	–61.2	n.a.	–8.20
KA3110A	2010-10-26 10:08	20.05	26.83	20361	Section	81.00	–10.00	1,635	30	89.80	–33.60	809	38	27.1	4.1	–58.3	n.a.	–7.80
KA3110A	2010-11-16 09:55	20.05	26.83	20363	Section	82.40	–6.30	1,500	30	88.20	–30.00	952	50	27.7	–4.9	–59.1	n.a.	–7.80
KA3110A	2010-12-07 16:48	20.05	26.83	20372	Section	82.80	–9.10	1,458	30	90.90	–26.50	711	37	26.7	0.0	–75.4	n.a.	–7.90
KA3110A	2011-04-21 08:45	20.05	26.83	20717	Fracture	80.90	–9.90	1,641	30	n.a.	n.a.	n.a.	n.a.	n.a.	n.a.	n.a.	n.a.	n.a.

Circulation experiments – Stable isotopes in gases.

Idcode	Sampling date	Secup (m)	Seclow (m)	SKB no.	Water type	$\delta^{13}C$ in CH4 dev PDB	$\delta^{13}C$ in CO2 dev PDB	$\delta^{2}H$ in CH4 dev PDB	$\delta^{2}H$ in H2 dev PDB	$\delta^{18}O$ in CO2 dev PDB
KA3110A	2010-10-05 09:49	20.05	26.83	20357	Section	–41.3	–19.5	–117.0	–830	35.7
KA3110A	2010-10-05 14:23	20.05	26.83	20359	Fracture	–46.1	–19.5	–97.7	–837	34.3
KA3110A	2010-10-26 09:36	20.05	26.83	20361	Section	–49.1	–23.7	–142.7	–817	28.2
KA3110A	2010-11-16 09:41	20.05	26.83	20363	Section	–49.3	–23.9	–131.3	b.d	29.6
KA3110A	2010-12-07 16:20	20.05	26.83	20372	Section	–46.9	–19.3	–160.0	b.d	35.8
KA3110A	2010-10-05 10:23	20.05	26.83	20358	Fracture	n.a.	n.a.	n.a.	n.a	n.a.
KA3385A	2010-10-06 08:33	32.05	34.18	20346	Section	–47.5	–22.7	–120.2	b.d	28.5
KA3385A	2010-10-06 11:00	32.05	34.18	20348	Fracture	–46.4	–23.3	–113.9	b.d	27.1
KA3385A	2011-01-20 09:11	32.05	34.18	20573	Section	–46.3	–24.2	–111.1	b.d	31.6
KA3385A	2010-10-06 09:25	32.05	34.18	20347	Fracture	n.a.	n.a.	n.a.	n.a	n.a.

b.d = below detection limit

Circulation experiments – Sulphide and iron (II) during discharge and circulation (section volumes: KA3110A:1: 14.5 L and KA3385A:1: 5 L).

Idcode	Sampling date	Secup (m)	Seclow (m)	SKB no.	pH	Fe^{2+}	HS^{-} (mg L^{-1})	Water type	Discharged volume (l)
KA3110A	2010-04-21 08:50	20.05	26.83	20158	n.a.	0.79	0.81	Section	1.00
KA3110A	2010-04-21 08:56	20.05	26.83	20159	n.a.	0.76	0.89	Section	2.00
KA3110A	2010-04-21 09:04	20.05	26.83	20161	n.a.	0.47	1.38	Section	3.00
KA3110A	2010-04-21 09:13	20.05	26.83	20162	n.a.	0.41	2.05	Section	4.00
KA3110A	2010-04-21 09:20	20.05	26.83	20163	n.a.	0.34	2.4	Section	5.00
KA3110A	2010-04-21 09:28	20.05	26.83	20164	n.a.	0.29	3.48	Section	6.00
KA3110A	2010-04-21 09:36	20.05	26.83	20165	n.a.	0.26	3.23	Section	7.00
KA3110A	2010-04-21 09:43	20.05	26.83	20166	n.a.	0.21	2.58	Section	8.00
KA3110A	2010-04-21 09:51	20.05	26.83	20167	n.a.	0.18	2.26	Section	9.00
KA3110A	2010-04-21 09:59	20.05	26.83	20168	n.a.	0.17	2.23	Section	10.00
KA3110A	2010-04-21 10:06	20.05	26.83	20169	n.a.	0.19	2.21	Section	11.00
KA3110A	2010-04-21 10:14	20.05	26.83	20170	n.a.	0.22	2.23	Section	12.00
KA3110A	2010-04-21 10:21	20.05	26.83	20171	n.a.	0.27	2.01	Section	13.00
KA3110A	2010-04-21 10:29	20.05	26.83	20172	n.a.	0.33	1.86	Section	14.00
KA3110A	2010-05-11 08:53	20.05	26.83	20182	n.a.	0.0	106.65	Section	0.25
KA3110A	2010-05-11 09:00	20.05	26.83	20183	n.a.	0.0	99.82	Section	0.46
KA3110A	2010-05-11 09:07	20.05	26.83	20184	n.a.	0.01	98.59	Section	0.71
KA3110A	2010-05-11 09:11	20.05	26.83	20185	n.a.	0.0	100.84	Section	1.00
KA3110A	2010-05-11 09:19	20.05	26.83	20186	n.a.	0.01	108.7	Section	2.00
KA3110A	2010-05-11 09:26	20.05	26.83	20187	n.a.	0.0	58.38	Section	3.00
KA3110A	2010-05-11 09:33	20.05	26.83	20188	n.a.	0.16	24.39	Section	4.00
KA3110A	2010-05-11 09:39	20.05	26.83	20189	n.a.	0.18	18.68	Section	5.00
KA3110A	2010-05-11 09:47	20.05	26.83	20190	n.a.	0.23	19.39	Section	6.00
KA3110A	2010-05-11 09:54	20.05	26.83	20191	n.a.	0.21	15.72	Section	7.00
KA3110A	2010-05-11 10:01	20.05	26.83	20192	n.a.	0.23	20.82	Section	8.00
KA3110A	2010-05-11 10:07	20.05	26.83	20193	n.a.	0.22	19.6	Section	9.00
KA3110A	2010-05-11 10:13	20.05	26.83	20194	n.a.	0.23	14.7	Section	10.00
KA3110A	2010-05-11 10:20	20.05	26.83	20195	n.a.	0.27	14.9	Section	11.00
KA3110A	2010-05-11 10:27	20.05	26.83	20196	n.a.	0.3	11.74	Section	12.00
KA3110A	2010-05-11 10:33	20.05	26.83	20197	n.a.	0.33	10.00	Section	13.00
KA3110A	2010-05-11 10:37	20.05	26.83	20198	n.a.	0.33	9.8	Section	14.00
KA3110A	2010-06-01 08:47	20.05	26.83	20218	n.a.	0.01	55.62	Section	0.25
KA3110A	2010-06-01 08:49	20.05	26.83	20219	n.a.	0.04	53.79	Section	0.5

Idcode	Sampling date	Secup (m)	Seclow (m)	SKB no.	pH	Fe^{2+}	HS^- (mg L^{-1})	Water type	Discharged volume (l)
KA3110A	2010-06-01 08:53	20.05	26.83	20220	n.a.	0.01	48.58	Section	0.75
KA3110A	2010-06-01 08:56	20.05	26.83	20221	n.a.	0.05	43.58	Section	1.00
KA3110A	2010-06-01 09:02	20.05	26.83	20222	n.a.	0.02	41.13	Section	2.00
KA3110A	2010-06-01 09:07	20.05	26.83	20223	n.a.	0.05	29.9	Section	3.00
KA3110A	2010-06-01 09:13	20.05	26.83	20224	n.a.	0.27	23.98	Section	4.00
KA3110A	2010-06-01 09:18	20.05	26.83	20225	n.a.	0.42	13.17	Section	5.00
KA3110A	2010-06-01 09:24	20.05	26.83	20226	n.a.	0.44	6.53	Section	6.00
KA3110A	2010-06-01 09:29	20.05	26.83	20227	n.a.	0.37	7.76	Section	7.00
KA3110A	2010-06-01 09:34	20.05	26.83	20228	n.a.	0.34	8.37	Section	8.00
KA3110A	2010-06-01 09:39	20.05	26.83	20229	n.a.	0.36	8.06	Section	9.00
KA3110A	2010-06-01 09:44	20.05	26.83	20230	n.a.	0.38	7.96	Section	10.00
KA3110A	2010-06-01 09:50	20.05	26.83	20231	n.a.	0.38	8.47	Section	11.00
KA3110A	2010-06-01 09:55	20.05	26.83	20232	n.a.	0.38	7.25	Section	12.00
KA3110A	2010-06-01 10:00	20.05	26.83	20233	n.a.	0.42	5.82	Section	13.00
KA3110A	2010-06-01 10:05	20.05	26.83	20234	n.a.	0.42	5.41	Section	14.00
KA3110A	2010-06-15 08:23	20.05	26.83	20265	n.a.	0.07	28.48	Section	0.25
KA3110A	2010-06-15 08:26	20.05	26.83	20266	n.a.	0.08	27.35	Section	0.5
KA3110A	2010-06-15 08:29	20.05	26.83	20267	n.a.	0.07	27.76	Section	0.75
KA3110A	2010-06-15 08:31	20.05	26.83	20268	n.a.	0.05	27.05	Section	1.00
KA3110A	2010-06-15 08:38	20.05	26.83	20269	n.a.	0.1	26.84	Section	2.00
KA3110A	2010-06-15 08:44	20.05	26.83	20270	n.a.	0.1	20.41	Section	3.00
KA3110A	2010-06-15 08:51	20.05	26.83	20271	n.a.	0.19	15.11	Section	4.00
KA3110A	2010-06-15 08:57	20.05	26.83	20272	n.a.	0.4	6.23	Section	5.00
KA3110A	2010-06-15 09:03	20.05	26.83	20273	n.a.	0.52	7.04	Section	6.00
KA3110A	2010-06-15 09:10	20.05	26.83	20274	n.a.	0.5	5.82	Section	7.00
KA3110A	2010-06-15 09:16	20.05	26.83	20275	n.a.	0.53	6.74	Section	8.00
KA3110A	2010-06-15 09:22	20.05	26.83	20276	n.a.	0.51	5.61	Section	9.00
KA3110A	2010-06-15 09:28	20.05	26.83	20277	n.a.	0.55	5.31	Section	10.00
KA3110A	2010-06-15 09:34	20.05	26.83	20278	n.a.	0.52	4.18	Section	11.00
KA3110A	2010-06-15 09:40	20.05	26.83	20279	n.a.	0.53	3.98	Section	12.00
KA3110A	2010-06-15 09:46	20.05	26.83	20281	n.a.	0.64	3.37	Section	13.00
KA3110A	2010-06-15 09:52	20.05	26.83	20282	n.a.	0.65	3.27	Section	14.00
KA3110A	2010-10-05 08:37	20.05	26.83	20349	n.a.	0.05	72.97	Section	0.00
KA3110A	2010-10-05 08:44	20.05	26.83	20350	n.a.	0.00	65.73	Section	1.00
KA3110A	2010-10-05 08:51	20.05	26.83	20351	n.a.	0.02	39.19	Section	2.00
KA3110A	2010-10-05 09:03	20.05	26.83	20352	n.a.	0.28	5.82	Section	4.00
KA3110A	2010-10-05 09:15	20.05	26.83	20353	n.a.	0.28	7.55	Section	6.00
KA3110A	2010-10-05 09:26	20.05	26.83	20354	n.a.	0.31	6.84	Section	8.00
KA3110A	2010-10-05 09:37	20.05	26.83	20355	n.a.	0.3	5.41	Section	10.00
KA3110A	2010-10-05 09:47	20.05	26.83	20356	n.a.	0.44	3.27	Section	12.00
KA3110A	2010-10-05 09:49	20.05	26.83	20357	7.84	0.56	4.17	Section	14.00
KA3110A	2010-10-05 14:23	20.05	26.83	20359	7.89	1.1	0.12	fracture	140.00
KA3110A	2010-10-26 08:18	32.05	34.18	20360	n.a.	0.01	16.84	Section	0.4
KA3110A	2010-10-26 09:36	20.05	26.83	20361	7.6	0.7	0.67	Section	14.00
KA3110A	2010-11-16 08:24	32.05	34.18	20362	n.a.	0.00	10.92	Section	0.4
KA3110A	2010-11-16 09:41	20.05	26.83	20363	7.59	0.51	0.34	Section	14.00
KA3110A	2010-12-07 14:42	32.05	34.18	20364	n.a.	0.11	8.77	Section	0.00
KA3110A	2010-12-07 14:55	32.05	34.18	20365	n.a.	0.05	4.95	Section	1.00
KA3110A	2010-12-07 15:01	32.05	34.18	20366	n.a.	0.08	4.95	Section	2.00
KA3110A	2010-12-07 15:13	32.05	34.18	20367	n.a.	0.1	1.8	Section	4.00
KA3110A	2010-12-07 15:23	32.05	34.18	20368	n.a.	0.73	0.67	Section	6.00

Idcode	Sampling date	Secup (m)	Seclow (m)	SKB no.	pH	Fe^{2+}	HS^- (mg L^{-1})	Water type	Discharged volume (l)
KA3110A	2010-12-07 15:40	32.05	34.18	20369	n.a.	0.8	0.8	Section	8.00
KA3110A	2010-12-07 15:51	32.05	34.18	20370	n.a.	0.77	0.57	Section	10.00
KA3110A	2010-12-07 16:08	32.05	34.18	20371	n.a.	0.83	0.44	Section	12.00
KA3110A	2010-12-07 16:20	20.05	26.83	20372	7.79	0.93	0.23	Section	14.00
KA3385A	2010-05-11 13:09	32.05	34.18	20200	n.a.	0.8	1.01	Section	1.00
KA3385A	2010-05-11 13:17	32.05	34.18	20201	n.a.	0.17	0.59	Section	2.00
KA3385A	2010-05-11 13:26	32.05	34.18	20202	n.a.	0.22	0.1	Section	3.00
KA3385A	2010-05-11 13:35	32.05	34.18	20203	n.a.	0.2	0.02	Section	4.00
KA3385A	2010-06-01 12:38	32.05	34.18	20236	n.a.	0.12	0.08	Section	1.00
KA3385A	2010-06-01 12:45	32.05	34.18	20237	n.a.	0.33	0.83	Section	2.00
KA3385A	2010-06-01 12:51	32.05	34.18	20238	n.a.	0.22	0.43	Section	3.00
KA3385A	2010-06-01 12:58	32.05	34.18	20239	n.a.	0.27	0.31	Section	4.00
KA3385A	2010-06-15 12:24	32.05	34.18	20284	n.a.	0.31	2.6	Section	1.00
KA3385A	2010-06-15 12:32	32.05	34.18	20285	n.a.	0.32	4.67	Section	2.00
KA3385A	2010-06-15 12:40	32.05	34.18	20286	n.a.	0.29	4.03	Section	3.00
KA3385A	2010-06-15 12:47	32.05	34.18	20287	n.a.	0.3	3.85	Section	4.00
KA3385A	2010-10-06 08:00	32.05	34.18	20343	n.a.	0.58	2.76	Section	0.00
KA3385A	2010-10-06 08:08	32.05	34.18	20344	n.a.	0.46	1.1	Section	1.00
KA3385A	2010-10-06 08:16	32.05	34.18	20345	n.a.	0.35	3.52	Section	2.00
KA3385A	2010-10-06 08:33	32.05	34.18	20346	7.57	0.25	3.61	Section	4.00
KA3385A	2011-01-20 08:36	32.05	34.18	20576	n.a.	0.00	26.94	Section	0.00
KA3385A	2011-01-20 08:36	32.05	34.18	20577	n.a.	0.11	23.17	Section	1.00
KA3385A	2011-01-20 08:36	32.05	34.18	20578	n.a.	0.11	0.00	Section	2.00
KA3385A	2011-01-20 08:36	32.05	34.18	20579	n.a.	0.00	1.00	Section	4.00

Acetate.

Idcode	Sampling date	Secup (m)	Seclow (m)	SKB no.	Water type	Acetate mg L^{-1}
KA3110A	2010-03-30 11:15	20.05	26.83	20136	Section	5.12
KA3110A	2010-03-30 15:30	20.05	26.83	20137	Fracture	3.42
KA3110A	2010-04-21 10:25	20.05	26.83	20154	Section	5.15
KA3110A	2010-05-11 10:42	20.05	26.83	20180	Section	38.89
KA3110A	2010-06-01 08:26	20.05	26.83	20216	Section	147.41
KA3110A	2010-06-01 10:07	20.05	26.83	20248	Section	16.96
KA3110A	2010-06-15 09:53	20.05	26.83	20262	Section	6.8
KA3110A	2010-10-26 09:36	20.05	26.83	20361	Section	1.74
KA3110A	2010-11-16 09:41	20.05	26.83	20363	Section	2.3
KA3110A	2010-12-07 16:20	20.05	26.83	20372	Section	2.35
KA3385A	2010-03-30 09:40	32.05	34.18	20134	Section	1.73
KA3385A	2010-03-30 14:20	32.05	34.18	20135	Fracture	1.16
KA3385A	2010-04-21 11:26	32.05	34.18	20153	Section	4.02
KA3385A	2010-05-11 13:41	32.05	34.18	20179	Section	6.35
KA3385A	2010-06-01 13:00	32.05	34.18	20247	Section	9.54
KA3385A	2010-06-15 12:49	32.05	34.18	20263	Section	25.1
KA3385A	2010-10-06 08:33	32.05	34.18	20346	Section	74.42
KA3385A	2011-01-20 09:11	32.05	34.18	20573	Section	26.86

Microbial numbers.

Idcode	Sampling date	Secup (m)	Seclow (m)	SKB no.	Water type	TOTAL_NUMBER (cells mL^{-1})	TOTAL_NUMBER_SD (cells mL^{-1})	IRB (cells mL^{-1})	IRB_LLIM (cells mL^{-1})	IRB_ULIM (cells mL^{-1})
KA3110A	2010-03-30 11:15	20.05	26.83	20136	Section	64,000	11,000	5.0	2.0	15.0
KA3110A	2010-03-30 15:30	20.05	26.83	20137	Fracture	17,000	2,100	1.4	0.6	3.5
KA3110A	2010-04-21 10:25	20.05	26.83	20154	Section	160,000	8,300	1.7	0.7	4.6
KA3110A	2010-05-11 10:42	20.05	26.83	20180	Section	270,000	72,000	9.0	4.0	25.0
KA3110A	2010-06-01 08:26	20.05	26.83	20216	Section	1200,000	400,000	n.a.	n.a.	n.a.
KA3110A	2010-06-01 10:07	20.05	26.83	20248	Section	260,000	24,000	500.0	200.0	2,000.0
KA3110A	2010-06-15 09:53	20.05	26.83	20262	Section	150,000	54,000	130.0	50.0	390.0
KA3110A	2010-06-15 12:24	20.05	26.83	20216	Section	1,100,000	260,000	n.a.	n.a.	n.a.
KA3110A	2010-10-05 09:49	20.05	26.83	20357	Section	200,000	15,000	1.1	0.4	2.9
KA3110A	2010-10-05 14:23	20.05	26.83	20359	Fracture	110,000	23,000	2.3	0.9	8.6
KA3110A	2010-12-07 16:20	20.05	26.83	20372	Section	130,000	1,400	1.1	0.4	2.9
KA3385A	2010-03-30 09:40	32.05	34.18	20134	Section	23,000	5,000	1.3	0.5	3.8
KA3385A	2010-03-30 14:20	32.05	34.18	20135	Fracture	4,700	2,100	0.4	0.1	1.5
KA3385A	2010-04-21 11:26	32.05	34.18	20153	Section	5,200	2,000	0.7	0.2	2.0
KA3385A	2010-05-11 13:41	32.05	34.18	20179	Section	6,100	2,200	1.1	0.4	2.9
KA3385A	2010-06-01 13:00	32.05	34.18	20247	Section	710,000	64,000	3.0	1.0	12.0
KA3385A	2010-06-15 12:14	32.05	34.18	20283	Section	350,000	59,000	n.a.	n.a.	n.a.
KA3385A	2010-06-15 12:49	32.05	34.18	20263	Section	330,000	20,000	5.0	2.0	15.0
KA3385A	2010-10-06 08:33	32.05	34.18	20346	Section	330,000	54,000	3.0	1.0	12.0
KA3385A	2011-01-20 09:11	32.05	34.18	20573	Section	1,500,000	84,000	5.0	2.0	15.0

Microbial numbers, continued.

Idcode	Sampling date	Secup (m)	Seclow (m)	SKB no.	Water type	AA (cells mL^{-1})	AA_LLIM (cells mL^{-1})	AA_ULIM (cells mL^{-1})	SRB (cells mL^{-1})	SRB_LLIM (cells mL^{-1})	SRB_ULIM (cells mL^{-1})
KA3110A	2010-03-30 11:15	20.05	26.83	20136	Section	17.0	7.0	48.0	11,000	4,000	30,000
KA3110A	2010-03-30 15:30	20.05	26.83	20137	Fracture	9.0	4.0	25.0	800	300	2,500
KA3110A	2010-04-21 10:25	20.05	26.83	20154	Section	50.0	20.0	170.0	8,000	3,000	25,000
KA3110A	2010-05-11 10:42	20.05	26.83	20180	Section	160.0	60.0	530.0	30,000	10,000	120,000
KA3110A	2010-06-01 08:26	20.05	26.83	20216	Section	n.a.	n.a.	n.a.	30,000	10,000	130,000
KA3110A	2010-06-01 10:07	20.05	26.83	20248	Section	8.0	3.0	25.0	14,000	6,000	36,000
KA3110A	2010-06-15 09:53	20.05	26.83	20262	Section	280.0	120.0	690.0	35,000	16,000	82,000
KA3110A	2010-06-15 12:24	20.05	26.83	20216	Section	n.a.	n.a.	n.a.	110,000	40,000	300,000
KA3110A	2010-10-05 09:49	20.05	26.83	20357	Section	130.0	50.0	390.0	3,000	1,000	12,000
KA3110A	2010-10-05 14:23	20.05	26.83	20359	Fracture	5.0	2.0	17.0	3,000	1,000	12,000
KA3110A	2010-12-07 16:20	20.05	26.83	20372	Section	8.0	3.0	25.0	2,300	900	8,600
KA3385A	2010-03-30 09:40	32.05	34.18	20134	Section	1.3	0.5	3.8	50	20	150
KA3385A	2010-03-30 14:20	32.05	34.18	20135	Fracture	2.3	0.9	8.6	13	5	39
KA3385A	2010-04-21 11:26	32.05	34.18	20153	Section	1.7	0.7	4.6	110	40	300
KA3385A	2010-05-11 13:41	32.05	34.18	20179	Section	13.0	5.0	39.0	1,300	500	3,900
KA3385A	2010-06-01 13:00	32.05	34.18	20247	Section	11.0	4.0	30.0	160,000	60,000	530,000
KA3385A	2010-06-15 12:14	32.05	34.18	20283	Section	n.a.	n.a.	n.a.	7,000	3,000	21,000
KA3385A	2010-06-15 12:49	32.05	34.18	20263	Section	130.0	50.0	390.0	1,700	700	4,800
KA3385A	2010-10-06 08:33	32.05	34.18	20346	Section	1.7	0.7	4.0	300,000	100,000	1,200,000
KA3385A	2011-01-20 09:11	32.05	34.18	20573	Section	8.0	3.0	25.0	>1,600,000		

Circulation experiments – Dissolved gases.

Idcode	Sampling date	Secup (m)	Seclow (m)	SKB no.	Water type	He (mL L^{-1})	Ar (mL L^{-1})	N_2 (mL L^{-1})	CO_2 (mL L^{-1})	CH_4 (mL L^{-1})	H2 (µL L^{-1})	CO (µL L^{-1})	C_2H_2 (µL L^{-1})	C_2H4 (µL L^{-1})	C_2H_6 (µL L^{-1})	C_3H_8 (µL L^{-1})	C_3H_6 (µL L^{-1})	Gas volume (mL)	Volume extracted water (g)
Sulphide 1																			
KA3385A	2010-03-30 09:40	32.05	34.18	20134	Section	6.23		62.500	0.142	0.146	13.6	1.400						69.30	
KA3110A	2010-03-30 11:15	20.05	26.83	20136	Section	0.32		42.300	2.740	0.212	135.0	0.440						43.30	
KA3385A	2010-03-30 14:20	32.05	34.18	20135	Fracture	7.87		65.800	0.073	0.114	156.0	0.560						74.60	
KA3110A	2010-03-30 15:30	20.05	26.83	20137	Fracture	0.38		41.300	2.240	0.202	32.8	0.380						44.40	
KA3110A	2010-04-21 10:25	20.05	26.83	20154	Section	0.41		4.290	2.160	0.236	180.7	1.000						46.30	
KA3385A	2010-04-21 11:26	32.05	34.18	20153	Section	5.82		53.800	0.136	0.130	11.3	2.060						60.40	
KA3110A	2010-05-11 10:42	20.05	26.83	20180	Section	0.41		45.800	1.680	0.286	95.8	0.800						48.90	
KA3385A	2010-05-11 13:41	32.05	34.18	20179	Section	9.5		57.100	0.107	0.132	2.6	1.940						80.00	
KA3110A	2010-06-01 10:07	20.05	26.83	20248	Section	0.41		47.000	2.610	0.252	94.5	0.580						50.80	
KA3385A	2010-06-01 13:00	32.05	34.18	20247	Section	6.35		55.100	0.156	0.138	35.5	2.090						61.10	
KA3110A	2010-06-15 09:53	20.05	26.83	20262	Section	0.36		49.600	2.000	0.259	0.5	1.300						52.90	
KA3385A	2010-06-15 12:49	32.05	34.18	20263	Section	6.21		64.600	0.292	0.135	11.7	1.930						71.30	
Sulphide2																			
KA3110A	2010-10-05 09:49	20.05	26.83	20357	Section	0.409	0.172	42.9	0.264	0.238	65.6	0.21	–0.8	–0.8	–0.8	–0.8	–0.8	44.1	193
KA3110A	2010-10-05 14:23	20.05	26.83	20359	Fracture	0.406	0.415	55.8	1.48	0.241	20.5	0.74	–0.1	–0.1	–0.09	–0.1	–0.1	58.4	193
KA3385A	2010-10-06 08:33	20.05	26.83	20346	Section	6.01	0.568	60.3	0.122	0.132	0.63	0.3	–0.11	–0.11	0.07	–0.11	–0.11	67.2	190
KA3385A	2010-10-06 11:00	20.05	26.83	20348	Fracture	5.14	–0.1	65.7	0.194	0.137	3.98	0.66	-0.13	–0.13	–0.12	–0.13	–0.13	71.2	192
KA3110A	2010-10-26 09:36	32.05	34.18	20361	Section	0.438	0.56		0.798	0.291	23.7	0.79	–0.21	–0.21	–0.2	–0.2	–0.21	129.0	193
KA3110A	2010-11-16 09:41	32.05	34.18	20363	Section	0.426	0.423	82.9	1.02	0.263	7.31	0.65	–0.14	–0.15	–0.14	–0.14	–0.14	85.1	194
KA3110A	2010-12-07 16:20	20.05	26.83	20372	Section	0.124	0.204	52.9	1.4	0.242	5.15	0.29	–0.09	–0.09	–0.09	–0.09	–0.09	54.9	192
KA3385A	2011-01-20 09:11	32.05	34.18	20573	Section	6.48	b.d.	65.9	0.916	0.138	2.42	1.21	–0.16	–0.14	0.04	–0.15	–0.16	72.2	196

Appendix G

Hydraulic tests and groundwater flow measurements in KA3110A and KA3385A

Tests within the Sulphide project

Calle Hjerne, Anna Lindquist, Pernilla Thur, Jan-Erik Ludvigson
Geosigma. June 2012

Abstract

In Äspö Hard Rock Laboratory an investigation about sulphide production in deep groundwater is in progress. Groundwater flow measurements using the tracers Uranine and iodine and hydraulic tests will complement the chemical investigations with hydrogeological information. The aim of the tests is to determine the magnitude of the natural groundwater flow through the borehole sections and to estimate the transmissivity in the tested sections.

The tests in KA3385A:1 indicates a groundwater flow of 40 mL/h and a transmissivity of 2×10^{-8} m^2/s.

During circulation of water in KA3110A:1, an unexpected and continuous pressure response was observed. A check of the pressure during earlier water sampling events in the section showed that the unexpected pressure response is recurrent. The conclusion is that the groundwater flow measurement, hydraulic test and water samplings probably are significantly affected by some hydraulic effect and should not be regarded as representative for an undisturbed section.

Sammanfattning

I Äspö laboratoriet pågår ett projekt rörande undersökning av sulfidproduktion i djupa grundvatten. Med hjälp av hydrauliska tester och utspädningsmätningar med uranin och jodid som spårämnen ska de kemiska undersökningarna kompletteras med hydrogeologisk information. Målet med testerna är att bestämma storleken på det naturliga grundvattenflödet genom sektionerna samt att beräkna transmissiviteten för de undersökta sektionerna.

Mätningar i KA3885A:1 tyder på ett grundvattenflöde på 40 mL/timme och en transmissivitet på 2×10^{-8} m^2/s.

Under cirkulation av vatten i KA3110A:1 observerades en oväntad och ihållande tryckrespons. En kontroll av tryck under tidigare vattenprovtagningar i sektionen visade att den oväntade tryckresponsen är återkommande. Slutsatsen är att utspädningsmätningen, det hydrauliska testet samt vattenprovtagningarna troligtvis är betydligt påverkade av någon hydraulisk effekt och att dessa inte bör anses representera en ostörd sektion.

G1 Execution and equipment

Tests performed

Dilution measurements and hydraulic tests were carried out in two borehole sections in the Äspö Hard Rock Laboratory according to Table G-1. The performed tests followed the activity plan AP TD KBP4001-11-019. The borehole equipment used for all test was the permanently installed packer system.

Table G-1. Events.

Event	Borehole: Section	Secup [m]	Seclow [m]	Start test	Stop test
Hydraulic test	KA3385A:1	32.05	34.18	2011-04-04 16:22:00	2011-04-04 19:22:00
Groundwater flow measurement	KA3385A:1	32.05	34.18	2011-04-04 13:21:00	2011-04-12 10:30:00
Hydraulic test	KA3110A:1	20.05	26.83	2011-04-06 08:30:00	2011-04-06 11:30:00
Water sampling	KA3110A:1	20.05	26.83	2011-04-06 09:22:00	2011-04-06 09:29:00
Groundwater flow measurement	KA3110A:1	20.05	26.83	2011-04-06 16:00:00	2011-04-12 10:30:00

Hydraulic test

Prior to the hydraulic test the flow meter used was calibrated at the test sites. Raw values were registered during a few minutes and the actual flow rate was simultaneously measured (Table G-2). The relation between raw-value and flow rate was plotted and a straight-line was fitted (Figure G-1).

The hydraulic test was carried out with a flow period lasting for 3 hours (Table G-1). The flow rate from the test section was kept constant at 150 mL/min (KA3385A) and 590 mL/min (KA3110A) by using a flow meter with a regulation unit. Flow rate and the pressure were logged with HMS (HydroMonitoringSystem). After the flow period the pressure recovery was also registered.

During the hydraulic test in KA3110A a water sample (SKB no: 20665) was collected after 52 minutes of flow period and the volume discharged at that time (30.7 L) corresponded to two section volumes.

Groundwater flow measurements

To determine the natural groundwater flow through the investigated section, groundwater flow measurements using the dilution technique was performed. The principle of a dilution test is to inject a tracer solution into a borehole section and then monitor the decrease in tracer concentration over time as illustrated in Figure G-2. Groundwater flow measurements were carried out in both KA3110A:1 and KA3385A:1 with Iodide (10,000 ppm) and with the tracer dye Uranine (50 ppm). A drawing of the principal experimental setup is shown in Figure G-3.

Table G-2. Calibration of the flow meter used in the hydraulic tests.

Borehole	Measured flow rate (ml/min)	Mean raw value (%)
KA3385A	50	5.668
	102.5	11.080
	205	22.453
	308	33.750
	154.5	17.027
	154	17.236
	154	17.216
KA3110A	510	56.102
	770	84.383
	589	64.701
	588	64.685
	587	64.877

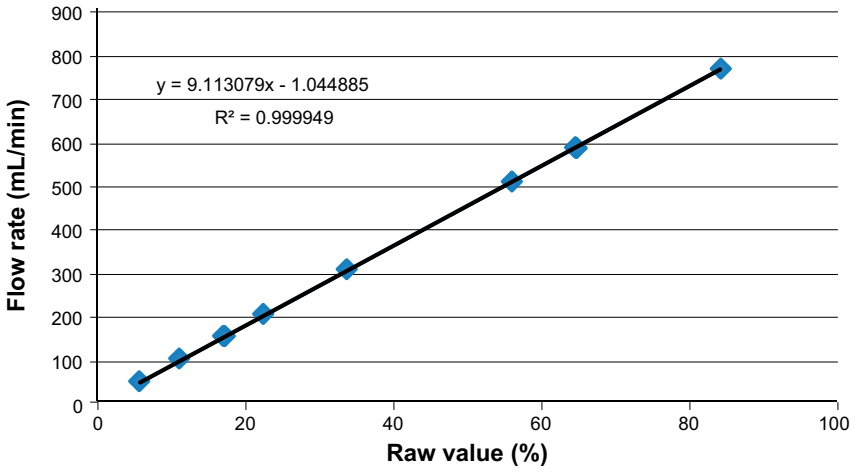

Figure G-1. *Calibration curve for the flow meter used in the hydraulic tests.*

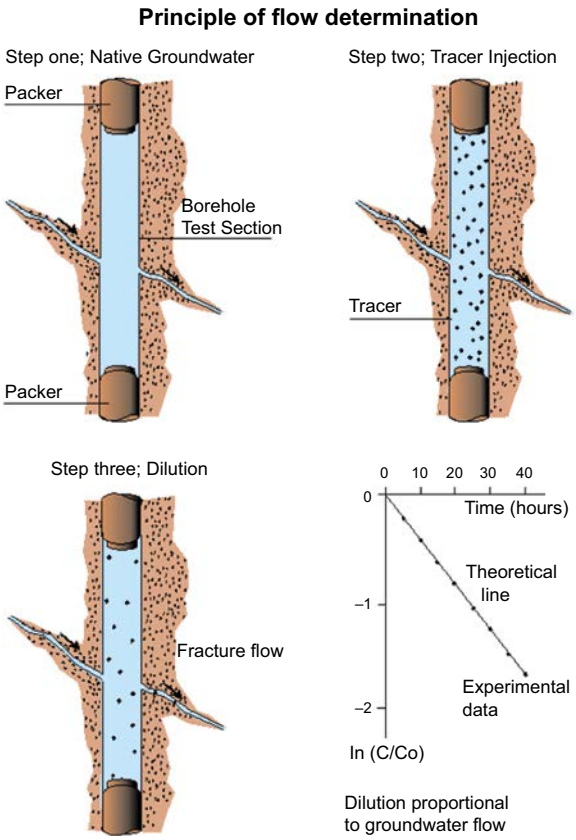

Figure G-2. *General principle of the dilution method.*

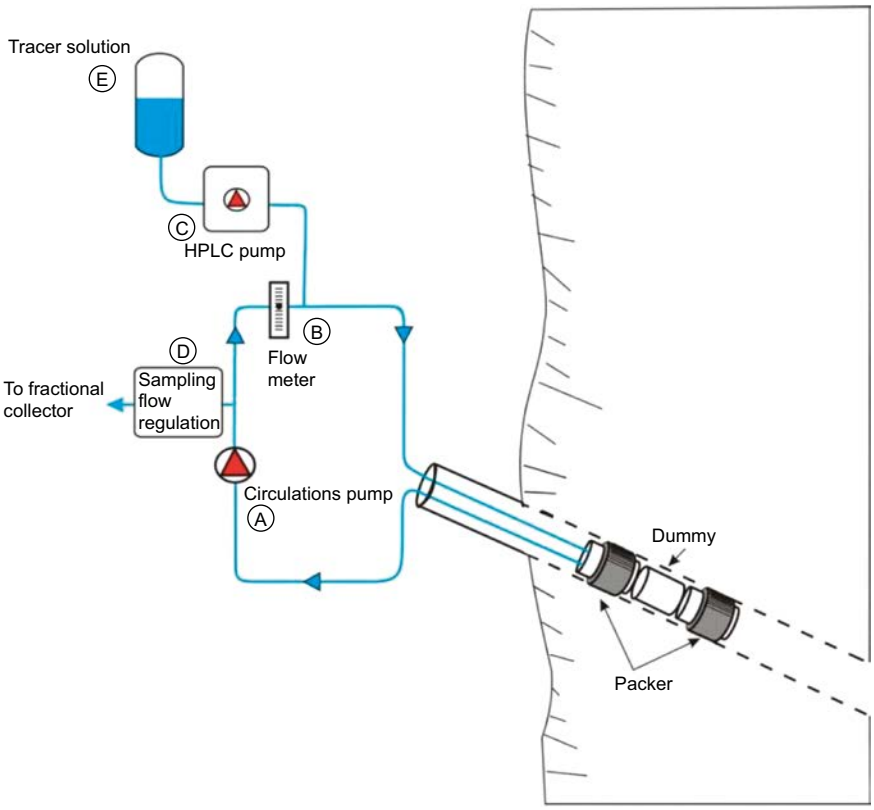

Figure G-3. *Principal drawing of the experimental setup of the groundwater flow measurements with the dilution technique.*

The water was circulated and during the time it takes to exchange one section volume the tracer was injected with a flow rate corresponding to 1/100 of the circulation flow rate. That implies that the theoretical initial concentration in the section was 0.5 ppm Uranine and 100 ppm Iodide (Table G-3). Information about injection times and flow rates are found in Table G-4. During the injection phase the sampling flow rate was increased to match the injection flow rate.

Continuous sampling was carried out during circulation by extracting a constant small flow (constant leak) which was collected by a fractional sampler. Depending on the sampling interval used, the sampling flow rate was adjusted so that a suitable sample volume (c. 15 ml) was collected in each sample tube. The sampling intervals and sample flow rates are found in Table G-5.

Flow rates were calculated from the decrease in tracer concentration versus time through dilution with natural unlabelled groundwater, c.f. Gustafsson (2002). The so-called "dilution curves" were plotted as the natural logarithm of concentration versus time as shown in Figure G-9 and Figure G-10. Theoretically, a straight-line relationship exists between the natural logarithm of the relative tracer concentration (c/c_0) and time (t):

$$Q_{flow} = \frac{-V \cdot \Delta \ln(c/c_0)}{\Delta t} \qquad \text{Equation G-1}$$

where Q_{flow} (m^3/s) is the observed groundwater flow rate through the borehole section and V (m^3) is the volume of the borehole section.

The sampling method where a small sampling volume is continuously withdrawn (constant leak) also causes a dilution of the tracer. The sampling flow is subtracted from the flow calculated in:

$$Q_{bh} = Q_{flow} - Q_{sample} \qquad \text{Equation G-2}$$

Table G-3. Background information.

	Unit	KA3385A Uranine	KA3385A Iodide	KA3110A Uranine	KA3110A Iodide
Background conc.	mg/L	0.01	0.6	0.01	0.5
Initial conc. in section	ppm	1.99	67	3.47	235
Theoretical initial conc. in section	ppm	0.5	100	0.5	100
Theoretical C_{00}	ppm	50	10,000	50	10,000
Injected volume	mL	55	55	152	152
Injected mass	mg	7.6	1,520	2.76	551

Table G-4. Injection times and flow rates.

	Unit	KA3385A	KA3110A
Volume (section + tubes)	L	5.67	15.11
Circulation flow	L/h	10	10
Injection flow	mL/min	1.67	1.67
Injection time	min	33	91
Start injection		2011-04-05 13:21:00	2011-04-06 16:00:00
Stop injection		2011-04-05 13:54:00	2011-04-06 17:31:00

Table G-5. Sampling interval and sampling flow rates.

Test	Sampling flow rate (mL/h)	Sampling interval (min)
KA3385A	13.3	60
KA3110A	13.8	60

G2 Results and interpretation

Hydraulic tests

Both hydraulic tests were evaluated as constant flow rate tests according to standard methods for flow in a porous homogeneous medium. Since the dominating flow regime was interpreted as pseudo spherical in both tests the model by Moench (1985) for flow in a leaky aquifer was used in the evaluation. Furthermore, it was assumed that the background pressure in the rock was stable during the tests. However, in the test in KA3385A a slightly increasing trend of the background pressure might be assumed during the test since water was flowing from the borehole section before the test in conjunction with calibration of the flow meter. The estimated transmissivity from the hydraulic tests is listed in Table G-6.

The transient evaluation of the test in KA3110A is showed in Figure G-4 and Figure G-5. The evaluation of the recovery period is considered as the most representative. No unambiguous evaluation could be made of the flow period. However, the responses during the flow and recovery period are consistent. A possible evaluation of the flow period is shown. The transient evaluation provides a slightly higher transmissivity than the specific capacity Q/s due to the rather high skin factor in this case.

In KA3385A the transient evaluation of the flow period, as showed in Figure G-6, is considered to be the most representative. As seen in Figure G-7, the estimated transmissivity from the recovery period is lower than that of the flow period. However, the transmissivity from the recovery period is considered as uncertain. However, as discussed further on in Section G3, the results from the hydraulic test in KA3110A:1 is quite questionable.

Table G-6. Estimated transmissivity from the hydraulic tests in KA3110A and KA3385A.

Borehole:section	Q/s [m²/s]	T_T [m²/s]
KA3110A:1	2.5×10^{-7}	5.1×10^{-7}
KA3385A:1	3.8×10^{-8}	1.6×10^{-8}

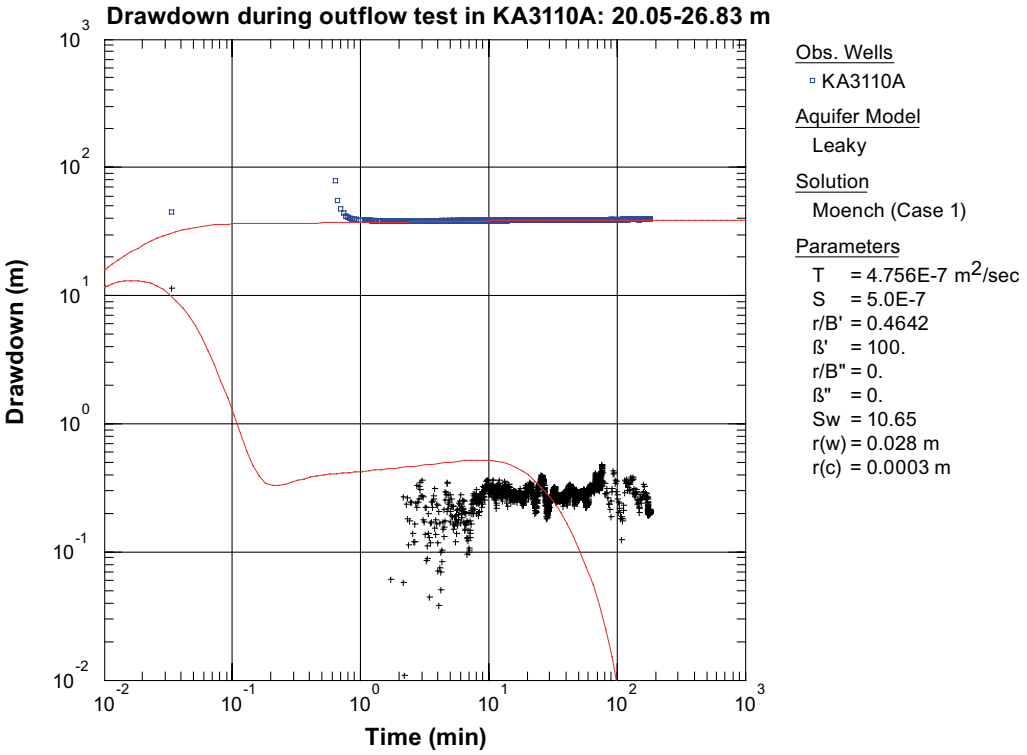

Figure G-4. *Log-log plot of drawdown (▫) and drawdown derivative, ds/d(ln t) (+), versus time in the flowing borehole section KA3110A: 20.05–26.83 m during the hydraulic test.*

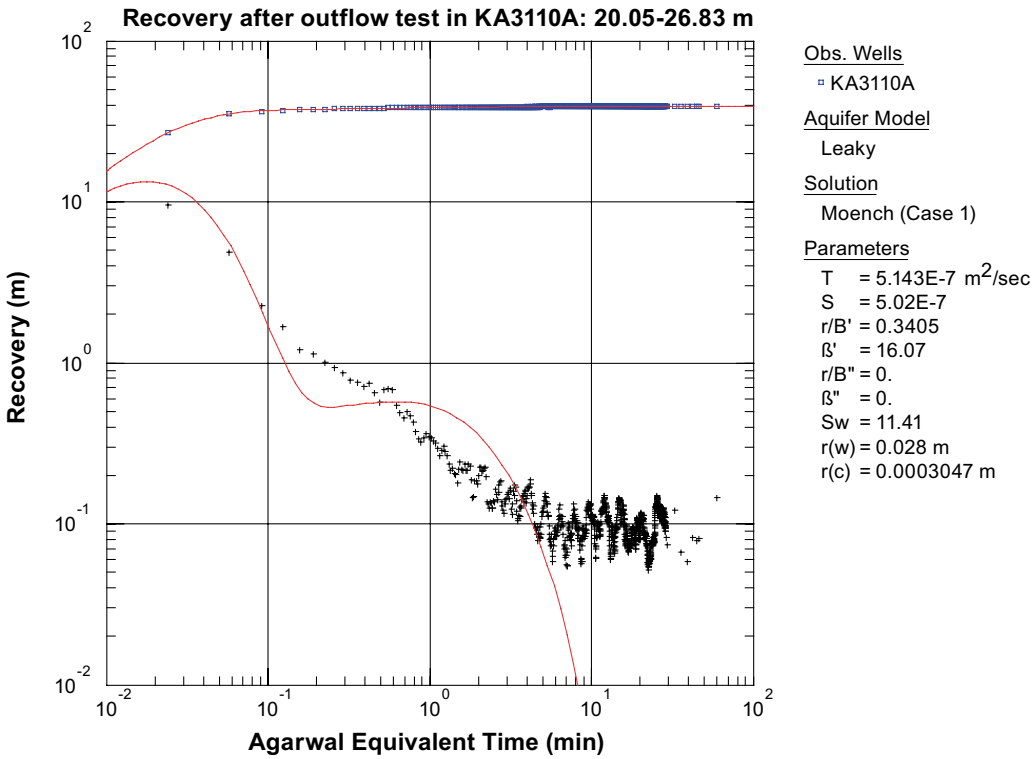

Figure G-5. *Log-log plot of recovery (▫) and recovery derivative, ds/d(ln t) (+), versus Agarwal equivalent time in the flowing borehole section KA3110A: 20.05–26.83 m during the hydraulic test.*

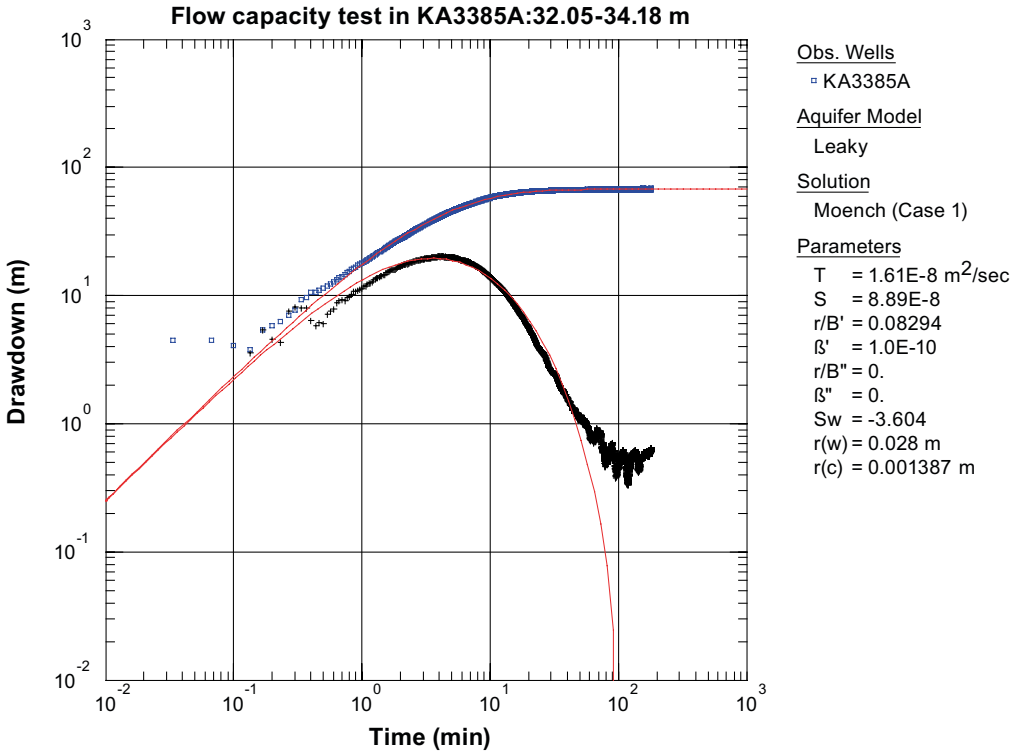

Figure G-6. *Log-log plot of drawdown (▫) and drawdown derivative, ds/d(ln t) (+), versus time in the flowing borehole section KA3385A: 32.05–34.18 m during the hydraulic test.*

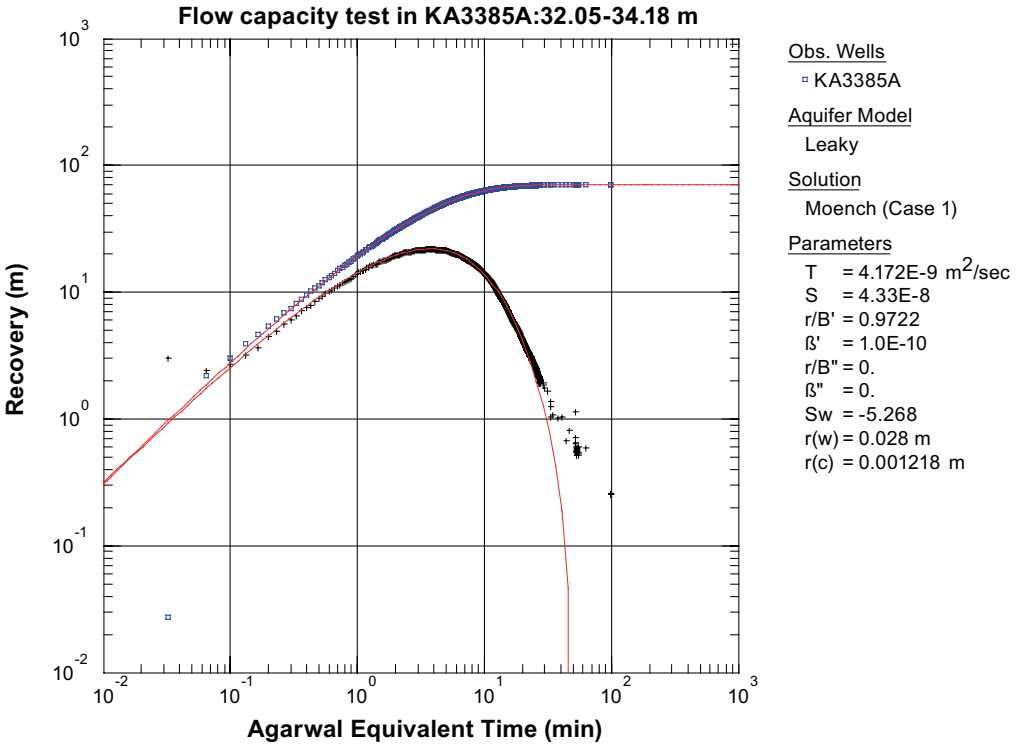

Figure G-7. *Log-log plot of recovery (▫) and recovery derivative, ds/d(ln t) (+), versus Agarwal equivalent time in the flowing borehole section KA3385A: 32.05–34.18 m during the hydraulic test.*

Groundwater flow measurements

KA3385A, comments on the test

The circulation did not cause any pressure change in the section, as seen in Figure G-8.

Generally the sampling worked well. However, there is a short period where samples are missing due to a temporary blocking of the thin tube from the sample flow regulator.

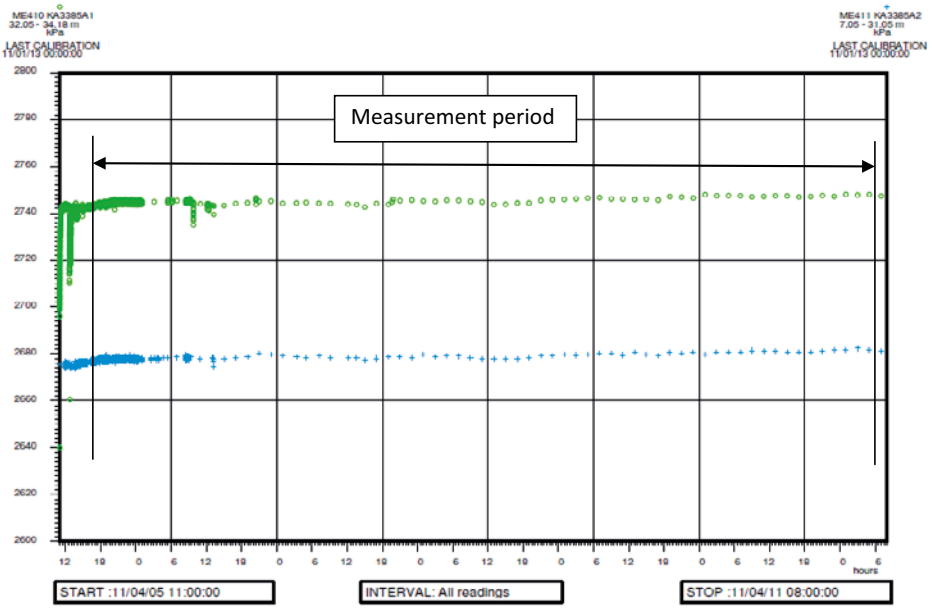

Figure G-8. *Pressure registrations of both sections in KA3385A (sections 1 and 2) during the groundwater flow measurements in section KA3385A:1.*

Dilution graphs for groundwater flow measurement with Uranine and Iodide are shown in Figure G-9 and Figure G-10. The groundwater flow according to the evaluation with Iodide is significantly larger than the corresponding evaluation using Uranine.

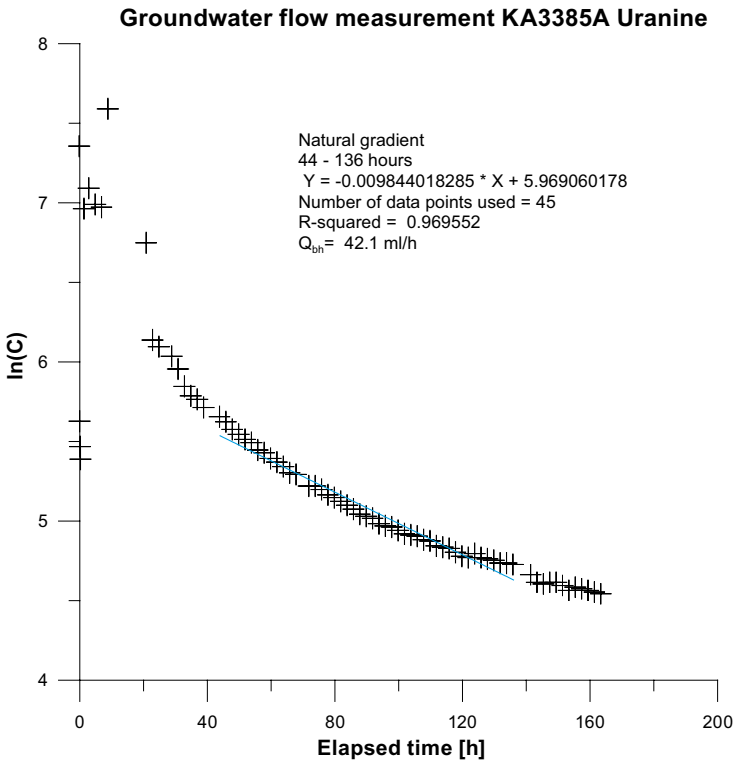

Figure G-9. *Dilution graph for the groundwater flow measurement in KA3385A:1 with Uranine.*

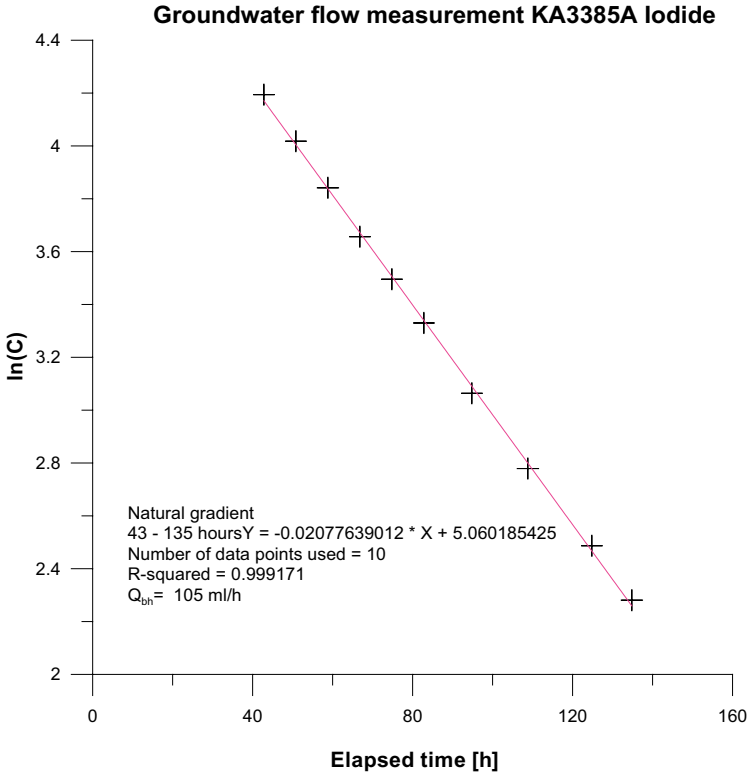

Figure G-10. *Dilution graph for the groundwater flow measurement in KA3385A:1 with Iodide.*

KA3110A, comments on the test

The circulation in the section caused a pressure increase (*dP*) of 80 kPa, see Figure G-11. This effect is discussed further in Section G3.

There was a gentle increasing pressure trend during the test period, see Figure G-12. This trend is an effect of the recovery period from pressure disturbances associated with the drilling, instrumentation and other activities performed in the new borehole KA2051A. Over the measurement period this is 10 kPa in 6 days and is not considered to have affected the evaluation of the test. Before the tests in KA3110A started the pressure was allowed to stabilize for 4 days.

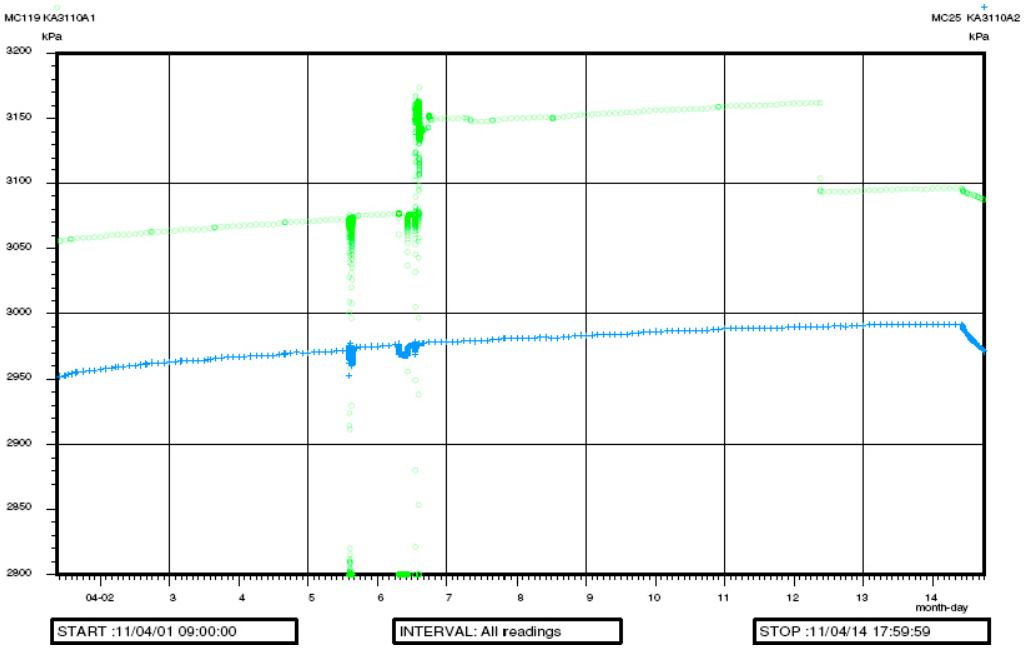

Figure G-11. *Pressure registration of both sections in KA3110A during the circulation of water in section 1.*

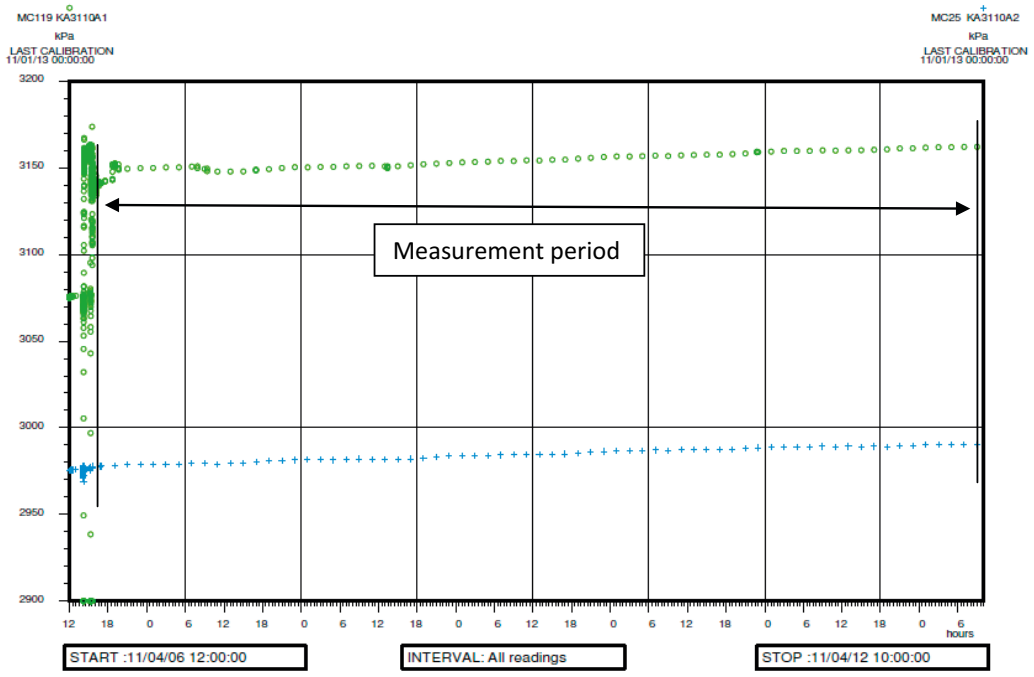

Figure G-12. *Pressure registrations of both sections in KA3110A during the groundwater flow measurements in section KA3110A:1.*

Dilution graphs for groundwater flow measurement with Uranine and Iodide are shown in Figure G-13 and Figure G-14. As in the case of evaluated groundwater flow in KA3385A, the flow according to the evaluation with Iodide is significantly larger than the corresponding evaluation using Uranine.

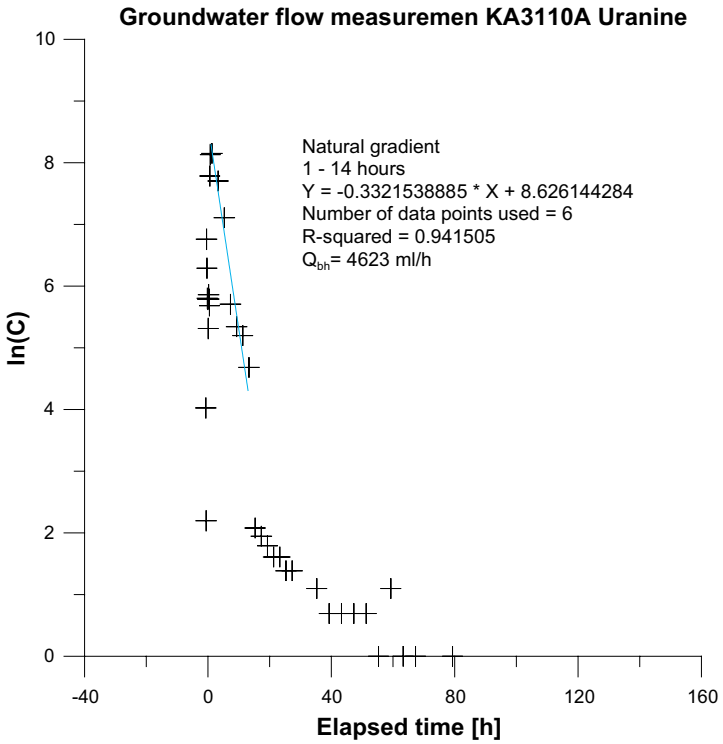

Figure G-13. *Dilution graph for the groundwater flow measurement in KA3110A:1 with Uranine.*

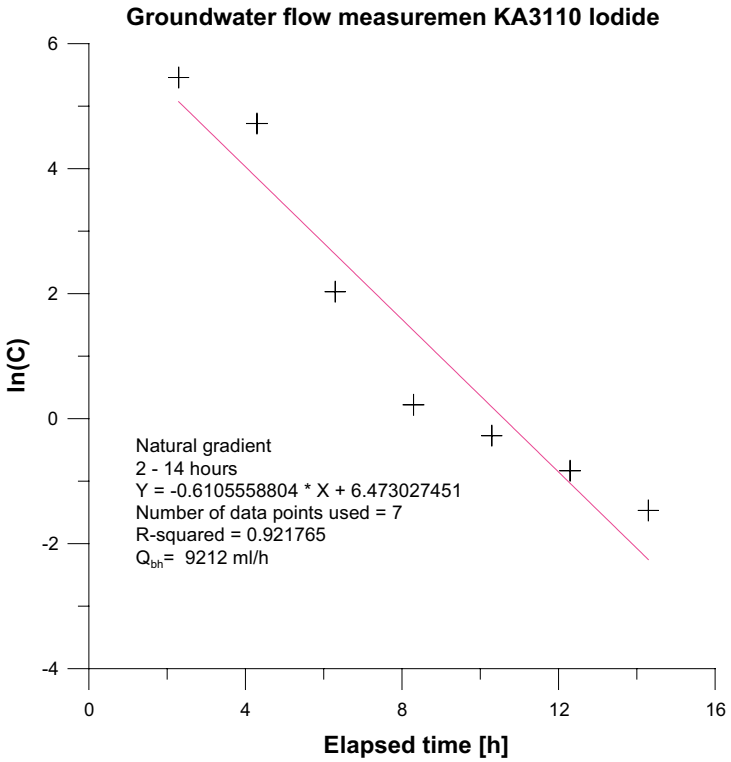

Figure G-14. *Dilution graph for the groundwater flow measurement in KA3110:1 with Iodide.*

Summary

The results from the two groundwater flow measurements are summarized in Table G-7. The dilution measurement with Iodide is not judged to be reliable due to questionable handling of the samples and the complexity of the compound as tracer element in natural environment. Hence, the results from the Uranine analysis are considered to be the most representative. However, as discussed further in Section G3, the results from the groundwater flow measurements in KA3310A:1 is not considered as representative for the natural flow rate through the section.

Table G-7. List of test data and results from ground water flow measurements.

	KA3385A:1	KA3310A:1
Start measurement	2011-04-05 13:57	2011-04-06 17:33
Stop measurement	2011-04-12 10:30	2011-04-12 10:10
Length measurement period (h)	165	137
Length evaluated period (h)	92	13
Evaluated groundwater flow Uranine (mL/h)	42	4,600

G3 Additional tests and discussion

During circulation of water in a borehole section the same volume of water is injected to the borehole section as being withdrawn since the circulation line should be closed. A significant and sustainable pressure response during circulation of a borehole section, as observed in KA3110A:1, is therefore quite unexpected. It has not, according the authors experience, been observed earlier at least not of this magnitude. Some additional tests and analysis were carried out to investigate this phenomenon and to assess the effect on previous tests in this section. Figure G-15 shows a schematic illustration of the borehole instrumentation used during the tests. Section 1 includes two tubes used for circulation and one tube for pressure registration. The circulation tube originating closest to the packer in section 1 are called *outer*, while the tube going furthest into the borehole are called *inner*. Section 2 only has one tube for pressure registration. The tubes for pressure registration are not shown in Figure G-15.

The first additional test made was to let water flow out from the borehole in one tube at the time (in total four tests, one for each tube). The pressure was logged with HMS while the flow rates were estimated by measuring the volume flowing per time unit. The results from the four tests are shown in Figure G-16 and Table G-8. The pressure responses were quite expected which indicates that the tubes are connected correctly in the borehole. However, note that the pressure decrease in section 1 was only 25 kPa while flowing the inner circulation tube, compared to 2,500 kPa while flowing the outer circulation tube, even though the flow rates are in the same range.

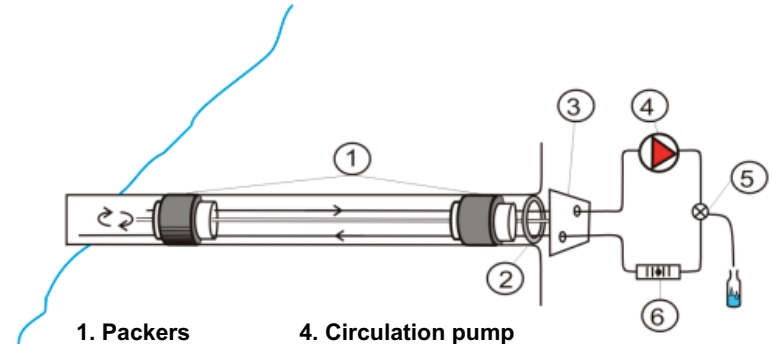

Figure G-15. *Illustration of the instrumentation in KA3110A.*

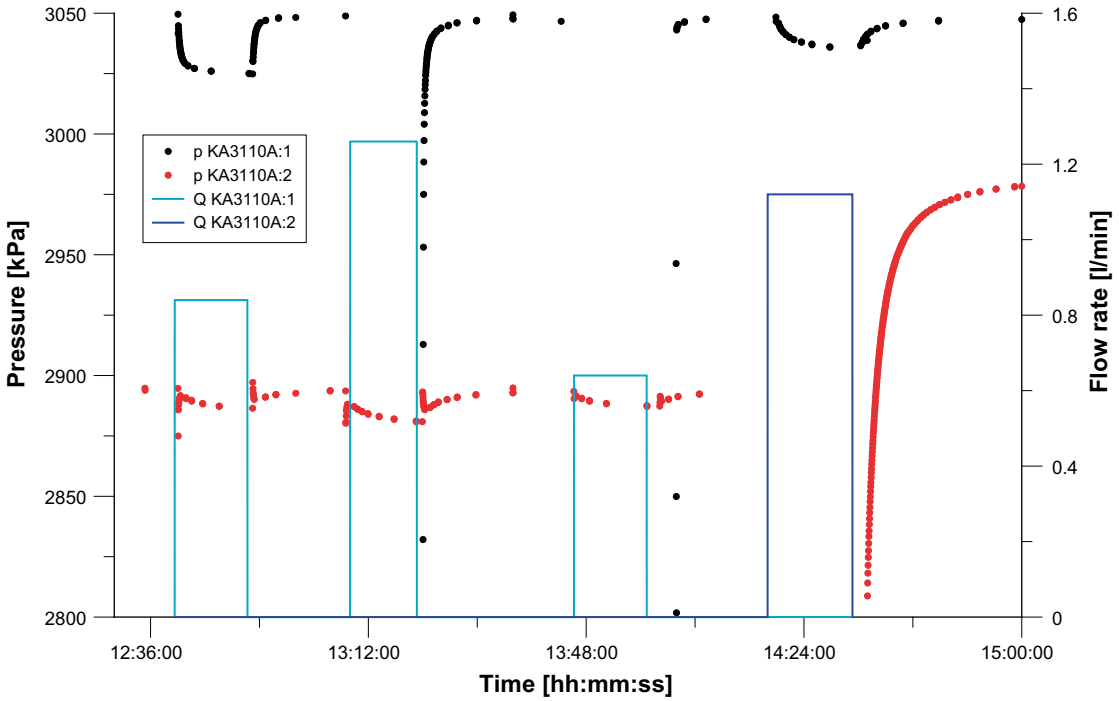

Figure G-16. *Pressure response and flow rates during additional tests. The tubes are tested in the order: section 1 inner circulation, section 1 outer circulation, section 1 pressure and finally section 2 pressure.*

Table G-8. Outflow tests in KA3110A.

Flowing tube	Q [ml/min]	dP_{sec1} [kPa]	dP_{sec2} [kPa]	Comment
Section 1, inner circulation	800	–25	–9	
Section 1, outer circulation	1,300	–2,500	–13	
Section 1, pressure	600		–6	No pressure registration in section 1
Section 2, pressure	1,100	–12		No pressure registration in section 2

A second complementary test was carried out by circulating the water in section 1 in both directions while observing the pressure. Unfortunately, due to technical problems it was not possible to execute this with an equally high flow rate as during previous tests. The results from this test are shown in Table G-9 and Figure G-17. When extracting water from the outer circulation tube and injecting the same volume in the inner tube, a small pressure decrease in section 1 is observed. The pressure in section 1 increases when the circulation is reversed.

Pressure in section 1 during the previous water sampling for sulphide was also checked. Three longer periods of circulation without disturbance of water sampling were found. The circulation flow rate during the periods was c. 12 L/h, i.e. slightly higher than during the groundwater flow measurement when it was 10 L/h. As seen in Figure G-18 the pressure response was significantly larger (c. 200 kPa) than during the groundwater flow measurement (c. 80 kPa). The earliest period in Figure G-18 shows a pressure increase while the other two has a pressure decrease. This indicates that different circulation directions have been used during the water sampling.

In January 2012 an attempt to dismantle the borehole instrumentation of KA3110A was made with the purpose of examining the equipment for micro film etc. However, the borehole instrumentation was not possible to move at all. It was also discovered during the attempt that the flow rate from the inner circulation tube was independent of the inflation of the packers.

Table G-9. Circulation test of KA3110A:1.

Circulation direction					
Flowing tube	**Injection tube**	**Start**	**Stop**	**Circulation flow [L/h]**	**dP_{sec1} [kPa]**
Outer	Inner	110622 08:55	110622 09:26	3.0	–3
Inner	Outer	110622 09:30	110622 10:00	3.6	+8

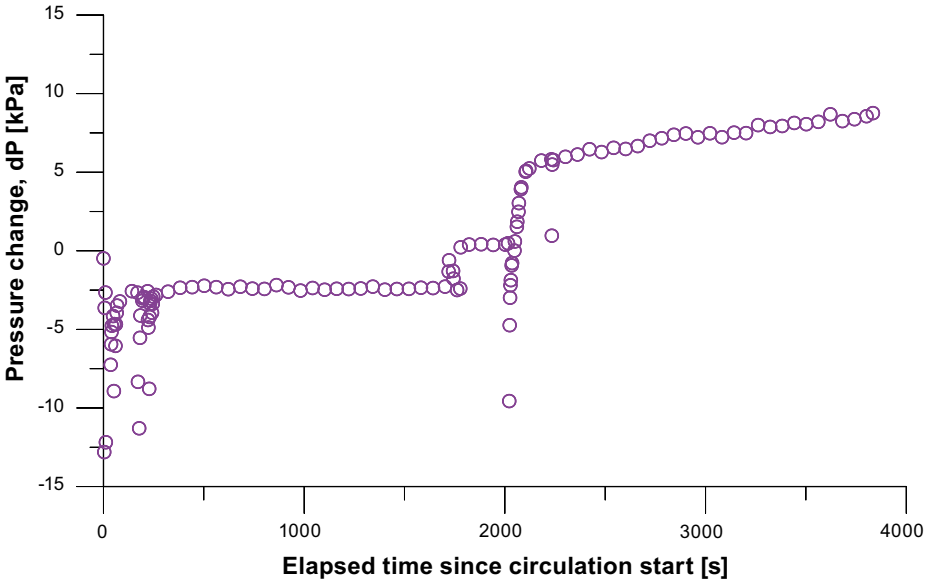

Figure G-17. Circulation test of KA3110A:1.

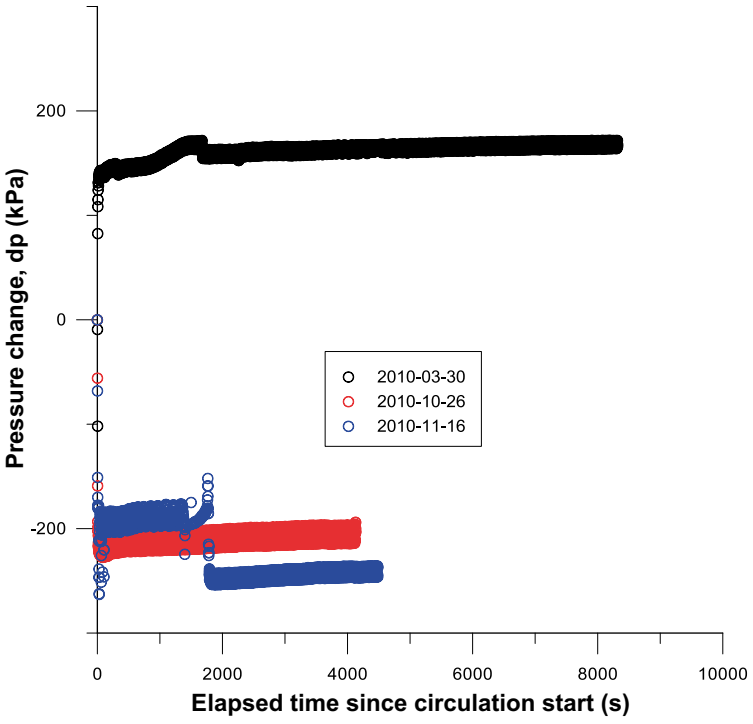

Figure G-18. Pressure response in KA3110A:1 during circulation in conjunction with water sampling.

It is possible that grouting has penetrated KA3110A since grouting has been carried out earlier in the vicinity. The effects observed in KA3110A may be explained if grouting exists in KA3110A:1 between the outlets of the inner and outer circulation tubes as illustrated with a grey area in Figure G-19. The blue line in Figure G-19 represents the circulation tube while the red line represents the pressure tube to KA3110A:1.

If circulation is performed with the inner circulation tube as flowing and the outer tube as injection, KA3110A:1 is expected to show an increasing pressure in the outer part of the section as shown in Figure G-20. This is consistent with observations made during circulations in KA3110A:1. A pressure decrease would then be expected on the other side of the grouting in KA3110A:1. It is then likely that the flow would go from on side of the grouting to the other as illustrated in the upper part of Figure G-20. However, depending on the fracture network, the water flowing to the pressure decreasing side could originate from some other area as shown in the lower part of Figure G-20.

The reverse situation is expected if the circulation direction is from the outer tube to the inner tube as shown in Figure G-21. This is also consistent with observations in KA3110A:1.

The explanation above for the unexpected pressure response in KA3110A:1 during circulation may not be proven in this report. Instead it should be considered as a theory that the authors not could dismiss. The authors have tried, but not succeeded, to come up with alternative theories that may explain the unexpected results from the investigations in KA3110A:1.

The borehole section KA3110A:1 was circulated also during other water sampling events during the Sulphide project. Due to the pressure response (decrease or increase) in KA3110A:1 displayed in Figure G-18 during these samplings it is not possible to consider the samples to represent a borehole section under natural undisturbed conditions.

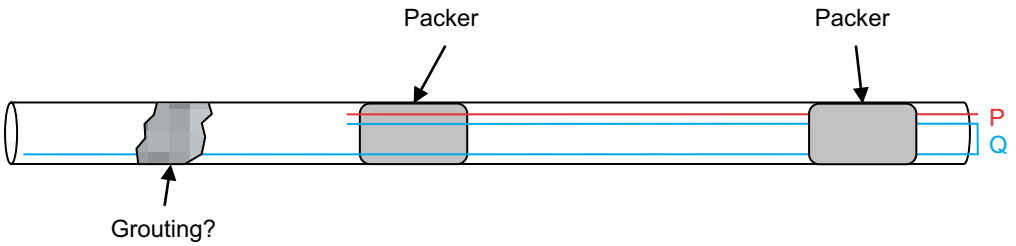

Figure G-19. *Illustration of possible grouting in KA3110A:1.*

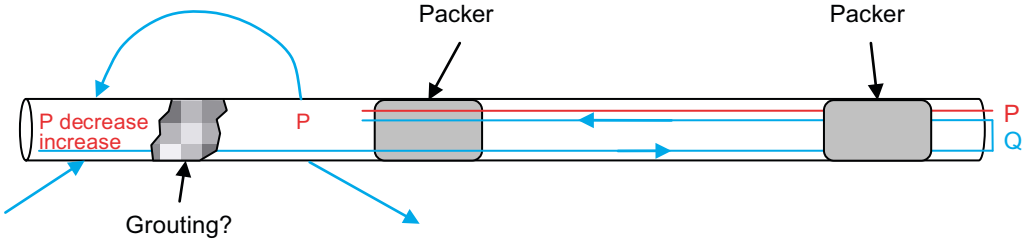

Figure G-20. *Illustration of possible flow and pressure response due to circulation from the inner to the outer circulation tube.*

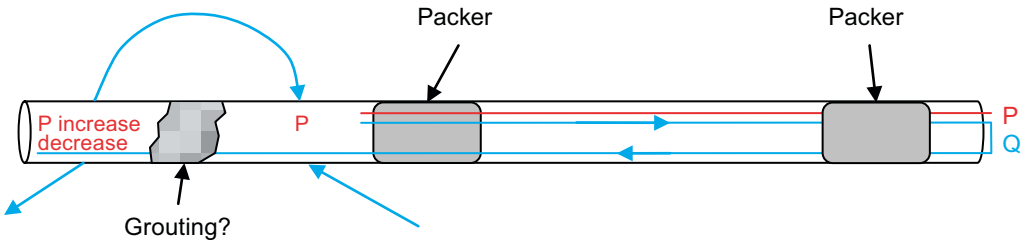

Figure G-21. *Illustration of possible flow and pressure response due to circulation from the outer to the inner circulation tube.*

G4 Conclusions

The results from the groundwater flow measurements and hydraulic tests in KA3385A:1 and KA3110A:1 may be summarised in the following conclusions:

- The tests in KA3385A:1 indicates a groundwater flow of 40 mL/h and a transmissivity of 2×10^{-8} m^2/s.
- During circulation of KA3110A:1 unexpected pressure responses were found.
- The results from groundwater flow measurement in KA3110A:1, hydraulic test as well as earlier water sampling, are probably significantly affected by some unfavourable condition in the bore-hole section and should not be regarded as representative for undisturbed conditions.
- A likely theory is that grouting has penetrated KA3110A:1 in between the outlets of the inner and outer circulation tubes.

Appendix H

Sample descriptions (SEM-observations and qualitative EDS analyses)

Samples were analysed using low-vacuum mode meaning that samples could be examined uncoated (i.e. they could be reused for other analyses). The acceleration voltage was 20 kV, and working distance 9.9 mm. Simple oxide and element calibration standards were used, linked to a cobalt drift standard. The uneven morphology of the samples disabled semi-quantitative EDS analyses to be carried out. The analyses were therefore only qualitative. However, the EDS spectra, element ratios and major element chemistry could be used to give important chemical information about the major constituents in the precipitates (e.g. about products of Al-corrosion and mineralogy of sulphides using the Fe/S-ratio revealing dominance of FeS or FeS_2 [pyrite]). Spot size was about 6 µm and analyses of fine-grained phases often gave a slightly mixed signal from several minerals.

Sample 22101, borehole KA3385A, 0 m.

Precipitates: Gypsum, Ca-Cl-Al-S-rich precipitate, halite, Al-Cl-rich precipitate and more pure Al-precipitate.

Photograph of sample 22101.

SEM-images:

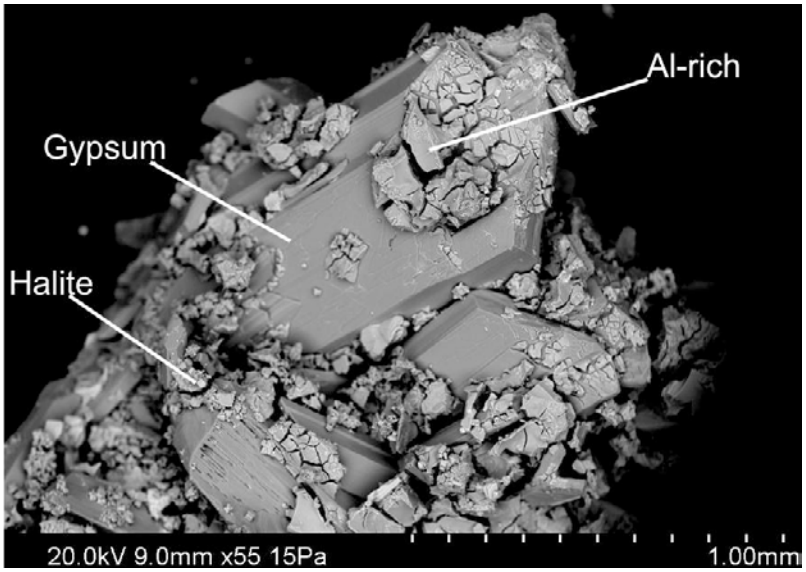

Back-scattered SEM image showing euhedral gypsum and brighter Cl-rich precipitates, such as NaCl (halite; bright and cubic).

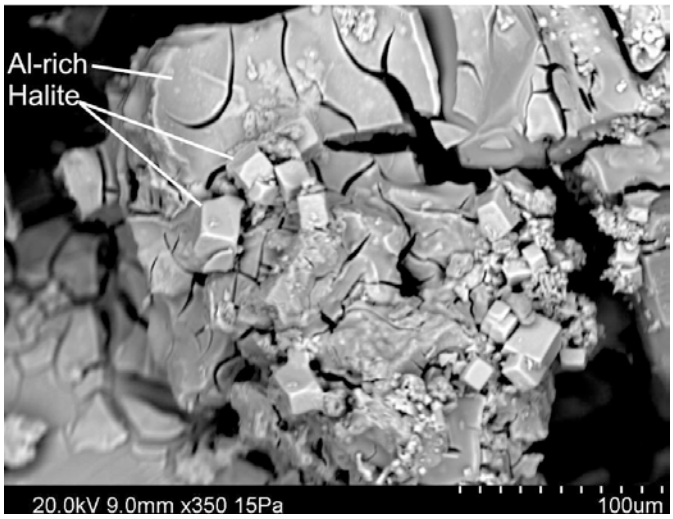

Back-scattered SEM image showing euhedral halite (NaCl – cubic) on an Al-rich substance.

EDS analysis locations and related spectra for 22101:

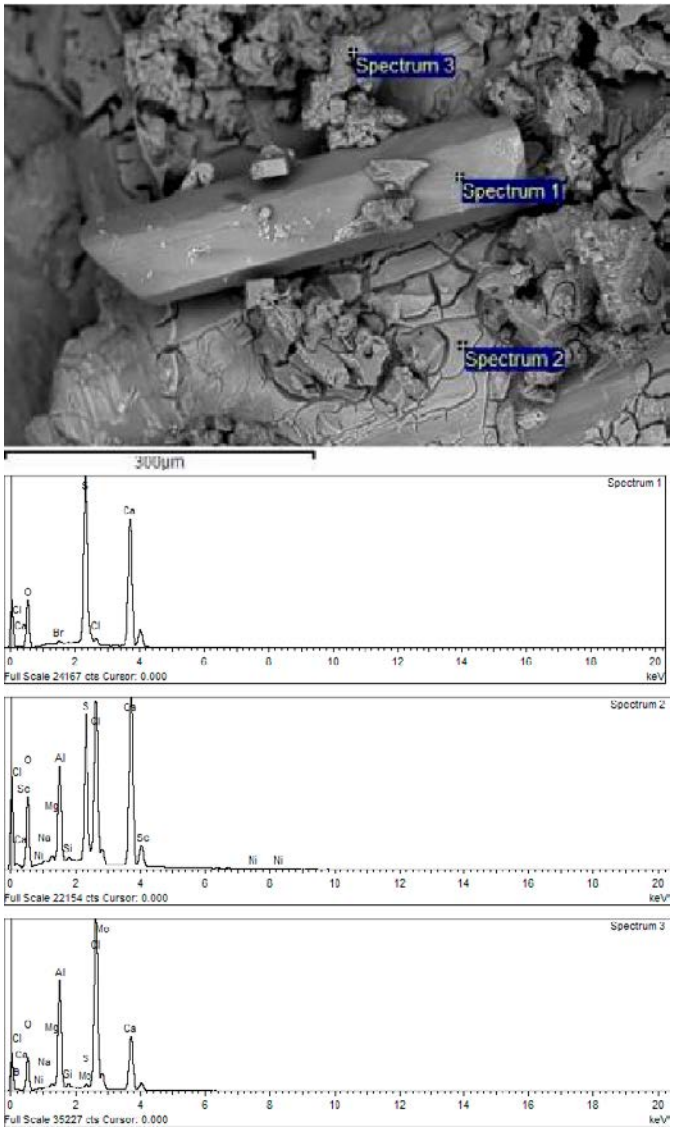

Spectrum 1: Gypsum, Spectrum 2: Gypsum+AlCl, Spectrum 3: Al-rich precipitate.

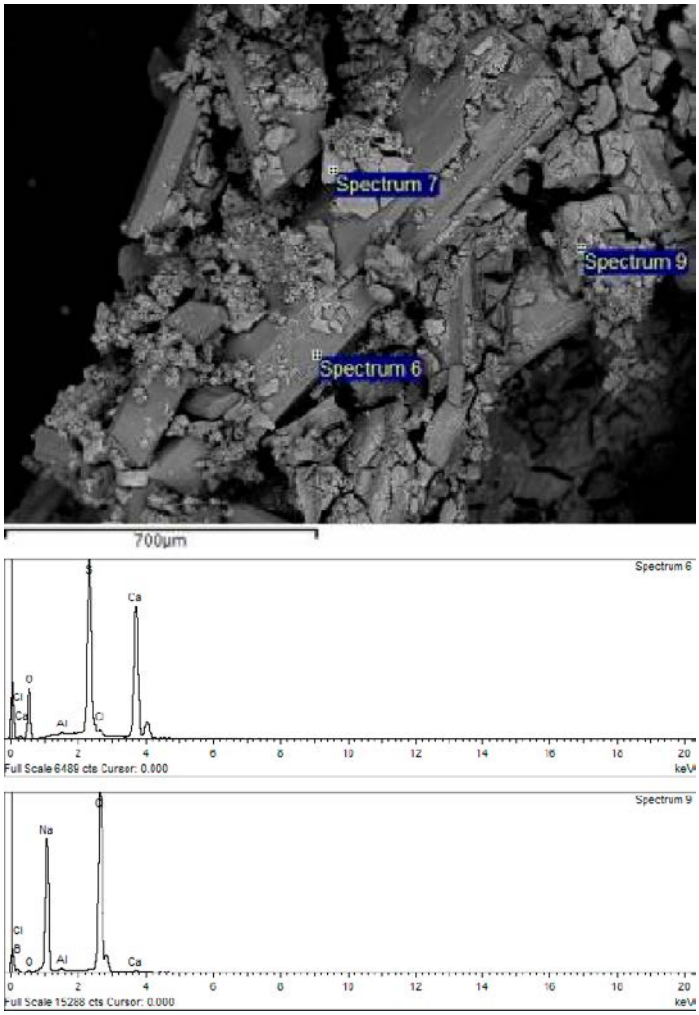

Spectrum 6: Gypsum, Spectrum 7: Ca-Al-Cl_2, Spectrum 9: Halite(NaCl). Spectrum 7 is missing, but analysis is shown in the table of EDS analysis.

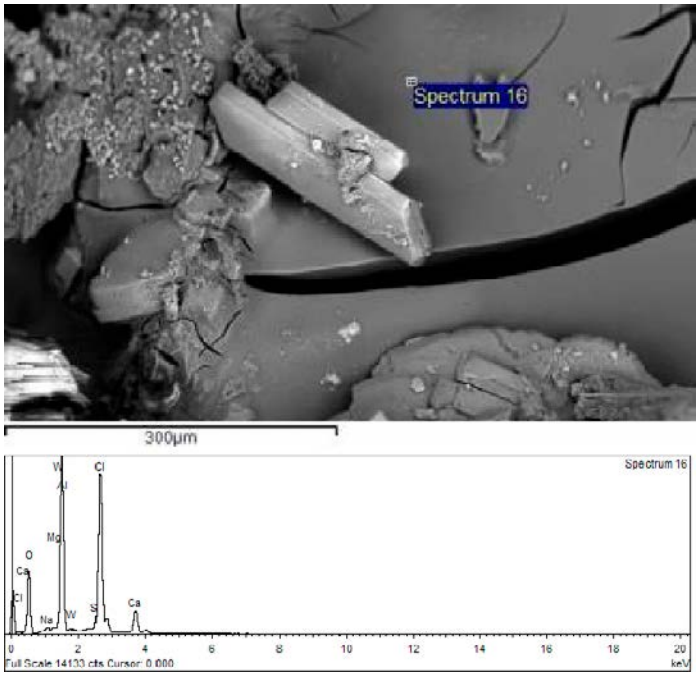

Spectrum 16: AlCl-precipitate.

Sample 22102, KA3385A, 0.4 m.

Al-rich substance with some Si. Ratio of Si:Al is 1:2. There are also variable amounts of S, Cl, Ca. When these elements are increased, Si decreases. There are also FeOOH and very-fine-grained calcite is indicated.

Photograph of sample 22102.

EDS analysis locations and related spectra for 22102:

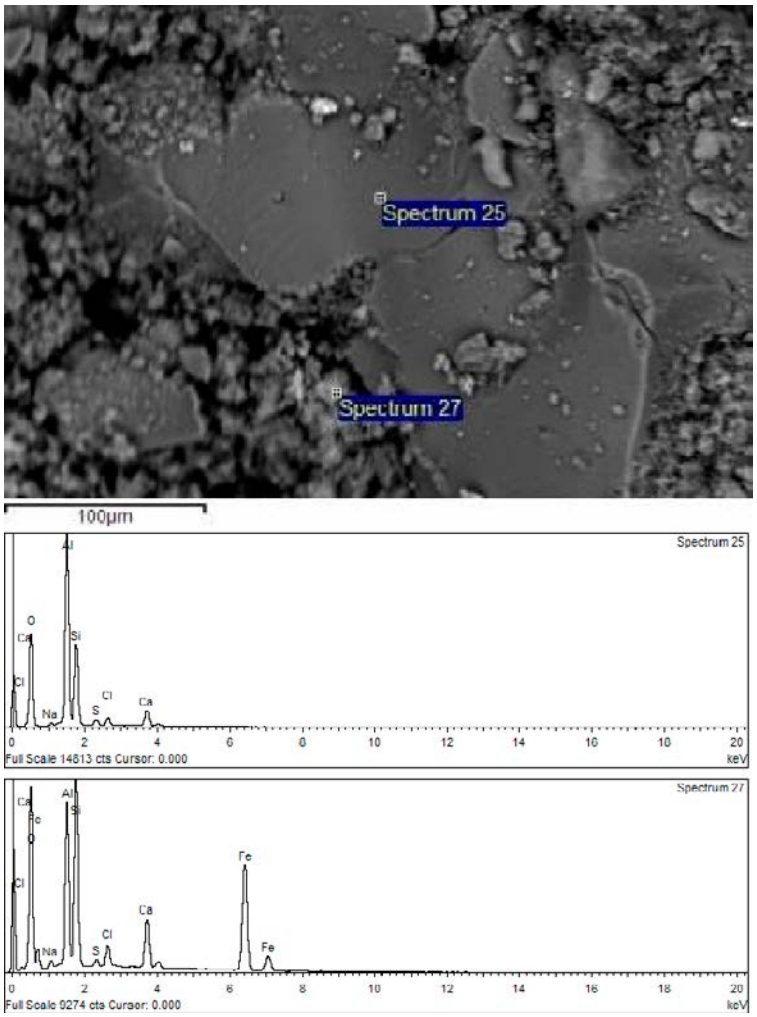

Spectrum 25: Al_2Si-precipitate, Spectrum 27: FeOOH+AlSi-precipitate.

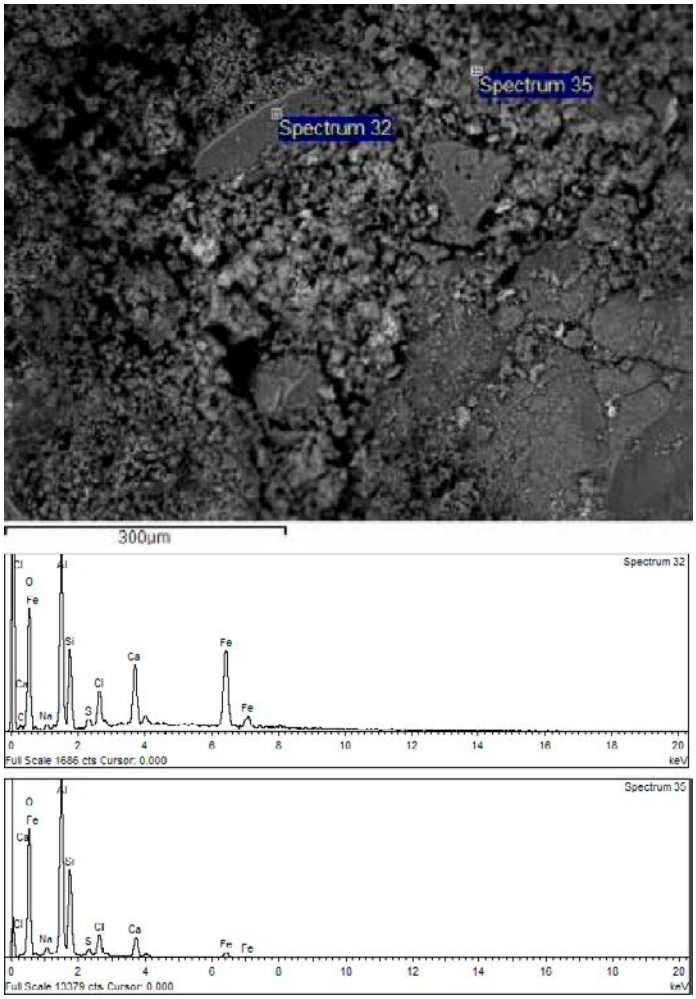

Spectrum 32: FeOOH+Al(Si)-precipitate, Spectrum 35: Al_2Si-precipitate.

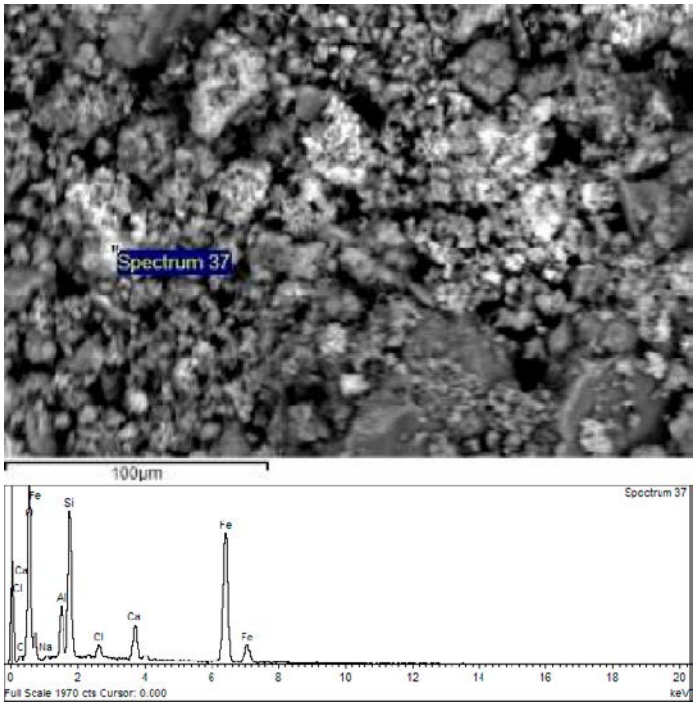

Spectrum 37: FeOOH+Al,Si etc.

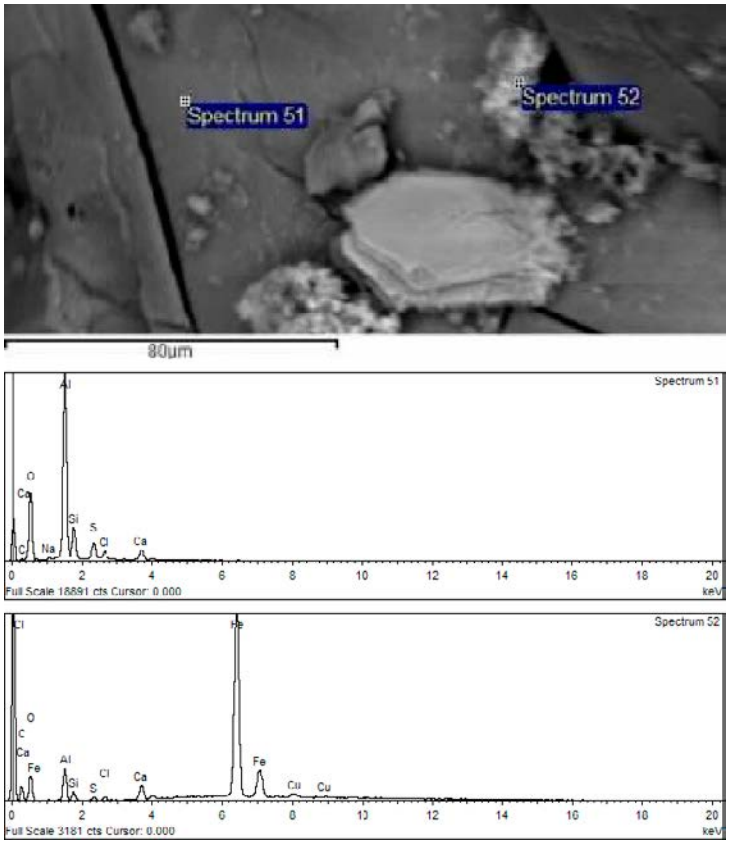

Spectrum 51: Al-rich precipitate, Spectrum 52: FeOOH.

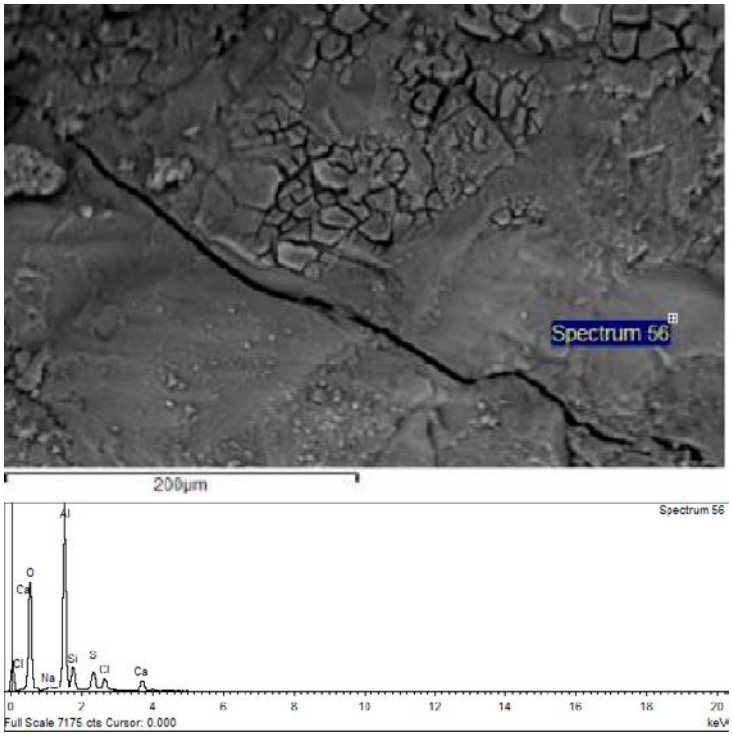

Spectrum 56: Al-rich precipitate.

Sample 22103, KA3385A, 4.2 m.

Precipitates: Al-rich substance. In addition, a small number of < 20 µm pyrite crystals were identified.

Photograph of sample 22103 (the white substance adjacent to the black tape in the left part of the rod).

SEM-images:

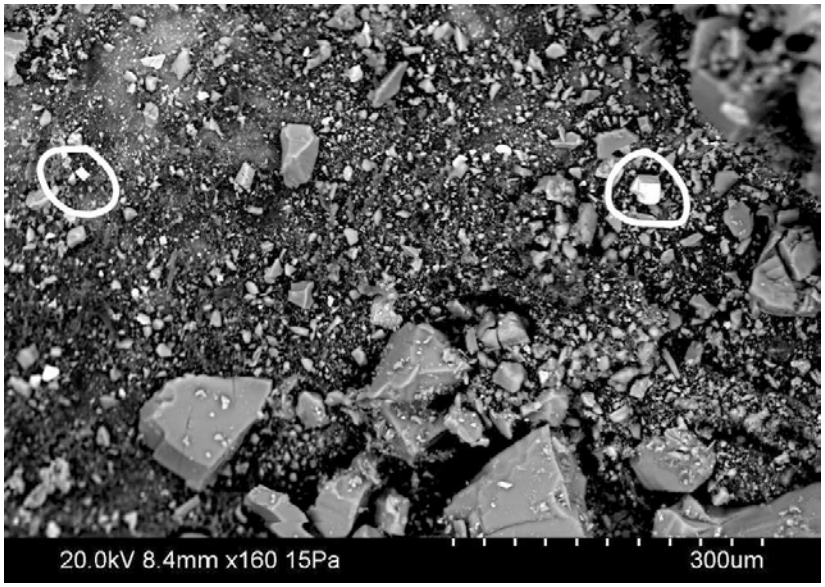

Back-scattered SEM image showing euhedral pyrite crystals (encircled) on the tape.

EDS analysis locations and related spectra for 22103:

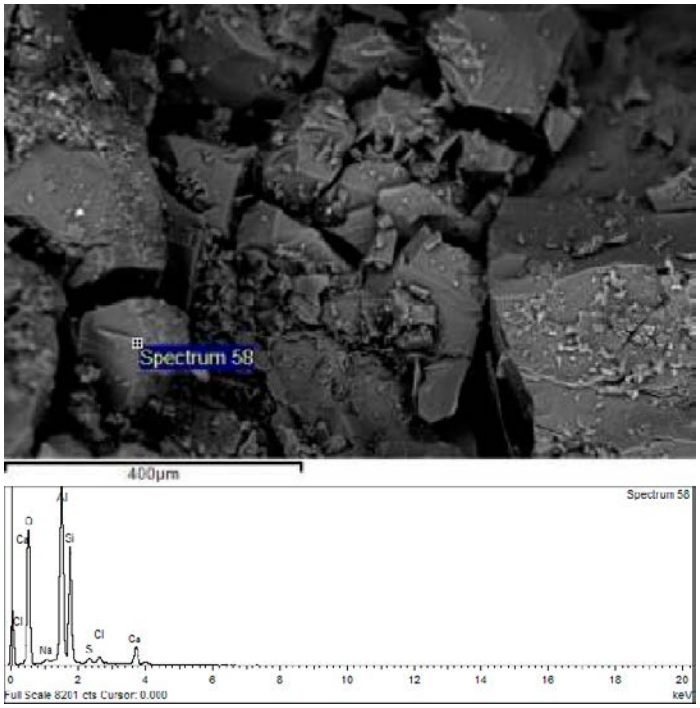

Spectrum 58: AlSi-precipitate.

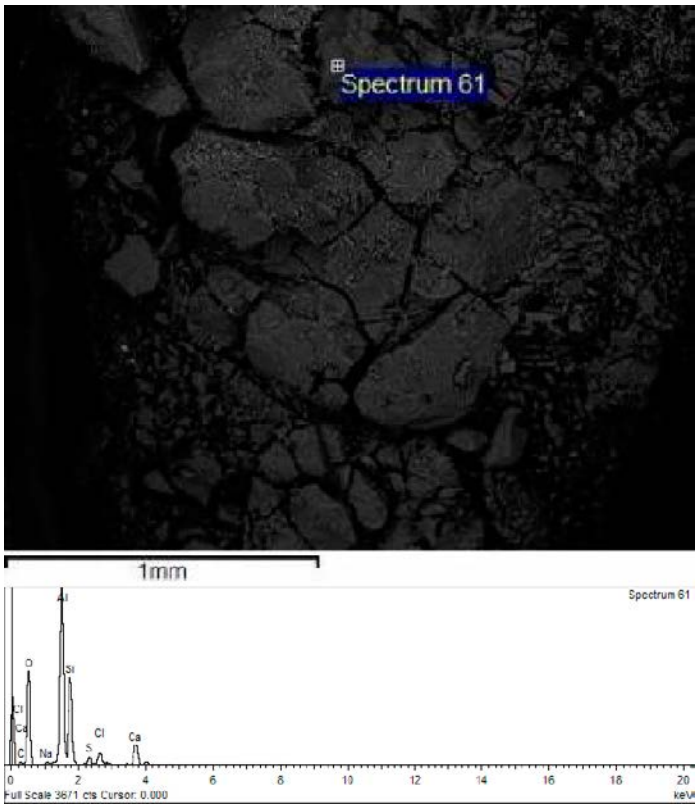

Spectrum 61: Al-rich precipitate.

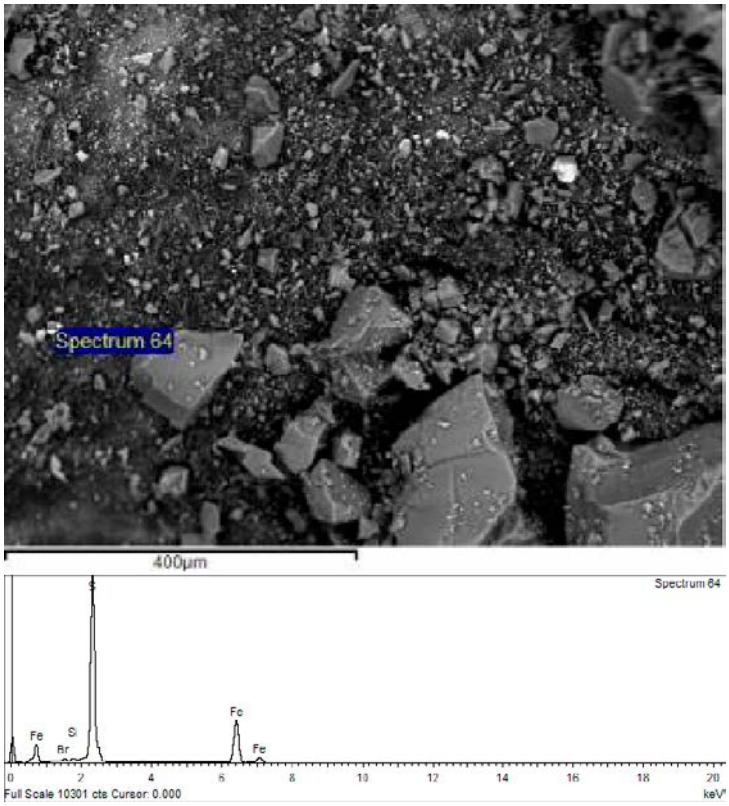

Spectrum 64: Pyrite.

Sample 22104, KA3385A, 7.2 m.

Biofilm with halite (NaCl) and CaCl2 precitates and Al-rich substance with some related Si, Cl and S.

Photograph of sample 22104 (the white substance adjacent to the black tape).

SEM-images:

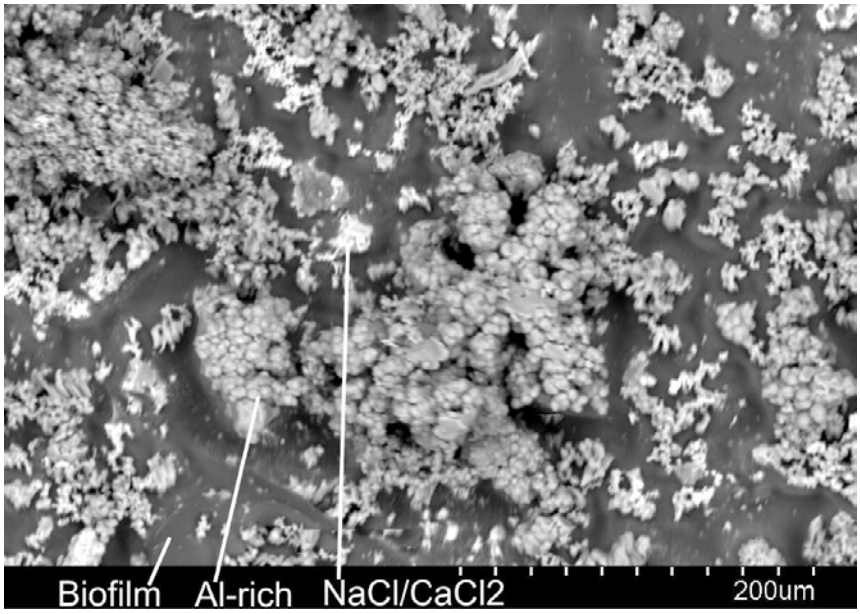

Back-scattered SEM image showing biofilm, Al-rich substance and NaCl/$CaCl_2$.

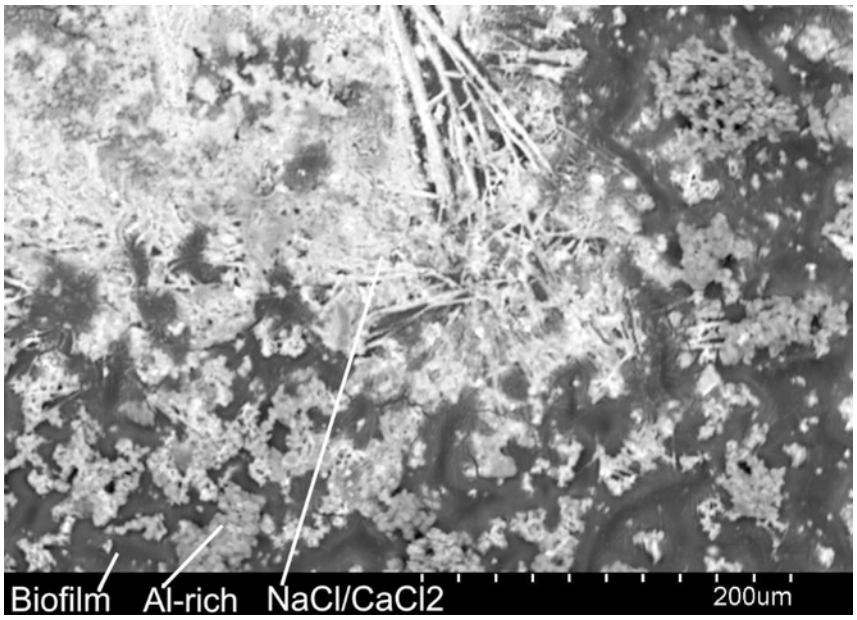

Back-scattered SEM image showing biofilm, Al-rich substance and NaCl/$CaCl_2$, close to the border of the sample where the sample has dried out and NaCl/$CaCl_2$ dominates.

EDS analysis locations and related spectra for 22104:

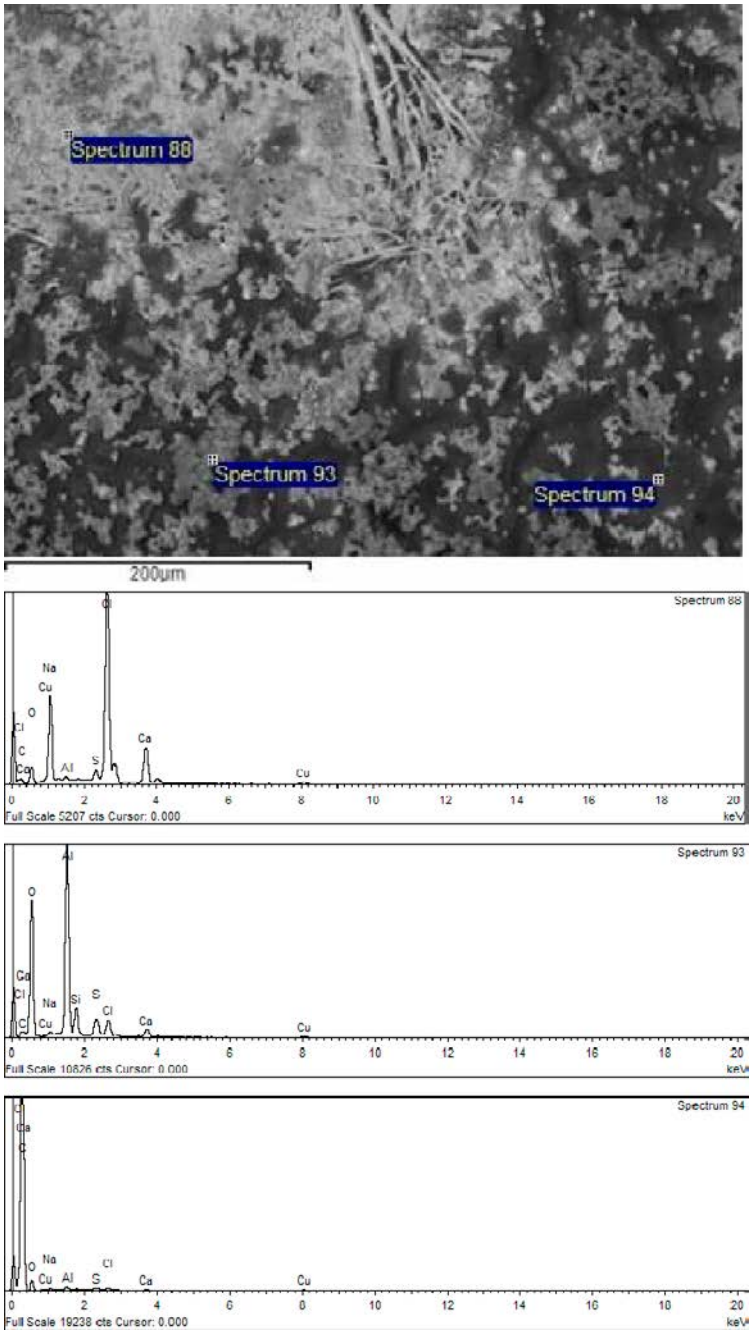

Spectrum 88: Biofilm+NaCl, Spectrum 93: Al-rich precipitate+biofilm, Spectrum 94: Biofilm.

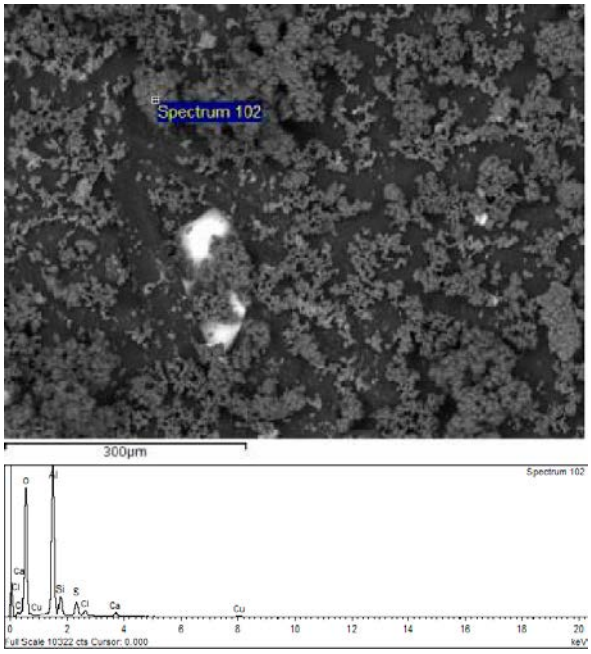

Spectrum 102: Al-rich precipitate+biofilm.

Sample 22105, KA3385A, 7.5 m.

Sample is dominated by euhedral calcite (scalenohedral habit). Very small amounts of barite is also indicated. Photograph of this sample is shown above (grey precipitates on the packer connections in the photograph for sample 22104).

SEM-images:

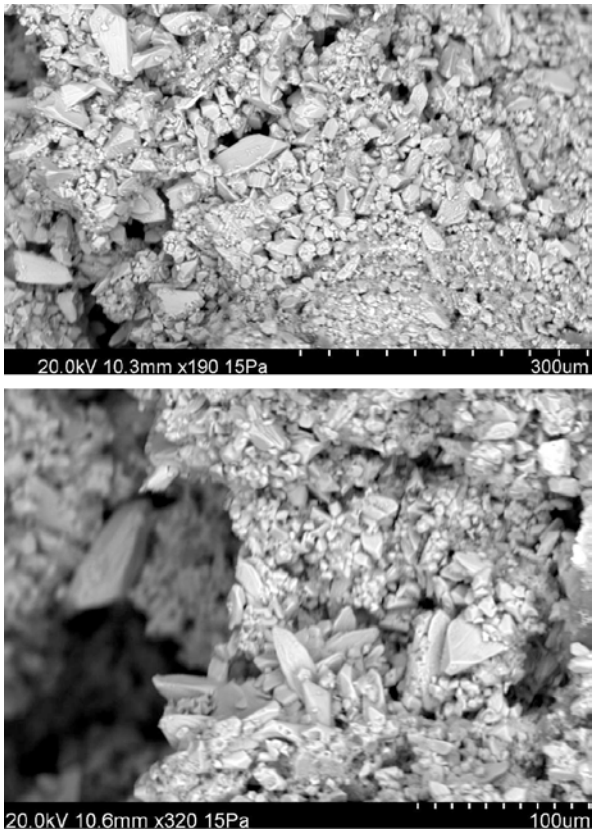

Back-scattered SEM images showing euhedral calcite crystals.

EDS analysis locations and related spectra for 22105:

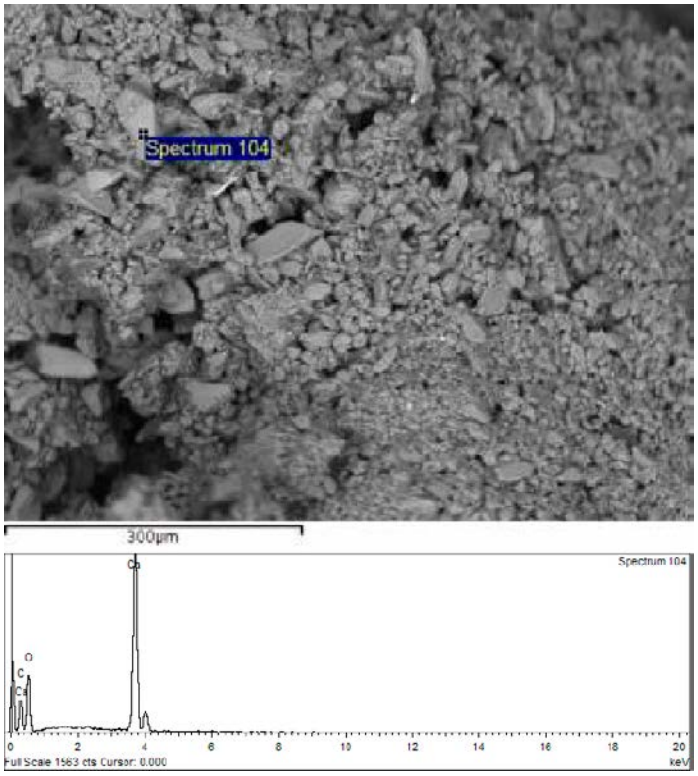

Spectrum 104: Calcite.

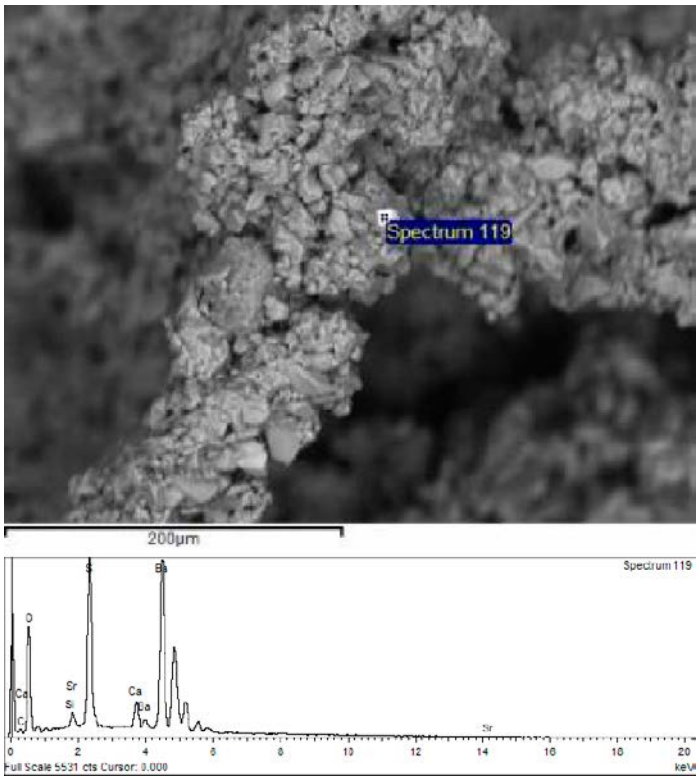

Spectrum 119: Barite.

Sample 22106, KA3385A, 9.65 m.

The sample consists of an Al-rich substance (with variable amounts of Si, S, Ca and Cl), and $NaCl/CaCl_2$ and limited amounts of biofilm.

Photograph of sample 22106 (the white substance adjacent to the black tape).

SEM-images:

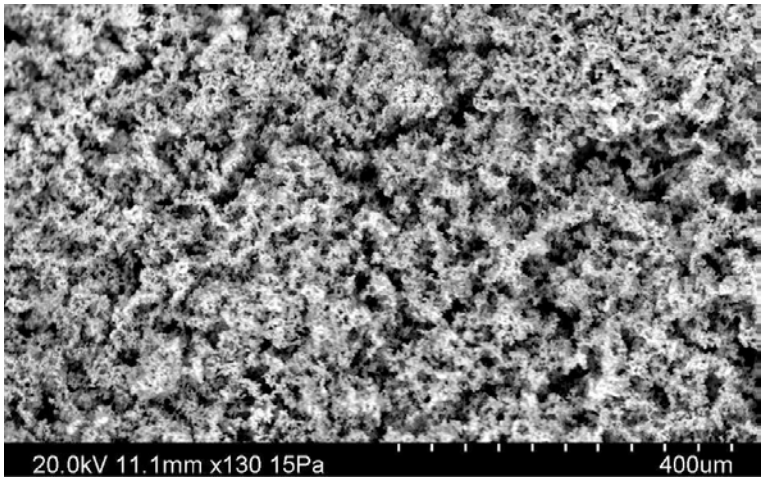

Back-scattered SEM image showing an Al-rich substance (with variable amounts of Si, S, Ca and Cl), and $NaCl/CaCl_2$ (brightest).

EDS analysis locations and related spectra for 22106:

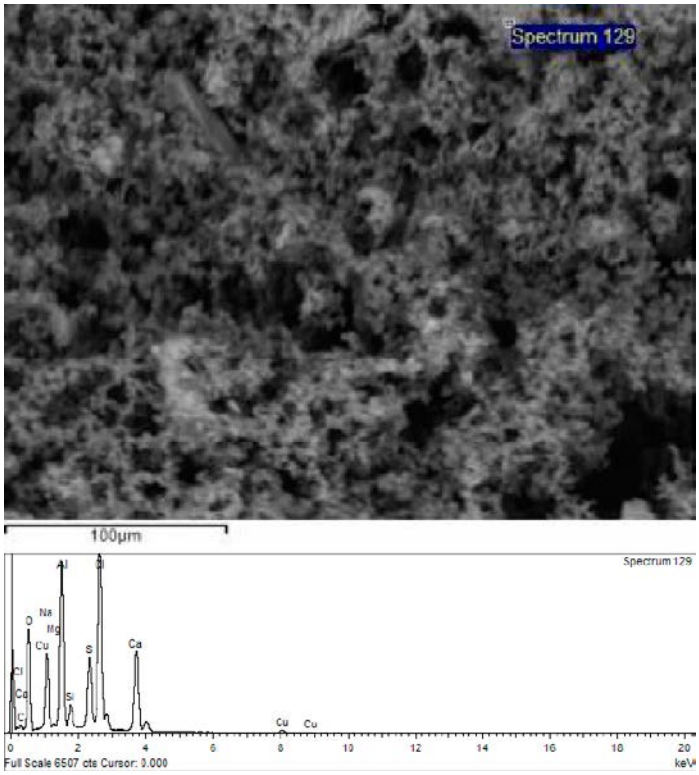

Spectrum 129: Al-rich precipitate and NaCl/($CaCl_2$).

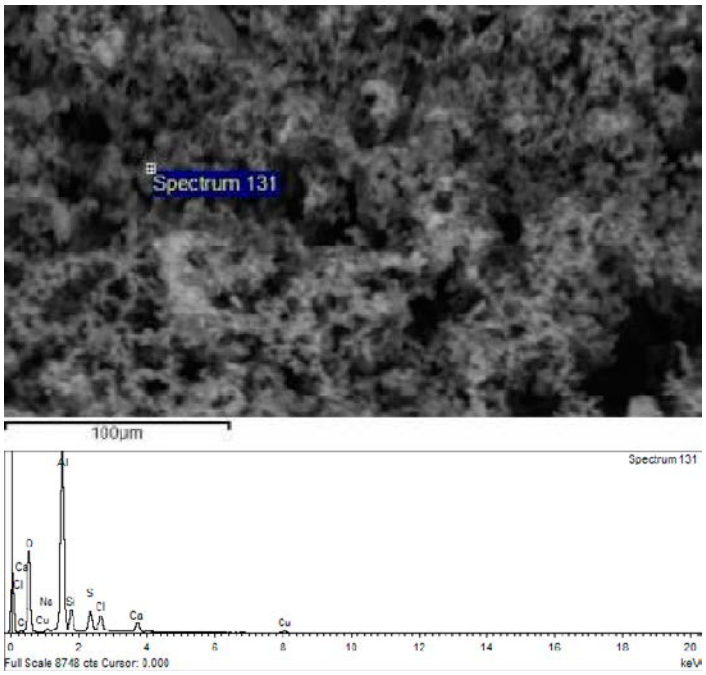

Spectrum 131: Al-rich precipitate, $CaCl_2$ and biofilm.

Sample 22107, KA3385A, 18.65 m.

Sample is dominated by Al-S rich substance (white soft material).

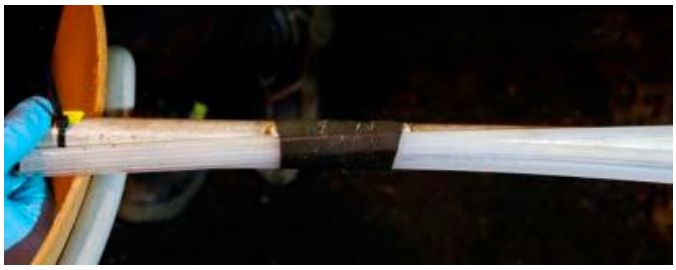

Photograph of sample 22107 (the white substance adjacent to the black tape).

SEM-images:

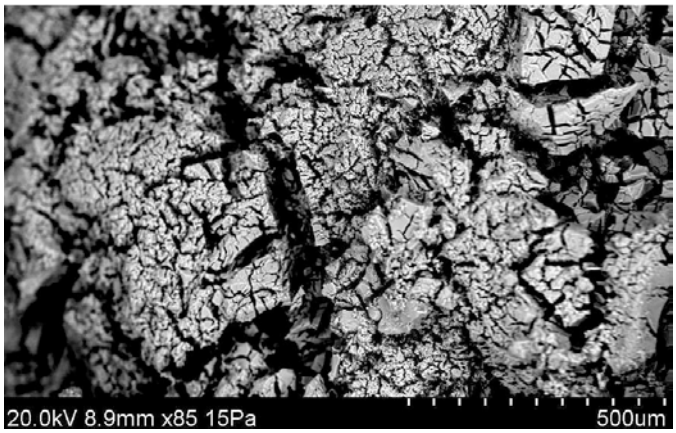

Back-scattered SEM image showing Al-rich substance (dry-cracked).

EDS analysis locations and related spectra for 22107:

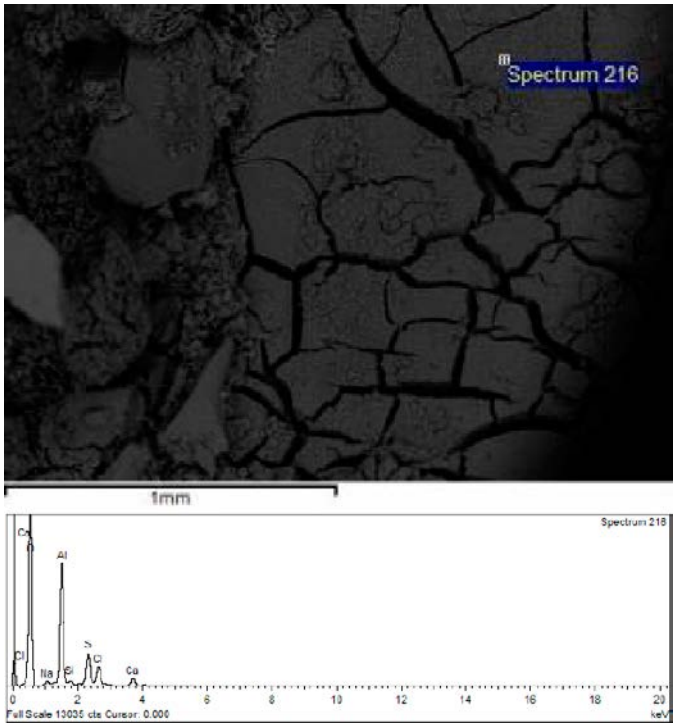

Spectrum 216: Al-rich substance (+S,CaNaCl).

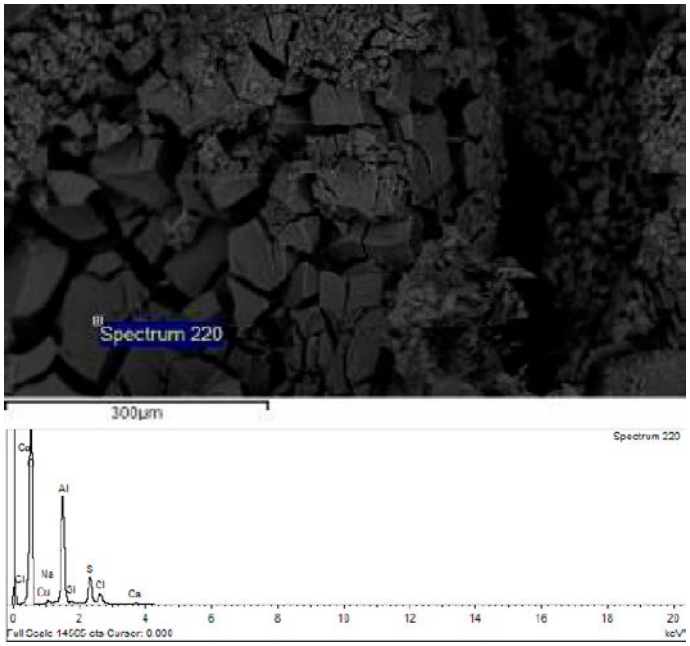

Spectrum 220: Al-rich substance (+S,Cl).

Sample 22108, KA3385A, 7.5 m.

Sample is dominated by calcite (scalenohedral habit). There is also a greenish, glassy coating dominated by Si+Mg-Cl-(Fe-Na). Very fine-grained FeS is present on the calcite crystals. Single cubic pyrite crystals were also identified.

SEM-images:

Back-scattered SEM image showing euhedral calcite.

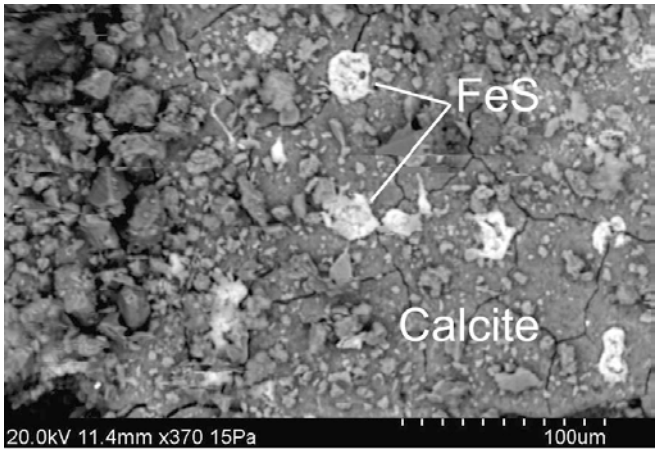

Back-scattered SEM image showing fine-grained FeS on the surface of a calcite crystal.

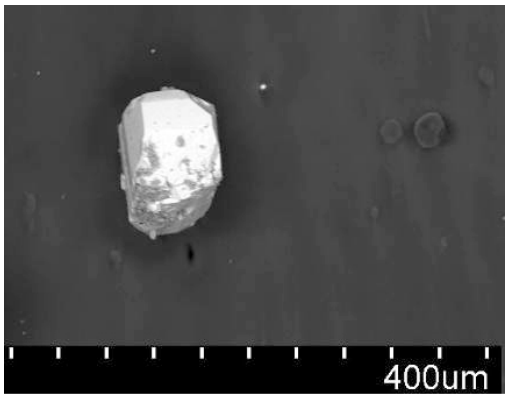

Back-scattered SEM image showing an euhedral pyrite crystal (on Cu tape-used during SEM investigations).

EDS analysis locations and related spectra for 22108:

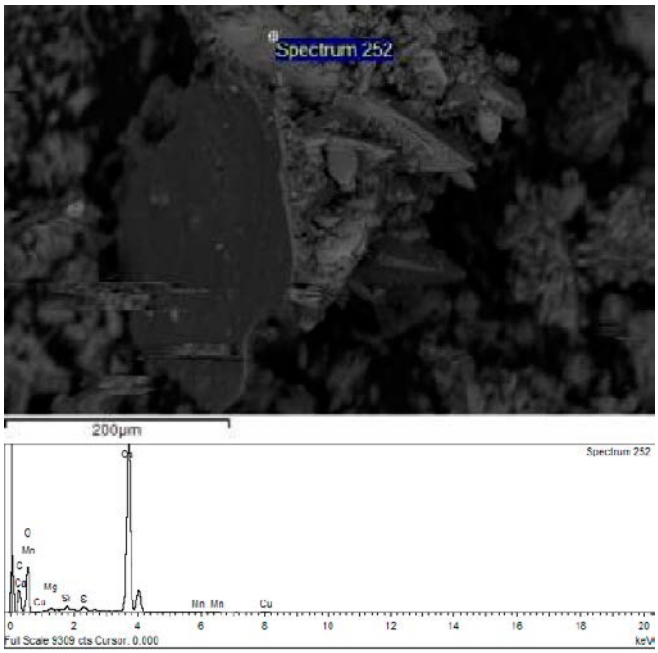

Spectrum 252: Calcite.

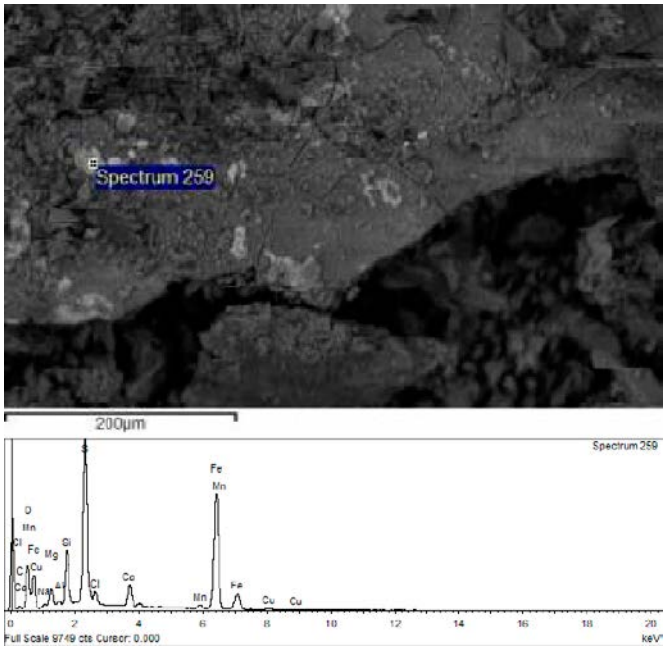

Spectrum 259: FeS.

Sample 22109, KA3385A, 32.3 m.

Sample is dominated by Al-S rich substance (white soft material, with some $CaCl_2$, and very small amounts of barite).

Photograph of sample 22109 (the white substance adjacent to the black tape).

SEM-images:

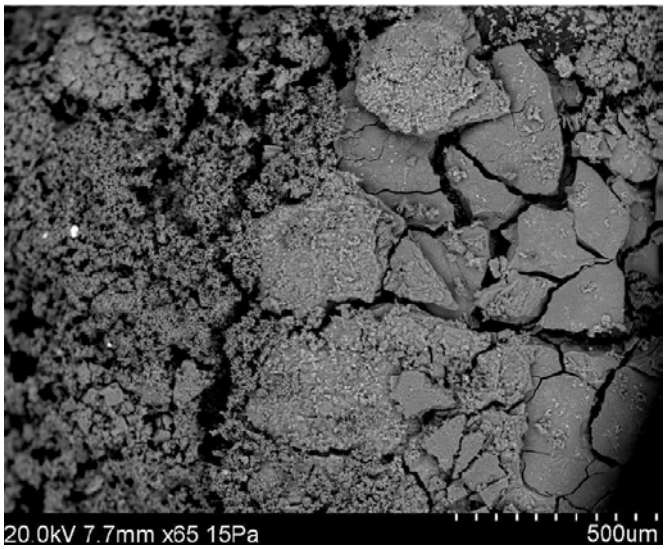

Back-scattered SEM image showing AlS-rich substance (dry-cracked).

EDS analysis locations and related spectra for 22109:

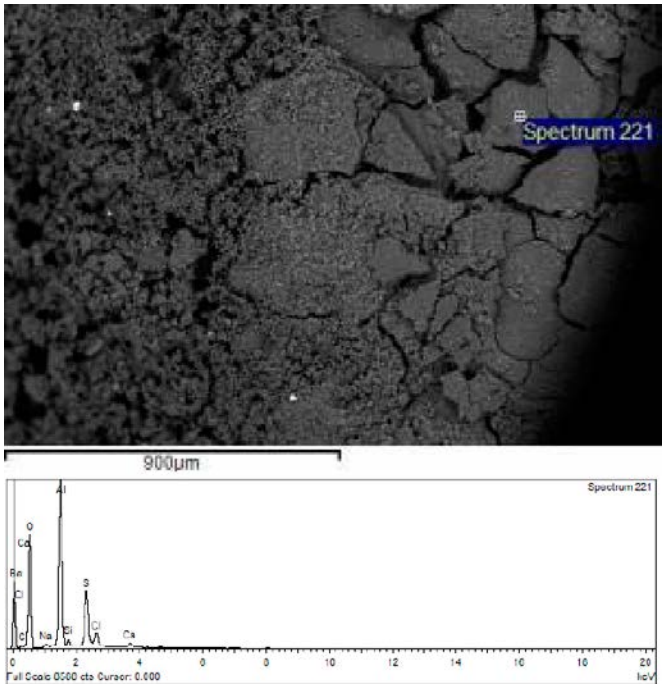

Spectrum 221: Al-S-rich substance.

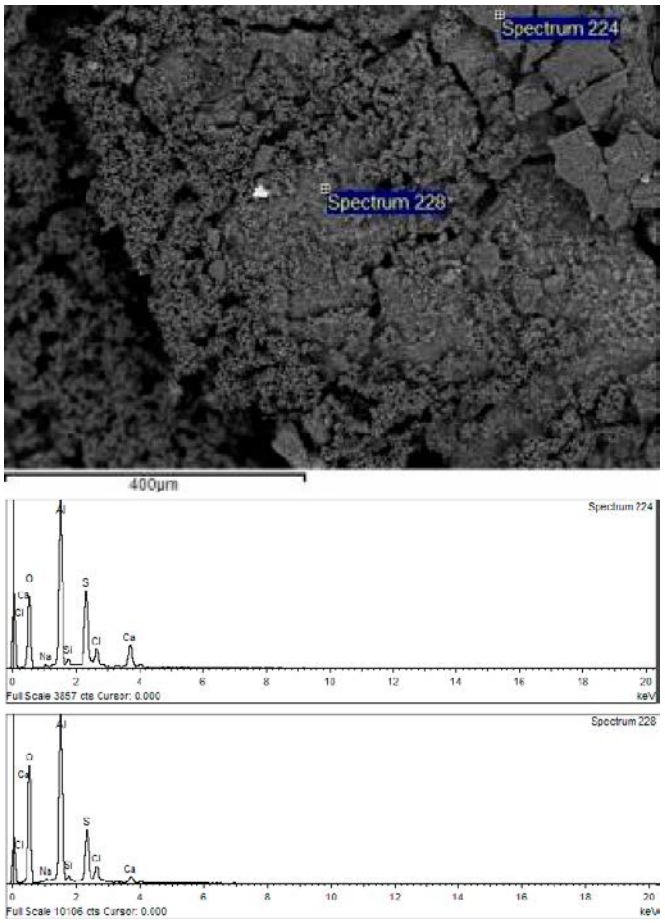

Spectrum 224: Al-S rich substance with some (Na)CaCl. Spectrum 228: Al-S rich substance with some (Na)CaCl.

Sample 22110, KA3385A, 30 m.

Sample is dominated by calcite (scalenohedral habit). There are also cubic pyrite crystals (~60 µm), barite (up to 50 µm), Si-rich precipitates and a greenish, glassy coating dominated by Si+Mg-Cl-(Fe-Na).

SEM-images:

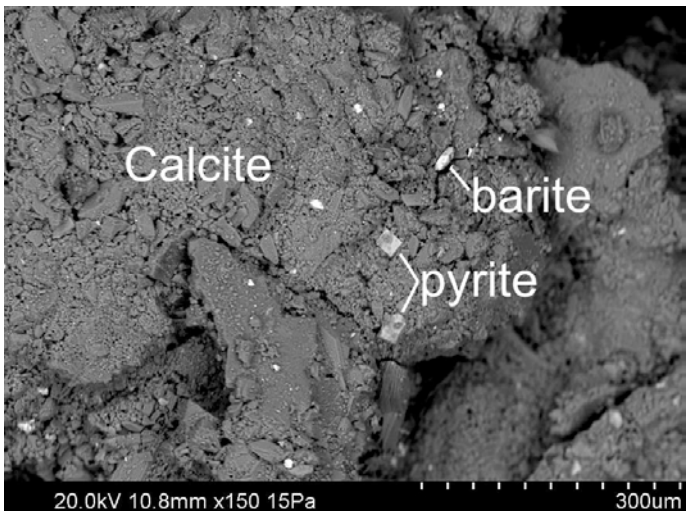

Back-scattered SEM image showing pyrite and barite on top of and in-mixed with calcite.

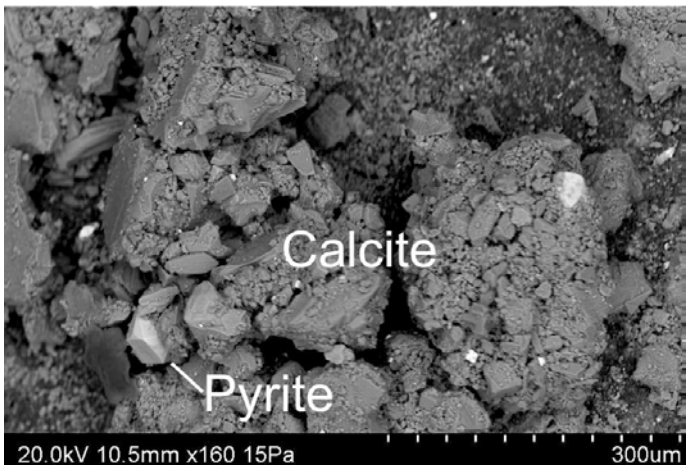

Back-scattered SEM image showing pyrite with calcite.

EDS analysis locations and related spectra for 22110:

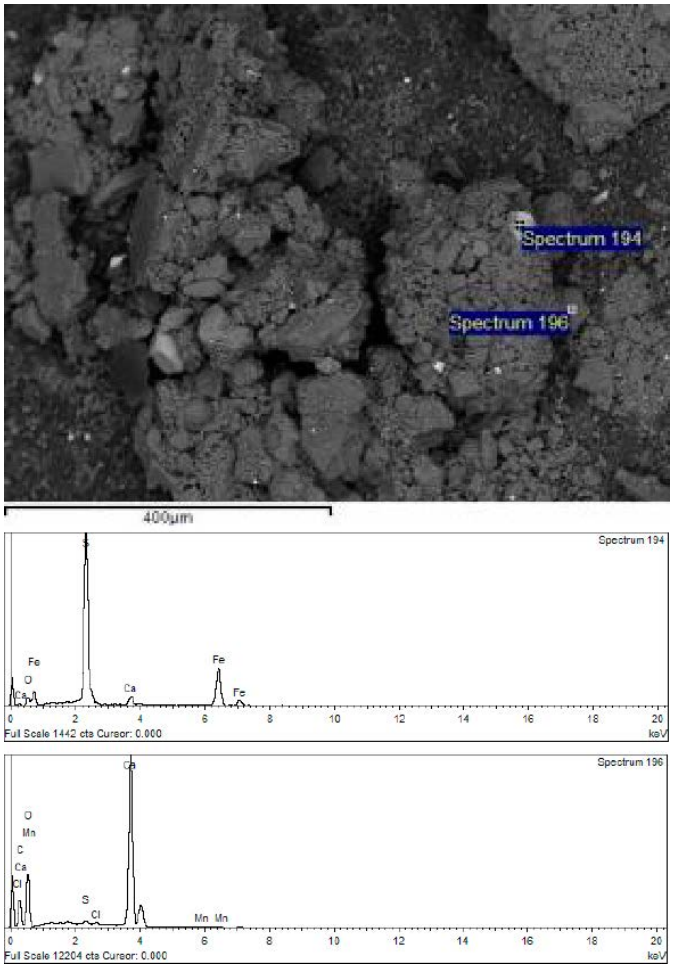

Spectrum 194: Pyrite, Spectrum 196: Calcite.

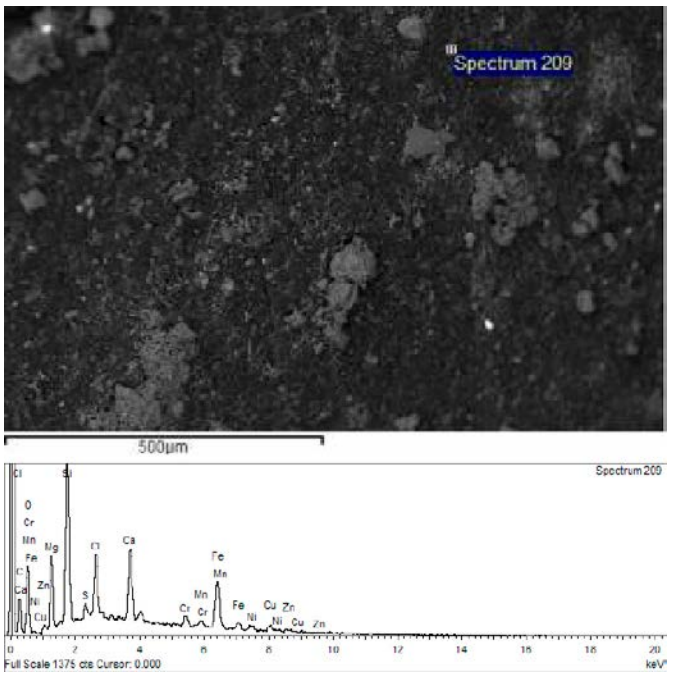

NaCaCl+Fe+Mg+Si+biofilm.

Sample 22111, KA3385A, 31.5 m.

Sample is dominated by calcite (scalenohedral habit). There are also cubic pyrite crystals (20–60 µm), fluorite, barite and fine-grained FeS on the surface of calcite crystals.

Photograph of location of sample 22111 (scraped off from packer connections).

SEM-images:

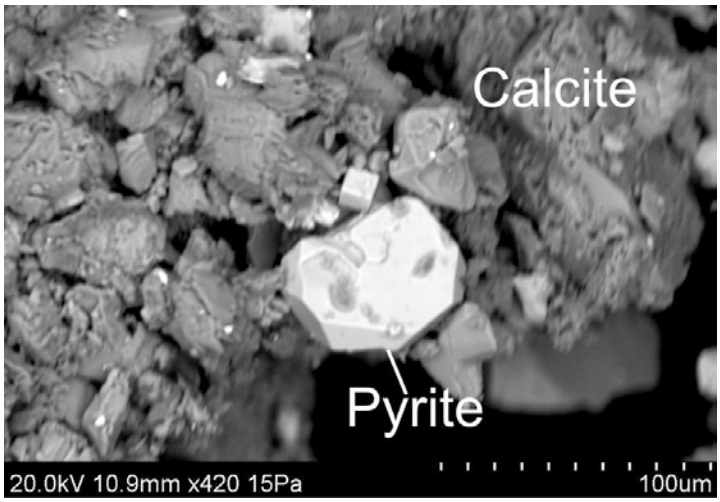

Back-scattered SEM image showing pyrite with calcite.

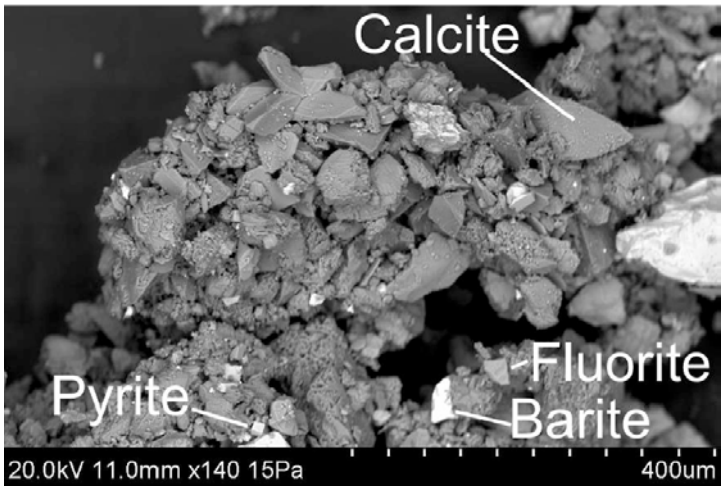

Back-scattered SEM image showing pyrite with calcite (dominates), barite, and fluorite.

EDS analysis locations and related spectra for 22111:

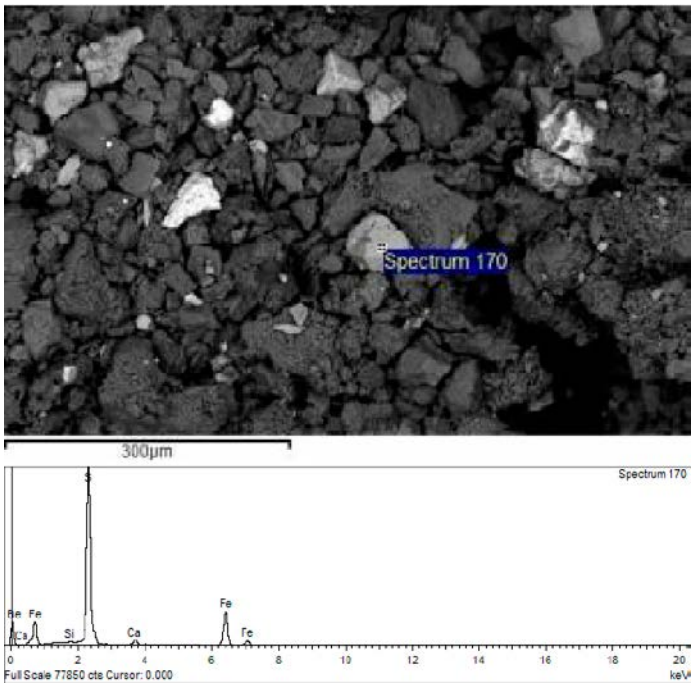

Spectrum 170: pyrite.

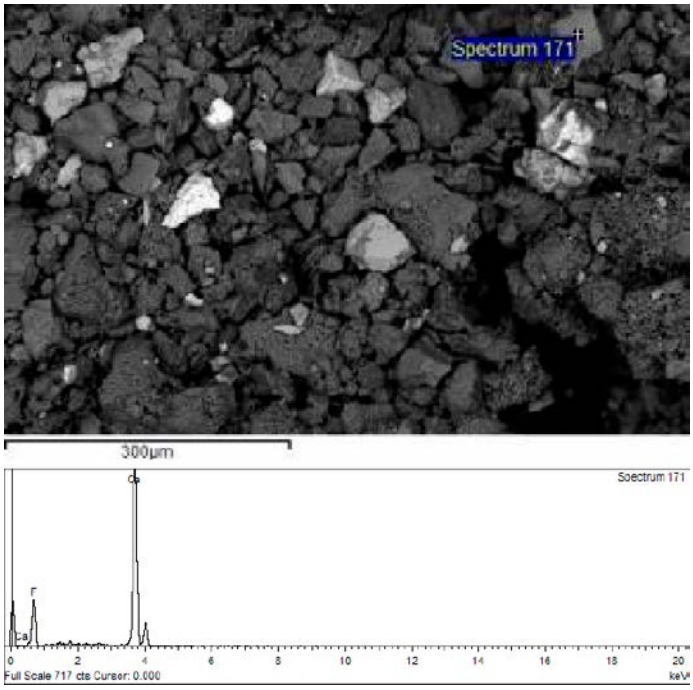

Spectrum 171: fluorite.

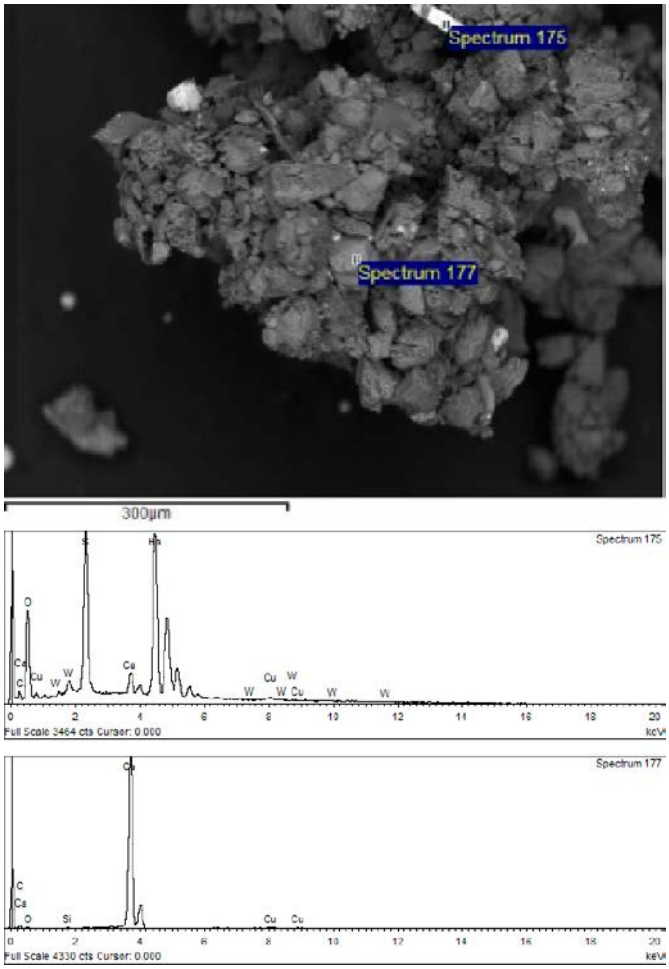

Spectrum 175: barite. Spectrum 177: calcite.

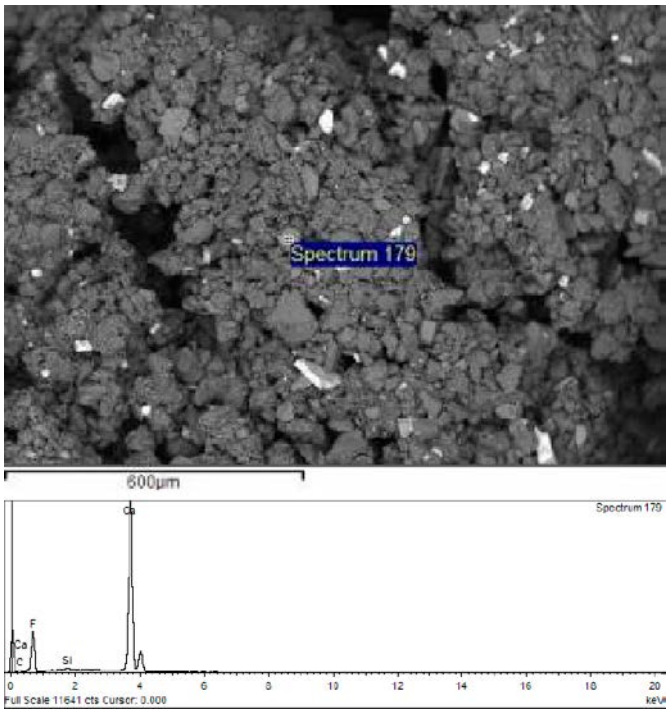

Spectrum 179: fluorite.

Sample 22112, KA3385A, 31.5–32.3 m.

Sample is dominated by calcite (~200 µm crystals with scalenohedral habit). There are also very few cubic pyrite crystals, barite and fine-grained FeS on the surface of calcite crystals. Some fine-grained Si- and Cl-precipitates were also observed.

Photograph of location of sample 22113 (scraped off from packer connections).

SEM-images:

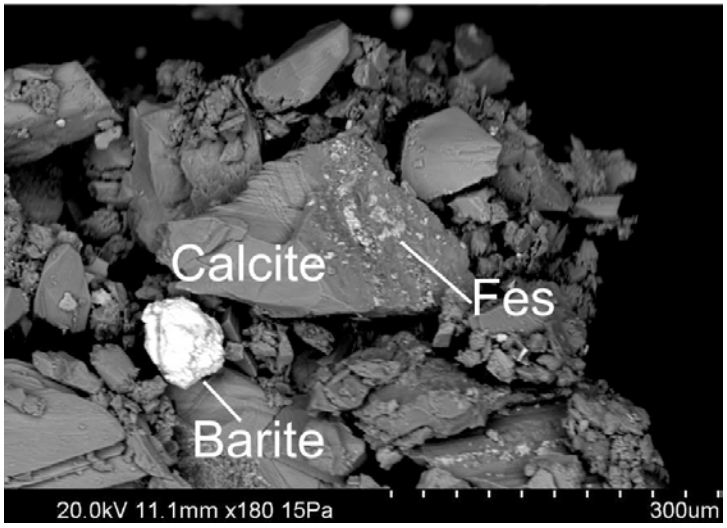

Back-scattered SEM image showing calcite with fine-grained FeS on the surface, and a barite crystal.

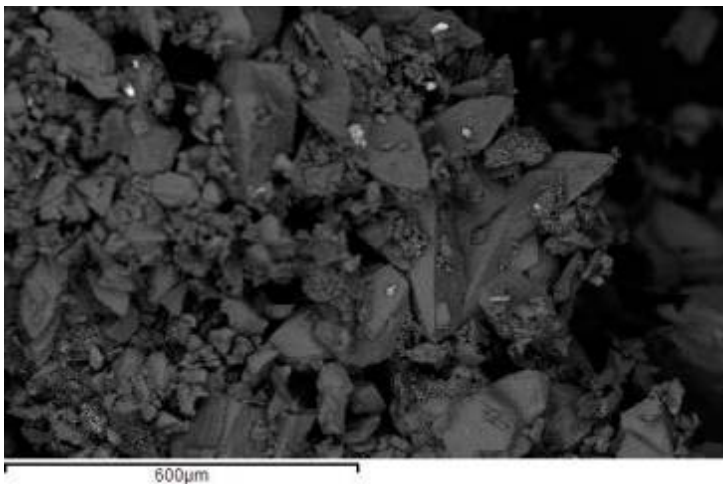

Back-scattered SEM image showing scalenohedral calcite.

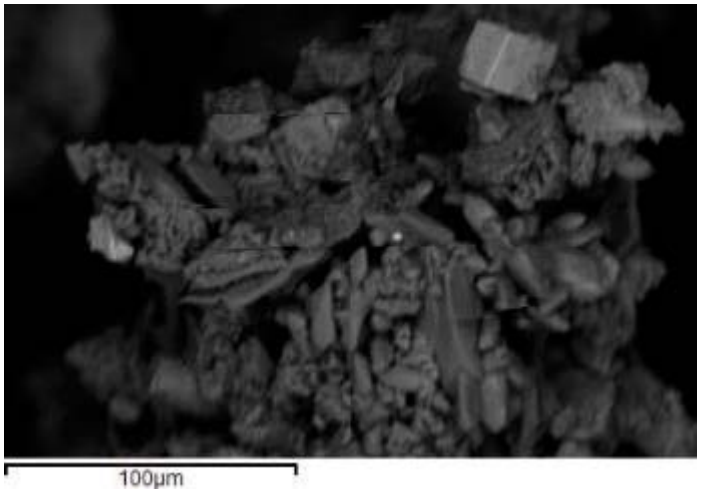

Back-scattered SEM image showing a cubic pyrite crystal with calcite (dominates).

EDS analysis locations and related spectra for 22112:

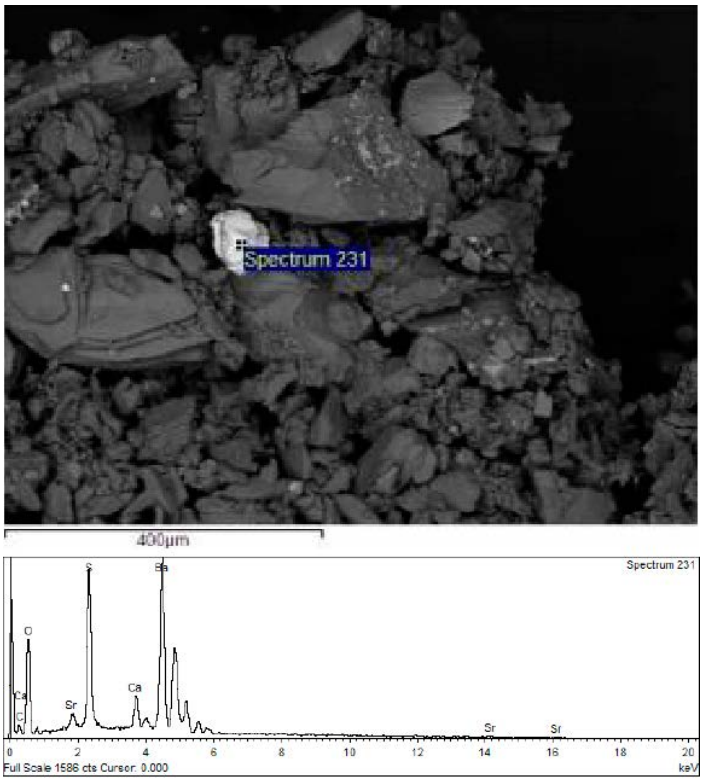

Spectrum 231: Barite (+small amount of calcite).

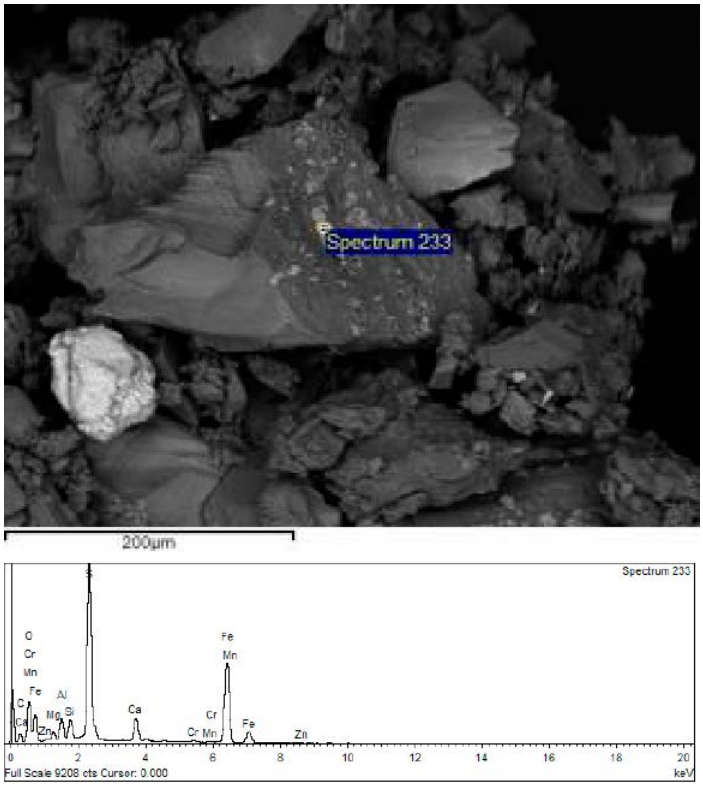

Spectrum 233: FeS.

Sample 22113, KA3385A, 31.5 m.

Sample is dominated by calcite (crystals with scalenohedral habit), with small amounts of cubic pyrite crystals (max 50 µm), barite and fine-grained FeS on the surface of calcite crystals.

SEM-images:

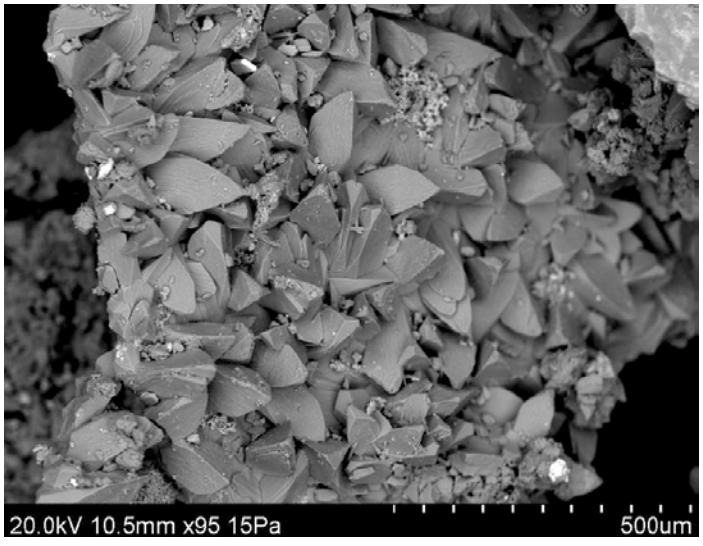

Back-scattered SEM image showing euhedral calcite crystals (bright crystals are barite and pyrite).

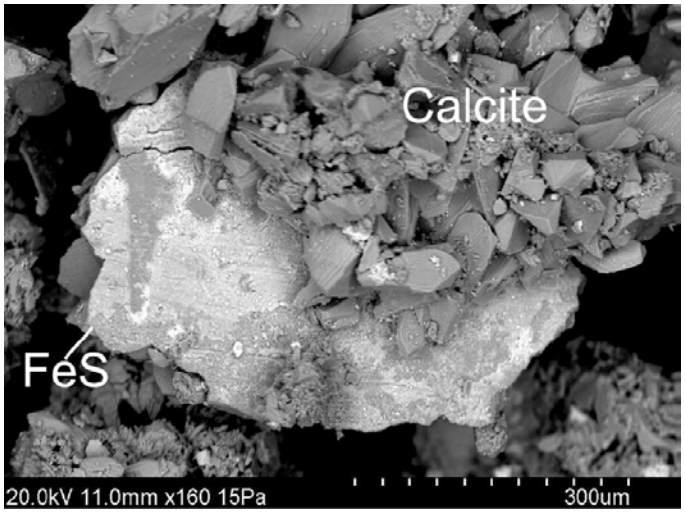

Back-scattered SEM image showing scalenohedral calcite and FeS (making up a surface which has been closest to the packer connection [iron], calcite has then grown on top of FeS).

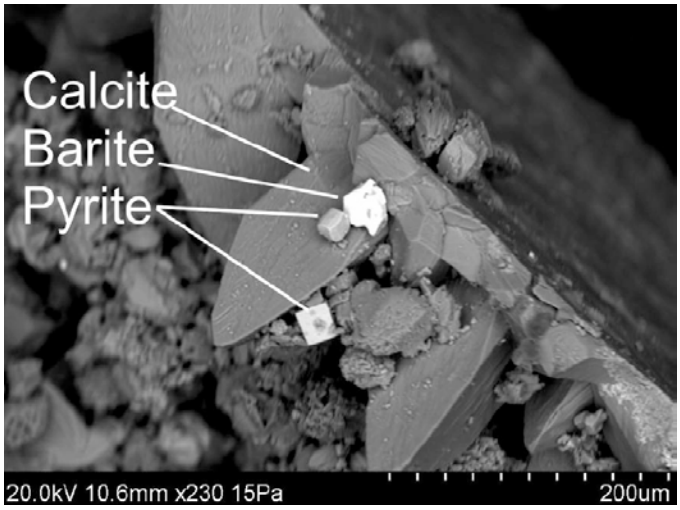

Back-scattered SEM image showing calcite (scalenohedral), with cubic pyrite crystals and barite.

EDS analysis locations and related spectra for 22113:

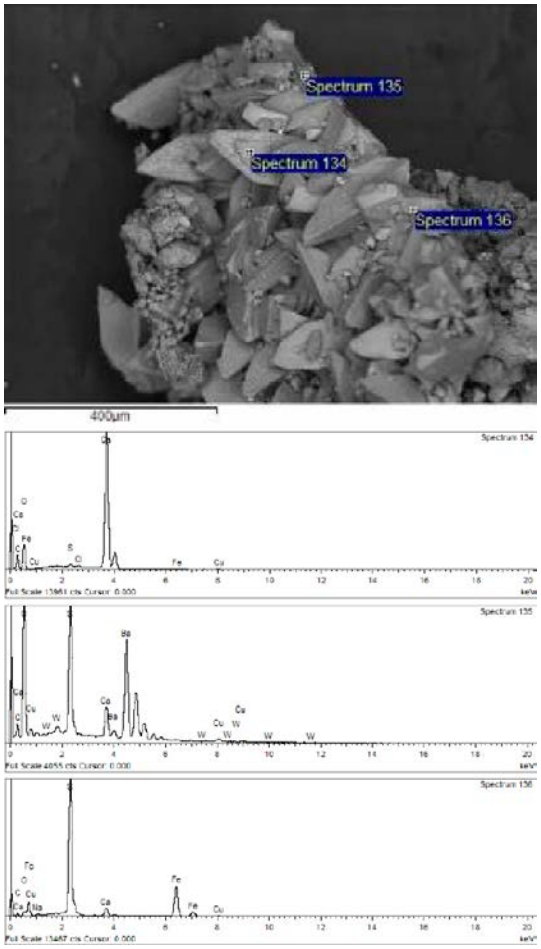

Spectrum 134: Calcite. Spectrum 135: Barite, Spectrum 137: Pyrite.

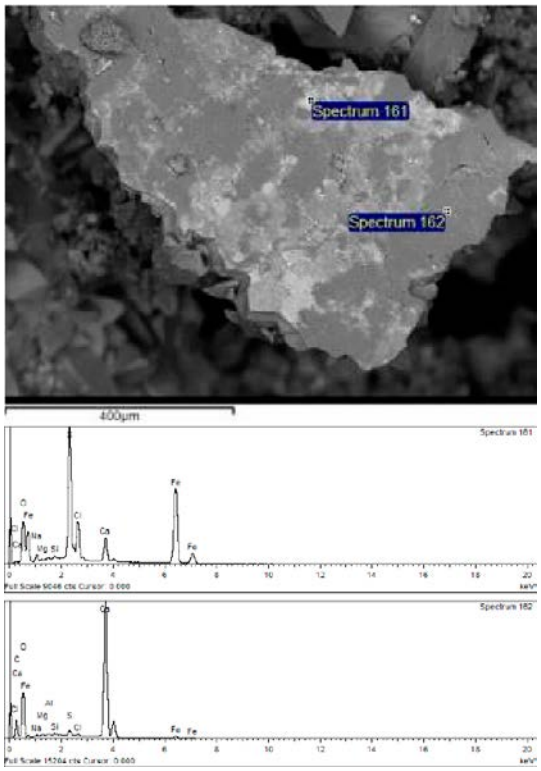

Spectrum 161: FeS (+Calcite and NaCl). Spectrum 162: Calcite.

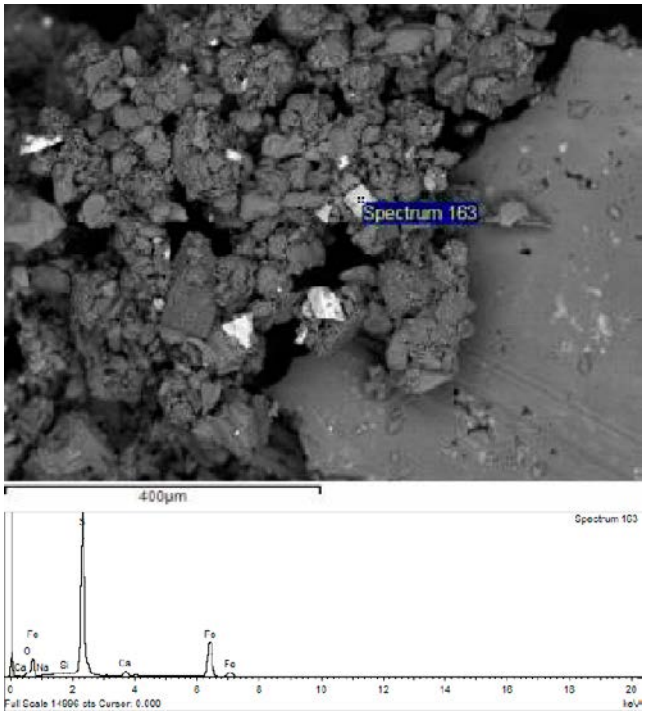

Spectrum 163: Pyrite.

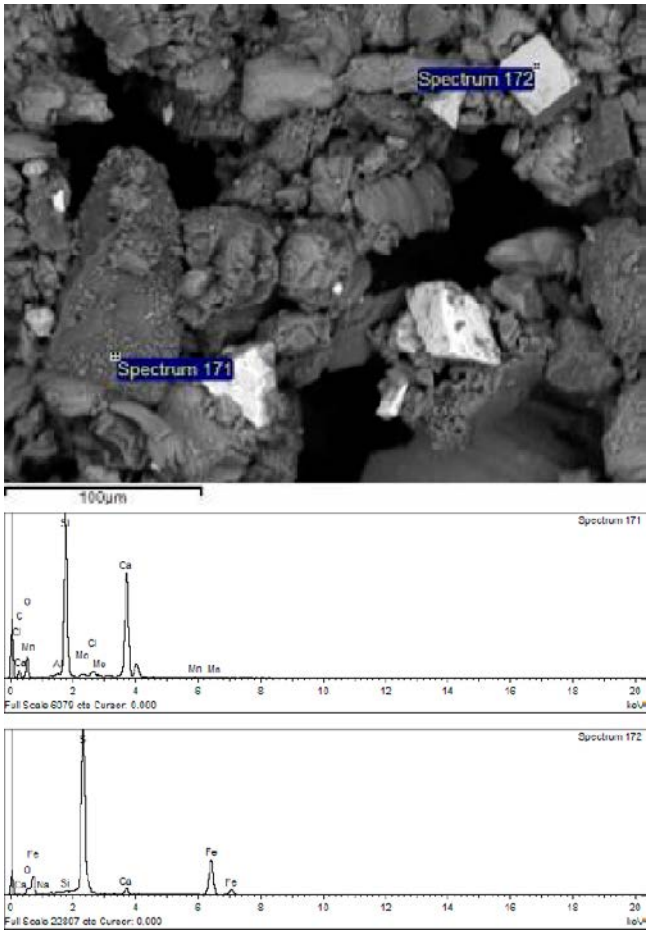

Spectrum 171 : Calcite+Si(quartz?). Spectrum 172: Pyrite.

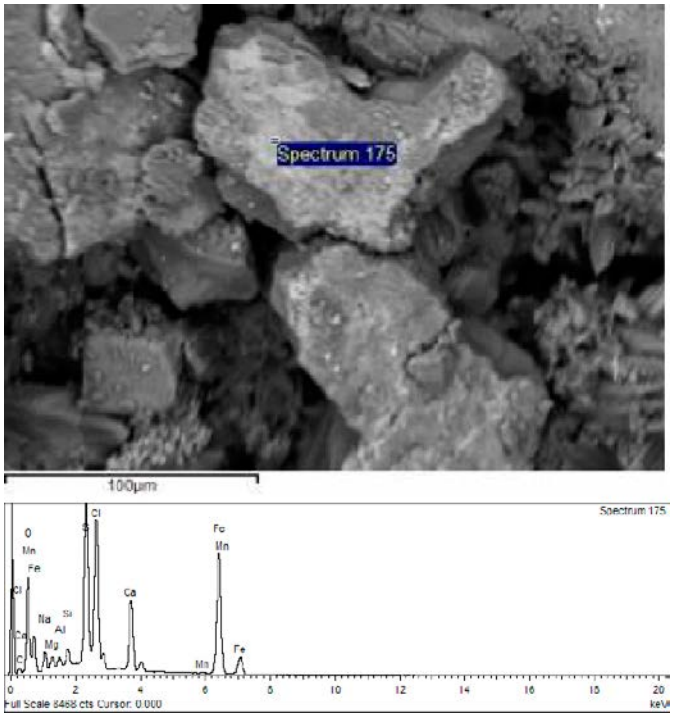

Spectrum 175: FeS+NaCaCl.

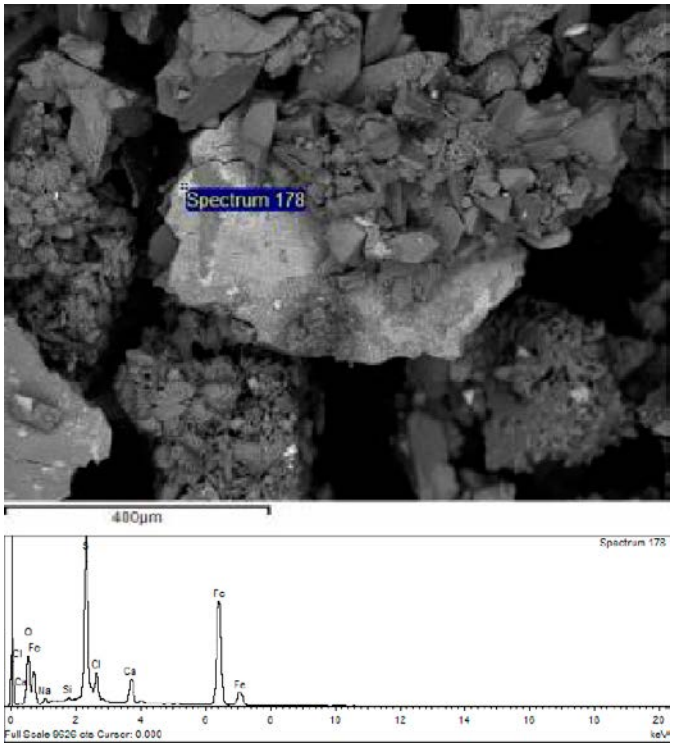

Spectrum 178: FeS.

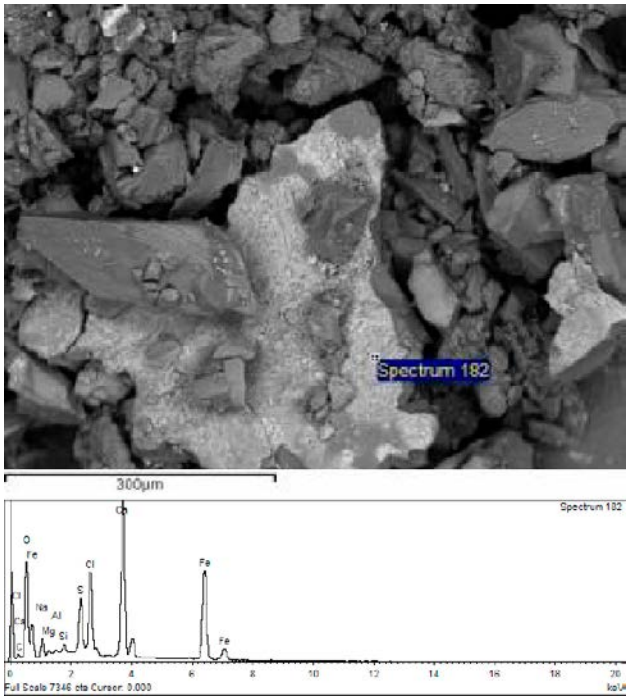

Spectrum 182 : FeS+NaCaCl.

Sample 22125, KA3105A, 17 m.

Sample is dominated by calcite (crystals is of scalenohedral [c-axis > a-axes] and equant [c-axis ≈ a-axes] habit), with very small amounts of cubic pyrite crystals (max 20–30 µm), barite (up to 100 µm), and quite commonly, fine-grained FeS has precipitated on the surface of calcite crystals.

SEM-images:

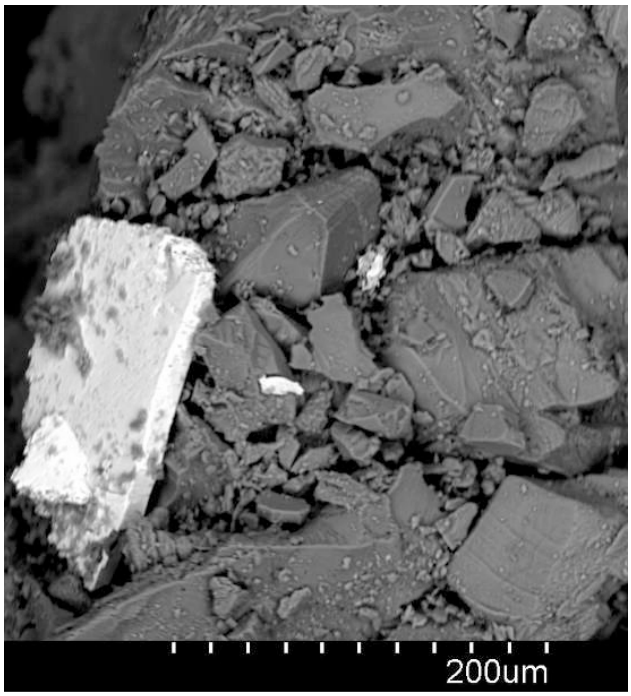

Back-scattered SEM image showing euhedral calcite crystals (dark) and barite (bright).

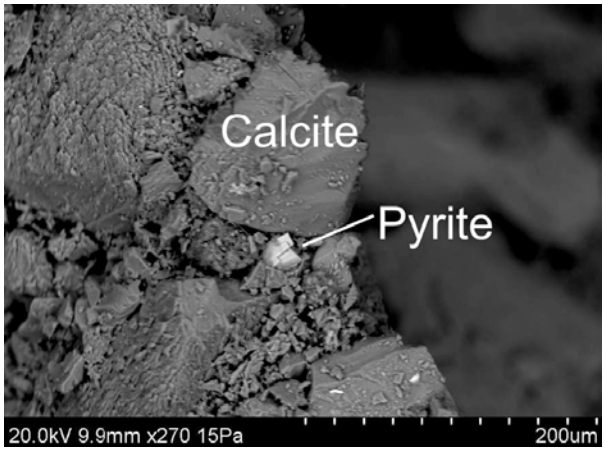

Back-scattered SEM image showing euhedral calcite and pyrite.

Back-scattered SEM image showing calcite, occasionally with a bright FeS cover.

EDS analysis locations and related spectra for 22125:

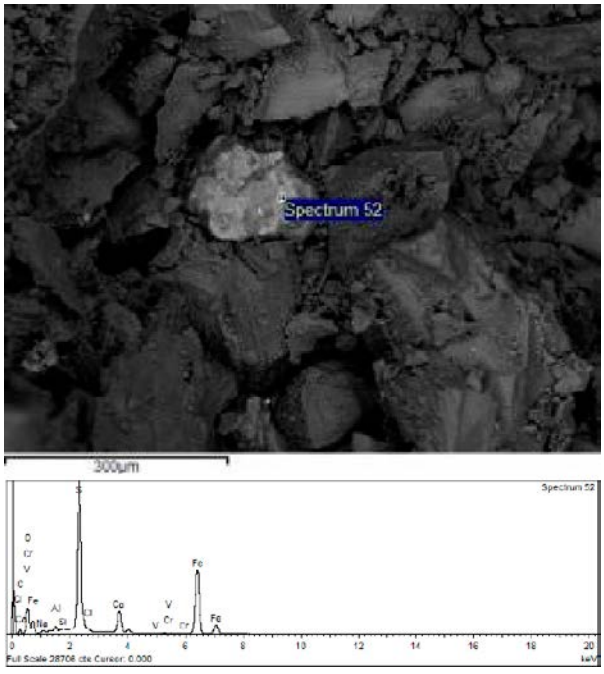

Spectrum 52: FeS (and calcite).

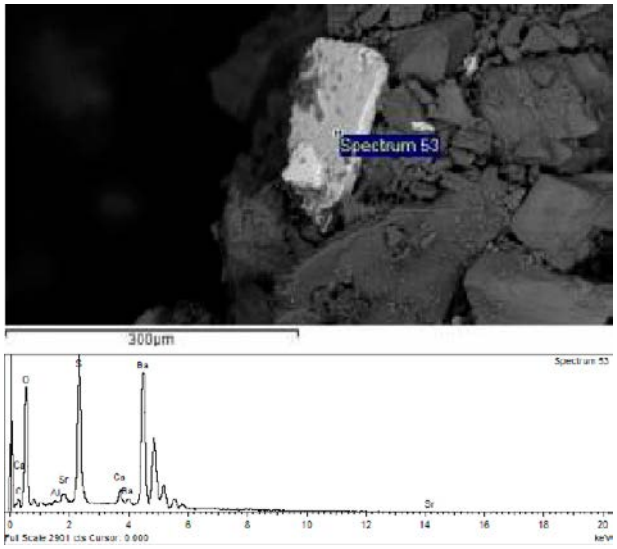

Spectrum 53: Barite.

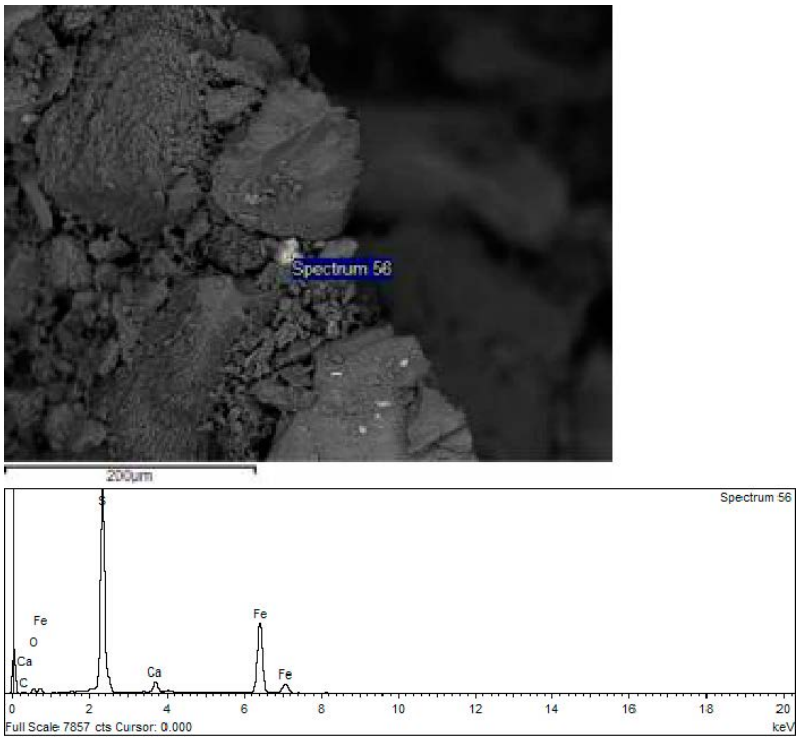

Spectrum 56: Pyrite/FeS.

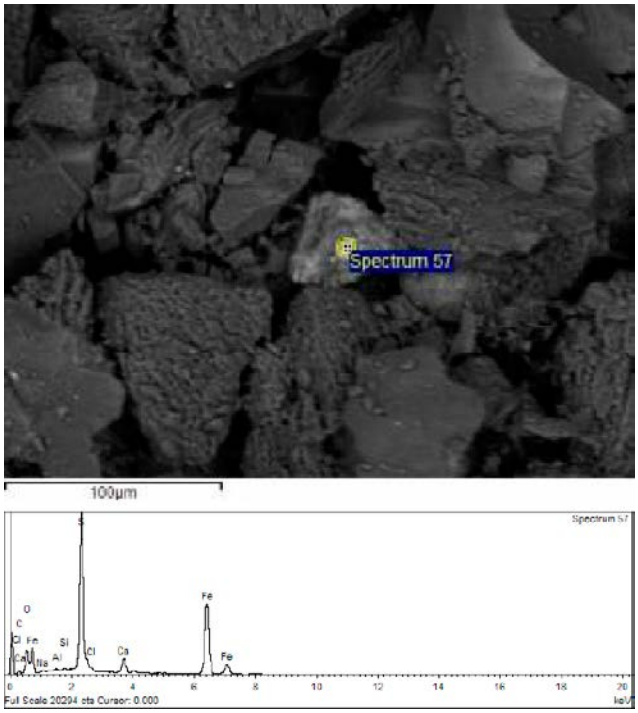

Spectrum 57: FeS.

Sample 22126, KA3105A, 19.5 m.

Sample is dominated by calcite (crystals are of scalenohedral [c-axis > a-axes] and equant [c-axis ≈ a-axes] habit), with very small amounts of barite, chalcopyrite (one crystal), FeS (fine-grained [< 5 µm] on calcite, but also larger aggregates [up to 50 µm]).

SEM-images:

Back-scattered SEM image showing calcite (with variable c-axis to a-axes ratio).

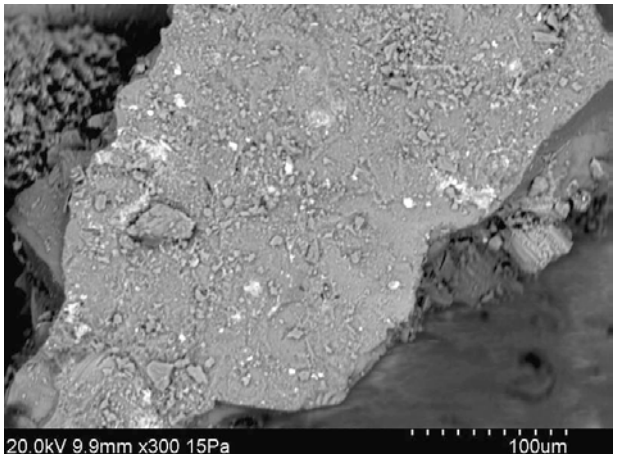

Back-scattered SEM image showing calcite with very fine-grained FeS on the surface (bright spots).

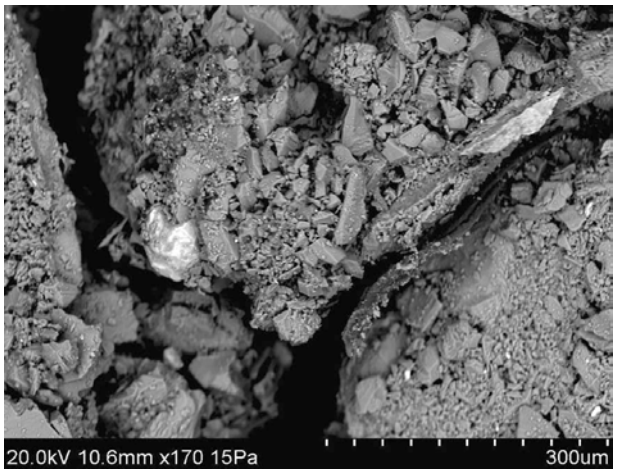

Back-scattered SEM image showing calcite along with aggregates of FeS crystals (bright).

EDS analysis locations and related spectra for 22126:

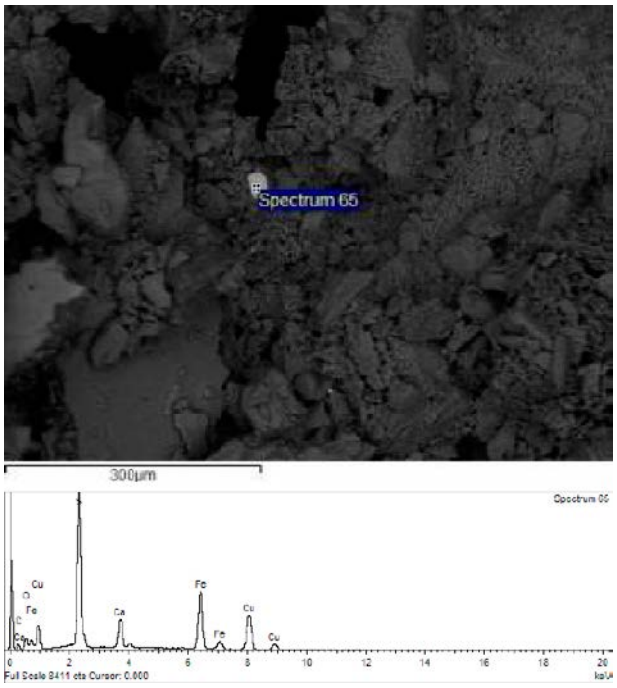

Spectrum 65: Chalcopyrite.

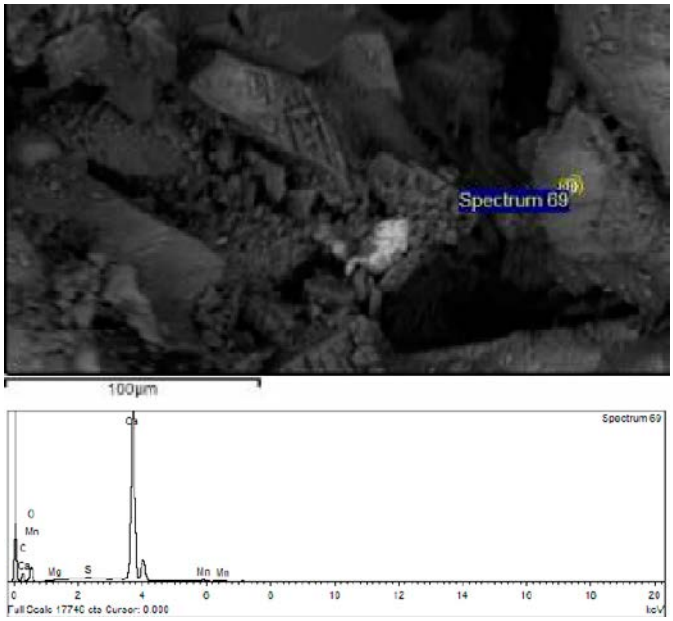

Spectrum 69: Calcite.

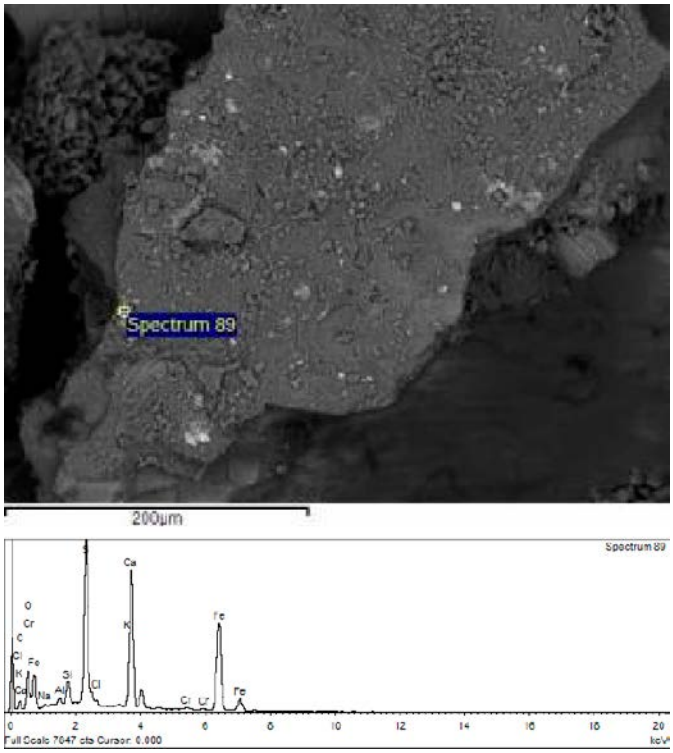

Spectrum 89: FeS+calcite.

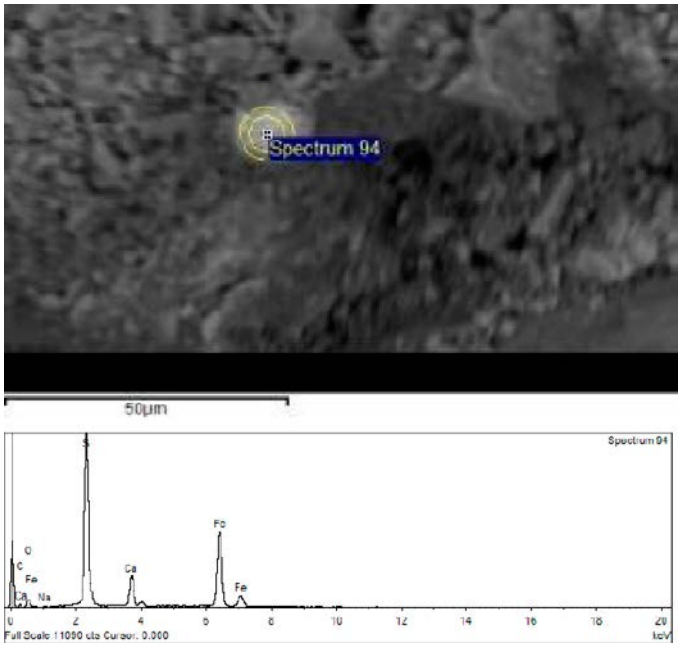

Spectrum 94: FeS(+calcite).

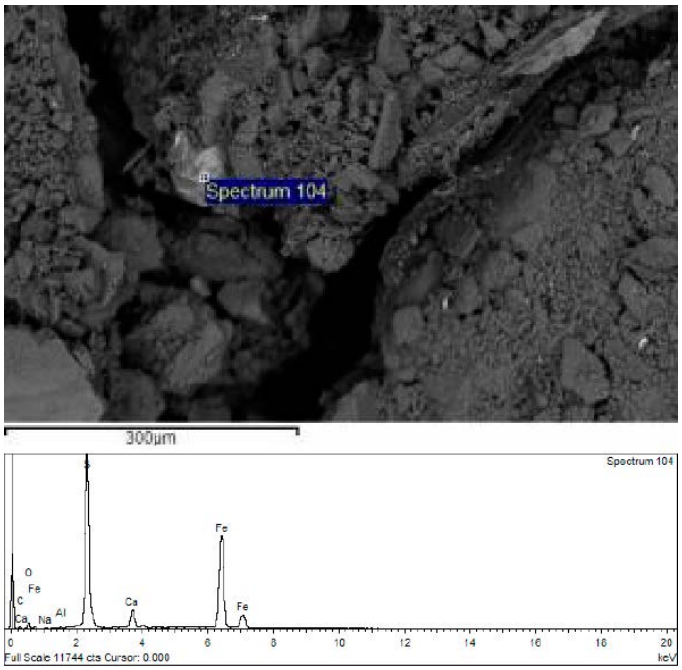

Spectrum 104: FeS(+calcite).

Sample 22127, KA3105A, 18.2 m.

Al-rich, glassy encrustation (+Si,S,Cl,Ca, Na).

SEM-images:

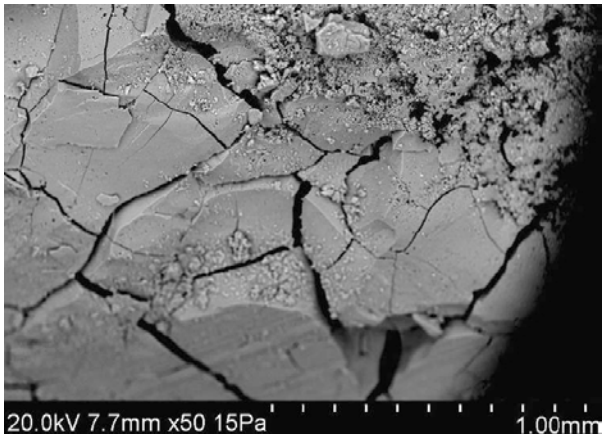

Back-scattered SEM image showing Al-rich substance (with dry cracks).

EDS analysis locations and related spectra for 22127:

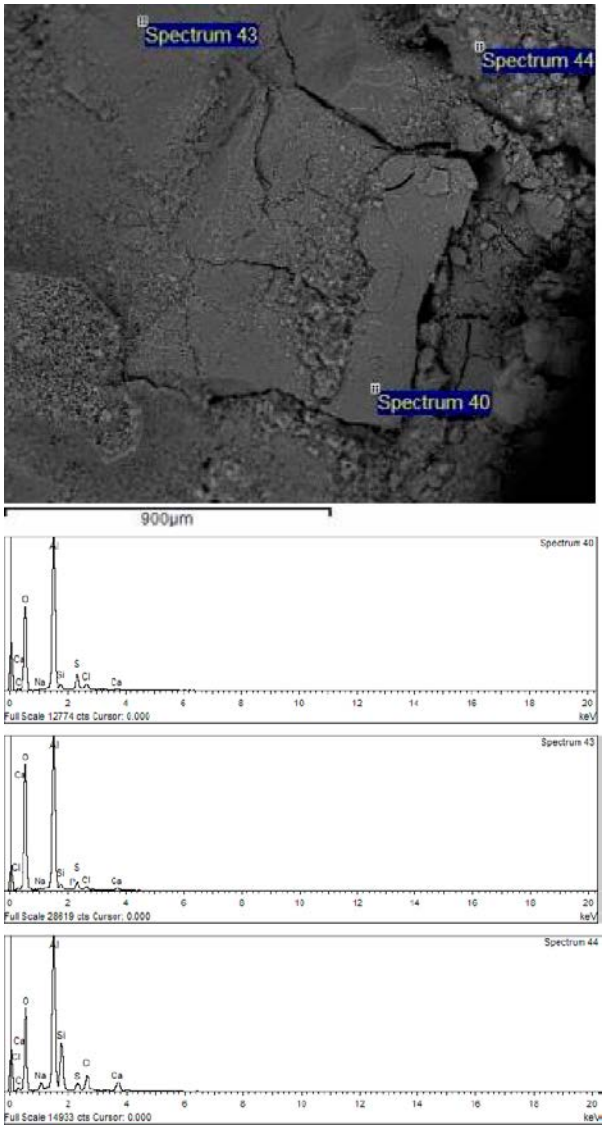

Spectrum 40: Al-S rich encrustation. Spectrum 43: Al-rich precipitate, Spectrum 44: Al(+Si,CaNaCl+S).

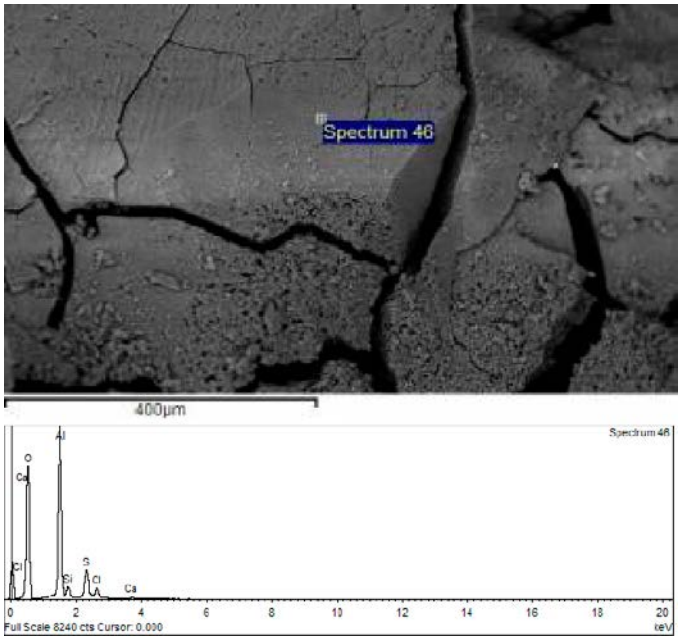

Spectrum 46: Al(+S,Cl,Si).

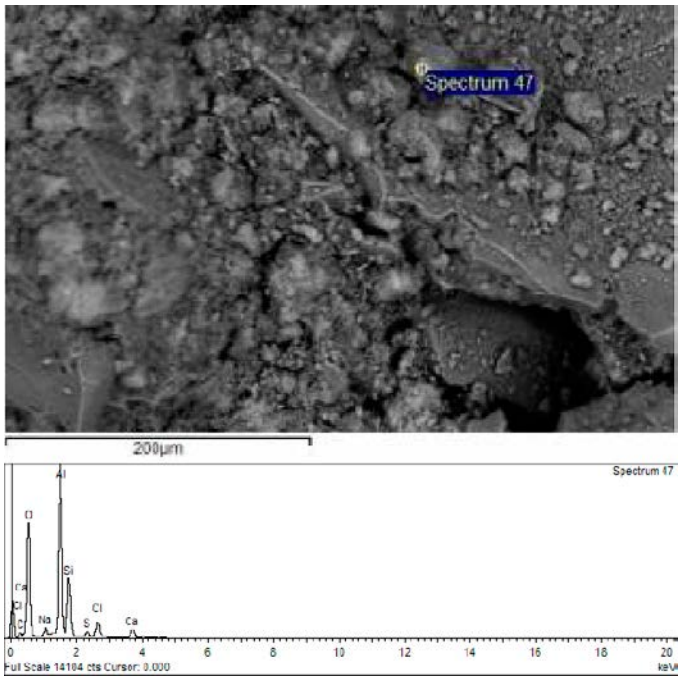

Spectrum 47: Al(+Si,CaNaCl+biofilm?)

Sample 22128, KA3105A, 4–5 m.

The sample is dominated by calcite (scalenohedral, up to 1 mm). Small barite crystals (up to 80 μm) and cubic pyrite crystals (5–10 μm) are present.

SEM images:

Back-scattered SEM image showing scalenohedral calcite.

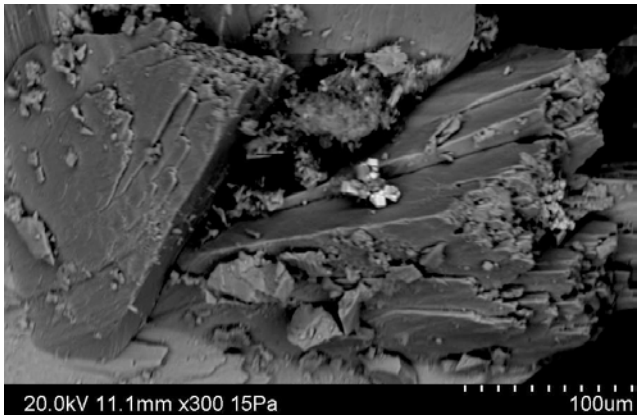

Back-scattered SEM image showing scalenohedral calcite with cubic pyrite (bright).

Back-scattered SEM image showing cubic pyrite (bright) on calcite.

EDS analysis locations and related spectra for 22128:

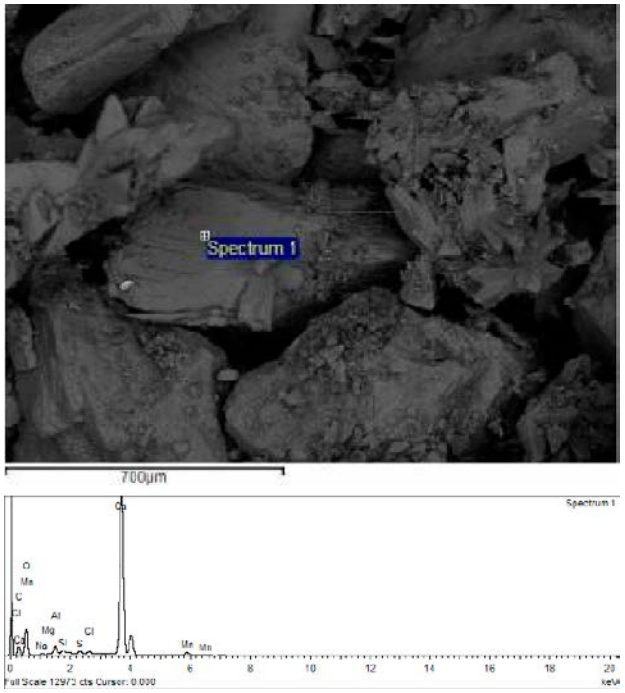

Spectrum 1: Calcite.

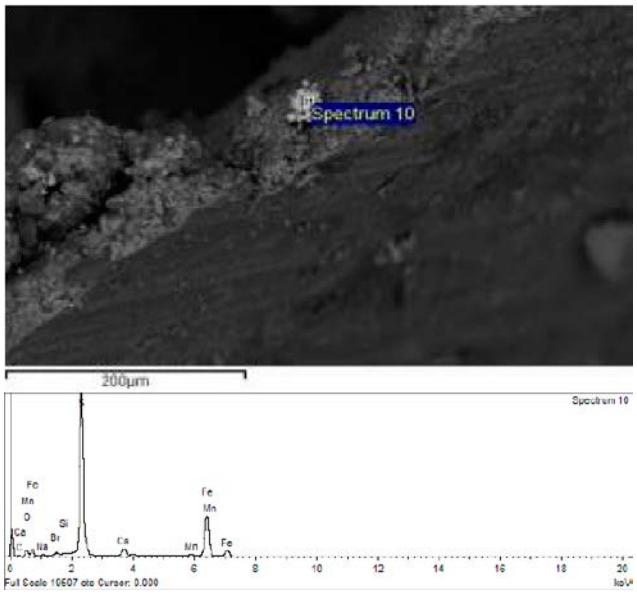

Spectrum 10: Pyrite.

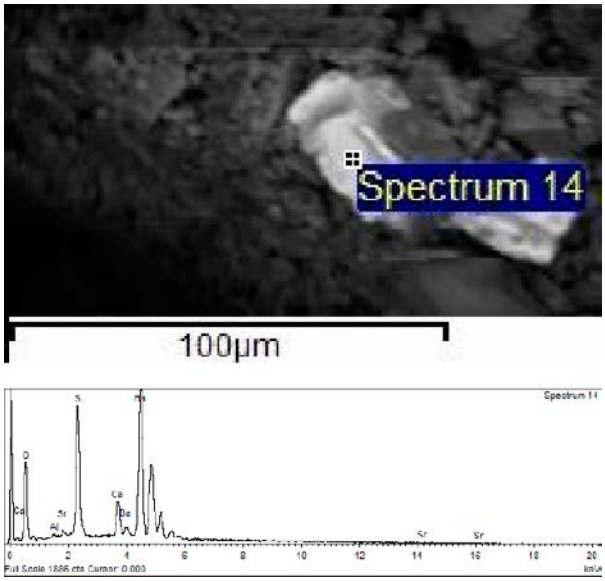

Spectrum 14: barite.

Sample 22129, KA3105A, 18.2 m.

The sample is dominated by an Al-rich encrustation/substance (with some S och Cl, and smaller but detectable amounts of Si, and in one case also Zn). Sample was taken beneath the tape. A FeAlSi-mineral was also detected (may be a clay mineral) and one small pyrite crystal was also detected.

SEM images:

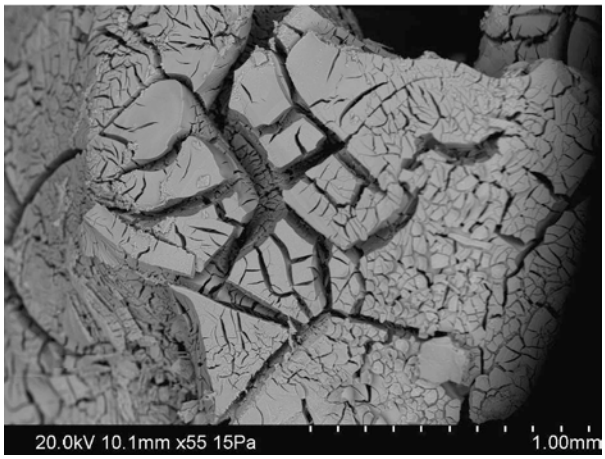

Back-scattered SEM image showing Al-rich substance (with dry cracks).

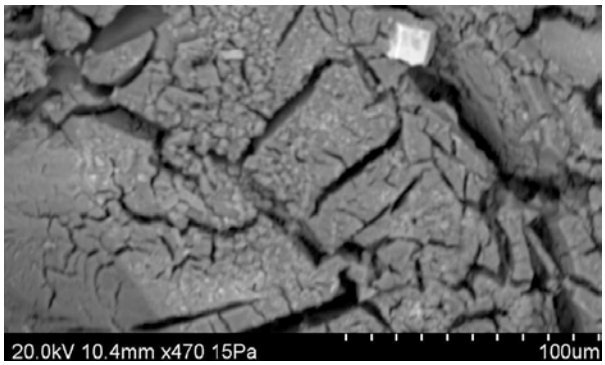

Back-scattered SEM image showing Al-rich substance (with dry cracks) and a single pyrite crystal.

EDS analysis locations and related spectra for 22129:

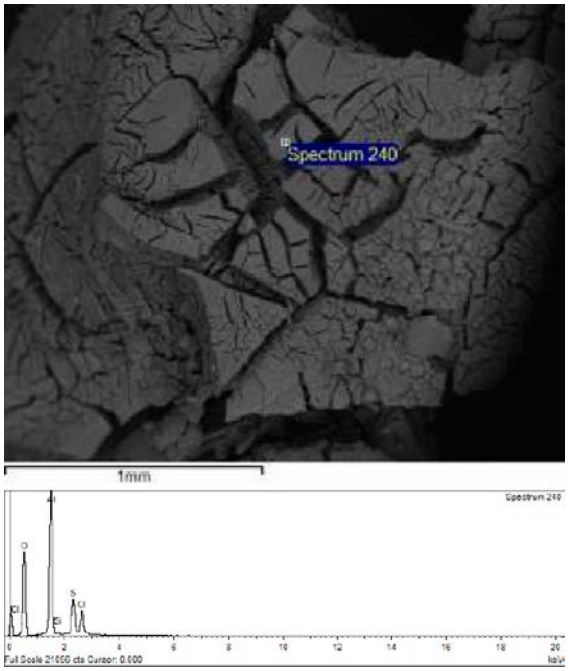

Spectrum 240: Al(+S,Cl).

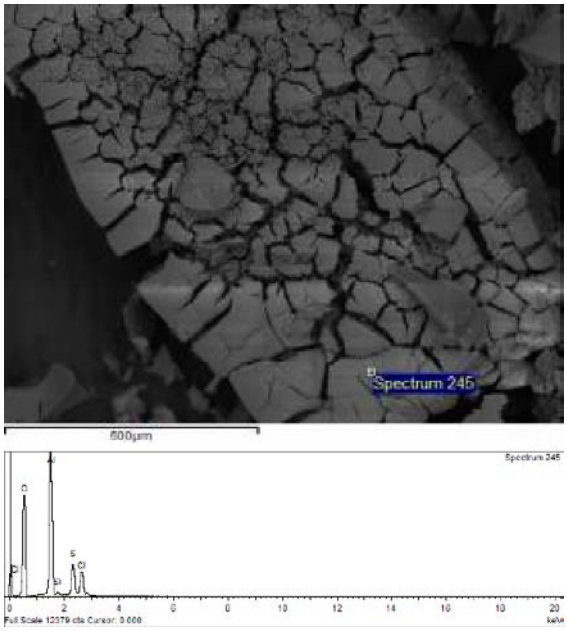

Spectrum 245: Al(+S,Cl).

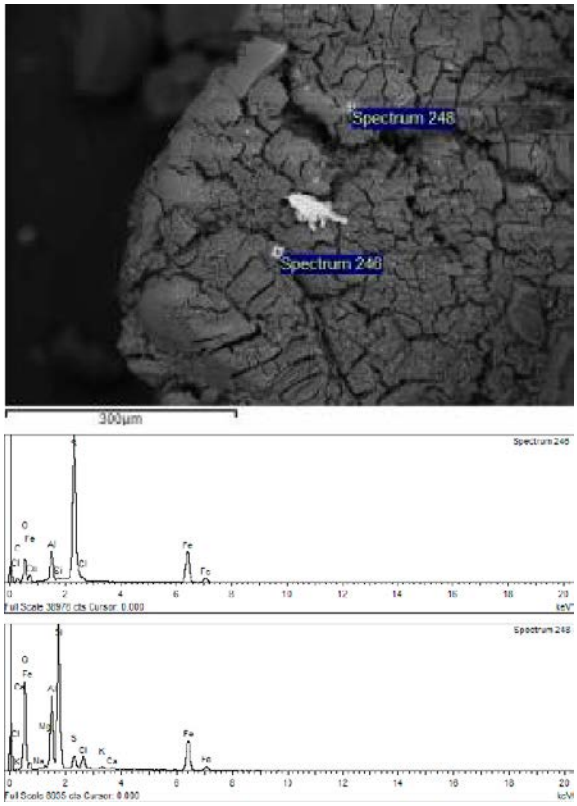

Spectrum 246: Pyrite, Spectrum 248; $FeAlSi_2$.

Sample 22130, KA3105A, 22.5 m.

Sample is dominated by calcite (crystals are of scalenohedral [c-axis > a-axes] and equant [c-axis ≈ a-axes] habit), with very thin cover of FeS and pyrite on its surface. Occasional single pyrite crystals were detected (cubic 20 µm-sized). Some Si-crystals (SiO_2?) also exist.

Photograph of sample 22130 (sample material was scraped off from packer connections).

SEM images:

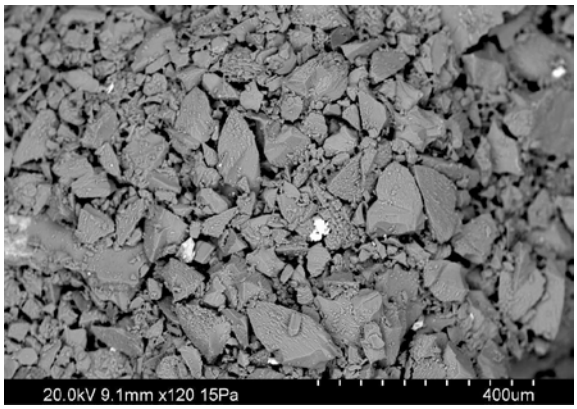

Back-scattered SEM image showing dominantly calcite.

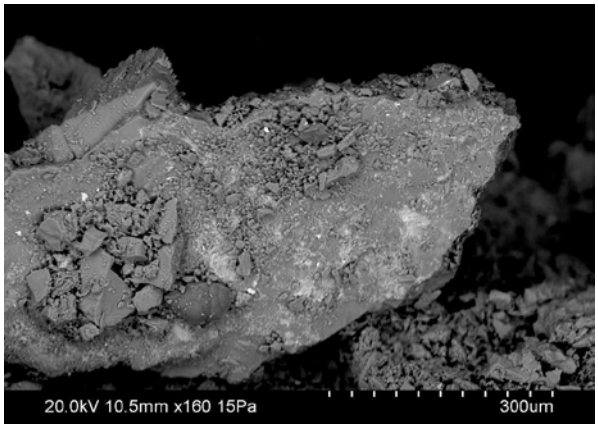

Back-scattered SEM image showing calcite with fine-grained FeS (bright) on the crystal surface.

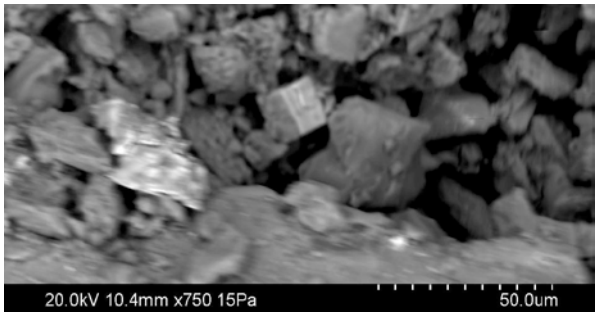

Back-scattered SEM image showing calcite and a cubic pyrite crystal.

EDS analysis locations and related spectra for 22130:

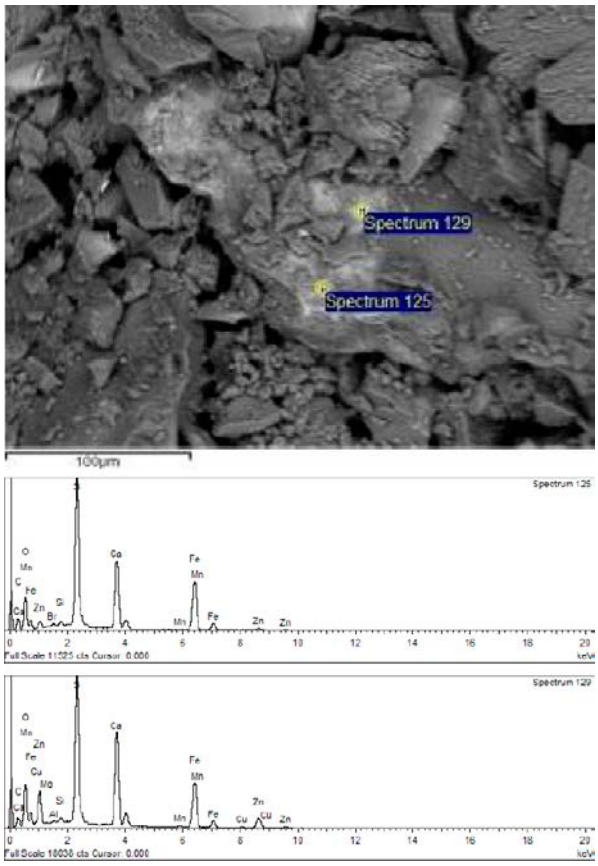

Spectrum 125: FeS/pyrite+calcite, Spectrum 129: FeS/pyrite+calcite.

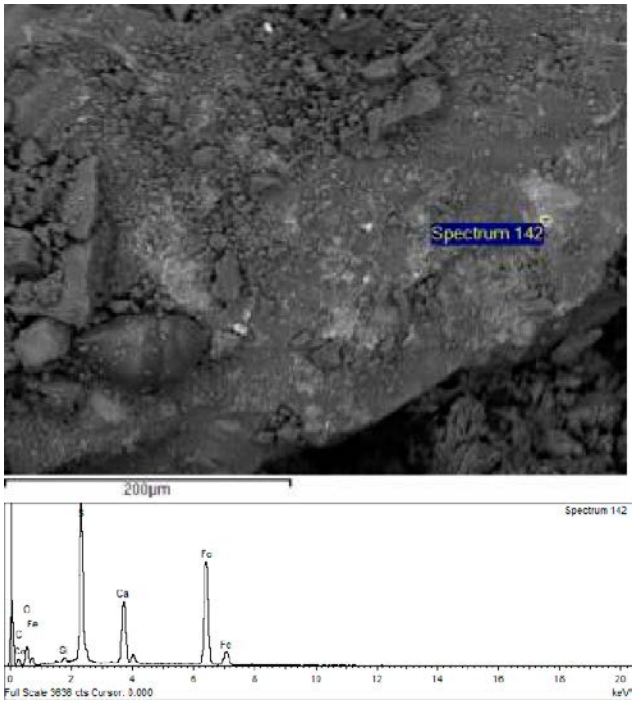

Spectrum 142: FeS/pyrite+calcite

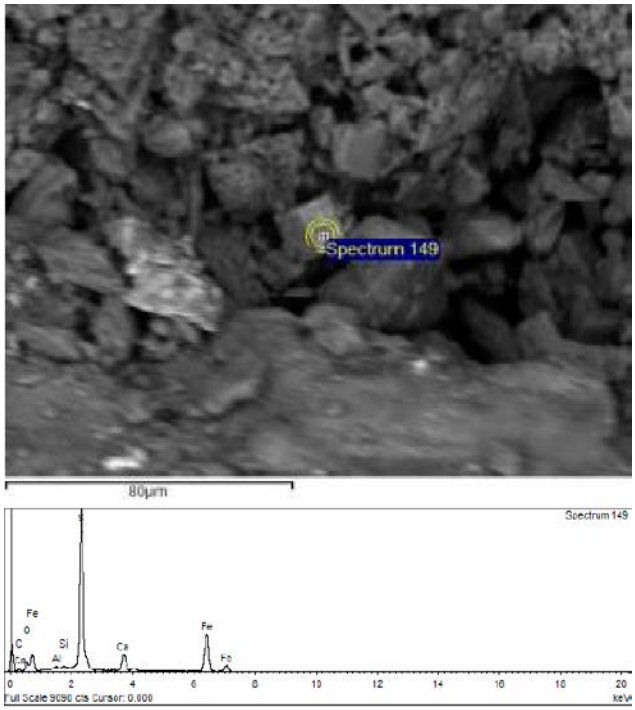

Spectrum 149: Pyrite+calcite.

Sample 22131, KA3105A, 22.5–24.5 m.

Sample is dominated by calcite (crystals are of scalenohedral [c-axis > a-axes] habit). Pyrite crystals exist (50 µm crystals, but smaller also exist: 1–2 µm). An Al-rich substance is also present, as well as a Si-rich mineral with some Al. Chalcopyrite, FeS, quartz (euhedral) and barite (up to 100 µm crystals) were also detected, as well as rock fragments (titanite, apatite, chlorite).

Photograph of sample 22131 (sample material was scraped off from the rod).

SEM images:

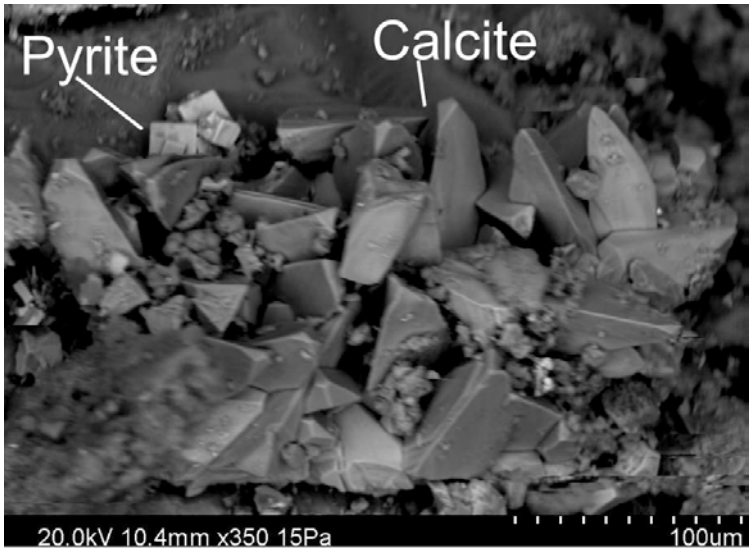

Back-scattered SEM image showing dominantly calcite and cubic pyrite.

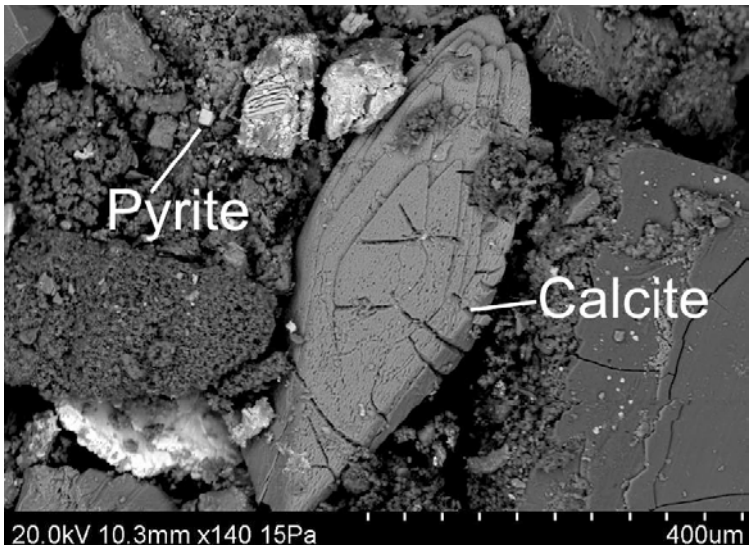

Back-scattered SEM image showing a scalenohedral calcite crystal, cubic pyrite etc.

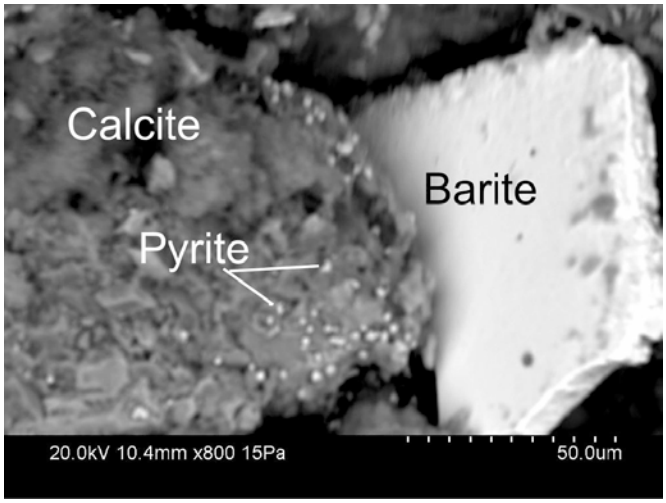

Back-scattered SEM image showing barite, as well as very fine-grained pyrite crystals on calcite.

EDS analysis locations and related spectra for 22131:

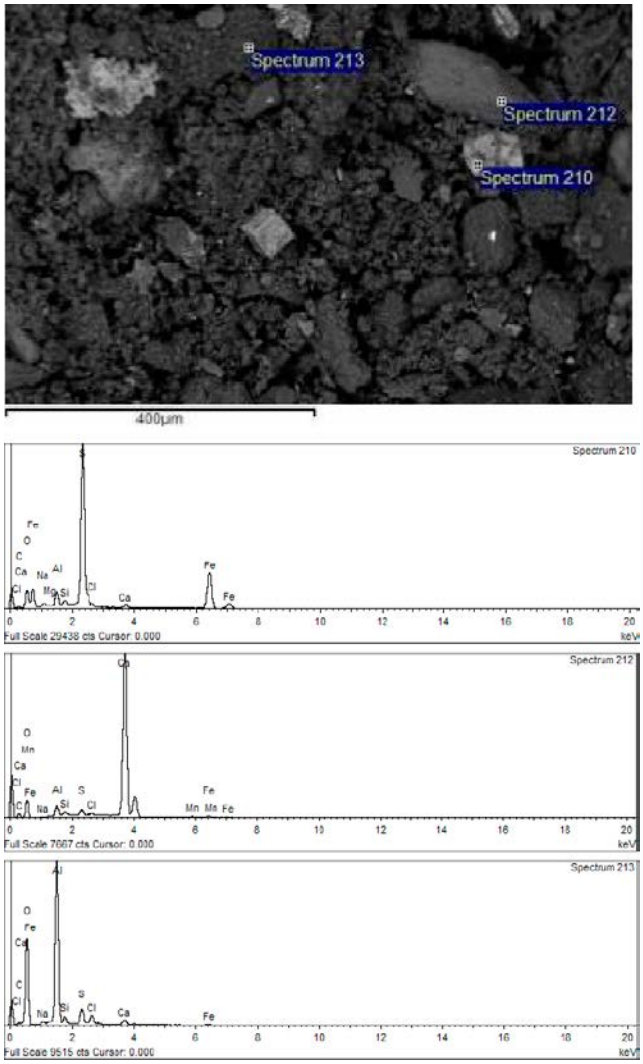

Spectrum 210: Pyrite, Spectrum 212: Calcite, Spectrum 213: Al-rich substance.

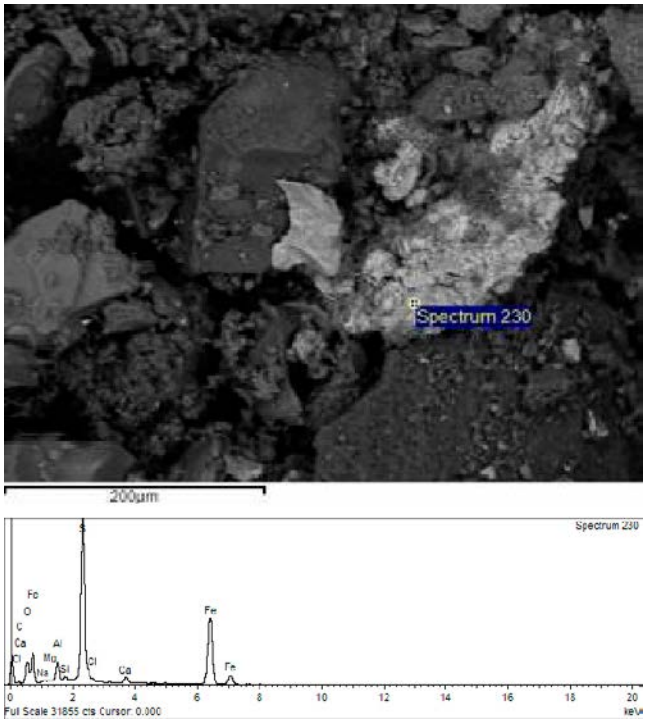

Spectrum 230: FeS.

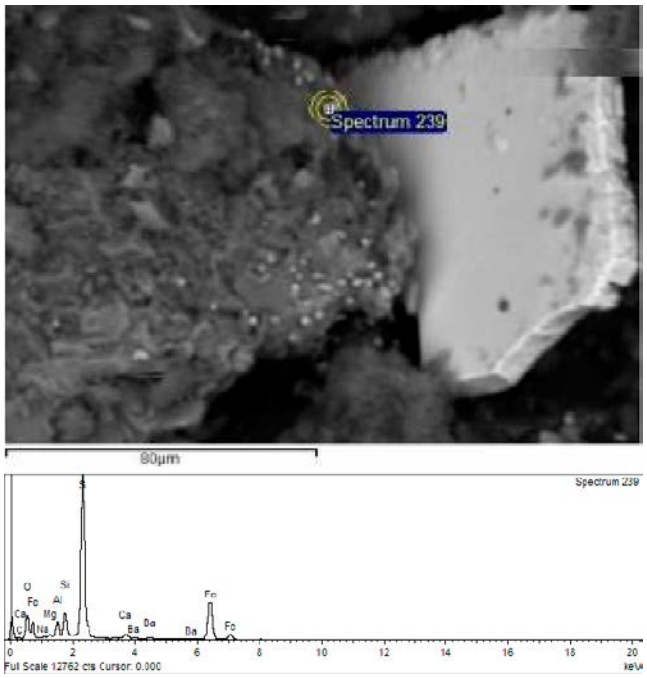

Spectrum 239: Pyrite.

Sample 22132, KA3105A, 24.5 m.

Sample is dominated by calcite (crystals are of scalenohedral [c-axis > a-axes] and equant [c-axis ≈ a-axes] habit). Pyrite and FeS exist as fine-grained crystals on the crystal surfaces of calcite. Largest pyrite crystals are 40–80 µm. An Al-rich substance is also present (also including smaller amounts of Si, S, Ca, Cl, Na).

Photograph of sample 22132 (sample material was scraped off from the packer connections).

SEM images:

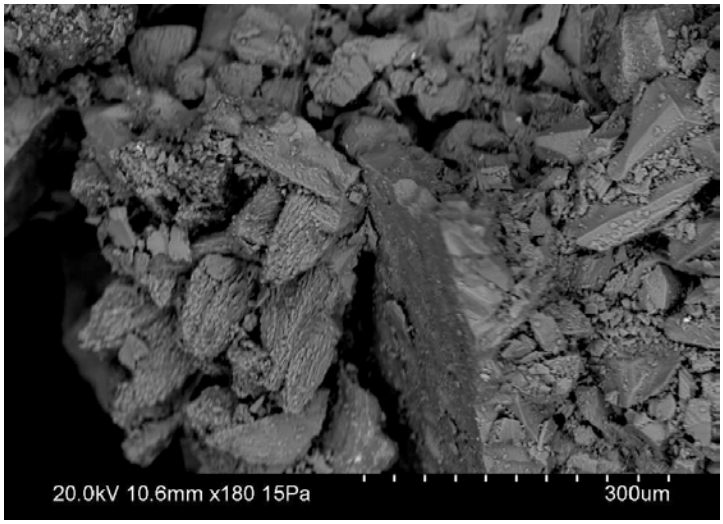

Back-scattered SEM image showing dominantly calcite.

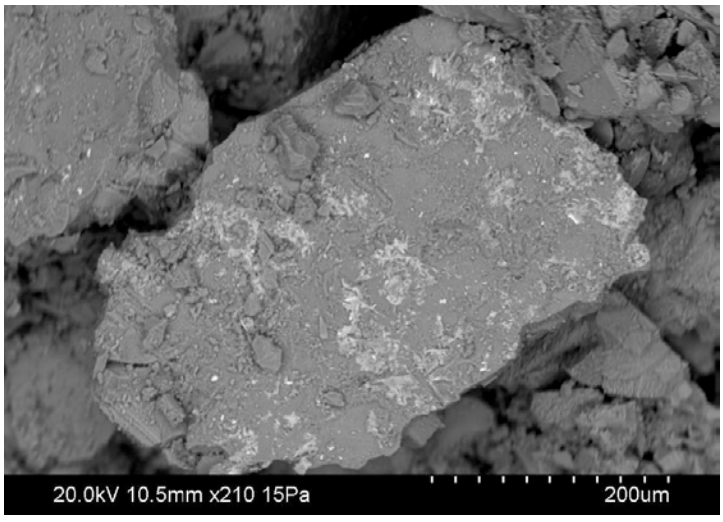

Back-scattered SEM image showing fine-grained FeS (bright) on calcite.

Back-scattered SEM image showing cubic pyrite (bright) with calcite.

EDS analysis locations and related spectra for 22132:

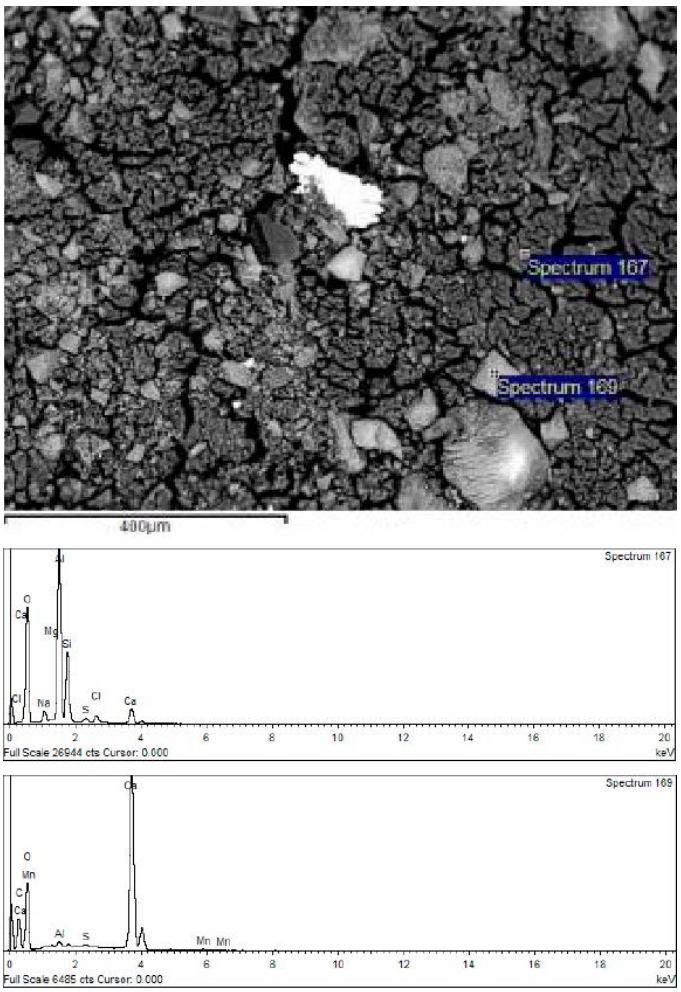

Spectrum 167: Al-rich substance. Spectrum 169: Calcite.

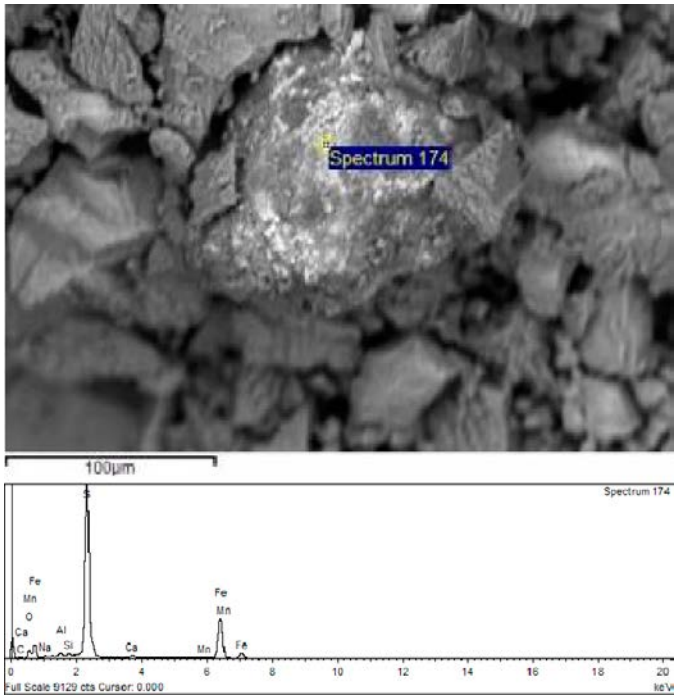

Spectrum 174: Pyrite.

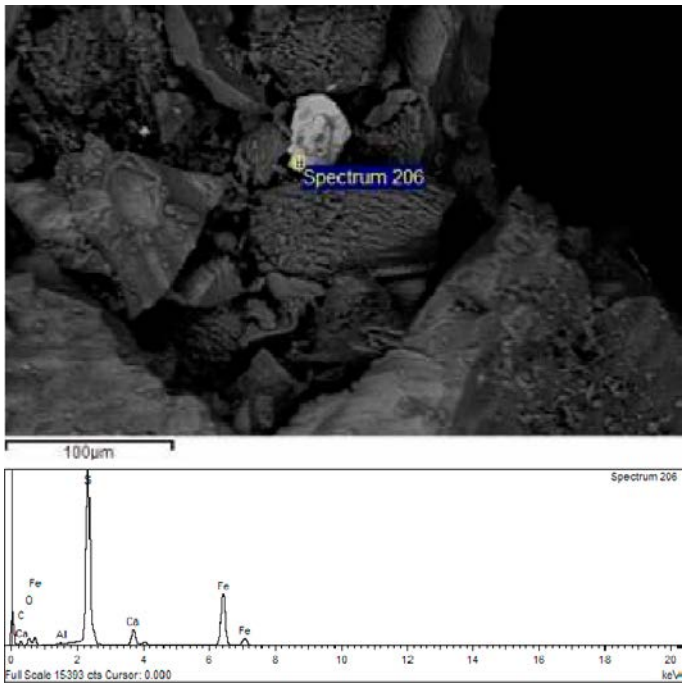

Spectrum 206: FeS/pyrite+calcite.

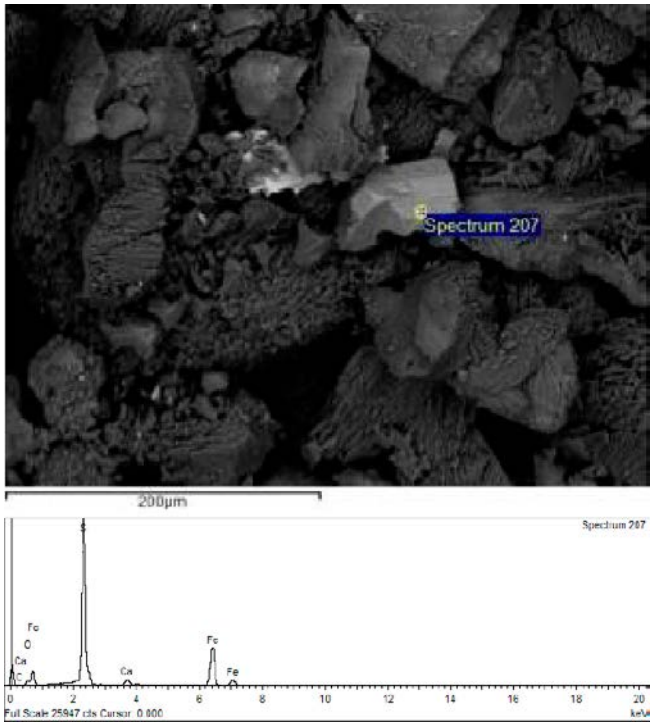

Spectrum 207: Pyrite.

Sample 22133, KA3105A, 23.2 m.

Sample consists of a white to yellowish substance, occasionally hardened. The substance consists of an Al-rich material, with significant components of S and Si (varying) and some NaCl/$CaCl_2$. A very small part of the sample is made up of FeS (~50 µm).

Photograph of sample 22133 (sample material was scraped off from the tape).

SEM images:

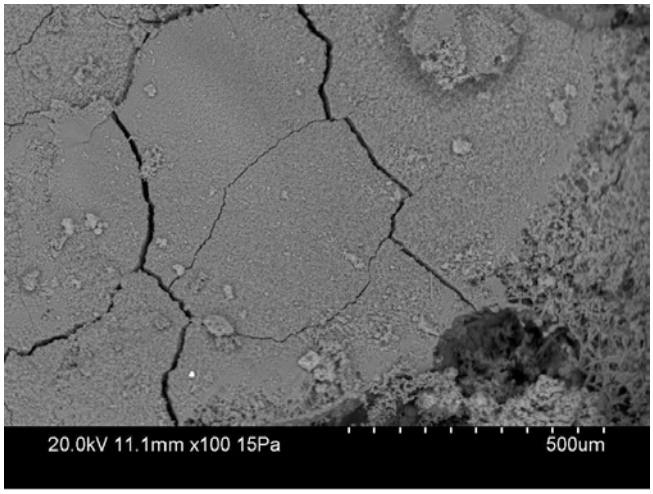

Back-scattered SEM image showing the hard Al-dominated crust.

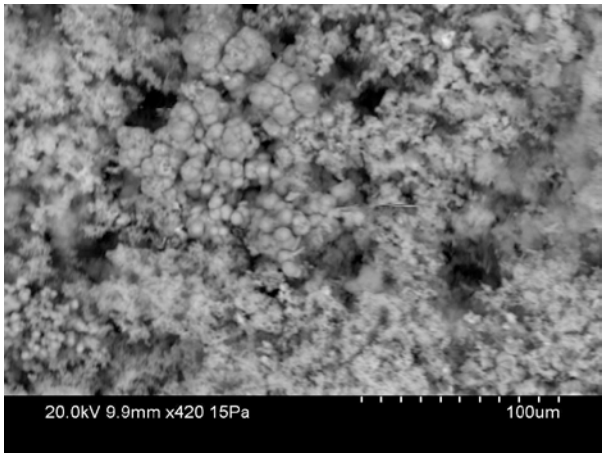

Back-scattered SEM image showing an Al-Si dominated part of the sample.

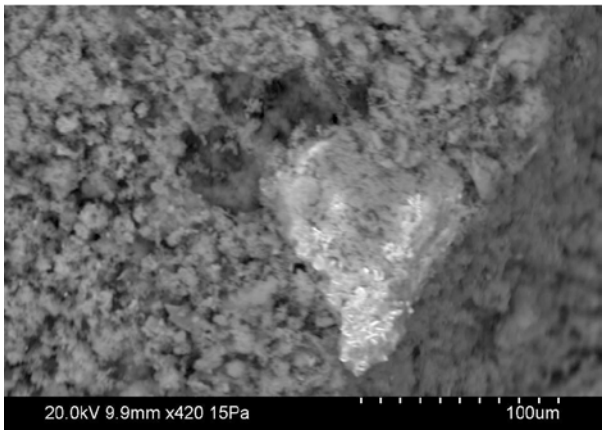

Back-scattered SEM image showing an FeS (bright) and the Al-dominated substance.

EDS analysis locations and related spectra for 22133:

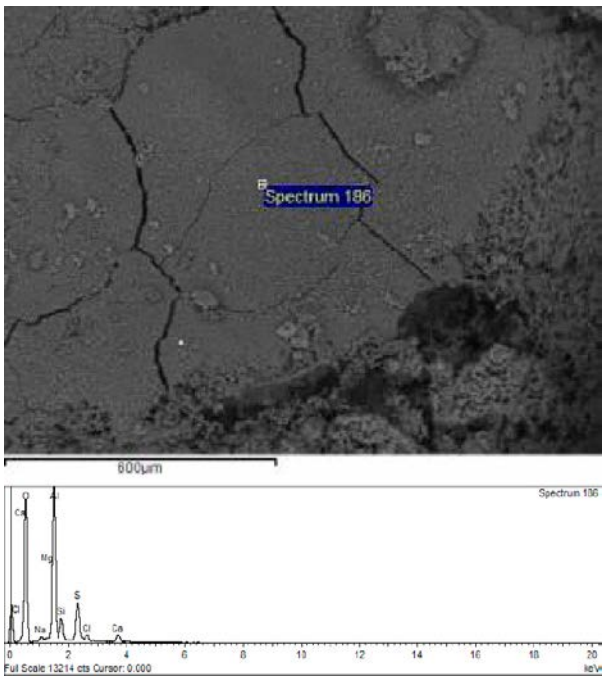

Spectrum 186: Al(S)-rich substance.

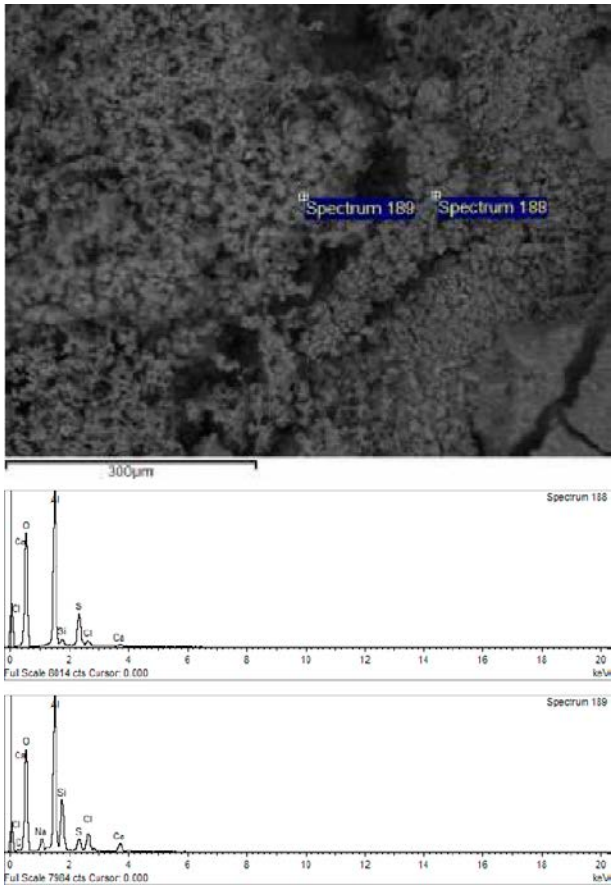

Spectrum 188: Al(S)-rich substance. Spectrum 189: Al(Si)-rich substance.

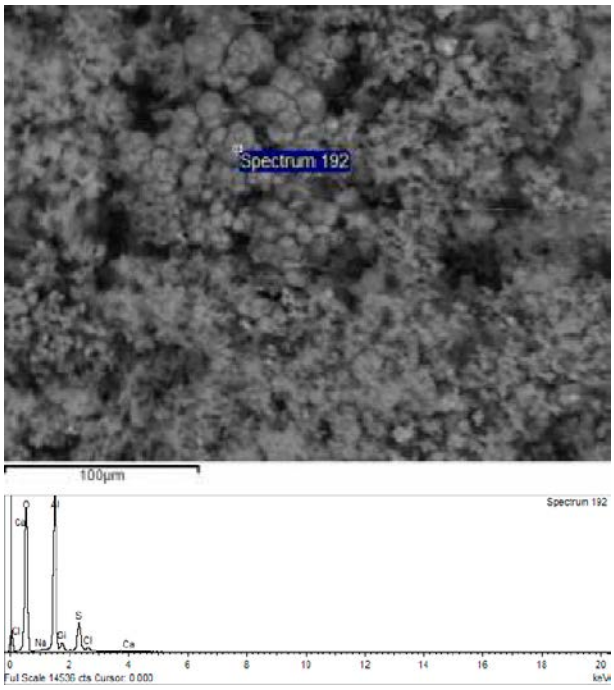

Spectrum 192: Al(S)-rich substance.

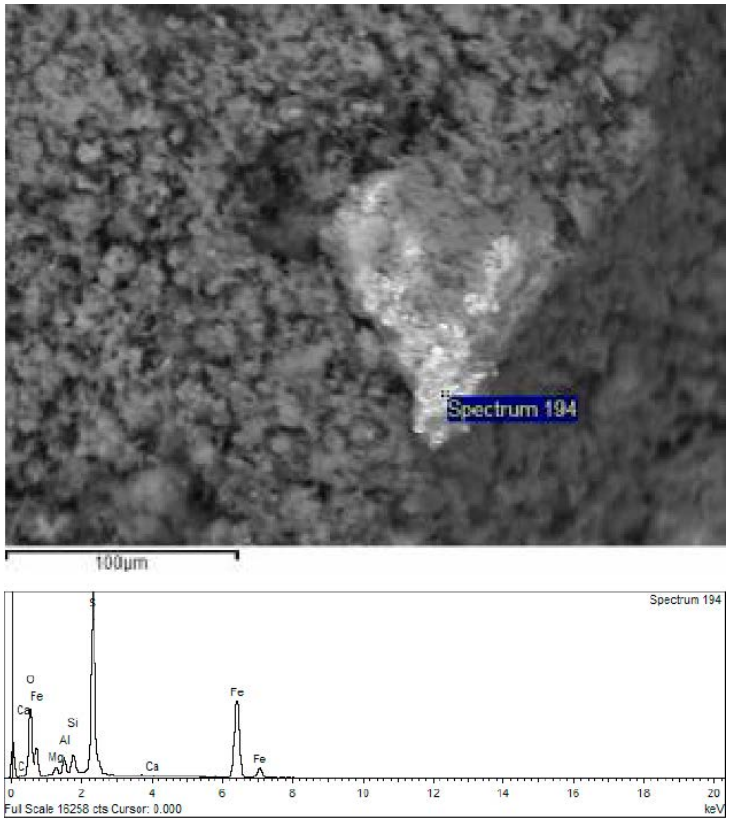

Spectrum 194: FeS.

Sample 22134, KA3105A, 25 m.

Sample is dominated by calcite with scalenohedral habit. Minor minerals are barite (more abundant than pyrite), pyrite (10–30 µm), and some FeS on surfaces of calcite crystals.

Photograph of sample 22134 (sample material was scraped off from the packer connections).

SEM images

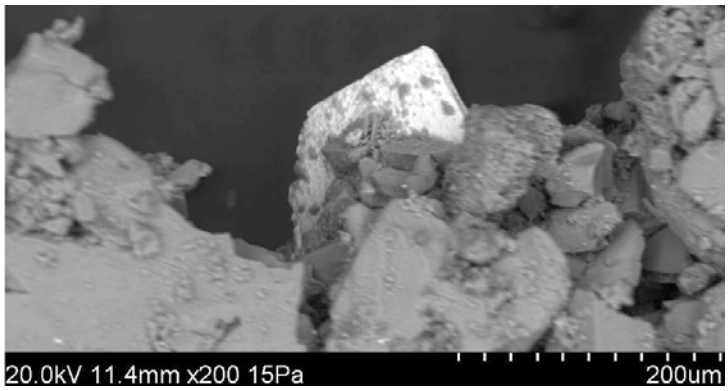

Back-scattered SEM-image of barite (bright) and calcite (the rest).

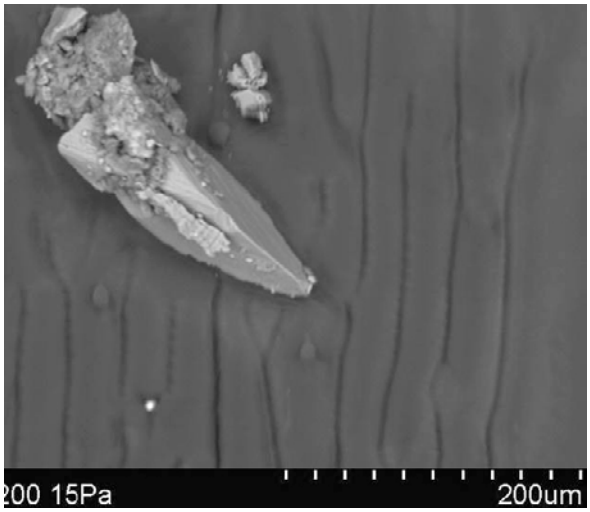

Back-scattered SEM-image of scalenohedral calcite on Cu-tape.

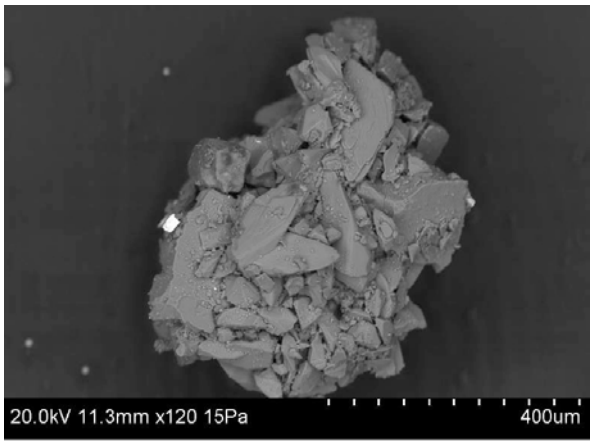

Back-scattered SEM-image of scalenohedral calcite aggregate with a small barite crystal (bright).

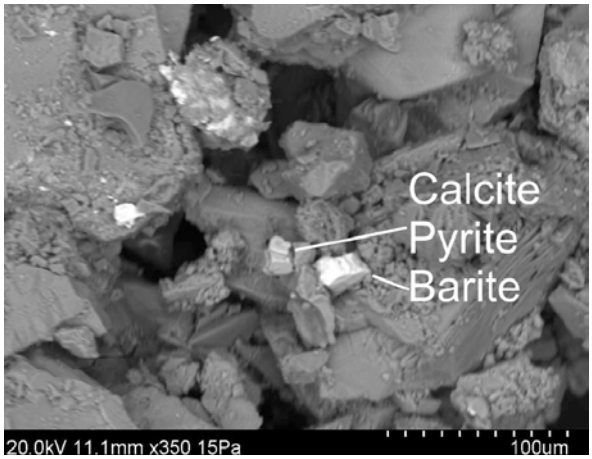

Back-scattered SEM-image of calcite (dominates) and fine-grained pyrite and barite.

EDS analysis locations and related spectra for 22134:

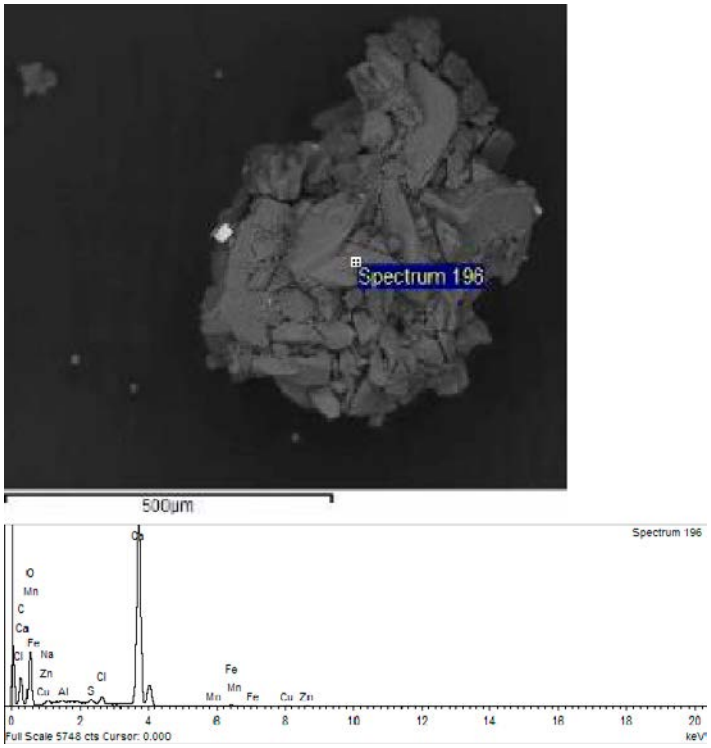

Spectrum 196: Calcite.

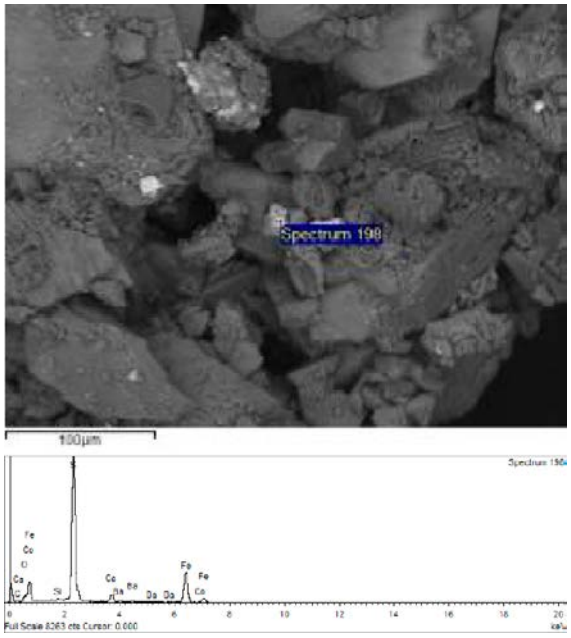

Spectrum 198: Pyrite.

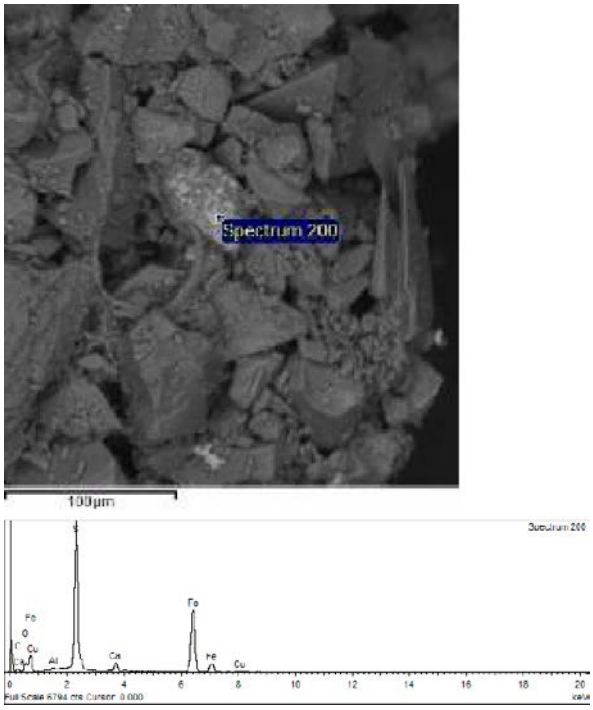

Spectrum 198: FeS.

Sample 22135, KA3105A, 25.2 m.

Sample is dominated by calcite with scalenohedral habit. Minor minerals are pyrite (cubic, up to 150 µm), barite (euhedral, up to 150 µm), FeS (fine-grained), quartz (euhedral), magnetite (up to 200 µm), and an Al-rich substance (dried out crust).

SEM images

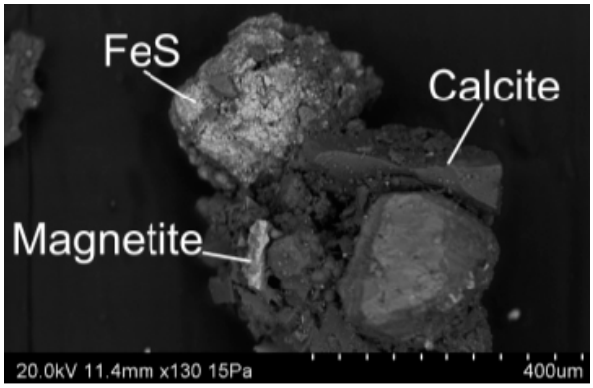

Back-scattered SEM-image of calcite, FeS (fine-grained) and magnetite.

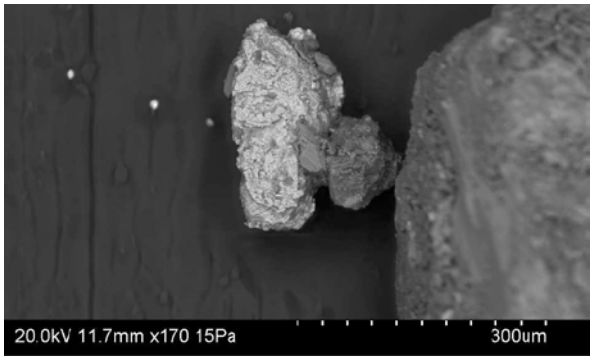

Back-scattered SEM-image of pyrite (bright) and calcite (dark).

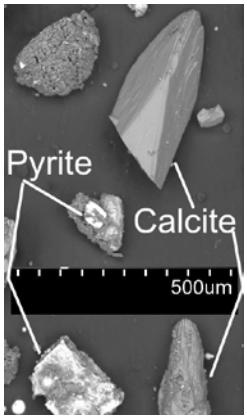

Back-scattered SEM-image of pyrite (bright) and calcite (dark).

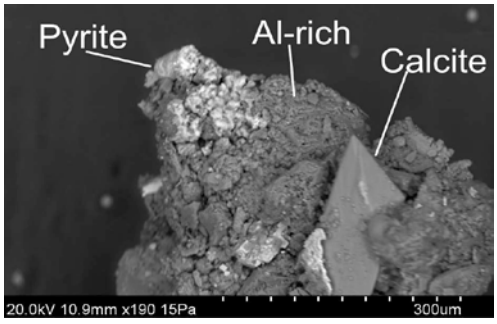

Back-scattered SEM-image of pyrite (bright), calcite and an Al-rich substance.

EDS analysis locations and related spectra for 22135:

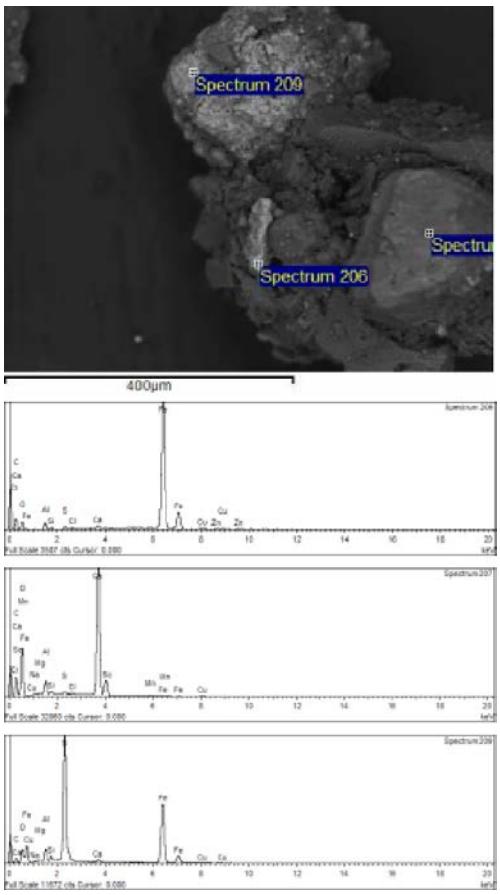

Spectrum 206: Fe-oxide (magnetite), Spectrum 207: Calcite, Spectrum 209: FeS.

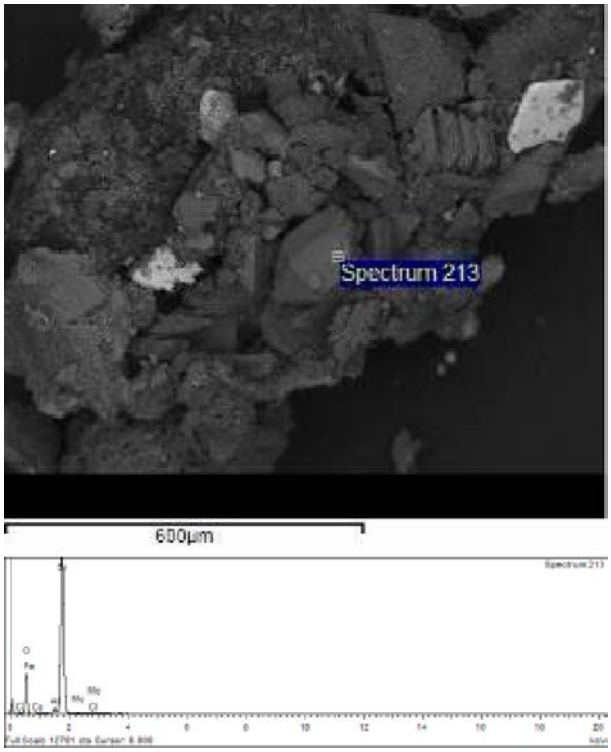

Spectrum 213: Si (quartz).

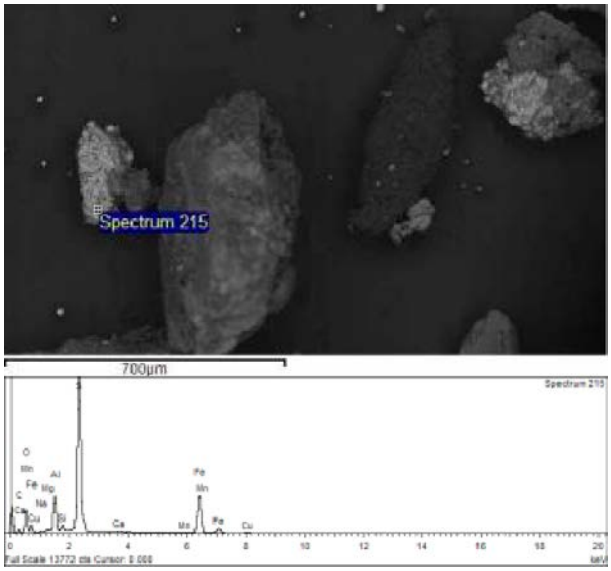

Spectrum 215: Pyrite.

Qualitative EDS analyses. Normalization to 100% total was applied, without calibration (due to the rough surfaces analysed).

Sample/Spectrum	Element	C	Na	Mg	Al	Si	S	Cl	Ca	Mn	Fe	Sr	Ba	K	Zn	F	O	Precipitate
22101_Spectrum1	Atomic%				0.32		16.28	1	16.53								65.9	Gypsum
22101_Spectrum2	Atomic%		0.46	0.43	7.47	0.14	9.39	12.83	14.35								54.8	Gypsum+AlCl
22101_Spectrum3	Atomic%		0.01	0.01	39.74	0.01		0.34	0.12								59.8	Al-rich precipitate
22101_Spectrum6	Atomic%	4.57			0.2		14.23	0.62	14.12								66.3	Gypsum
22101_Spectrum7	Atomic%			0.79	13.98		0.45	37.1	12.28								35.4	Ca-Al-Cl2
22101_Spectrum9	Atomic%		41.85		0.44		0.21	33.55	0.34								23.2	Halite(NaCl)
22101_Spectrum16	Atomic%		1.09	0.43	25.26		0.23	25.05	4.01								43.8	AlCl-precipitate
22102_Spectrum25	Atomic%		0.62		22.15	11.77	0.77	1.09	2.1								61.5	Al2Si-precipitate
22102_Spectrum27	Atomic%		1.34		10.92	11.21	0.37	1.21	2.75		11.56						60.7	FeOOH+AlSi-precip.
22102_Spectrum32	Atomic%	3.52	0.98		13.25	5.74	0.61	2.31	3.95		9.99						59.7	FeOOH+Al(Si)-precip.
22102_Spectrum35	Atomic%		1.72		20.06	11.33	0.76	2.67	2.4		1.11						60	Al2Si-precipitate
22102_Spectrum37	Atomic%	6.49	0.86		3.86	9.06		0.83	2.01		14.9						61.8	FeOOH+Al,Si etc
22102_Spectrum51	Atomic%	3.32	0.44		24.21	5.12	2.33	1.13	1.41								61.9	Al-rich prec.
22102_Spectrum52	Atomic%	12.71			2.68	0.49	0.15	0.16	0.76		20.06						62.4	FeOOH
22102_Spectrum56	Atomic%		0.62		27.61	4.29	3	1.7	1.73								61	Al-rich prec.
22103_Spectrum58	Atomic%		0.97		18.76	14.62	0.66	0.89	2.13								62	AlSi-precipitate
22103_Spectrum61	Atomic%	8.5	0.53		15.7	8.9	0.62	0.94	2.01		0.12						62.7	Al-rich prec.
22103_Spectrum64	Atomic%				0.22	0.16	18.64				9.76						71.2	Pyrite
22104_Spectrum88	Atomic%	16.55	15.7	0.21	0.31		0.75	14.5	3.46								47.9	Biofilm+NaCl
22104_Spectrum93	Atomic%	11.85	0.67		17.83	2.88	1.57	1.67	0.7								62.4	Al-rich prec.+biofilm
22104_Spectrum94	Atomic%	33.18	0.05		0.04		0.03	0.04	0.01								66.6	Biofilm
22104_Spectrum102	Atomic%	11.29	0.19		19.13	2.89	1.72	0.75	0.44								63.2	Al-rich prec.+biofilm
22105_Spectrum104	Atomic%	23.57							14.65								61.8	Calcite
22105_Spectrum119	Atomic%	5.59		0.35		0.28	12.06		1.84			0.77	13.9				65	Barite
22106_Spectrum129	Atomic%		10.39	0.28	13.21	1.74	4.75	12.22	6.56								50.2	Al-rich prec.+NaCl
22106_Spectrum131	Atomic%	4.87	0.84		23.17	3.37	2.54	2.2	1.19								61.1	Al-rich prec.+CaCl2+biofilm
22107_Spectrum216	Atomic%		1.38		24.61	0.7	6.59	4.55	1.53								60.5	Al(+S,CaNaCl)
22107_Spectrum220	Atomic%		0.73		26.38	0.45	6.9	2.83	0.32								62.1	Al(+S,Cl)
22109_Spectrum221	Atomic%	5.41	0.82		20.12	0.91	6.68	1.81	0.48								63.8	Al(+S,Cl)
22109_Spectrum224	Atomic%		0.44		20.41	0.85	9.4	2.61	2.78								63.5	Al(+S,CaCl)
22109_Spectrum228	Atomic%		0.72		24.16	1.01	7.68	2.82	0.97								62.6	Al(+S,Cl,Si)
22110_Spectrum194	Atomic%						18.5		1.07		9.54						70.9	Pyrite(+calcite)
22110_Spectrum196	Atomic%	22.25	0.23			0.11	0.2	0.14	15.72	0.1							61.3	Calcite

Sample/Spectrum	Element	C	Na	Mg	Al	Si	S	Cl	Ca	Mn	Fe	Sr	Ba	K	Zn	F	O	Precipitate
22110_Spectrum209	Atomic%	20.14	3.53			4.43	0.4	1.75	2.25	0.35	2.8						62.6	NaCaCl+Fe+Si+biofilm?
22111_Spectrum 170	Atomic%	0.98	0.13		0.06	0.09	18.58		0.54		8.42						71.2	Pyrite
22111_Spectrum 171	Atomic%								28.18							43.6	28.2	Fluorite
22111_Spectrum 175	Atomic%	10.09			0.29	10.11	1.35	0.43	0.19	0.34	11.7						65.5	FeS
22111_Spectrum 177	Atomic%	7.71	0.13		0.08	0.25			36.93		0.13						54.1	Calcite
22111_Spectrum 179	Atomic%	3.04	0.29	0.12	0.12	0.23		0.07	27.15		0.06					34.2	34.5	Fluorite(+calcite)
22112_Spectrum231	Atomic%	10.31					9.74		2.09			0.72	12.2				64.9	Barite(+calcite)
22112_Spectrum233	Atomic%	11.65	0.18	0.72	1.37	0.96	8.16		1.22	0.06	8.54						66.9	FeS
22112_Spectrum259	Atomic%	4.16	0.42	1.94	0.28	3.24	8.82	0.81	1.3	0.3	13.22						65.4	FeS
22113_Spectrum134	Atomic%	19.06	0.29				0.37	0.17	20		0.14						59.8	Calcite
22113_Spectrum135	Atomic%	15.28		0.22			8.03		1.98		0.11		7.28				66	Barite
22113_Spectrum136	Atomic%	9.75	0.37			0.06	12.89		0.78	0.05	6.61						69.4	Pyrite
22113_Spectrum148	Atomic%	22.71	5.35	0.15	0.13			14.06	3.71		0.13						53.4	Na/CaCl
22113_Spectrum161	Atomic%	4.42	2.2	0.25		0.22	10.23	3.55	2.27		13.31						63.6	FeS
22113_Spectrum162	Atomic%	20.98	0.36	0.15	0.12	0.17	0.56	0.2	15.94		0.44						61.1	Calcite
22113_Spectrum163	Atomic%		0.39		0.08	0.11	18.56		0.64	0.07	9.3						70.9	Pyrite
22113_Spectrum171	Atomic%	14.2	0.15		0.15	12.31	0.15	0.35	9.38	0.09							63.2	Calcite+Si(qz?)
22113_Spectrum172	Atomic%						18.73		0.67		9.51						71.1	Pyrite
22113_Spectrum175	Atomic%	7.81	2.7	0.96	0.53	0.72	6.4	6.94	3.36	0.09	11.07						59.4	FeS+NaCaCl
22113_Spectrum178	Atomic%	2.56	1.28	0.17		0.16	11.05	2.32	1.86		15.67						64.8	FeS
22113_Spectrum182	Atomic%	7.19	4.1	0.52	0.31	0.52	3.18	5.07	10.57	0.08	11.92						56.5	FeS+NaCaCl
22125_Spectrum 52	Atomic%	8.51	0.5		0.42	0.05	10.61	0.28	1.75		10.39						67.4	FeS
22125_Spectrum 53	Atomic%	11.6			0.32		10.01		0.96				10.8				66.1	Barite
22125_Spectrum 56	Atomic%	4.08			0.08		14.31		0.92		11.39						69.2	Pyrite/FeS
22125_Spectrum 57	Atomic%	6.88	0.6		0.15	0.09	11.53	0.3	1.2		11.6						67.7	FeS
22126_Spectrum 65	Atomic%	8.88					9.25		1.93		7.16						65.5	FeS/Pyrite+calcite
22126_Spectrum 69	Atomic%	13.05		0.19			0.19		29.39	0.32	0.11						56.8	Calcite
22126_Spectrum 89	Atomic%	13.48	0.52		0.3	0.9	6.06	0.22	5.97		7.44						64.9	FeS+calcite
22126_Spectrum 94	Atomic%	6.69	0.16		0.05		11.47		2.28		11.65						67.7	FeS(+calcite)
22126_Spectrum 104	Atomic%	5.27	0.17		0.1		11.46		1.38		14.02						67.6	FeS/Pyrite+calcite
22127_Spectrum 40	Atomic%				25.4	1.41	7.28	2.63	0.27								63	Al-S rich encrustation
22127_Spectrum 41	Atomic%	4.09	0.34	1.87	26.36	1.54	3.28	1.34	0.19								61	Al(+S,Cl,Si)
22127_Spectrum 43	Atomic%		0.44		33.67	1.57	1.93	0.76	0.61								60.8	Al-rich precip
22127_Spectrum 44	Atomic%	9.66	1.74		17.3	6.09	0.76	1.79	1.02								61.6	Al(+Si,CaNaCl+S)
22127_Spectrum 46	Atomic%				28.27	2.18	5.13	1.9	0.2								62.3	Al(+S,Cl,Si)

Sample/Spectrum	Element	C	Na	Mg	Al	Si	S	Cl	Ca	Mn	Fe	Sr	Ba	K	Zn	F	O	Precipitate
22127_Spectrum 47	Atomic%	11.76	1.6	0.18	15.67	5.92	0.49	1.32	0.86								62.2	Al(+Si,CaNaCl+biofilm?)
22128_Spectrum 1	Atomic%	13.65	0.69	0.22	1.12	0.37	0.23	0.24	25.32	0.94							57.2	Calcite
22128_Spectrum 10	Atomic%	4.72	0.32			0.08	15.26		0.76	0.25	8.76						69.7	Pyrite
22128_Spectrum 14	Atomic%	4.85					11.79		3.16			0.3	15.5				64.1	Barite(+calcite)
22129_Spectrum 240	Atomic%				26.26	0.46	6.92	5.27									61.1	Al(+S,Cl)
22129_Spectrum 245	Atomic%				26.86	0.63	6.34	5.32									60.7	Al(+S,Cl)
22129_Spectrum 246	Atomic%	7.55	0.1		2.95	0.19	13.15	0.37			6.45						69.2	Pyrite
22129_Spectrum 248	Atomic%		0.4	0.42	9	17.24	1.5	1.44	0.18		6.28			0.29			63	FeAlSi2
22129_Spectrum 249	Atomic%	8.18			19.58	1.02	4.6	4.13									62	Al(+S,Cl)+biofilm?
22130_Spectrum 125	Atomic%	14.87		0.09	0.13	0.2	7.57		4.11	0.06	5.9				0.46		66.6	FeS/Pyrite+calcite
22130_Spectrum 129	Atomic%	13.39				0.23	7.49		5.64	0.13	5.1				2.27		65.6	FeS/Pyrite+calcite
22130_Spectrum 142	Atomic%	9.04		0.15		0.3	8.24		3.78		12.42						66.1	FeS/Pyrite+calcite
22130_Spectrum 149	Atomic%	6.62			0.23	0.17	14.14		1.68		7.64						69.5	Pyrite+calcite
22131_Spectrum 210	Atomic%	7.97	0.84	0.11	1.61	0.46	12.99	0.28	0.23		6.6						68.9	Pyrite
22131_Spectrum 212	Atomic%	7.89	0.37	0.22	2.27	0.53	0.86	0.29	31.35	0.25	0.46						55.5	Calcite
22131_Spectrum 213	Atomic%	6.39	0.85		25.18	1.26	2.4	1.41	0.66		0.21						61.7	Al-rich substance
22131_Spectrum 230	Atomic%	5.24	0.41	0.12	1.9	0.27	12.19	0.25	0.42		11.2						68	FeS
22131_Spectrum 239	Atomic%	4.38	0.19	0.32	1.78	2.18	13.81		0.44		7.44		0.12				69.4	Pyrite
22132_Spectrum 167	Atomic%		2.68	0.31	21.9	11.09	0.58	0.89	2.07								60.5	Al(Si)-rich precip
22132_Spectrum 169	Atomic%	22.9		0.18	0.39	0.11	0.17		14.33	0.16							61.8	Calcite
22132_Spectrum 174	Atomic%	3.71	0.51		0.52	0.2	16.04		0.21	0.13	8.54						70.1	Pyrite
22132_Spectrum 206	Atomic%	9.31			0.09		12.1		1.29		8.36						68.9	FeS/Pyrite+calcite
22132_Spectrum 207	Atomic%	4.16	0.13				16.01		0.64		8.79						70.3	Pyrite
22133_Spectrum 186	Atomic%		0.91	0.27	22.98	3.94	6.35	1.05	1.18								63.3	Al(S)-rich substance
22133_Spectrum 188	Atomic%		0.29		27.19	1.57	6.25	1.17	0.37								63.2	Al(S)-rich substance
22133_Spectrum 189	Atomic%		3.46	0.27	22.27	8.83	1.94	1.84	1.26								60.1	Al(Si)-rich substance
22133_Spectrum 192	Atomic%		0.45		27.98	1.7	5.62	0.73	0.14								63.2	Al(S)-rich substance
22133_Spectrum 194	Atomic%	4.04	0.22	0.87	1.44	1.29	12.27		0.08		11.63						68.2	FeS
22134_Spectrum 196	Atomic%	22.82	0.54	0.12	0.15		0.23	0.38	13.76	0.12	0.21				0.15		61.4	Calcite
22134_Spectrum 198	Atomic%	5.53	0.3		0.09	0.14	15.35		0.88		7.59		0.09				70	Pyrite
22134_Spectrum 200	Atomic%	9.25			0.16		10.88		0.65		10.8						68.3	FeS
22135_Spectrum 206	Atomic%	16.48			0.55	0.11	0.13	0.07	0.21		19.03				0.08		63.3	Magnetite
22135_Spectrum 207	Atomic%	21.88	0.31	0.17	1.42	0.18	0.21	0.13	13.9	0.16	0.14						61.5	Calcite
22135_Spectrum 209	Atomic%	12.56	0.24	0.26	1.25	0.36	8.44		0.21		9.23						67.5	FeS
22135_Spectrum 213	Atomic%	4.51	0.18	0.13	1	27.59		0.08	0.09		0.16						66.3	Si(qz)
22135_Spectrum 215	Atomic%	10.36	0.21	0.25	3.3	0.37	10.78		0.13	0.06	6.1						68.4	Pyrite

Appendix I

Observations of corrosion on borehole equipment

Corrosion KA3385A

The borehole consisted of three areas, see below Figure I-1. The hole had no casing of stainless steel.

Both area 1 and 2 were anaerobic areas and the borehole was completely filled with water. Area 3 is aerobic as there was no sealing of the borehole towards the tunnel. The part that had been examined consisted of 18 rods, where the following observations were made:

Rod 1

- The first joint had a heavy corrosion on the aluminum (approximately 1 cm outside rock wall).
- Light brown deposits on the rod.
- Local pitting (adhering corrosion products).
- Joint to bar two little crevice corrosion (adhering corrosion products).
- Weak discoloration of polyamide tube.

Rod 2

- Severe corrosion under the PVC-tape (polyvinylchloride tape). Voluminous corrosion products, possibly al-oxide (white) and al-hydroxide (transparent).
- Local pitting (adhering corrosion products).
- No attack in the joint.
- Weak discoloration of the polyamide tubes.
- PH-value under tape was about 5 and about 7 on the outside.

Rod 3

- Severe corrosion under the PVC-tape. Voluminous corrosion products.
- Local pitting (adhering corrosion products).
- No attack in the joint.
- The glue on the tape dissolved, PVC-tape very brittle (valid for all tape samples).

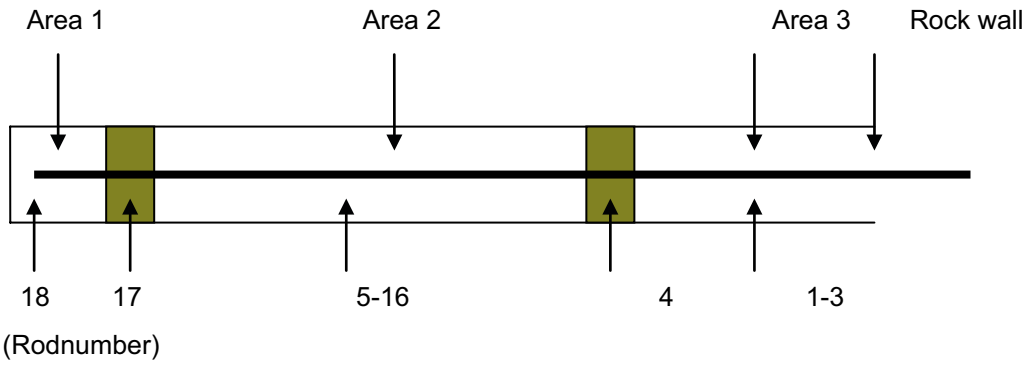

Figure I-1. *Schematic illustration of borehole KA3385A.*

Rod 4 (packer connection)

- The stainless steel surfaces (before packer connection) had calcite precipitations. No galvanic corrosion on al-rod due to contact with stainless steel (for both sides of packer connection).
- The metal surfaces after the packer connection (rod 5 and onwards) was slimy in contrast to the surfaces before the packer connection (biofilm?)
- Black deposits on the rod (FeS?).

Rod 5–7

- Severe corrosion under the PVC-tape.
- Black deposits on the rods but no pitting with adhering corrosion products.
- No crevice corrosion or galvanic corrosion in the joints between rods.

Rod 8

- Severe corrosion under the PVC-tape.
- Black deposits.
- A few pits on rods with adhering corrosion products.
- No crevice corrosion and galvanic corrosion in the joint.
- Maybe small attack on polyamide tube.

Rod 9

- Severe corrosion under the PVC-tape.
- Black deposits on the rods but no pitting with adhering corrosion products.
- No crevice corrosion and galvanic corrosion in the joint, even though the joint is not drawn in the bottom. There is a gap between the rods of 5 mm, where the stainless steel pin is exposed. Despite this, no galvanic corrosion.

Rod 10

- Black deposits on the rods but no pitting with adhering corrosion products.
- No crevice corrosion or galvanic corrosion in the joint.

Rod 11–15

- Severe corrosion under the PVC-tape.
- Black deposits.
- A few pits with adhering corrosion products.
- No crevice corrosion or galvanic corrosion in the joint.

Rod 16

- Severe corrosion under the PVC-tape.
- Very little deposits on aluminum surfaces.
- A few pits with adhering corrosion products.
- No crevice corrosion or galvanic corrosion in the joint.
- Heavy calcite precipitations on stainless steel pipe.

Rod 17 (packer connection)

- Heavy calcite precipitations and sulphide deposits on stainless steel pipe.

Rod 18

- Severe corrosion under the PVC-tape.
- Black deposits and local pitting on aluminum surfaces.
- No visible galvanic corrosion of aluminum near the stainless steel tubes. (The aluminum rods and the stainless steel tubes have good contact).

The observations made can be summarized as the following:

Outside the rock wall

Severe attack on joint located approximately 1 cm outside the rock wall.

Area 3

- Severe corrosion under the PVC-tape.
- Local pitting the on freely exposed aluminum surfaces.
- No crevice corrosion in the joints between the rods.
- No galvanic corrosion of the rod near the stainless steel tubes.
- No black (sulphide) deposits.

Area 2

- Severe corrosion under the PVC-tape.
- Black deposits but no or only a few local pits on freely exposed surfaces (bars 5–11).
- Very little black deposits and occasional pitting at freely exposed surfaces (bars 12–16).
- No crevice corrosion in the joints between the rods.
- No galvanic corrosion of the rod near the stainless steel tubes.
- Calcite precipitations on stainless steel pipes.

Area 1

- Severe corrosion under the PVC-tape.
- Black deposits and local pitting on the free surfaces.
- No galvanic corrosion of the rod near the stainless steel tubes.
- Some galvanic corrosion on the end of the rod having a freely exposed stainless pin.
- Calcite precipitations on stainless steel pipes.

The polymeric materials were consistently affected in a similar way independent in which area they had been exposed. PUR rubber in packer connections and polyamide in tubes were virtually unaffected. The PVC tape had become brittle and the glue been dissolved. Furthermore, the PVC-tape had also decreased in volume, which is most likely an indication of a loss in plasticizer. There were no visible indications (such as a change in color) that the PVC itself had been degraded.

Corrosion KA3105A

The borehole KA3105A consisted of six areas, 5 anaerobic and one external, probably partly aerobic (0–6 m in from the tunnel). The first part of the bore hole (0–2 m) had a casing of stainless steel.

A detailed documentation of each rod was not performed. Below is a more comprehensive description of the observations made.

Outer part (0–6 m)

The part of the rod having been situated inside the casing (first 2 m) was very strongly attacked by corrosion. No precipitations of sulphide on these first 2 m.

At the end of the casing both aluminum rod and polyamide tubes were covered with large amounts of sulphide precipitations (Figure I-2). In the distance 2–6 m there was heavy corrosion under the PVC-tape but no corrosion on freely exposed aluminum surfaces.

Section 5 (7–16 m)

Corrosion under the PVC-tape. No visible corrosion on freely exposed aluminum surfaces. Black sulphide deposits. Precipitation of calcite on stainless steel tubes at packer connection.

Section 4 / Blind section / Section 3 / Section 2

The same appearance as in section 5. One of the polyamide tubes had a slight dark discoloration, which most likely is explained as a quality defect from its production.

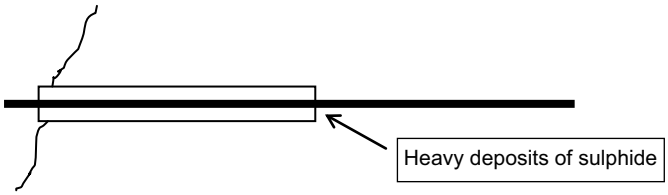

Figure I-2. *Casing and rod in borehole KA3105A.*

Appendix J

Investigation of equipment: precipitates, microbiology and hydrochemical data

Minerals – stable isotopes

Stable isotopes

Calcite

$\delta^{13}C$ and $\delta^{18}O$ analysis of calcite ($\delta^{13}C \pm 0.1‰$ and $\delta^{18}O \pm 0.2‰$ at 2σ, NBS-18 calibrated) were carried out at the Institute for Energy Technology (IFE), Norway. About 100 µg sample was transferred to a 10 ml vacutainer, put in a temperature controlled Al block and flushed with Helium (He) for 5 minutes. 0.1 ml 100% H_3PO_4 was added. The reaction was controlled at 30.0°C for 2 hours. The CO_2 gas produced was then flushed out with Helium flow on to a Poraplot Q GC column and analysed on a Finnigan MAT DeltaXP isotope ratio mass spectrometer.

Pyrite

SIMS-analyses of pyrite were carried out at Nordsim, at the Swedish Museum of Natural History, Stockholm. One to five crystals were analysed from each fracture coating and one to three analyses were made for each crystal, in transects. Microscale sulphur isotope ratio measurements were carried out using a Cameca IMS1280 ion microprobe. Analytical settings are described briefly below, and roughly follow those described in detail in Whitehouse et al. (2005). Sulphur was ionized by a $^{133}Cs^+$ primary beam with 20 kV incident energy (10 kV primary, –10 kV secondary) and a primary beam current of ~1.5 nA, producing ions from an elliptical area of ~10 µm. A normal incidence electron gun was used for charge compensation. Secondary ion signals for ^{32}S and ^{34}S were detected simultaneously by three Faraday detectors. Pyrite isotope standards were mounted together on the sample mounts and analyzed at regular intervals during the automated sample runs. Pyrite standards were Ruttan and Balmat pyrites (Crowe and Vaughan 1996), of which the Ruttan pyrite with a $\delta^{34}S$ value of 1.2‰ (measured at: 1.2 ± 0.1‰) was used for normalizing the results from unknowns. Typical precision on a single $\delta^{34}S$ value, after propagating the within run and external uncertainties from the standard measurements was ± 0.3–0.4‰. All results are reported with respect to the CDT standard (Canyon Diablo Troilite).

Minerals – SIMS analyses.

Idcode	Sampling date	Secup m	Seclow m	Section no.	SKB no.	Sample type	Mineral name	$\delta^{13}C$ V-PDB	$\delta^{18}O$ V-PDB	$\delta^{34}S$ CDT	Comment
KA3385A	2012-02-01	30.00	30.00	2	22110	Mineral – coating	Calcite	–13.92	–11.15		Grown on equipment in borehole
KA3385A	2012-02-01	30.00	30.00	2	22110	Mineral – coating	Pyrite			–2.8	Crystal1
KA3385A	2012-02-01	30.00	30.00	2	22110	Mineral – coating	Pyrite			–13.5	Crystal1
KA3385A	2012-02-01	30.00	30.00	2	22110	Mineral – coating	Pyrite			–13.7	Crystal1
KA3385A	2012-02-01	30.00	30.00	2	22110	Mineral – coating	Pyrite			28.1	Crystal2
KA3385A	2012-02-01	30.00	30.00	2	22110	Mineral – coating	Pyrite			27.9	Crystal2
KA3385A	2012-02-01	30.00	30.00	2	22110	Mineral – coating	Pyrite			28.3	Crystal2
KA3385A	2012-02-01	30.00	30.00	2	22110	Mineral – coating	Pyrite			33.8	Crystal3
KA3385A	2012-02-01	30.00	30.00	2	22110	Mineral – coating	Pyrite			–35.7	Crystal4
KA3385A	2012-02-01	30.00	30.00	2	22110	Mineral – coating	Pyrite			–34.9	Crystal4
KA3385A	2012-02-01	31.50	31.50	1	22111	Mineral – coating	Calcite	–22.94	–8.89		Grown on equipment in borehole
KA3385A	2012-02-01	31.50	31.50	1	22113	Mineral – coating	Calcite	–16.80	–10.47		Grown on equipment in borehole
KA3385A	2012-02-01	31.50	31.50	1	22111	Mineral – coating	Pyrite			–6.2	Crystal1
KA3385A	2012-02-01	31.50	31.50	1	22111	Mineral – coating	Pyrite			–3.2	Crystal1
KA3385A	2012-02-01	31.50	31.50	1	22111	Mineral – coating	Pyrite			20.1	Crystal2
KA3385A	2012-02-01	31.50	31.50	1	22111	Mineral – coating	Pyrite			28.2	Crystal2
KA3385A	2012-02-01	31.50	31.50	1	22111	Mineral – coating	Pyrite			29.2	Crystal2
KA3385A	2012-02-01	31.50	31.50	1	22111	Mineral – coating	Pyrite			–14.5	Crystal3
KA3385A	2012-02-01	31.50	31.50	1	22111	Mineral – coating	Pyrite			–16.4	Crystal3
KA3385A	2012-02-01	31.50	31.50	1	22111	Mineral – coating	Pyrite			–17.6	Crystal3
KA3385A	2012-02-01	31.50	31.50	1	22111	Mineral – coating	Pyrite			16.5	Crystal4
KA3385A	2012-02-01	31.50	31.50	1	22111	Mineral – coating	Pyrite			23.5	Crystal5
KA3385A	2012-02-01	31.50	31.50	1	22111	Mineral – coating	Pyrite			33.1	Crystal5
KA3385A	2012-02-01	31.50	31.50	1	22113	Mineral – coating	Pyrite			–9.5	Crystal1
KA3385A	2012-02-01	31.50	31.50	1	22113	Mineral – coating	Pyrite			–15.1	Crystal1
KA3385A	2012-02-01	31.50	31.50	1	22113	Mineral – coating	Pyrite			25.5	Crystal2
KA3385A	2012-02-01	31.50	31.50	1	22113	Mineral – coating	Pyrite			28.8	Crystal2
KA3385A	2012-02-01	31.50	31.50	1	22113	Mineral – coating	Pyrite			15.2	Crystal3
KA3385A	2012-02-01	31.50	32.30	1	22112	Mineral – coating	Calcite	–12.31	–10.57		Grown on equipment in borehole

Idcode	Sampling date	Secup m	Seclow m	Section no.	SKB no.	Sample type	Mineral name	$\delta^{13}C$ V-PDB	$\delta^{18}O$ V-PDB	$\delta^{34}S$ CDT	Comment
KA3105A	2012-02-07	17.00	17.00	4	22125	Mineral – coating	Calcite	–14.99	–9.83		Grown on equipment in borehole
KA3105A	2012-02-07	17.00	17.00	4	22125	Mineral – coating	Pyrite			9.9	Crystal1
KA3105A	2012-02-07	17.00	17.00	4	22125	Mineral – coating	Pyrite			10.7	Crystal2
KA3105A	2012-02-07	17.00	17.00	4	22125	Mineral – coating	Pyrite			5.5	Crystal3
KA3105A	2012-02-07	19.50	19.50	4	22126	Mineral – coating	Calcite	–12.68	–7.73		Grown on equipment in borehole
KA3105A	2012-02-07	22.50	22.50	3	22130	Mineral – coating	Calcite	–12.87	–7.86		Grown on equipment in borehole
KA3105A	2012-02-07	22.50	22.50	3	22130	Mineral – coating	Pyrite			13.1	Crystal1
KA3105A	2012-02-07	22.50	22.50	3	22130	Mineral – coating	Pyrite			8.2	Crystal1
KA3105A	2012-02-07	22.50	24.50	3	22131	Mineral – coating	Pyrite			6.2	Crystal1
KA3105A	2012-02-07	22.50	24.50	3	22131	Mineral – coating	Pyrite			4.1	Crystal2
KA3105A	2012-02-07	22.50	24.50	3	22131	Mineral – coating	Pyrite			2.9	Crystal2
KA3105A	2012-02-07	22.50	24.50	3	22131	Mineral – coating	Pyrite			–23.6	Crystal2
KA3105A	2012-02-07	24.50	24.50	3	22132	Mineral – coating	Calcite	–13.05	–7.70		Grown on equipment in borehole
KA3105A	2012-02-07	25.00	25.00	3	22134	Mineral – coating	Calcite	–16.15	–11.50		Grown on equipment in borehole
KA3105A	2012-02-07	25.00	25.00	3	22134	Mineral – coating	Pyrite			9.9	Crystal1
KA3105A	2012-02-07	25.00	25.00	3	22134	Mineral – coating	Pyrite			12.0	Crystal2
KA3105A	2012-02-07	25.20	25.20	3	22135	Mineral – coating	Calcite	–14.27	–8.59		Grown on equipment in borehole
KA3105A	2012-02-07	25.20	25.20	3	22135	Mineral – coating	Pyrite			–14.4	Crystal1
KA3105A	2012-02-07	25.20	25.20	3	22135	Mineral – coating	Pyrite			–23.1	Crystal1
KA3105A	2012-02-07	25.20	25.20	3	22135	Mineral – coating	Pyrite			12.5	Crystal2
KA3105A	2012-02-07	25.20	25.20	3	22135	Mineral – coating	Pyrite			–12.9	Crystal2
KA3105A	2012-02-07	25.20	25.20	3	22135	Mineral – coating	Pyrite			–40.8	Crystal2
KA3105A	2012-02-07	25.20	25.20	3	22135	Mineral – coating	Pyrite			33.3	Crystal3
KA3105A	2012-02-07	25.20	25.20	3	22135	Mineral – coating	Pyrite			27.9	Crystal3

Minerals – chemical analysis of “white precipitate” on tape

Two samples of white precipitates at the tape were analysed for major and trace elements using ICP-SFMS. The chemical analyses were carried out at ALS, Luleå, Sweden, accordingly. The samples were dried at 105°C. 0.1 g of the sample was melted by 0.375 g $LiBO_2$ and dissolved in HNO_3. Loss on ignition (LOI) was performed at 1,000°C. The analyses were carried out according to EPA methods 200.7 and 200.8 (modified). Sulphur was not analysed due to the small sample volumes. Results are listed below.

Minerals – table of chemical analysis of “white precipitate”.

Idcode	Sampling date	Secup	Seclow	Section	SKB no.	Sampling place	Al_2O_3	Cao	Fe_2O_3	MgO	MnO	Na_2O	P_2O_5	SiO_2	TiO_2	Ba	Be	Co	Cr	Ga	Hf
KA3385A	2012-02-01	18.65	18.65	2	22107	Beneath tape	49.90	0.75	–0.1	0.05	–0.0030	0.8230	0.014	1.60	0.011	15.40	–0.50	–5.0	17.4	7.2	0.44
KA3385A	2012-02-07	18.20	18.20	4	22127	Beside tape	50.70	0.86	–0.1	0.06	0.0045	0.3300	0.013	5.34	0.002	10.40	0.71	–6.0	–10.0	17.3	0.15
Idcode	**Sampling date**	**Secup**	**Seclow**	**Section**	**SKB no.**	**Sampling place**	**Mo**	**Nb**	**Ni**	**Rb**	**Sc**	**Sr**	**Ta**	**Th**	**U**	**V**	**W**	**Y**	**Zr**	**La**	**Ce**
KA3385A	2012-02-01	18.65	18.65	2	22107	Beneath tape	–5.0	–5.00	–10	7.99	–1.0	98.0	–0.07	–0.10	0.33	13.9	–50	–2.00	13.1	1.6	6.5
KA3385A	2012-02-07	18.20	18.20	4	22127	Beside tape	–6.0	–6.00	10	4.85	–1.0	217.0	–0.08	0.18	3.95	14.7	–60	–2.00	12.0	2.7	8.5
Idcode	**Sampling date**	**Secup**	**Seclow**	**Section**	**SKB no.**	**Sampling place**	**Pr**	**Nd**	**Sm**	**Eu**	**Gd**	**Tb**	**Dy**	**Ho**	**Er**	**Tm**	**Yb**	**Lu**	**TS**		
KA3385A	2012-02-01	18.65	18.65	2	22107	Beneath tape	–1.00	0.5	–0.4	–0.05	–0.4	–0.1	–0.10	–0.08	–0.1	–0.1	–0.3	–0.04	37.8		
KA3385A	2012-02-07	18.20	18.20	4	22127	Beside tape	–2.00	1.1	–0.5	–0.06	–0.5	–0.1	0.15	–0.09	–0.2	–0.2	–0.3	–0.05	57.1		

Minerals – Qualitative SEM observations.

Idcode	Sampling date	Secup m	Seclow m	Section no.	SKB no.	Sampling place	Sample type	Barite	Calcite	Chalcopyrite	Flourite	Goethite
KA3385A	2012-02-01	0.00	0.00	Outside	22101	Pipe string	Mineral – coating					
KA3385A	2012-02-01	0.40	0.40	Outside	22102	Pipe string	Mineral – coating		*			*
KA3385A	2012-02-01	4.20	4.20	Outside	22103	Pipe string/tape	Mineral – coating					
KA3385A	2012-02-01	7.20	7.20	2	22104	Tape	Mineral – coating					
KA3385A	2012-02-01	7.50	7.50	2	22105	Packer	Mineral – coating	*	***			
KA3385A	2012-02-01	9.65	9.65	2	22106	Tape	Mineral – coating					
KA3385A	2012-02-01	18.65	18.65	2	22107	Tape	Mineral – coating					
KA3385A	2012-02-01	30.00	30.00	2	22110	Packer	Mineral – coating	*	***			
KA3385A	2012-02-01	31.50	31.50	1	22111	Packer	Mineral – coating	*	***		*	
KA3385A	2012-02-01	31.50	32.30	1	22112	Pipe string	Mineral – coating	*	***			
KA3385A	2012-02-01	32.30	32.30	1	22109	Tape	Mineral – coating	*				
KA3105A	2012-02-07	3.00	4.00	Outside	22128	Pipe string	Mineral – coating	*	***			
KA3105A	2012-02-07	17.00	17.00	4	22125	Packer	Mineral – coating	*	***			
KA3105A	2012-02-07	18.20	18.20	4	22127	Tape	Mineral – coating					
KA3105A	2012-02-07	19.50	19.50	4	22126	Packer	Mineral – coating	*	***	*		
KA3105A	2012-02-07	22.50	22.50	3	22130	Packer	Mineral – coating		***			
KA3105A	2012-02-07	22.50	24.50	3	22131	Pipe stringt	Mineral – coating	*	***	*		
KA3105A	2012-02-07	23.20	23.20	3	22133	Tape	Mineral – coating					
KA3105A	2012-02-07	24.50	24.50	3	22132	Packer	Mineral – coating		***			
KA3105A	2012-02-07	25.00	25.00	3	22134	Packer	Mineral – coating	*	***			
KA3105A	2012-02-07	25.20	25.20	3	22135	Pipe string	Mineral – coating	*	***			

Minerals – Qualitative SEM observations, continued.

Idcode	Sampling date	Secup m	Seclow m	Section no.	SKB no.	Sampling place	Sample type	Gypsum	Magnetite	Pyrite	Quartz	Comment (other phases)
KA3385A	2012-02-01	0.00	0.00	Outside	22101	Pipe string	Mineral – coating	***				NaClAl(Cl-S)-rich precipitates
KA3385A	2012-02-01	0.40	0.40	Outside	22102	Pipe string	Mineral – coating					Al-rich precipitate(+Si,S,Cl,Ca)
KA3385A	2012-02-01	4.20	4.20	Outside	22103	Pipe string/tape	Mineral – coating			*		Al-rich precipitate (+Si,S,Cl,Ca)
KA3385A	2012-02-01	7.20	7.20	2	22104	Tape	Mineral – coating					Biofilm,CaCl2-NaCl,Al
KA3385A	2012-02-01	7.50	7.50	2	22105	Packer	Mineral – coating					
KA3385A	2012-02-01	9.65	9.65	2	22106	Tape	Mineral – coating					Al+SiSClCa,NaCaCl, biofilm
KA3385A	2012-02-01	18.65	18.65	2	22107	Tape	Mineral – coating					Al(+S,Si,Ca,Cl)-rich precipitate
KA3385A	2012-02-01	30.00	30.00	2	22110	Packer	Mineral – coating			*		Si+Mg-Cl(Fe-Na)-coating
KA3385A	2012-02-01	31.50	31.50	1	22111	Packer	Mineral – coating			*		FeS
KA3385A	2012-02-01	31.50	32.30	1	22112	Pipe string	Mineral – coating			*		FeS,Si-,Cl-rich precipitate
KA3385A	2012-02-01	32.30	32.30	1	22109	Tape	Mineral – coating					Al-S-rich(white,soft),CaCl2
KA3105A	2012-02-07	3.00	4.00	Outside	22128	Pipe string	Mineral – coating			*		
KA3105A	2012-02-07	17.00	17.00	4	22125	Packer	Mineral – coating			*		FeS
KA3105A	2012-02-07	18.20	18.20	4	22127	Tape	Mineral – coating					Al-rich(+Si,S,Cl,Ca,Na)
KA3105A	2012-02-07	19.50	19.50	4	22126	Packer	Mineral – coating					FeS
KA3105A	2012-02-07	22.50	22.50	3	22130	Packer	Mineral – coating			*	*	FeS
KA3105A	2012-02-07	22.50	24.50	3	22131	Pipe stringt	Mineral – coating			*	*	FeS,Al,wall rock fragments
KA3105A	2012-02-07	23.20	23.20	3	22133	Tape	Mineral – coating					Al(+S,Si),NaCaCl,FeS
KA3105A	2012-02-07	24.50	24.50	3	22132	Packer	Mineral – coating			*		FeS,Al-rich substance
KA3105A	2012-02-07	25.00	25.00	3	22134	Packer	Mineral – coating			*		FeS
KA3105A	2012-02-07	25.20	25.20	3	22135	Pipe string	Mineral – coating		*	*	*	FeS,Al-rich crust

Microbiology.

Idcode	Sampling date	Secup	Seclow	SKB no.	Sampling place	Sampler	SRB_from surface	SRB_surface_ (lower limit)	SRB_surface_ (upper limit)	Total number of cells (TNC)_surface	SD_TNC_surface
KA3385A	2012-02-01 00:00	32.05	34.18	22091	Packer-rubber	Cotton swab	777.78	1111.11	6444.44	350,000	180,000
KA3385A	2012-02-01 00:00	32.05	34.18	22092	Pipe string-Al	Cotton swab	1,222.22	222.22	1,888.89	150,000	83,000
KA3385A	2012-02-01 00:00	32.05	34.18	22093	Tubing	Cotton swab	88.89	333.33	2,777.78	57,000	29,000
KA3385A	2012-02-01 00:00	32.05	34.18	22094	Precipitation, tape	Spoon	n.a.	n.a.	n.a.	n.a.	n.a.
KA3385A	2012-02-01 00:00	32.05	34.18	22095	Packer-stainless steel	Cotton swab	0.26	0.10	0.96	61,000	44,000
KA3105A	2012-02-07 00:00	17.01	19.51	22096	Pipe string-Al	Cotton swab	2,444.44	333.33	2,333.33	440,000	270,000
KA3105A	2012-02-07 00:00	17.01	19.51	22097	Precipitation, tape	Spoon	n.a.	n.a.	n.a.	n.a.	n.a.
KA3105A	2012-02-07 00:00	17.01	19.51	22098	Tubing	Cotton swab	888.89	33.33	277.78	220,000	17,000
KA3105A	2012-02-07 00:00	17.01	19.51	22099	Packer-rubber	Cotton swab	55.56	22.22	188.89	64,000	46,000
KA3105A	2012-02-07 00:00	17.01	19.51	22100	Stainless steel	Cotton swab	0.26	0.10	0.96	59,000	31,000

Idcode	Sampling date	Secup	Seclow	SKB no.	Sampling place	Sampler	SRB_volume	SRB_volume_ (lower limit)	SRB_volume_ (upper limit)	Total number of cells (TNC)_volume	SD_TNC_volume
KA3385A	2012-02-01 00:00	32.05	34.18	22091	Packer-rubber	Cotton swab	n.a.	n.a.	n.a.	n.a.	n.a.
KA3385A	2012-02-01 00:00	32.05	34.18	22092	Pipe string-Al	Cotton swab	n.a.	n.a.	n.a.	n.a.	n.a.
KA3385A	2012-02-01 00:00	32.05	34.18	22093	Tubing	Cotton swab	n.a.	n.a.	n.a.	n.a.	n.a.
KA3385A	2012-02-01 00:00	32.05	34.18	22094	Precipitation, tape	Spoon	55	22	188	*	
KA3385A	2012-02-01 00:00	32.05	34.18	22095	Packer-stainless steel	Cotton swab	n.a.	n.a.	n.a.	n.a.	n.a.
KA3105A	2012-02-07 00:00	17.01	19.51	22096	Pipe string-Al	Cotton swab	n.a.	n.a.	n.a.	n.a.	n.a.
KA3105A	2012-02-07 00:00	17.01	19.51	22097	Precipitation, tape	Spoon	555	444	3,333	*	
KA3105A	2012-02-07 00:00	17.01	19.51	22098	Tubing	Cotton swab	n.a.	n.a.	n.a.	n.a.	n.a.
KA3105A	2012-02-07 00:00	17.01	19.51	22099	Packer-rubber	Cotton swab	n.a.	n.a.	n.a.	n.a.	n.a.
KA3105A	2012-02-07 00:00	17.01	19.51	22100	Stainless steel	Cotton swab	n.a.	n.a.	n.a.	n.a.	n.a.

***** No tnc value because of precipitates.

Water data – isotopes.

Idcode	Sampling date	Secup m	Seclow m	SKB no.	Water type	pmC	$\delta^{13}C$ V-PDB	$\delta^{34}S_{SO4}$ V-CDT	$\delta^{34}S_{HS}$ V-CDT	δD V-SMOW	TR TU	$\delta^{18}O_4$ V-SMOW
KA3105A	2012-02-06	25.51	52.01	22089	Section	59.10	–15.70	22.7	–7.3	–73.9	n.a.	–10
KA3105A	2012-02-06	22.51	24.51	22090	Section	70.60	–15.20	26.5	–14.5	–70.4	n.a.	–9.4
KA3105A	2012-02-06	17.01	19.51	22124	Section	77.10	–14.70	27.6	–16.2	–69.1	7.20	–9.20
KA3105A	2012-02-14	25.51	52.01	22147	Fracture	66.70	–15.30	23.9	–19.9	–77.3	5.60	–10.10
KA3105A	2012-02-14	22.51	24.51	22148	Fracture	78.50	–14.60	28.3	–20.9	–68.4	7.90	–9.00
KA3105A	2012-02-14	17.01	19.51	22149	Fracture	78.30	–14.50	28.3	–21.9	–70.3	8.70	–8.90
KA3385A	2012-02-14	32.05	34.18	22153	Fracture	47.80	–11.90	20.2	–10.7	–77.1	2.40	–10.70
KA3385A	2012-01-31	32.05	34.18	22088	Section	42.80	–13.00	18.6	–0.5	–77.4	2.10	–11.10
KA3385A	2012-01-31	32.05	34.18	22433	Section	39.46	–12.6	n.a.	n.a.	n.a.	n.a.	n.a.
KA3385A	2012-01-31	32.05	34.18	22435	Fracture	46.18	–10.90	n.a.	n.a.	n.a.	n.a.	n.a.

Water data – trace elements.

Idcode	Sampling date	Secup m	Seclow m	SKB no.	Water type	U µg L^{-1}	Th µg L^{-1}	Sc µg L^{-1}	Rb µg L^{-1}	Y µg L^{-1}	Zr µg L^{-1}	Sb µg L^{-1}	Cs µg L^{-1}	Hf µg L^{-1}	Tl µg L^{-1}
KA3105A	2012-02-06	25.51	52.01	22089	Section	n.a.	n.a.	n.a.	n.a.	n.a.	n.a.	n.a.	n.a.	n.a.	n.a.
KA3105A	2012-02-06	22.51	24.51	22090	Section	n.a.	n.a.	n.a.	n.a.	n.a.	n.a.	n.a.	n.a.	n.a.	n.a.
KA3105A	2012-02-06	17.01	19.51	22124	Section	n.a.	n.a.	n.a.	n.a.	n.a.	n.a.	n.a.	n.a.	n.a.	n.a.
KA3105A	2012-02-14	25.51	52.01	22147	Fracture	n.a.	n.a.	n.a.	n.a.	n.a.	n.a.	n.a.	n.a.	n.a.	n.a.
KA3105A	2012-02-14	22.51	24.51	22148	Fracture	n.a.	n.a.	n.a.	n.a.	n.a.	n.a.	n.a.	n.a.	n.a.	n.a.
KA3105A	2012-02-14	17.01	19.51	22149	Fracture	1.2600	<0.20	<0.40	28.4000	0.4230	0.4340	<0.1000	2.5300	<0.02	<0.0500
KA3385A	2012-02-14	32.05	34.18	22153	Fracture	n.a.	n.a.	n.a.	n.a.	n.a.	n.a.	n.a.	n.a.	n.a.	n.a.
KA3385A	2012-01-31	32.05	34.18	22088	Section	n.a.	n.a.	n.a.	n.a.	n.a.	n.a.	n.a.	n.a.	n.a.	n.a.
KA3110A	2012-01-31	20.05	26.83	22087	Section	n.a.	n.a.	n.a.	n.a.	n.a.	n.a.	n.a.	n.a.	n.a.	n.a.

Idcode	Sampling date	Secup m	Seclow m	SKB no.	Water type	La µg L^{-1}	Ce µg L^{-1}	Pr µg L^{-1}	Nd µg L^{-1}	Sm µg L^{-1}	Eu µg L^{-1}	Gd µg L^{-1}	Tb µg L^{-1}	Dy µg L^{-1}	Ho µg L^{-1}
KA3105A	2012-02-06	25.51	52.01	22089	Section	n.a.	n.a.	n.a.	n.a.	n.a.	n.a.	n.a.	n.a.	n.a.	n.a.
KA3105A	2012-02-06	22.51	24.51	22090	Section	n.a.	n.a.	n.a.	n.a.	n.a.	n.a.	n.a.	n.a.	n.a.	n.a.
KA3105A	2012-02-06	17.01	19.51	22124	Section	n.a.	n.a.	n.a.	n.a.	n.a.	n.a.	n.a.	n.a.	n.a.	n.a.
KA3105A	2012-02-14	25.51	52.01	22147	Fracture	n.a.	n.a.	n.a.	n.a.	n.a.	n.a.	n.a.	n.a.	n.a.	n.a.
KA3105A	2012-02-14	22.51	24.51	22148	Fracture	n.a.	n.a.	n.a.	n.a.	n.a.	n.a.	n.a.	n.a.	n.a.	n.a.
KA3105A	2012-02-14	17.01	19.51	22149	Fracture	0.2920	0.3920	0.0451	0.2010	0.0302	–0.0200	0.0393	–0.0200	0.0297	–0.0200
KA3385A	2012-02-14	32.05	34.18	22153	Fracture	n.a.	n.a.	n.a.	n.a.	n.a.	n.a.	n.a.	n.a.	n.a.	n.a.
KA3385A	2012-01-31	32.05	34.18	22088	Section	n.a.	n.a.	n.a.	n.a.	n.a.	n.a.	n.a.	n.a.	n.a.	n.a.
KA3110A	2012-01-31	20.05	26.83	22087	Section	n.a.	n.a.	n.a.	n.a.	n.a.	n.a.	n.a.	n.a.	n.a.	n.a.

Idcode	Sampling date	Secup m	Seclow m	SKB no.	Water type	Er µg L^{-1}	Tm µg L^{-1}	Yb µg L^{-1}	Lu µg L^{-1}
KA3105A	2012-02-06	25.51	52.01	22089	Section	n.a.	n.a.	n.a.	n.a.
KA3105A	2012-02-06	22.51	24.51	22090	Section	n.a.	n.a.	n.a.	n.a.
KA3105A	2012-02-06	17.01	19.51	22124	Section	n.a.	n.a.	n.a.	n.a.
KA3105A	2012-02-14	25.51	52.01	22147	Fracture	n.a.	n.a.	n.a.	n.a.
KA3105A	2012-02-14	22.51	24.51	22148	Fracture	n.a.	n.a.	n.a.	n.a.
KA3105A	2012-02-14	17.01	19.51	22149	Fracture	0.0282	–0.0200	0.0252	–0.0200
KA3385A	2012-02-14	32.05	34.18	22153	Fracture	n.a.	n.a.	n.a.	n.a.
KA3385A	2012-01-31	32.05	34.18	22088	Section	n.a.	n.a.	n.a.	n.a.
KA3110A	2012-01-31	20.05	26.83	22087	Section	n.a.	n.a.	n.a.	n.a.

Water data – environmental metals.

Idcode	Sampling date	Secup m	Seclow m	SKB no.	Water type	Al µg L^{-1}	Ba µg L^{-1}	Cd µg L^{-1}	Cr µg L^{-1}	Cu µg L^{-1}	Co µg L^{-1}	Hg µg L^{-1}	Ni µg L^{-1}	Mo µg L^{-1}	Pb µg L^{-1}	V µg L^{-1}	Zn µg L^{-1}
KA3105A	2012-02-06 10:50	25.51	52.01	22089	Section	13.70	41.00	<0.02	0.35	0.81	0.06	0.00	0.89	13.90	0.44	0.11	12.00
KA3105A	2012-02-06 11:27	22.51	24.51	22090	Section	124.00	51.90	>0.02	0.14	<0.20	0.15	0.00	0.66	9.12	<0.10	0.68	2.21
KA3105A	2012-02-06 11:46	17.01	19.51	22124	Section	20.20	40.40	<0.02	0.20	<0.20	0.02	0.00	0.39	5.71	<0.10	0.33	<0.80
KA3105A	2012-02-14 08:45	25.51	52.01	22147	Fracture	3.32	34.50	<0.20	0.15	<0.20	0.05	0.00	<0.20	14.40	0.11	0.14	<0.80
KA3105A	2012-02-14 09:48	22.51	24.51	22148	Fracture	1.38	36.80	<0.20	0.21	<0.20	0.09	0.00	<0.20	4.63	<0.10	0.41	<0.80
KA3105A	2012-02-14 09:49	17.01	19.51	22149	Fracture	0.60	38.90	<0.02	0.13	<0.20	0.03	0.00	<0.20	4.40	<0.10	0.45	<0.80
KA3385A	2012-02-14 09:28	32.05	34.18	22153	Fracture	2.67	66.80	<0.05	0.19	<0.50	<0.05	0.00	<0.50	33.20	<0.30	<0.05	<2.00
KA3385A	2012-01-31 09:16	32.05	34.18	22088	Section	361.00	75.80	<0.05	–0.10	<0.50	<0.05	0.00	2.22	36.70	<0.30	0.62	<2.00

Water chemistry.

Idcode	Sampling date	Secup m	Seclow m	SKB no.	Water type	Na^+ mg L^{-1}	K^+ mg L^{-1}	Ca^{2+} mg L^{-1}	Mg^{2+} mg L^{-1}	HCO_3^- mg L^{-1}	Cl^- mg L^{-1}	SO_4^{2-} mg L^{-1}	SO_4_S mg L^{-1}	Br^- mg L^{-1}	F^- mg L^{-1}	Si^{2+} mg L^{-1}	Fe mg L^{-1}
KA3105A	2012-02-06	25.51	52.01	22089	Section	1,230	7.45	608	42.3	n.a.	2,672	251.6	98.2	10.2	n.a.	7.17	0.241
KA3105A	2012-02-06	22.51	24.51	22090	Section	1,150	8.00	494	52.4	n.a.	2,613	225.0	92.0	8.6	n.a.	7.73	0.410
KA3105A	2012-02-06	17.01	19.51	22124	Section	1,090	10.60	390	66.7	n.a.	2,341	222.8	85.2	7.6	n.a.	7.31	0.279
KA3105A	2012-02-14	25.51	52.01	22147	Fracture	1,130	6.32	612	43.2	123.3	2,769	253.5	89.6	9.7	1.52	7.73	0.167
KA3105A	2012-02-14	22.51	24.51	22148	Fracture	1,050	9.01	373	70.7	222.3	2,280	222.4	77.9	6.7	1.70	7.65	0.257
KA3105A	2012-02-14	17.01	19.51	22149	Fracture	1,030	11.30	353	78.0	225.5	2,303	219.9	77.9	6.5	1.57	7.49	0.393
KA3385A	2012-02-14	32.05	34.18	22153	Fracture	2,010	11.20	1,710	69.3	n.a.	n.a.	n.a.	132	n.a.	n.a.	6.65	0.211
KA3385A	2012-01-31	32.05	34.18	22088	Section	2,280	11.2	1,950	63.0	n.a.	n.a.	n.a.	150	n.a.	n.a.	6.36	0.173
KA3110A	2012-01-31	20.05	26.83	22087	Section	n.a.	n.a.	n.a.	n.a.	n.a.	n.a.	n.a.	n.a.	n.a.	n.a.	n.a.	n.a.
KA3385A	2012-01-31	32.05	34.18	22150	Section	n.a.	n.a.	n.a.	n.a.	n.a.	n.a.	n.a.	n.a.	n.a.	n.a.	n.a.	n.a.
KA3385A	2012-01-31	32.05	34.18	22151	Section	n.a.	n.a.	n.a.	n.a.	n.a.	n.a.	n.a.	n.a.	n.a.	n.a.	n.a.	n.a.
KA3385A	2012-01-31	7.05	31.05	22152	Section	n.a.	n.a.	n.a.	n.a.	n.a.	n.a.	n.a.	n.a.	n.a.	n.a.	n.a.	n.a.

Idcode	Sampling date	Secup m	Seclow m	SKB no.	Water type	Fe-tot mg L^{-1}	Fe^{2+} mg L^{-1}	Mn^{2+} mg L^{-1}	Li^+ mg L^{-1}	Sr^{2+} mg L^{-1}	pH	Conductivity mS m^{-1}	TOC mg L^{-1}	DOC mg L^{-1}	HS^- mg L^{-1}	P-tot mg L^{-1}
KA3105A	2012-02-06	25.51	52.01	22089	Section	n.a.	n.a.	0.290	0.402	11.000	7.67	887	n.a.	5.0	0.185	0.0087
KA3105A	2012-02-06	22.51	24.51	22090	Section	n.a.	n.a.	0.366	0.288	8.920	7.73	779	n.a.	6.0	0.230	<0.005
KA3105A	2012-02-06	17.01	19.51	22124	Section	n.a.	n.a.	0.473	0.187	6.670	7.62	739	n.a.	6.8	0.399	<0.005
KA3105A	2012-02-14	25.51	52.01	22147	Fracture	0.180	0.170	0.302	0.368	10.100	7.61	895	n.a.	5.1	0.062	<0.005
KA3105A	2012-02-14	22.51	24.51	22148	Fracture	0.260	0.260	0.474	0.133	5.770	7.59	754	n.a.	7.3	0.113	<0.005
KA3105A	2012-02-14	17.01	19.51	22149	Fracture	0.400	0.400	0.571	0.121	5.180	7.57	753	n.a.	7.5	0.087	<0.04
KA3385A	2012-02-14	32.05	34.18	22153	Fracture	n.a.	n.a.	0.489	1.090	29.900	n.a.	n.a.	n.a.	n.a.	<0,019	<0.05
KA3385A	2012-01-31	32.05	34.18	22088	Section	n.a.	n.a.	0.435	0.138	37.300	7.56	1,953	n.a.	n.a.	0.189	<0.05
KA3110A	2012-01-31	20.05	26.83	22087	Section	n.a.	n.a.	n.a.	n.a.	n.a.	8.00	998	n.a.	n.a.	14.413	n.a.
KA3385A	2012-01-31	32.05	34.18	22150	Section	n.a.	n.a.	n.a.	n.a.	n.a.	n.a.	n.a.	n.a.	n.a.	0.02	n.a.
KA3385A	2012-01-31	32.05	34.18	22151	Section	n.a.	n.a.	n.a.	n.a.	n.a.	n.a.	n.a.	n.a.	n.a.	<0,019	n.a.
KA3385A	2012-01-31	7.05	31.05	22152	Section	n.a.	n.a.	n.a.	n.a.	n.a.	n.a.	n.a.	n.a.	n.a.	<0,019	n.a.